SUPRAMOLECULAR MODIFICATION OF SELECTED ANTIRETROVIRAL DRUGS

Emile Richard Engel

Dissertation presented for the degree of Master of Science

in the Department of Chemistry
University of Cape Town

August 2011

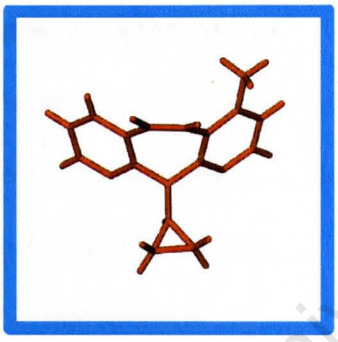

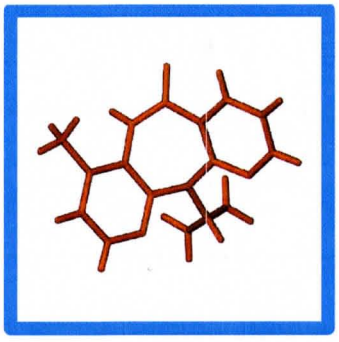

Supervisors: Professors Mino Caira and Susan Bourne

Table of Contents

ACKNOWLEDGEMENTS

My special thanks to:

Professor Mino Caira for his committed supervision, kindness, support and insistence on excellence

Professor Susan Bourne for her co-supervision, care and valuable words of praise and encouragement

Dr Hong Su for collection of the single crystal X-ray data

My colleagues at the Centre for Supramolecular Chemistry Research who became my good friends and with whom I shall share many fond memories

Dr Mircea Bogdan and staff at the National Institute for Research and Development of Isotopic and Molecular Technologies in Cluj-Napoca, Romania for their hospitality and instruction in the NMR analysis of cyclodextrin inclusion complexes

Drs Wilna Liebenberg, Nicole Stieger and Marique Aucamp of the Unit of Drug Research and Development at North-West University, and Dr Halima Samsodien of the School of Pharmacy at the University of the Western Cape for their gracious assistance with solubility studies

The Mandela Rhodes Foundation for financial support

My family whose love and endless support made this work possible

ABSTRACT

A number of antiretroviral drugs that are currently in use for anti-HIV therapy have extremely poor aqueous solubility. This, along with the fact that many of these pharmaceutical compounds possess potential hydrogen bond donor and acceptor functionalities, makes them ideal candidates for attempted supramolecular derivatisation. The primary objective of this study was to carry out co-crystal screening and attempt cyclodextrin complexation with nevirapine, efavirenz, lamivudine and zidovudine, with a view to identifying and isolating new solid forms of these drugs. Any new forms were to be characterised by a variety of analytical techniques, including thermal, spectroscopic and X-ray analysis and, where possible, such derivatives would be tested for any enhancements of drug solubility.

Three novel co-crystals of nevirapine with carboxylic acid co-formers were isolated. Each could be prepared by a simple, rapid liquid-assisted grinding procedure and single crystals were grown by slow evaporation for subsequent X-ray structure elucidation. It was found that upon melting each of the co-crystals, the nevirapine that had been co-crystallised was able to recrystallise as the original, anhydrous form. This is a rare phenomenon in co-crystal chemistry. Quite remarkably, the aqueous solubility of nevirapine for one of these co-crystals was shown to be *five* times greater than that of the untreated form of the drug.

During liquid-assisted co-grinding for the purposes of co-crystal screening, efavirenz underwent phase transformations in several experiments. Subsequently, a very efficient liquid-assisted grinding method was developed for the preparation of a known polymorph of efavirenz. This preparative procedure has not been reported hitherto.

Zidovudine was successfully included in β-cyclodextrin and the complex characterised fully, both in the solid state (by single crystal X-ray diffraction) and in solution (by proton NMR spectroscopy). The association constant for the complex in solution was determined and it indicated that the host-guest interactions in water are extremely weak. By employing water-assisted kneading and powder X-ray diffraction analysis, γ-cyclodextrin was also shown to form an inclusion complex with this active pharmaceutical ingredient.

Two pharmaceutical salts and a β-cyclodextrin inclusion complex of lamivudine were isolated and characterised. Furthermore, reaction products of lamivudine with glutaric acid and succinic acid were prepared and studied. The β-cyclodextrin complex was found to crystallise in a unique packing arrangement. Both the solution- and solid-state behaviours of this complex were investigated by methods that included thermal analysis, X-ray diffraction analysis, isothermal titration calorimetry and proton NMR spectroscopy.

A variety of nine new pharmaceutical salts, co-crystals and cyclodextrin inclusion complexes were prepared using the selected antiretroviral drugs. Of these, single crystal X-ray structures were determined for seven. A number of interesting novel results presented in this dissertation provide strong motivation for further studies of a similar nature.

Chapter 1: Introduction

Supramolecular Modification of Pharmaceuticals

It was Hermann Emil Fischer who in 1894 pre-empted the importance of supramolecular chemistry as a field of study when he used the analogy of a lock and key in describing the enzyme-substrate interaction. In 1987 Charles Pedersen, Donald Cram and Jean-Marie Lehn won the Nobel Prize for their work on crown ethers and cryptands, which could selectively bind metal cations, and this was a milestone that legitimised supramolecular chemistry as an independent field of research.[1] The crown ethers are simple cyclic arrays of ether groups, with organic spacers – anything from ethyl chains to bulkier groups like cyclohexyl or phenyl rings – and cryptands are effectively three-dimensional analogues of these.[2] Lehn, who coined the term 'supramolecular chemistry', described the process of this research field's development as beginning with the selective binding of alkali metal cations by macrocyclic ligands (cryptands and crown ethers) and *exploding* with the arrival of synthetic receptor molecules.[3] Some areas within the field rely heavily on large synthetic molecules while in other areas, commonly available small molecules are utilised with great success.

More recently the term 'crystal engineering' has been used to describe the process of designing supramolecular assemblies. In an effort to predict and control the properties of a crystal, the molecular building blocks and conditions are chosen so that the process of assembly (crystallisation) occurs as desired.[4] The two main principles are still molecular recognition and supramolecular function[1] so crystal engineers make use of their knowledge of hydrogen bond complementarity and common supramolecular synthons, examples of which are illustrated in Figure 1.

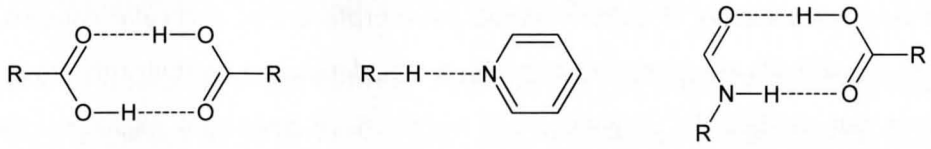

Figure 1: Some highly prevalent supramolecular synthons.

Supramolecular modification (or crystal engineering) of active pharmaceutical ingredients (APIs) entails the harnessing of long-range interactions (particularly hydrogen bonds) for the preparation of new, superior solid forms. The motivation lies in the fact that many drugs with poor aqueous solubility are currently in development or in use and they are not ideal because of their potentially low or unpredictable bioavailability. To overcome such problems, a number of techniques have been employed including micronisation and the preparation of micellar solutions.[5] Inclusion of drugs in

cyclodextrins and the preparation of salt forms are widely-employed, reliable strategies, examples of which are presented in this dissertation. The formation of pharmaceutical co-crystals is a more novel technique that is also exhibited here. There is evidence that through these types of modifications, chemists are able to enhance in particular dissolution and solubility – in some cases dramatically – as well as modify properties such as thermal stability. This study will refer to polymorphs and solvates but will focus on novel results related to co-crystals, salts and cyclodextrin inclusion complexes of some antiretroviral drugs.

John Maddox's famous 1988 assertion that it is a "continuing scandal" that we are not able to predict how compounds will pack in the solid state based on their molecular structure[6] is still very relevant today and partly the inspiration for this and other studies like it. While we are in pursuit here of improved physicochemical performance of a selection of antiretroviral drugs, this study serves also as an exploration of molecular behaviour, adding to the body of knowledge that will in time provide an understanding of how molecules collectively 'choose' a crystal packing arrangement and align themselves accordingly.

Polymorphs and Solvates

In an article entitled "Pharmaceutical Applications of Polymorphism", Haleblian and McCrone defined a polymorph as "a solid crystalline phase of a given compound resulting from the possibility of at least two different arrangements of the molecules of that compound in the solid state". Polymorphs of a given molecule would be identical when converted to liquid or gaseous form, which distinguishes them from geometric isomers and tautomers.[7]

Pharmaceutical polymorphs are of particular interest because different forms often exhibit different physicochemical properties, which translate into variations in bioavailability. Differences in thermal stability and aqueous solubility of closely-related polymorphs are of particular concern. Often the principal weak interactions are preserved between forms, depending on their robustness.[8] The case of the "elusive but predictable" polymorph of aspirin is an important example, where a very commonly used drug could exist as a different polymorph that had gone unidentified until 2005.[9] Even more important and relevant to this thesis is the example of ritonavir, where a commercial batch failed dissolution testing and was later identified as a conformational polymorph of the known form. This newly-discovered Form II was far less water-soluble than Form I.[10]

Joel Bernstein discusses the use of the term pseudopolymorph, which has in the past incorporated solvates and hydrates.[11] The term solvate refers to a crystal that incorporates molecules of the solvent from which it was grown, hydrates being the special case where water is the included

solvent.[12] In most cases the solvent molecules form an integral part of the crystal and their removal causes the structure to collapse. The problem is that there are other cases in which the solvent may be removed easily and returned to the crystal without disrupting the host packing arrangement. A test to distinguish between these and genuine polymorphs is to check for bubbles upon heating, or to check for a loss of mass using thermogravimetric analysis.[11] Pharmaceutical solvates are permissible where the solvent incorporated is not harmful or is present at non-toxic levels. Thus, hydrates are permissible and very common, and other potentially acceptable solvents are ethanol and acetone.[13]

Pharmaceutical Salts

A salt is usually the product of an acid-base reaction. The salt form of an organic substance has different physicochemical properties to those of the neutral compound. Pharmaceutical salts have been of interest for many years because of their ability to increase the dissolution and solubility of a drug.[14] The standard method of pharmaceutical salt preparation is to dissolve the drug and salt former in a common solvent and recrystallise the salt product. A solution-based method that is used less commonly is salt exchange, where one of the components is already in salt form, while the other is still a free acid or base.[15] Trask and co-workers demonstrated the effectiveness of neat grinding and solvent-drop grinding as alternative methods of salt screening and preparation.[16]

A variety of important physicochemical considerations accompanies pharmaceutical salt selection. The salt form must preferably have a high degree of crystallinity, low hygroscopicity, and be stable under conditions of elevated temperature (40 °C) and high relative humidity (75 %).[15] One must be sure that the salt will dissociate into its constituent free acid and base, which depends on factors such as the intrinsic solubility, solubility product and the pH of maximum solubility. An investigation of the effect of common ions is particularly important for basic drugs.[17]

In Serajuddin's consideration of salt forms approved by the FDA during 1995-2006, relatively strong acids were used in the salt forms of 77 % of basic APIs. It appears that the more common carboxylic acids are usually suitable for salt formation of the majority of basic drugs.[17] The development of salt forms is not always feasible, since the difference in pK_a values of the drug and salt former must be, in general, at least 2 pH units.[15] In cases where salt formation is simply not possible, co-crystals are a potential alternative.

Pharmaceutical Co-crystals

Definition

An official definition of the term co-crystal still eludes us. This is the cause of a great deal of confusion, some of which was addressed in a series of letters during 2003-2007, published by Desiraju, Dunitz and Bond in *CrystEngComm*. Desiraju argued that the well-established term 'molecular complex' is sufficient but that if we retain the term co-crystal, it should at least refer to multi-component crystals where some properties of the free components are still evident.[18] Dunitz stated that the term molecular complex had been used for many years without appropriately specific reference to the crystalline state. It encompassed too broad a variety of entities that were solid, liquid or even gaseous at room temperature. He believed the term co-crystal (the hyphen essential) implied a crystal comprising more than one component, that the class should encompass solvates, clathrates and inclusion compounds, and that the term would in any case "be difficult to displace".[19] Bond argued that there is no basis for the assertion that the term should refer to, in particular, a complex of which all components are *solid* at room temperature; that this additional burden is attributed to the term is "contrived and inappropriate". He prefers that co-crystal be used purely as a synonym for the term 'multi-component molecular crystal'.[12]

In their definition of a co-crystal, Shan and Zaworotko have included the stipulation of the components being solid at room temperature because of certain practical implications. In particular, this detail distinguishes them from solvates (including hydrates), which are often less stable upon heating, and addresses the amenability of co-crystals to be discovered and prepared by solid-state methods, as will be discussed in a later section of this chapter.

This thesis deals particularly with the subset of co-crystals called pharmaceutical co-crystals, where at least one of the components is a neutral API. Here, a narrowing of the definition is accepted, so that it includes the condition that any co-formers must be pharmaceutically acceptable.[20] Furthermore it is accepted to include only co-formers that are solids at room temperature for the reasons mentioned by Shan and Zaworotko,[21] which are relevant to our co-crystal screening procedures. So, importantly, in this thesis the term co-crystal refers to a pharmaceutical co-crystal, which is taken to be a molecular complex incorporating a neutral API and at least one other component that is pharmaceutically acceptable and a solid at room temperature.

Often, the components of a co-crystal are co-operatively hydrogen bonded and certainly in the engineering of co-crystals, it is usually necessary to make use of hydrogen bond complementarities. Where solution-based preparative methods are employed, the goal is to recrystallise heteromerically

(Figure 2) so that the starting components combine rather than separate (homomeric recrystallisation). In that sense, recrystallisation is used here in a very different way than in purification during molecular synthesis.[22]

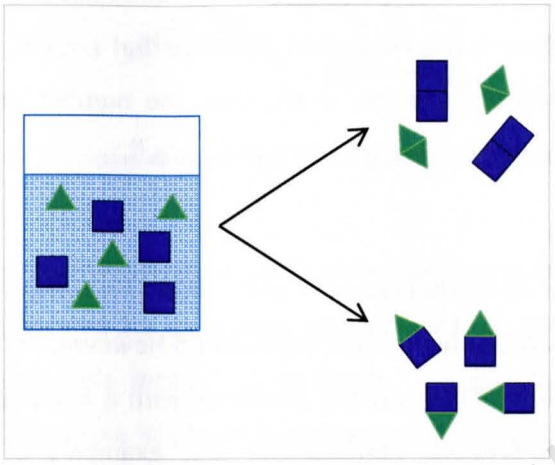

Figure 2: The difference between homomeric recrystallisation (above) and co-crystallisation (below).

Utility

Pharmaceutical co-crystals incorporate APIs and non-drug partner molecules that are safe for consumption – usually meaning that the substance is on the FDA's list of Generally Regarded as Safe (GRAS) substances. This list includes food additives and pharmaceutical excipients. Having established that the molecules of a co-crystal must be in neutral, not ionic form, we have identified the main difference between these and pharmaceutical salts, since the formation of salts involves some kind of charge transfer. In this regard, it is very important, in crystallographic studies, to be able to unambiguously identify the position of acidic protons that may have been transferred during the preparative procedure.

One of the main implications for the distinction between co-crystals and salts has been with regard to the rational design of new forms. It has been shown that the predictability of the form is reduced when proton transfer takes place. In other words, when a salt is formed, the resulting structure is often more complex than in similar cases where there has been no proton transfer. It may result in an obscure stoichiometry, the inclusion of solvent molecules and complex patterns of hydrogen bonding. One rationalisation has been the tendency of carboxylates to bond with multiple acceptors.[23]

Regarding their usefulness, both salts and co-crystals provide new forms with potentially more desirable properties than the parent API. The main difference lies in the vastly greater possibilities within the realm of co-crystals and the seemingly greater predictability of co-crystal structure as

compared with the unpredictability of salts. Importantly also, when compared with pharmaceutical salts, the number of possible co-crystals is vastly greater than the number of potential salt forms. This is because the primary requirement for obtaining a salt, is that the two starting components must engage in an acid-base reaction, and this is not a requirement for co-crystal formation. Thus, where the possibility of salt formation is limited for drugs that are not readily ionisable, this factor does not limit co-crysallisation formation at all. Also, the number of suitable co-formers often exceeds the number of potential salt formers for a given API.[24]

Examples

The majority of studies in co-crystallisation – even those involving APIs – have not specifically involved pharmaceutically acceptable partner molecules.5 However, the realisation of their utility in producing superior formulations has resulted in studies with a more specific focus on discovering pharmaceutically viable co-crystals. Perhaps the first examples of crystal engineering of a pharmaceutically relevant organic compound were the studies on substituted barbituric acid conducted by Zerkowski.[25] By varying the barbituric acid substituents and incorporating different melamine derivatives, over 60 different co-crystals were constructed with linear tape, crinkle tape and rosette tape motifs. The research demonstrated how relatively minor changes in the structure of self-assembling molecular building blocks affected the crystal architecture.

In terms of strategy for the rational design of co-crystals, carbamazepine is an interesting example. Crystal engineers have used two approaches. The first was to engage the 'peripheral' groups with hydrogen bonding potential i.e. to make use of available hydrogen bonding potential without disrupting the primary hydrogen bonding motif of the free drug. An example of how this was achieved with saccharin is shown in Figure 3. The second strategy was to compete directly with the amide-amide self-association of carbamazepine.[21] Fleischman and co-workers reported a set of 13 new multi-component crystalline phases of carbamazepine using this strategy. Most importantly, the group showed it was possible to produce a great variety of new forms with existing, commonly available compounds, where the greatest challenge was not to invent and synthesise but to choose carefully from a readily available list.[26]

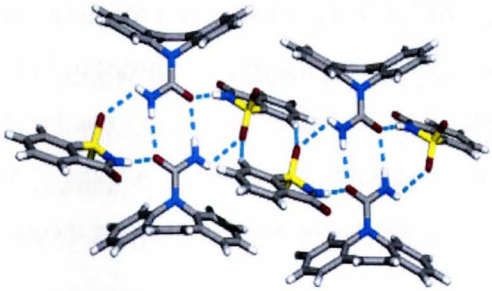

Figure 3: Carbamazepine-saccharin co-crystal reported by Fleischman *et al.*[26]

Itraconazole was modified by co-crystallisation with dicarboxylic acids that belong to the FDA's list of GRAS compounds. The drug formed 2:1 complexes with similar hydrogen bonding motifs in the six co-crystals reported by Remenar's group.[27] Importantly, the groups found that solvent-drug interactions played an important role in determining the success of co-crystallisation. The aqueous dissolution of the co-crystals was tested and it was found that the dissolution profiles were more similar to those of an amorphous form of the drug* than the crystalline form of itraconazole. For the co-crystals, the itraconazole solubility was enhanced 4-20 fold over that of the free crystalline form.

Intellectual property

The increasing prominence of pharmaceutical co-crystal research is also driven by the implications for intellectual property protection. For an invention to be considered worthy of patenting it must be novel, useful and non-obvious. The novelty aspect is no concern because pharmaceutical salts have for many years been considered patentable. Co-crystallisation has the potential to improve a variety of physicochemical properties and is still highly unpredictable (non-obvious). Thus, co-crystals satisfy the basic criteria and the implication is that inventors must identify and protect co-crystals in addition to useful polymorphs, solvates and salts of the drug. This is a mammoth task considering the 2000+ compounds that may be potential co-formers.[28]

Co-crystal Screening

Recent activity in the area of co-crystal screening has incorporated various methods. All of the following have been used in varying degrees in high-throughput co-crystal screening.

Dry co-grinding (or neat co-grinding) of the API and co-former involves combining the two, in a given molar ratio, in a mortar and grinding them together lightly for a recorded period of time. The process of grinding facilitates the reaction. It is considered an example of green chemistry because harmful organic solvents are not required.

* Itraconazole is sold as Sporanox beads, which are amorphous

For *liquid-assisted co-grinding* (LAG), also called solvent-drop grinding or solvent-assisted grinding, a few drops of solvent are introduced during the grinding process. The solvent is usually one in which at least one of the components is partially soluble. There has been evidence to suggest that the solubility of one of the components lends itself to an increase in the rate of the supramolecular reaction, while a lack of solubility is less likely to result in a rate increase.[29]

Co-precipitation from solution by various methods is most commonly carried out by the well-known slow evaporation method. Here a solution containing the API and co-former is allowed to evaporate slowly, yielding crystals after a period of hours to weeks. It is the most widely employed method of crystal growth and the main method used for co-crystal screening. Slow cooling may also be employed and this method is particularly useful for single crystal growth. The solution is prepared at high temperature and then slowly allowed to cool – over a period of hours or days – to control the recrystallisation. Vapour diffusion and layering are also useful when the above methods fail.

Reaction co-crystallisation, also called the slurry method or solution-mediated phase transformation, is a method claimed to be a highly efficient way of screening for co-crystals.[30,31] The difficulty with this procedure is that generally larger amounts of starting material are required than for the grinding methods and the solvent effect is still not fully accounted for. If the co-crystal is more soluble than the components, which it may well be, then this will not be effective.

There is no protocol accepted to produce the best results for any given API and co-former. Effective protocols have been varying combinations of the above methods. In some reported cases, several co-crystals have been produced by both grinding and slow evaporation.[20] However, there have also been reports of co-crystals that could only be prepared by one of the two methods or where *different* co-crystals resulted from grinding and slow evaporation.[32,33] Herein, a recent paper detailing an industrially relevant protocol was used as a guide for the co-crystal screening of the antiretrovirals.[34]

For a co-crystal to form, it requires complementarity of the hydrogen bonding groups and conformational flexibility of the drug. To illustrate the generally low rates of success with co-crystal screening, observe a particularly rewarding example, that of carbamazepine. While the hit rate was considered very high, a variety of screening experiments incorporated 50 co-crystal formers (not necessarily GRAS) and produced only 10 new co-crystals. Most drugs produce hit rates far lower than this during co-crystal screening, and the process is still largely trial-and-error based.

Considerations of pK_a

Predictions of whether the resultant species of reaction between an API and co-former will be a salt or a co-crystal have been based on the value of ΔpK_a where $\Delta pK_a = pK_a(base) - pK_a(acid)$. It has been shown that the outcome is reasonably predictable when $\Delta pK_a < 0$ (most likely a co-crystal) or $\Delta pK_a > 3$ (most likely a salt), but when $0 < \Delta pK_a < 3$ it is not possible to predict co-crystal or salt formation, and there is the added complication that there exists a type of continuum between these extremes. The phenomenon of 'shared' protons may result, where the proton is not fully transferred but exists at an intermediate position between the acidic and basic components.[35] In other words, there may be a statistical distribution within the crystal between the cases of protons transferred and retained.

Cyclodextrin Inclusion

Cyclodextrins (CDs) are macrocyclic oligosaccharides derived from an enzymatic process involving cyclodextrin glucosyl transferase. These compounds were first described by A. Villiers in 1891 after he isolated them from starch, calling them 'cellulosine'.[36] However, it is Franz Schardinger who is widely regarded as having laid the foundation for cyclodextrin chemistry by demonstrating that the occurrence of what he called "α and β dextrin" in the bacterial digest of *Bacillus macerans* was largely independent of the type of starch substrate used. During the period 1935-1954, the combined work of Freudenberg, Jacobi and Cramer (among others) served to identify the three main naturally occurring cyclodextrins and to fully characterise their physicochemical properties and molecular structure. Chemists also became aware of the ability of cyclodextrins to both stabilise and destabilise chemically labile compounds, solubilise lipophilic compounds and to complex organic guest molecules.[37]

Structural features and properties

CDs are made up D-glucopyranoside units, linked by α-1,4-glycosidic bonds (Figure 4). The group of α-, β- and γ-CD occur naturally and are referred to as the native, parent or first-generation cyclodextrins. They are made up of six, seven and eight glucopyranoside units, respectively. There are also derivatised forms. A number of modified cyclodextrins have also been synthetically produced. Most commonly, they have been derivatised by substitution at the hydroxyl groups. The ones of interest in this study are dimethylated β-CD (DIMEB), trimethylated β-CD (TRIMEB), randomly-methylated β-CD (RAMEB) and hydroxypropyl β-CD (HP-β-CD).

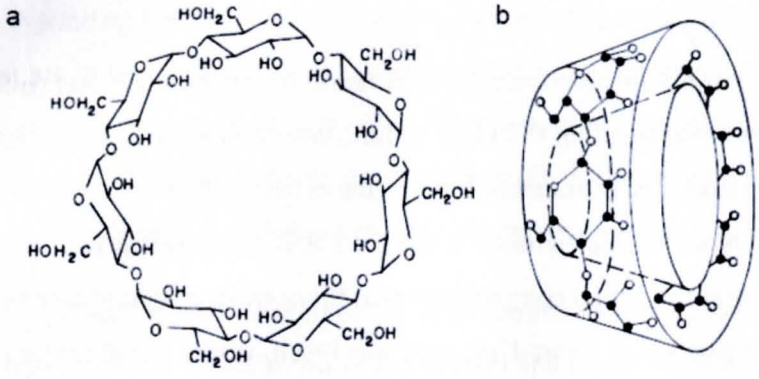

Figure 4: (a) β-CD with seven glucose units, (b) the truncated cone shape. Reproduced from reference 42.

The cyclodextrins are often represented as a truncated cones (Figure 4). The primary rim is the narrow end of the torus, where the $-CH_2OH$ groups are located. The wider secondary rim is made up of secondary hydroxyl groups. These engage in intramolecular O-H···O hydrogen bonding to form a 'belt' that stabilises the shape of the cyclodextrin, which would otherwise be far less rigid.[38] The positioning of these hydroxyl groups at both surfaces is responsible for the fact that the outer portion is hydrophilic and the cavity of the CD is hydrophobic. It is this feature in particular that makes them well-suited to inclusion complexation of hydrophobic molecules or large molecules with a hydrophobic portion. Figure 5 is a molecular structure of a glucopyranoside unit with conventional labelling. The hydroxyl groups of the primary rim are referred to the OH6 hydroxyls and those of the secondary rim the OH2 and OH3 groups. The oxygen atom of the glycosidic linker is O4 and the one within the ring is O5.

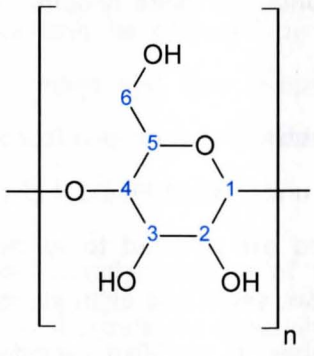

Figure 5: Glucopyranoside unit with carbon atoms labelled conventionally. The index n is equal to 6, 7 or 8 for α-, β- and γ-CD, respectively.

Properties of the cyclodextrins used in this study are provided in Table 1. Of particular relevance is the difference in aqueous solubility. The reason that β-CD has a much lower solubility than both α-CD and γ-CD is that the other two have six and eight fold symmetry, which is more compatible with

the aqueous solvent cage because of its even number of hydrogen bond donors and acceptors. Also, the hydrogen bonding belt at the secondary rim limits the hydroxyl-water interactions, whereas for α- and γ-CD, this belt of hydrogen bonds is incomplete so the hydroxyl groups are more accessible. Herein also lies the main reason why the derivatised β-CDs have particularly high aqueous solubility – on average > 500 mg cm^{-3} at 25 °C.[39] The derivatised CDs become less soluble at elevated temperature, so co-precipitation experiments with these are usually conducted at 60 °C.

Table 1: Properties of the native cyclodextrins.[36,40]

Property	α-CD	β-CD	γ-CD
Molecular mass (g mol^{-1})	972	1135	1297
Aqueous solubility at 25 °C (mg cm^{-3})	145	18.5	232
Diameter of cavity (Å)	4.7-5.3	6.0-6.5	7.5-8.3
Outer diameter (Å)	14.6	15.4	17.5
Cavity Volume ($Å^3$)	174	262	472
Mean K for 1:1 complexes	130(8)	490(8)	350(9)

Inclusion complexes

An inclusion complex involves a host molecule and a smaller guest molecule, where the guest is included within the host cavity by non-covalent forces.[41] For a cyclodextrin inclusion complex to form, the cavity must of course be large enough to accommodate the guest but it is possible for larger molecules to form complexes by insertion of certain groups or side chains. Important also is the polarity of the guest molecule. Hydrophobic molecules usually form more stable complexes, while polar molecules that are highly water-soluble are less amenable to inclusion. Similarly it has been shown that ionic forms of a guest form weaker complexes than the neutral molecule.[42]

Interestingly these inclusion complexes may form stereoselectively and chemically unstable compounds may be stabilised against photosensitivity or oxidation by complexation. Cyclodextrins have also been useful in masking bad smells and tastes, and increasing the aqueous solubility of hydrophobic compounds.[43]

Cyclodextrin complexes may be prepared by a variety of methods including dry kneading, water-assisted kneading, co-precipitation by slow cooling and co-precipitation at elevated temperature. The dry kneading method is exactly the same as was described for co-crystals, where the cyclodextrin and guest compounds are simply ground together so that the powdered materials are mixed intimately. Water may be added to facilitate the inclusion reaction. Depending on the nature of the guest and the quantities used, the complex formation may be complete after a few minutes or as many as several hours of kneading. The slow cooling method is particularly useful when attempting to study cyclodextrin complexes by single crystal X-ray diffraction analysis. The crystals

obtained by normal slow evaporation are often very small, while slow cooling tends to yield large, single crystals more frequently.

Crystal packing

Two major patterns of cyclodextrin crystal packing have been recognised and examples of both are illustrated in Figure 6. The *cage type* pattern has the cyclodextrin cavities shut off from one another. In these crystals, a guest molecule in one cavity is not able to interact with guests in other cavities. The two typical examples of cage type packing are the herringbone arrangement and brickwork arrangements.

The *channel type* patterns are broadly divided into head-to-head or head-to-tail arrangements. The head-to-head arrangements form dimeric pairs. Within the channel type packing arrangements there are several variations, including the helical channel, screw channel and intermediate channel types. The formation of these channels often allows guest molecules to be positioned in multiple orientations along the length of the channel.

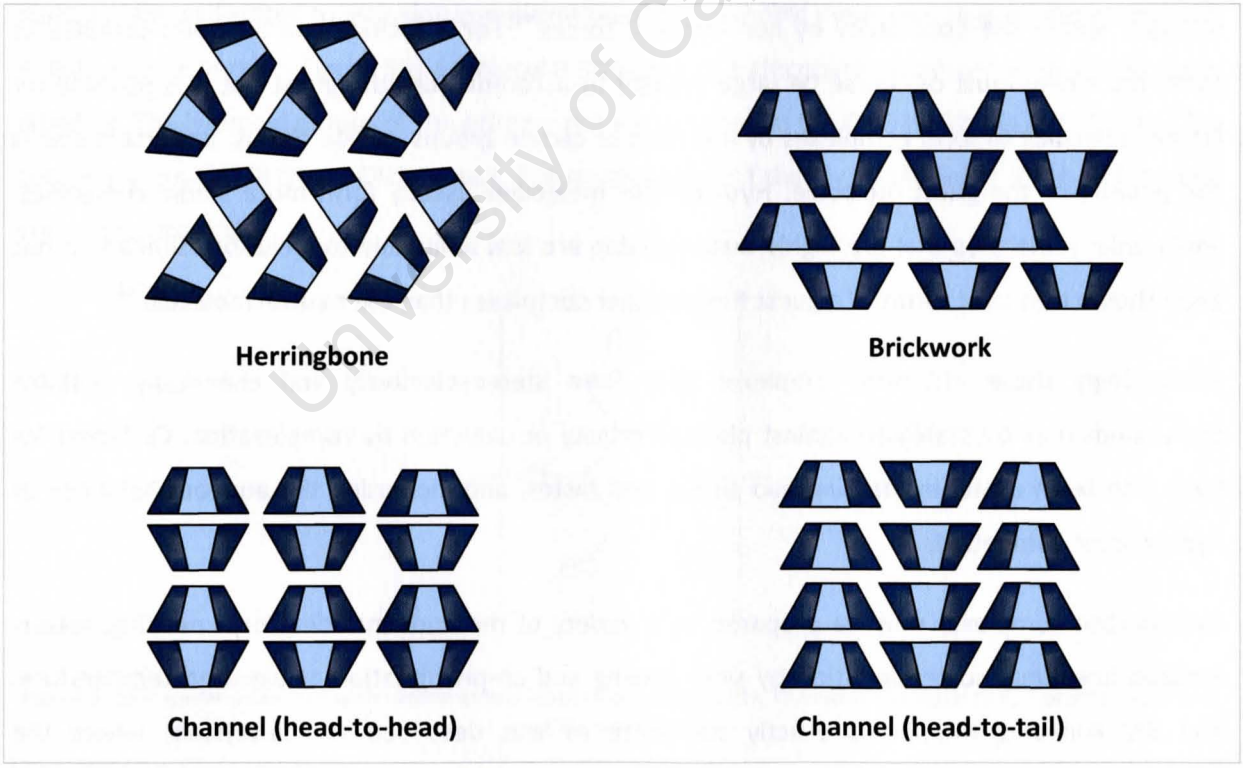

Figure 6: Examples of cyclodextrin packing. The cage type arrangements are above and the channel type below.

The herringbone and layer type structures above are typical examples of monomeric packing arrangements. Dimeric structures like the head-to-head channel type are common for β-CD inclusion complexes. The dimer is stabilised by hydrogen bonding between the hydroxyls of one secondary rim and the other. Other examples are the screw channel and chessboard packing arrangements, illustrated in Figure 7.

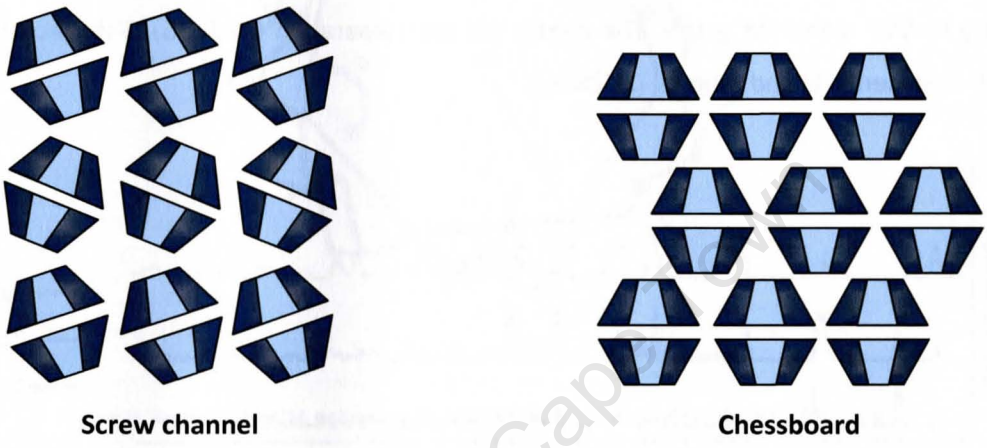

Figure 7: Examples of dimeric packing – the screw channel and chessboard arrangements.

An important concept related to cyclodextrin packing arrangements is that of isostructurality. Two crystals are said to be isostructural when they are of the same crystal system, Bravais lattice and space group. Surveys have been conducted and the known inclusion complexes categorised according to isostructurality.[44,45] Both Caira and Lubhelwana made extensive use of the Cambridge Crystal Structural Database (CSD),[46] which is a collection of thousands of reported single-crystal X-ray structures. Two examples pertaining to β-CD that are particularly relevant to this thesis will be mentioned here. The series 7 (B1) is the one containing the pure host hydrate as well as other guest molecules that do not cause significant changes in the packing arrangement. These crystallise in the space group $P2_1$ with unit cell dimensions a ~ 15 Å, b ~ 10 Å, c ~ 21 Å and β ~ 110°. The series of $C2$ structures with cell dimensions a ~ 19 Å, b ~ 24.5 Å, c ~ 16 Å and β ~ 110°, and classified as series 11 (B6) includes solvent guests and small organic molecules, including the API ibuprofen. For γ-CD, there is only one isostructural series of complexes, with tetragonal space group $P42_12$ and unit cell dimensions a = b ~ 24 Å and c ~ 23 Å.

An important consequence of this level of categorisation, and indeed the main reason it was carried out in the first place, is that the gross packing arrangement may be easily determined by simple

powder X-ray diffraction (PXRD) analysis. Within a given isostructural series, the PXRD traces of all of the inclusion complexes have the same principal features, despite the fact that the guest molecules may be very different. Previously, using PXRD analysis to confirm complexation meant comparing the pattern of the suspected complex with those of the guest, the free host and a physical mixture of the two. By using the CSD to generate reference patterns that are an average of the patterns within a given isostructural series, it is possible to unequivocally confirm that complexation has occurred if the pattern of the sample matches one of the reference patterns.[44] PXRD traces of structures from the isostructural series 11 are provided in Figure 8 to demonstrate their similarity. They are labelled according to CSD reference codes. The guests are methylparaben (AJUVEG), *S*-ibuprofen (TUXKUS) and (Z)-9-dodecen-1-ol and ethanol (ZUZXOH).

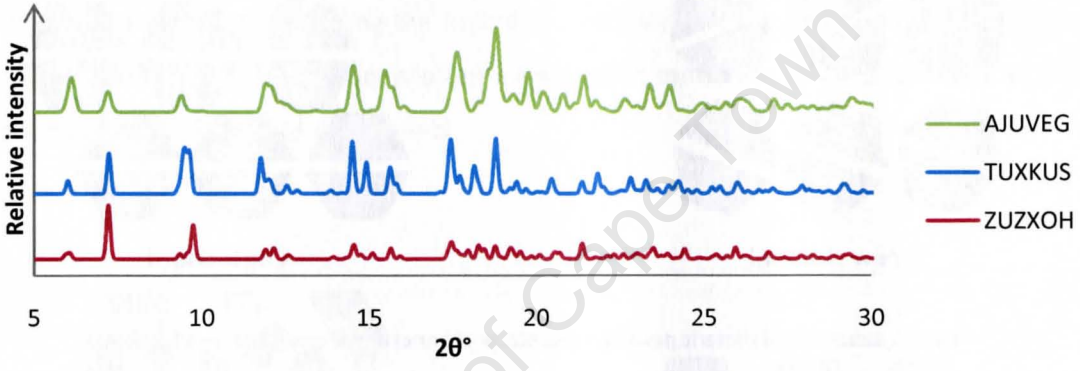

Figure 8: PXRD traces of representative structures from the isostructural series 11.

Another utility of isostructural classification relates to the use of isomorphous replacement (formally 'isostructural replacement' according to IUPAC) as a tool for structure solution. The technique involves using the coordinates of the host in a known (solved) structure as the coordinates of the host atoms in an unknown structure, where both the known and unknown at least belong to the same isostructural series by virtue of a similarity in unit cell dimensions. The technique is based on the premise that, particularly in cyclodextrin inclusion complexes, the host framework is both dominant in determining the X-ray diffraction pattern and has coordinates that are very similar to the coordinates of other host frameworks within the isostructural series to which it belongs.

Molecular geometry

Of particular interest in the study of cyclodextrin inclusion complexes is the conformation of the host molecule. There are several parameters defined by Saenger[47] and Harata[43] used to quantify the extent to which the guest influences the host geometry. These parameters may be compared with those for free host (hydrated) as well as with other complexes. An important basis for extracting

geometrical information is the O4 polygon, which in the case of β-CD is a pseudo-heptagon whose vertices are the O4 oxygen atoms. An idealised version, with important distances and angles, is represented in Figure 9.

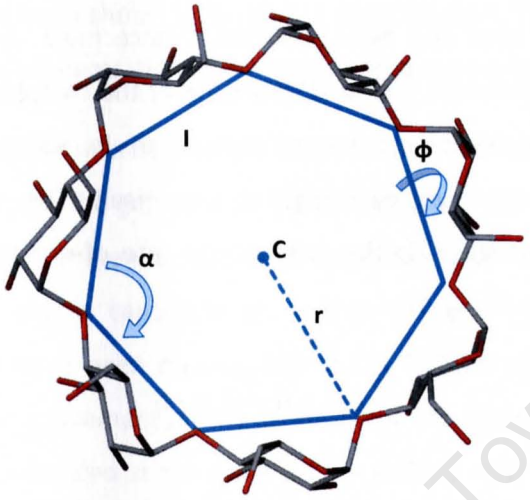

Figure 9: An idealised O4 polygon with important geometrical parameters indicated.

For a glucopyranoside residue labelled n, l is the length of the O4(n-1)-O4(n) side of the polygon. The value r is the centroid-O4n distance. The parameters α and ϕ are the angle O4(n-1)-O4(n)-O4(n+1) and the torsion angle O4(n-2)-O4(n-1)-O4(n)-O4(n+1) respectively. There are a few parameters not represented in the figure. The distance d is the displacement of O4n from the mean plane of all the O4 atoms and D_3 is the distance between consecutive interglucose hydroxyls (O3(n)-O2(n+1)) of the secondary rim. Also important are the tilt angles τ_1 and τ_2. The first is the angle between the mean plane of the ring C1→O5 for a given residue and the line orthogonal to the O4 mean plane. For the residue n, τ_2 is the angle at which the mean plane of O4(n), C4(n), C1(n) and O4(n+1) intersects the O4 mean plane. The τ_1 and τ_2 angles are expected to be similar.

Complexes in solution

It has been said that an understanding of the forces that drive cyclodextrin inclusion is not important in the field of cyclodextrin chemistry alone but is of fundamental importance to supramolecular chemistry as a whole. The primary factors that contribute to the complex formation with a neutral guest are electrostatic interactions, van der Waals interactions, the hydrophobic interaction and hydrogen bonding. While the expulsion of water molecules from the cyclodextrin cavity may appear to be a strong driving force, this is not the case because enthalpy-entropy compensation comes into

effect – when the high-energy water molecules are released, hydrogen bonding within the complex generally lowers their conformational freedom. [48]

Obviously, cyclodextrin molecules are far less rigid in solution but it is important to realise that they are able to adopt several very different conformations. In solution, 1:1 stoichiometric ratios are most common but other ratios have also been reported.[38] Since most complexes are prepared from solution – usually aqueous solution – an understanding of the complexation reaction in solution is extremely useful. While evidence of strong association in solution implies that solid-state complexation is likely, it does not guarantee such a result. The reaction below governs the complexation in solution where K is the ratio of the rate of dissociation (k_D) and the rate of recombination (k_R).[49]

$$CD + G \overset{K}{\leftrightarrow} CD \cdot G$$

$$K = {}^{k_D}/_{k_R}$$

The measurement of K may be highly dependent on the experimental method employed, particularly because the simple model used to describe guest inclusion in solution does not account for the multitude of other possible modes of interaction, and this must be considered when drawing comparisons between different systems.[50] Characterisation of the complexes involves primarily determining the stoichiometric ratio, the association constant and the mode of inclusion. The characterisation of complexes in solution is achieved by a variety of methods that includes UV/Vis spectroscopy, NMR spectroscopy, circular dichroism and isothermal titration calorimetry (ITC).[38]

NMR spectroscopy is used in the continuous variation method to determine Job plots from which these parameters may be derived. ITC is particularly useful and unique because it allows the direct determination of the enthalpy of binding. Curve-fitting and a series of simple calculations allow the further determination of other thermodynamic parameters *viz.* entropy and Gibbs free energy of complex formation. Both the continuous variation method and ITC are employed in this study and these methods are explained in detail in Chapter 2.

Pharmaceutical applications

Lipophilic drugs with low aqueous solubility are particularly good candidates for bioavailability improvement through cyclodextrin inclusion. This is because there is evidence that cyclodextrins enhance the oral bioavailability of FDA's Class II (poor aqueous solubility, high permeability) drugs. On the other hand, cyclodextrin complexes of the Class I (high solubility, high permeability) and Class III (high solubility, poor permeability) drugs generally show reduced bioavailability.[51]

The utility of a drug complex is highly dependent on the magnitude of K. Generally, higher K values are an indication that the complex may be stable enough to isolate in the solid state. Stable cyclodextrin-drug complexes have association constants in the range 100-20,000. While there is the danger that the complex may be so tightly bound that the drug is not adequately released, even highly stable complexes have been shown to dissociate upon dilution. Typically a 1:100 dilution will cause a 70 % reduction in the concentration of complexed drug molecules.[42]

Recent human trials of a topical microbicide gel incorporating the antiretroviral drug tenofovir[52] produced very promising results. The gel reduced the acquisition of HIV by 39 % overall and for the subset with a high rate of adherence, a 54 % reduction was achieved. The experimental antiretroviral drug UC781[53] was a candidate for use in similar topical formulations. Inclusion complexes of this molecule have been formed with β-CD, RAMEB and HP-β-CD, and tested for solubility enhancement and improvements in the inhibition of HIV. Experimental results showed that the solubility of UC781 was enhanced in the order β-CD < RAMEB < HP-β-CD and that the HP-β-CD complex yielded a remarkable 30-fold enhancement in inhibition of the virus. This provides strong motivation for further attempts at cyclodextrin inclusion of anti-HIV drugs, both for traditional oral administration *and* the more novel topical formulations.

The Selected Antiretrovirals

The antiretrovirals (ARVs) were chosen primarily on the basis of hydrogen bonding capability and limited evidence of supramolecular modification in literature. In addition, polymorphism was considered an important indicator of the potential to yield new forms.

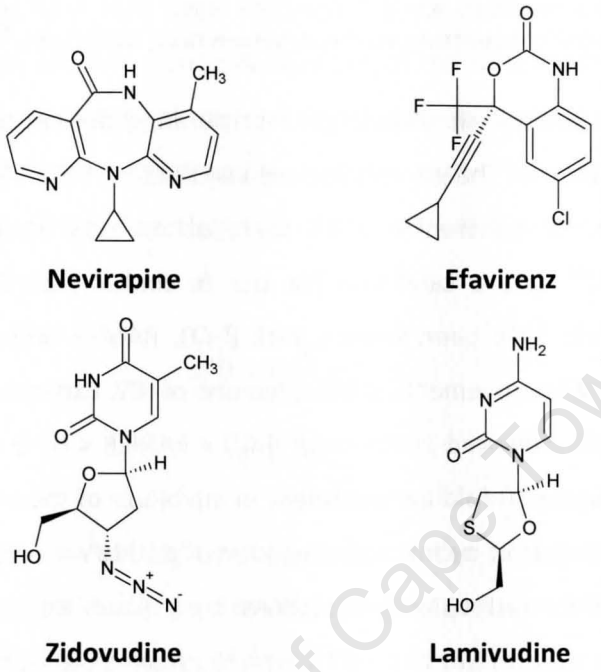

Figure 10: Molecular structures of the ARVs that were the subject of this study.

Relevant properties of the drugs are listed in Table 2. Note the particularly low aqueous solubility values for nevirapine and efavirenz. All are of relatively low molecular mass and nevirapine is the most chemically stable, melting at 247-249 °C. Lamivudine is the only one for which salt forms have been reported,[54,55] despite the fact that nevirapine is more acidic and should be more readily ionised.

Table 2: Properties of the selected antiretrovirals.[56,57]

Property	Nevirapine	Efavirenz	Lamivudine	Zidovudine
Molecular formula	$C_{15}H_{14}N_4O$	$C_{14}H_9ClF_3NO_2$	$C_8H_{11}N_3O_3S$	$C_{10}H_{13}N_5O_4$
Molecular mass (g mol^{-1})	266.30	315.68	229.26	267.24
Solubility at 25 °C (mg cm^{-3})	0.1	9	70*	25
pK_a	2.8	10.2	4.3	9.7
Melting point (°C)	247-249	139-141	160-162	106-112
Known polymorphs	3	several	1	1

*At 20 °C

Nevirapine

Nevirapine (systematic name 11-cyclopropyl-5,11-dihydro-4-methyl-6*H*-dipyrido[3,2-*b*:2′,3′-*e*] diazepin-6-one) is a non-nucleoside reverse transcriptase inhibitor effective against HIV-1. The drug is available commercially as Viramune. The anhydrous form is administered as tablets, while the hydrate is taken as a suspension.[58] Its crystal structure was first reported in 1992, while the drug was still in clinical trials.[59] Numerous solvates have been produced and recently, two co-crystals have emerged.[60] There have been limited attempts at cyclodextrin inclusion.[61]

Nevirapine is an ideal candidate for supramolecular modification because it is hydrophobic and exhibits polymorphic behaviour. An ability to form numerous solvates suggests that the drug can accommodate guest molecules and is at least structurally flexible enough to exist in new forms.

Solute-solvent interactions have been shown to have an observable effect on nevirapine crystal habit. It has been shown that the crystal habit of nevirapine is polarity-dependent. More polar solvent produced elongated crystals because of stronger interactions with the nevirapine molecules, while less polar solvents produced tabular crystals.[62] These interactions are an important consideration, given that co-crystals and cyclodextrin complexes are usually prepared from solution or in the presence of some solvent.

Efavirenz

Efavirenz is widely employed in first-line anti-HIV therapy. Marketed under the name Sustiva or Stocrin, its systematic name is (4*S*)-6-chloro-4-(cyclopropylethynyl)-1,4-dihydro-4-(trifluoromethyl)-2*H*-3,1-benzoxazin-2-one. It is a non-nucleoside HIV-1 reverse transcriptase inhibitor and was approved by the FDA in 1998 and the EMEA in 1999.[56,63] Recently, it has been administered in a single tablet combination that incorporates emtricitabine and tenofovir disoproxil fumarate.[64]

There is a report of efavirenz cyclodextrin complexes with β-CD, randomly methylated β-CD and hydroxypropyl β-CD.[65] The structure of the pure drug and hydrate were known before this study was undertaken, and a few pharmaceutically unacceptable solvates and co-crystals had been discovered in a study where efavirenz produced a low hit-rate during co-crystal screening.[66] As with nevirapine, it has been shown to exhibit polymorphism. In fact, there are many existing patents and patent applications – representative examples of which are referenced here – that describe several polymorphs and different preparative methods.[67,68,69] This implied conformational flexibility suggests that the hydrogen bonding groups may be sufficiently accessible for supramolecular modification. However, a foreseeable problem is that the drug does not crystallise readily and that it has been necessary to employ unconventional solvents for recrystallisation.[66,70]

Zidovudine

Also known as azidothymidine or AZT, it has the systematic name 3′-azido-3′-deoxythymidine. Sold as Retrovir and Retrovis, it is a nucleoside analogue reverse transcriptase inhibitor and was the first drug approved for the treatment of AIDS.[71]

The single crystal X-ray structure of zidovudine has been determined by a number of research groups.[72,73,74] However, there were no solvates or polymorphs of this drug reported at the time of writing. Its moderate but acceptable aqueous solubility of 25 mg cm^{-3} may be the reason it has not received as much attention with respect to supramolecular modification as have other more hydrophobic drugs.

The only co-crystals that are known were formed with lamivudine (to be discussed) and (2,4,6)-triaminopyrimidine. The co-crystal that incorporated lamivudine is actually a ternary co-crystal that incorporates water as well.[54] This zidovudine-lamivudine co-crystal hydrate, which forms a one-dimensional ribbon type packing arrangement as seen in Figure 11, is of particular interest because of the fact that the constituent antiretrovirals are often administered as part of a combination therapy. The successful incorporation of two drugs in the same solid phase opens the possibility to combination therapies where all of the constituents are combined in one stable solid phase, bearing in mind that dosage aspects might complicate such formulations.

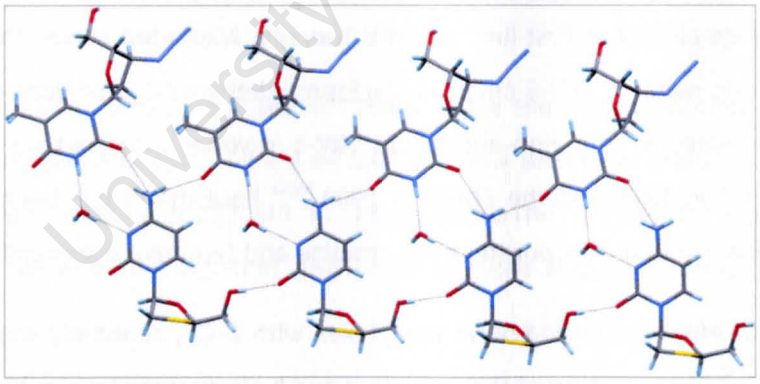

Figure 11: Crystal packing of the zidovudine-lamivudine co-crystal hydrate, reproduced from reference 54. Lamivudine molecules make up the lower layer and zidovudine molecules are in the upper layer.

Lamivudine

Lamivudine (systematic name (2*R*-cis)-4-amino-1-[2-(hydroxymethyl)-1,3-oxathiolan-5-yl]-2(1H)-pyrimidinone) is sold under the trade name Epivir. It is a chiral drug that is one of the most widely employed nucleoside reverse transcriptase inhibitors in the treatment of HIV infection.[75] In addition to its anti-HIV utility it is also used in the treatment of hepatitis B infection.[76]

This API is ionisable. It has a pK_a of 4.3 and has been incorporated into salts with 3,5-dinitrosalicylic acid, saccharin and maleic acid.[54,54] The saccharinate and maleate crystal packing arrangements are practically identical, and the authors of the paper declaring the saccharinate have hailed it as an example of rational design. Importantly, they predicted that other similar salts of lamivudine could result from similar rational design processes. Lamivudine has been incorporated in an interesting co-crystal with zidovudine, as mentioned above. In the same paper there is also the report of a co-crystal with 4-quinoline.[54] The drug is known to exist in the crystalline state as an anhydrous form (the most thermodynamically stable solid form)[77] and as two hydrates; one is a hemihydrate and the other incorporates 0.2 molar equivalents of water per mole of lamivudine. Single crystal structures have been reported for all three of these forms.[78]

Also of importance is a patent that claims a cyclodextrin inclusion complex with β-CD, where a PXRD pattern is provided as the main evidence of complex formation.[79] This patent is evidence that there is existing commercial interest in new solid forms of this API.

Objectives

The aims of the project described in this dissertation were to prepare new solid forms of the selected antiretroviral drugs by supramolecular modification and to investigate the physicochemical properties of these. The specific objectives were as follows:

1. Carry out co-crystal screening with each of the APIs
2. Attempt cyclodextrin inclusion with each of the APIs
3. Where a new form is identified, prepare samples of the co-crystal/salt/inclusion complex for analysis
4. Characterise the new forms by a variety of spectroscopic, thermal and X-ray analytical techniques
5. Where possible, investigate whether or not enhancements in stability and/or solubility have been achieved

References

1 Desiraju GR (2001) Nature 412: 397

2 Steed JW, Atwood JL (2009) Supramolecular Chemistry, 2nd edition. John Wiley & Sons, Chichester, West Sussex, UK, p 122

3 Lehn J-M (1993) Science 260: 1762

4 Braga D, Brammer L, Champness NR (2005) CrystEngComm 7: 1

5 Blagden N, de Matas M, Gavan PT, York P (2007) Adv Drug Delivery Rev 59: 617

6 Maddox J (1988) Nature 335: 201

7 Haleblian J, McCrone W (1969) J Pharm Sci 58: 911

8 Rodríguez-Spong B, Price CP, Jayasankar A, Matzger AJ, Rodríguez-Hornedo N (2004) Adv Drug Delivery Rev 56: 241

9 Vishweshwar P, McMahon JA, Bis JA, Zaworotko MJ (2006) J Pharm Sci 95: 499

10 Bauer J, Spanton S, Henry R, Quick J, Dziki W, Porter W, Morris J (2001) Pharm Res 18: 859

11 Bernstein J (2002) Polymorphism in Molecular Crystals. Caledon Press, Oxford, UK, p 4

12 Bond AD (2007) CrystEngComm 9: 833

13 Haleblian J, McCrone W (1969) J Pharm Sci 58:911

14 Patel A, Jones SA, Ferro A (2009) Br J Cardiol 16: 281

15 Kumar L, Amin A, Bansal AK (2008) Pharmaceutical Technol 3, http://pharmtech.findpharma.com/pharmtech/article/articleDetail.jsp?id=500407&sk=&date=&pageID=7 (accessed on 28 March 2011)

16 Trask AV, Haynes DA, Motherwell WDS, Jones W (2006) Chem Commun (1): 51

17 Serajuddin ATM (2007) Adv Drug Delivery Rev 59: 603

18 Desiraju GR (2003) CrystEngComm 5: 466

19 Dunitz JD (2003) CrystEngComm 5: 506

20 Weyna DR, Shattock T, Vishweshwar P, Zaworotko MJ (2008) Cryst Growth Des 9: 1106

21 Shan N, Zaworotko M (2008) Drug Discovery Today 13: 440

22 Aakeröy CB, Salmon DJ. (2005) CrystEngComm 7: 439

23 Aakeröy CB, Fasulo ME, Desper J (2007) Mol Pharmaceutics 4: 317

24 Good DJ, Rodríguez-Hornedo N (2009) Cryst Growth Des 9: 2252

25 Zerkowski JA, Seto CT, Whitesides GM (1992) J Am Chem Soc 114: 5473

26 Fleischman SG, Kuduva SS, McMahon JA, Moulton B, Bailey Walsh RD, Rodríguez-Hornedo N, Zaworotko MJ (2003) Cryst Growth Des 3: 909

27 Remenar JF, Morissette SL, Peterson ML, Moulton B, MacPhee JM, Guzmán HR, Almarsson Ö (2003) J Am Chem Soc 125: 8456

28 Trask AV (2007) Mol Pharmaceutics 4: 301

29 Shan N, Toda F, Jones W (2002) Chem Commun (20): 2372

30 Zhang GGZ, Henry RF, Borchardt TB, Lou X (2007) J Pharm Sci 96: 990

31 Childs SL, Rodríguez-Hornedo N, Reddy LS, Jayasankar A, Maheshwari C, McCausland L, Shipplett R, Stahly BC (2008) CrystEngComm 10: 856

32 Trask AV, van de Streek J, Motherwell WDS, Jones W (2005) Crystal Growth Des 5: 2233

33 Blagden N, Berry DJ, Parkin A, Javed H, Ibrahim A, Gavan PT, De Matos LL, Seaton CC (2008) New J Chem 32: 1659

34 Li Z, Yang B-S, Jiang M, Eriksson M, Spinelli E, Yee N, Senanayake C (2009) Org Process Res Dev 13: 1307

35 Childs SL, Stahly GP, Park A (2007) Mol Pharmaceutics 4: 323

36 Brewster M, Loftsson T (2007) Adv Drug Delivery Rev 59: 645

37 Loftsson T, Duchene D (2007) Int J Pharm 329: 1

38 Connors KA (1997) Chem Rev 97: 1325

39 Steed JW, Atwood JL (2009) Supramolecular Chemistry, 2nd edition. John Wiley & Sons, Chichester, West Sussex, UK, p 330

40 Del Valle EMM (2004) Process Biochem 39: 1033

41 Frömming K-H, Szejtli J (1994) In: Davies JED (ed) Topics in Inclusion Science, vol 5. Kluwer Academic Publishers, Dordrecht, The Netherlands, p 45

42 Challa R, Ahuja A, Ali J, Khar RK (2005) AAPS PharmSciTech 6: E329

43 Harata K (1993) Seimei Kogaku Kogyo Gijutsi Kenkyusho Kenkyu Hokoku 1: 1

44 Caira MR (2001) Rev Roum Chim 46: 371

45 Lubhelwana S (2005) Crystal Isostructurality and X-ray Diffraction Studies of Cyclodextrin Inclusion Compounds, MSc Thesis, University of Cape Town, South Africa

46 Cambridge Structural Database and Cambridge Structural Database System (Feb, 2011) Version 5.32, Cambridge Crystallographic Data Centre, University Chemical Laboratory, Cambridge, England

47 Saenger W (1984) In: Atwood JL, Davies JED, MacNicol DD (eds) Inclusion Compounds, vol 2. Oxford University Press, London, UK, ch 8

48 Liu L, Guo Q-X (2002) J Inclusion Phenom Macrocyclic Chem 42:1

49 Frömming K-H, Szejtli J (1994) In: Davies JED (ed) Topics in Inclusion Science, vol 5. Kluwer Academic Publishers, Dordrecht, The Netherlands, p 50

50 Loftsson T, Másson M, Brewster ME (2004) J Pharm Sci 93:1091

51 Loftsson T, Duchene D (2007) Int J Pharm 329: 1

52 Abdool Karim Q, Abdool Karim SS, Frohlich JA, Grobler AC, Baxter C, Mansoor LE, Kharsany ABM, Sibeko S, Mlisana KP, Omar Z, Gengiah TN, Maarschalk S, Arulappan N, Mlotshwa M, Morris L, Taylor D (2010) Science 329: 1168

53 Yang H (2008) AAPS J 10: 606

54 Bhatt PM, Azim Y, Thakur TS, Desiraju GR (2009) Cryst Growth Des 9: 951

55 Martins FT, Paparidis N, Doriguetto AC, Ellena J (2009) Cryst Growth Des 9: 5283

56 O' Neil MJ, Heckelman PE, Koch CB, Roman KJ (eds) (2006) Merck Index, 14th edition, New Jersey, USA

57 Gennaro AR (1995) Remington: The Science and Practice of Pharmacy, 19th edition, vol 2. Mack Publishing, Easton, Pennsylvania, USA, p 1336

58 Bardsley-Elliot A, Perry CM (2000) Paediatr Drugs 2: 373

59 Mui PW, Jacober SP, Hargrave KD, Adams J (1992) J Med Chem 35: 201

60 Samsodien H (2010) Supramolecular Derivatives of Selected Bioactive Compounds: A Physicochemical Study, PhD Thesis, University of Cape Town, South Africa

61 Lokamatha KM, Barathi A, Shanta Kumar SM, Rama Rao, N (2010) Research Journal of Pharmaceutical, Biological and Chemical Sciences 1: 372

62 Sarkar M, Perumal OP, Panchagnula R (2008) Indian J Pharm Sci 70: 619

63 Vrouenraets SM, Wit FW, Tongeren J van, Lange JM (2007) Expert Opin Pharmacother 8: 851

64 Rakhmanina NY, van den Anker JN (2010) Expert Opin Drug Metab Toxicol 6: 95

65 Sathigari S, Chadha G, Lee Y-HP, Wright N, Parsons DL, Rangari VK, Fasina O, Babu RJ (2009) AAPS PharmSciTech 10: 81

66 Mahapatra S, Thakur TS, Joseph S, Varughese S, Desiraju GR (2010) Cryst Growth Des 10: 3191

67 Radesca LA, Maurin MB, Rabel SR, Moore JR (1999) International Patent Application 64405

68 Reddy BP, Rathnakar K, Reddy RR, Reddy MD, Reddy KSC (2006) US Patent Application 0235008

69 Sharma R, Bhushan KH, Aryan RC, Singh N, Pandya B, Kumar Y (2006) International Patent Application 040643

70 Ravikumar K, Sridhar B (2009) Mol Cryst Liq Cryst 515: 190

71 http://www.fda.gov/ForConsumers/ByAudience/ForPatientAdvocates/HIVandAIDSActivities/ucm151074.htm (accessed on 20 July 2011)

72 Birnbaum GI, Giziewicz J, Gabe EJ, Lin T-S, Prusoff WH (1987) Can J Chem 65: 2135

73 Camerman A, Mastraopaolo D, Camerman N (1987) Proc Natl Acad Sci USA 84: 8239

74 Dyer I, Low JN, Tollin P, Wilson HR, Alan Howie R (1988) Acta Crystallogr C44: 767

75 Coates JA, Cammack N, Jenkinson HJ, Mutton IM, Pearson BA, Storer R, Cameron JM, Penn CR (1992) Antimicrob Agents Chemother 36: 202

76 Chang CN, Skalskiv V, Zhou JH, Cheng YCJ (1992) Biol Chem 267: 22414

77 Jozwiakowski MJ, Nguyen N-AT, Sisco JM, Spancake CW (1996) J Pharm Sci 85: 193

78 Bhattacharya A, Roy BN, Singh GP, Srivastava D, Mukherjee AK (2010) Acta Crystallogr C66: o329

79 Llorret Perez S, Puigvert Colomer M (2009) International Patent Application 031026

Chapter 2: Experimental

Materials

Nevirapine ($C_{15}H_{14}N_4O$) was purchased from Cipla Ltd. (batch 1001003, Mumbai, India), while efavirenz ($C_{14}H_9ClF_3NO_2$), lamivudine ($C_8H_{11}N_3O_3S$) and zidovudine ($C_{10}H_{13}N_5O_4$) were supplied by Brunel (batches HEVC0870007, 040803 and 040903, respectively; Pretoria, South Africa). The purity of all four drug batches was confirmed by proton NMR spectroscopy and DSC analysis.

β-cyclodextrin (β-CD; $C_{42}H_{70}O_{35}$), γ-cyclodextrin (γ-CD; $C_{48}H_{80}O_{40}$), dimethylated β-CD (DIMEB; $C_{56}H_{98}O_{35}$) and trimethylated β-CD (TRIMEB; $C_{63}H_{112}O_{35}$) were supplied by Cyclolab (Budapest, Hungary). Randomly methylated β-CD (RAMEB; $(C_{42}H_{70-n}O_{35})(CH_3)_n$[*]) and hydroxypropyl β-CD (HP-β-CD; $(C_{42}H_{70-n}O_{35})(C_3H_7O)_n$[†]) were obtained from Sigma-Aldrich Chemie Gmbh (Steinheim, Germany). All cyclodextrins were used as received and it was determined by TGA analysis that the native CDs contained ~7 water molecules of crystallisation per CD molecule at room temperature.

Co-crystal and salt formers were obtained from Sigma-Aldrich Chemie Gmbh (Steinheim, Germany) and Acros Organics (New Jersey, USA). The full list of co-formers is provided in the appendix.

Co-crystal Screening

A three-stage co-crystal screening protocol similar to the one described by Li *et al.* was employed here.[1] The first two stages involved co-grinding and served as a high-throughput means of identifying co-formers that might produce one or more co-crystals with a given active pharmaceutical ingredient (API). The third stage involved more time-consuming co-precipitation experiments. Importantly, stages one and two informed the choices in stage three of which co-formers, solvents and molar ratios to prioritise. Where warranted, there were deviations from the protocol.

Stage one of the screening process was dry co-grinding. The experiments involved combining the API with one of a selection of co-formers and neat grinding with a pestle and mortar for at least 5 min. The resultant material was analysed by PXRD and its trace compared with PXRD traces of the free starting reagents. The appearance of new peaks and the disappearance of free component peaks served as evidence of possible co-crystallisation. In general the API and co-former were first combined in 1:1 molar ratio before other molar ratios were attempted, based on the predicted supramolecular synthons of potential co-crystals.

[*] n = 0.6-0.8
[†] n = 1.5-2.1

Solvent-assisted or liquid-assisted co-grinding (LAG) was the next stage. Here, a few drops of solvent were added during the grinding process – periodically where necessary – and the resultant paste/gel kneaded for at least 5 min. As for the dry co-grinding experiments, the API and co-former were mixed according to the predicted stoichiometries of hypothetical co-crystals.

Co-precipitation experiments followed with co-former candidates that presented favourable results in stages one and two. The co-precipitation was achieved by the common method of slow evaporation from solution. With a vast number of possible combinations of co-former, solvent and molar ratio, it was important to choose carefully. Where LAG produced a phase change for a particular co-former-API combination, the solvent that had been used was then also used for slow evaporation. Along with this, the information available in literature was considered, particularly where various recrystallisation experiments had been reported. In general, the API and co-former were combined stoichiometrically – in some cases pre-ground together – and dissolved in an appropriate solvent or mixture of solvents at near saturation, while heated to a few degrees below the solvent boiling point. The warm solution was carefully filtered through 0.45 µm microfilters and allowed to crystallise at ~20 °C.

Confirmation of quantitative co-crystal formation required:

1. Confirmation of no component peaks in the PXRD trace
2. Confirmation of no component melting peaks in the DSC record
3. Unambiguous evidence that no acid-base reaction had occurred, so that the resultant complex may be considered a genuine co-crystal and not a salt

The typical API mass used for grinding experiments was ~10 mg. Larger masses (~20-30 mg) were required for the slow evaporation stage. It must be noted that the co-crystal screening in this study cannot be considered comprehensive. In the case of solvent-assisted co-grinding at least one solvent was employed; however, different solvents may have produced very different results. Also, not all of the products of slow evaporation experiments were analysed. There were simply too many experiments so, except in a few select cases, only the unit cells of single crystals were checked on the four-circle diffractometer. In the majority of cases, powdered products were not analysed. Where single crystals could not be grown for structure determination, FTIR was employed to provide some evidence of whether or not there had been proton transfer resulting in a salt and not a co-crystal. Details of particular co-crystallisation experiments conducted for each of the APIs in this study are given in the relevant chapters. Comprehensive lists of co-crystal screening experiments and outcomes are provided in the appendix.

Cyclodextrin Inclusion

Inclusion of the selected antiretroviral drugs in cyclodextrins was attempted by well-known kneading and co-precipitation methods. For kneading experiments, in general, the API and cyclodextrin were mixed in equimolar ratio and kneaded in the presence of a small quantity of water for 30-90 min. In some cases, water was replaced with ethanol, methanol, or aqueous solutions of these.

Co-precipitation experiments with the β-CD and γ-CD were carried out by dissolving the API and cyclodextrin in 1-5 cm^3 $MilliQ^2$ water, and stirring for 6-24 h depending on the solubility at 40-60 °C. Thereafter, the solutions were filtered using 0.45 μm microfilters to remove any undissolved material and other debris, and allowed to cool slowly over 2-3 days in a vacuum flask.

Where derivatised cyclodextrins were used, the guest and drug were combined in 1-5 cm^3 MilliQ water. The solution or suspension was maintained at low temperature (ice bath) and stirred for approximately 24 h. While still cold, it was filtered as mentioned above and the resultant clear solution placed in a 60 °C oven to crystallise.

To determine whether or not complexes had formed, single crystals were selected for unit cell determination and powders were analysed by PXRD. With PXRD it was possible to compare the resultant powder patterns with known calculated patterns for various common isostructural complexes. Matching a new complex with a known trace from the isostructural series made it possible to know the gross packing arrangement of a new complex.

Thermal Analysis

The methods employed were Hot Stage Microscopy (HSM), Differential Scanning Calorimetry (DSC) and Thermogravimetric Analysis (TGA). The three were used in combination to analyse changes in the physical state of API forms as a function of temperature.

Hot stage microscopy

The hot stage microscopy (HSM) apparatus comprises a microscope coupled with a digital video camera. The 'hot stage' is a plate upon which small samples may be subjected to a temperature programme, administered via a digital controller. Hot stage microscopy was used to record visible changes that occurred as a function of temperature. Samples were placed in silicone oil for the purpose of even heat distribution and so that release of vapour was easily observable. In general the events of interest were: desolvation (bubbles), melting, recrystallisation and decomposition. The data in the form of still images were analysed along with DSC and TGA profiles.

A Linkam TP92 manual temperature controller was used in conjunction with a Linkam THMS600 hot stage. The samples were monitored and images recorded via a Sony Digital Hyper HAD colour video camera fitted to a Nikon stereomicroscope. A heating rate of 10 K min^{-1} was used for all experiments.

Thermogravimetry and differential scanning calorimetry

During thermogravimetric analysis (TGA) a thermobalance records minute changes in mass as the temperature is varied. The method allows for the observation of mass loss as a result of volatile guest loss and decomposition.

Differential scanning calorimetry (DSC) involves a sample pan and reference pan subjected to a controlled temperature programme, during which both pans are maintained at a constant temperature. The heat required to maintain this state is monitored and allows the plotting of heat flow against temperature, displaying peaks at the occurrence of endothermic and exothermic thermal events.

A TA-Q500 Thermogravimetric Analyzer and DSC-Q200 Differential Scanning Calorimeter, TA instruments, with Universal Analysis 2000 software (v4.5A, TA Instruments-Waters LLC), were employed. Both TGA and DSC instruments were run at a nitrogen purge gas flow rate of 50 cm^3 min^{-1}. A heating rate of 10 K min^{-1} was used for most experiments to be consistent with the data collected by HSM; however, the temperature range for each experiment was varied according to the nature of the sample. Sample masses were typically 0.5-2 mg.

Spectroscopic Studies

FTIR spectroscopy

Fourier Transform Infrared (FTIR) Spectroscopy is used routinely to identify and analyse chemical bonds by their natural frequencies of vibration. In the present study, the technique was used to investigate whether or not proton transfer had taken place between the API and co-former by inspecting changes in the characteristic absorption bands of the acidic and basic groups. Spectra were collected on a Perkin Elmer 983 spectrophotometer. Samples were prepared using the Nujol mull method and pressed between sodium chloride windows.

Proton NMR spectroscopy

Routine proton NMR experiments were carried out with a Varian-VXR 300 (300 MHz), Varian-Unity 400 (400 MHz) or Bruker AMX 400 (400 MHz) spectrometer. The experiments were generally conducted to determine or confirm the stoichiometry of salts, co-crystals and inclusion complexes. All samples were dissolved in an appropriate deuterated solvent – either $CDCl_3$, d_6-DMSO or D_2O. The data were analysed using the program Topspin[3] or MestRe-C.[4]

The NMR spectrometer for continuous variation experiments was a Bruker AVANCE III 500 MHz spectrophotometer fitted with a 'broad band observe' probehead. Samples were dissolved in D_2O where possible and DMSO in the cases of very low aqueous solubility. Typical conditions were as follows: temperature at 298 K; 32 K data points; 16 ÷ 128 scans; sweep width of 7 ppm (2-9). A 90 ° pulse of 10.1 μs was used with a zq 30 program (30° pulse excitation). Four dummy scans were run before each experiment. The relaxation delay was 3 s and the acquisition time 4.68 s. Topspin was employed for data analyses.[3]

The continuous variation method

The continuous variation method has become known as Job's method, after the author of the original paper describing it.[5] In the present study, proton NMR spectroscopy was used to draw Job plots for cyclodextrin host-guest reactions in solution. The reactions are of the form:

$$aH + bG \leftrightarrow C \qquad (1)$$
$$\text{where } C = H_aG_b$$

The Job plot is a graph of some signal – here it is an NMR-derived signal, $\Delta\delta_{obs}$ – that is a linear function of the concentration of the complex. With respect to our host-guest system, the signal is plotted against the molar ratio $R = \frac{[X]}{[M]}$ with $[M]$ equal to the sum of the total concentrations of H and G, and X representing H or G. The resultant curve should reach a maximum at $R = \frac{a}{b}$ and approach linearity immediately above and below this value.[6] The dependent variable used in these experiments was $\Delta\delta_{obs}[X]$, where $\Delta\delta_{obs}$ is the difference in observed chemical shift for a solution of the pure X and a solution where the host *and* guest are present.

For a sample series of constant volume, the total molar concentration was kept constant while the molar ratio was varied stepwise. A 10 mM stock solution of each drug and partner cyclodextrin was prepared in DMSO or D_2O. A series of solutions was then prepared from these, usually 11, with molar ratios of 0-1 and analysed by proton NMR spectroscopy.

The association constant

The association constant, K, is defined, from reaction equation (1) as:

$$K = \frac{[C]}{[H]^a[G]^b} \tag{2}$$

Given that $[H]_T = [H] + a[C]$ and $[G]_T = [G] + b[C]$, where $[H]_T$ and $[G]_T$ are the total concentrations of H and G, equation (2) may be expressed as:

$$K = \frac{[C]}{([H]_t - a[C])^a([G]_T - b[C])^b} \tag{3}$$

If $a, b = 1$ as would be established from a Job plot, equation (3) becomes:

$$K = \frac{[C]}{([H]_t - a[C])([G]_T - b[C])} \tag{4}$$

With reference to the earlier comment about Job's method, the observed chemical shift δ_{obs} is taken as a linear function of $[C]$ where δ_{obs} is defined as the weighted average chemical shift for the free guest δ_f and complexed guest δ_c simultaneously present in a given solution. It may be expressed as:

$$\delta_{obs} = \frac{[G]\delta_f + [C]\delta_c}{[G]_T} \tag{5}$$

Since $[G]_T = [G] + [C]$, equation (5) may also be expressed as:

$$\delta_{obs} = \frac{[G]\delta_f + ([G]_T - [G])\delta_c}{[G]_T} = \frac{[G]}{[G]_T}\delta_f + \frac{[G]_T - [G]}{[G]_T}\delta_c$$

And if $= \frac{[G]}{[G]_T}$, then:

$$\delta_{obs} = z\delta_f + (1 - z)\delta_c \tag{6}$$

As $[G] \to 0$, $z \to 0$ such that $\delta_{obs} \to \delta_c$. When $[G] = [G]_T$ or $[G]_T \gg [H]_T$ then $z \to 1$ and $\delta_{obs} \to \delta_f$ (similarly proven for the host). Furthermore, if it is defined that $\Delta\delta = \delta_f - \delta_{obs}$ and $\Delta\delta_c = \delta_f - \delta_c$, then:

$$\Delta\delta_{obs}^{(X)} = \frac{[C]}{[X]_T}\Delta\delta_c^{(X)}$$

where $X = H, G$ for a 1:1 complex.

Substituting the above result into equation (4) gives:

$$[X]_T^2\left(\Delta\delta_{obs}^{(X)}\right)^2 - [X]_T\Delta\delta_{obs}^{(X)}\Delta\delta_c^{(X)}\left([M] + \frac{1}{K}\right) + [H]_T[G]_T\left(\Delta\delta_c^{(X)}\right)^2 = 0 \quad (7)$$

where $[M] = [H]_T + [G]_T$

And solving equation (7) for $\Delta\delta_{obs}^{(X)}$ gives:

$$\Delta\delta_{obs}^{(X)} = \frac{\Delta\delta_c^{(X)}}{2[X]_T}\left\{[M] + \frac{1}{K} \pm \left[\left([M] + \frac{1}{K}\right)^2 - 4[H]_T[G]_T\right]^2\right\} \quad (8)$$

The ratio $\Delta\delta_{obs}/\Delta\delta_c$ will always be less than 1, so only negative solutions of equation (8) are considered. For a set of n samples in an experiment, there will be n equations and only two independent variables that may be solved by taking the experimental $\Delta\delta_{obs}$ values as reference.[7]

ConstEQ and ConstEQV

The association constant was derived with the aid of CONSTEQ.[7] The program evaluates data obtained from the continuous variation experiment by non-linear least-squares fitting analysis according to equation (7), which, without approximations, correlates the total concentrations of host and guest with the chemical shift difference. During each step of the program's iterative fitting procedure, a quadratic equation is used to determine the direction of the search and the loss error function, E, is calculated according to the following equation:

$$E = \sum_{i,j}(\Delta\delta_{obs}^{(i,j)} - \Delta\delta_{calc}^{(i,j)})^2$$

i: sample number, j:proton index

E is the sum of squares of the deviations between the experimental and predicted values. The fitting procedure reaches convergence when the difference between two consecutive E-values is less than 10^{-6}. The entire set of studied protons (up to 15) for a given system may be included in the

calculation to give a single representative K value but the procedure may only be used for systems with a host-guest stoichiometry of 1:1.

ConstEQV, a modified version of ConstEQ, is used when the data from standard experiments do not result in convergence. In this case a second set of experiments is required, where the guest concentration is fixed and the host concentration varied so that the molar ratio varies from zero to values in excess of 10. So, when using ConstEQ, $[M]$ remains constant, while for ConstEQV it varies.

Isothermal Titration Calorimetry

Isothermal titration calorimetry (ITC) is a technique that involves measuring tiny amounts of heat associated with a μL-scale titration. Used to characterise the interactions between molecules in solution, the technique is commonly employed in the analysis of biological systems, to measure the heat of enzyme-substrate binding.[8] In general, the instrument comprises a sample cell and reference cell, which are maintained at the same temperature. A thermoelectric device measures the power required to maintain the sample cell temperature. The integral of this power value is proportional to heat generated or released by the reaction taking place in the sample cell.[9]

ITC experiments were performed at 298 K using a Nano ITC^{2G} (TA Instruments). Each titration comprised 28 injections of 10 μL cyclodextrin solution into the 1.4 cm^3 reaction cell, which contained the API solution of known concentration, details of which are provided in the relevant sections. The first step of each experiment was to measure the heat of dilution for the CD solution, so that this could be accounted for when measuring the heat of binding for each API-cyclodextrin system. NanoAnalyze (v2.1.13, TA Instruments) was the software program used for data analysis.

Determination of the binding parameters

The experiments in the present study were used to measure parameters of binding for cyclodextrin complexes in solution. The output signal from the ITC instrument is the value of the electrical power required to maintain $\Delta T = 0$ for the sample and reference cells. Integration of this power value yields the heat change (Δq_i) between consecutive injections $i - 1$ and i. Plotting $\frac{\Delta q_i}{[CD]_T}$ against $\frac{[CD]_T}{[G]_T}$, where $[CD]_T$ and $[G]_T$ are the total cyclodextrin and guest concentrations, respectively, results in a titration curve from which the values of the binding parameters K, n and ΔH^0 can be determined. These values are extracted using a least-squares non-linear adjustment method based on the Wiseman isotherm (equation (9)).[10,11,12] The parameter r is a composition variable (equation (10)), V_0 is the total volume of the reaction solution and X_R is the absolute value of the ratio $\frac{[G]_T}{[CD]_T}$. Using equations (11) and (12) made it possible to calculate the entropy and Gibbs free energy changes.

$$\frac{dq}{d[CD]_T} = \Delta H^0 V_0 \left[\frac{1}{2} + \frac{1 - X_R - r}{2\sqrt{(1 + X_R + r)^2 - 4X_R}}\right] \quad (9)$$

$$r = \frac{1}{[CD]_T K} \quad (10)$$

$$\Delta G^0 = -RT\ln K \quad (11)$$

$$\Delta G^0 = \Delta H^0 - T\Delta S^0 \quad (12)$$

X-ray Diffraction Analysis

Powder X-ray diffraction

PXRD analysis was used extensively in this study to verify the uniqueness of new forms. During co-crystal and cyclodextrin inclusion complex screening, samples of powdered material were checked routinely. The PXRD data were collected at room temperature, so in some cases where experimental traces are compared with traces calculated from single crystal X-ray data that was collected at low temperature (100 or 173 K), the peaks in the experimental trace appear to be shifted to slightly lower 2θ values. Two instruments were used for PXRD analysis.

Most of the powder X-ray diffractograms were recorded using a Philips PW1120/00 X-ray generator. The generator was fitted with a Huber long fine-focus tube PW2273/20 and a Huber Guinier

Monochromater Series 611/5 to produce CuKα_1 radiation (λ = 1.5405981 Å) at 20 mA and 40 kV. The PXRD patterns were recorded by a Huber Imaging Plate Camera 670. In cases of temperature-controlled PXRD, a Huber High Temperature Controller HTC 9634 unit was used with capillary rotation device 670.2. Samples were manually ground and a small amount (ca. 5 mg) packed into No. 14 Markröhrchen non-diffracting glass. In a few cases where capillary mounting was not possible, flat samples were prepared on Mylar® film.

The second instrument, employed for only a few samples, was a PANalytical X'Pert PRO MPD (Multi-Purpose Diffractometer) with X'Celerator detector and fixed divergence slits for the CuKα_1 radiation. Samples were placed on zero background silicon holders and loaded onto a reflection transmission spinner.

Single-crystal X-ray diffraction

All single crystals were mounted on a nylon loop and coated with Paratone oil.[13] Unit cell dimensions were determined on two instruments – a Nonius Kappa CCD (charge-coupled device) diffractometer and a Bruker KAPPA APEX II DUO single-crystal X-ray diffractometer. The Nonius Kappa CCD diffractometer, employing graphite-monochromated MoKα radiation (λ = 0.71069Å) generated by a Nonius FR590 generator (54 kV, 23 mA), was used only for unit cell determination. Unit cell refinement and data-reduction were performed using the programs DENZO and SCALEPACK.[14] Intensity data for all the structures reported herein were collected on the Bruker KAPPA APEX II DUO diffractometer. This instrument accommodates both Cu and Mo sources. In all structures reported here, Mo-Kα radiation, generated by a Bruker K780 generator (50 kV, 30 mA), was used. For unit cell refinement and data-reduction, the program SAINT[15] was used and corrections for absorption by the crystals containing sulphur were carried out with the program SADABS.[16] Low temperature collection made use of a Cryostream cooler (Oxford Cryostreams UK) with N_2 gas flowing at a rate of 20 cm^3 min^{-1}. Space group determinations were verified using the program XPREP,[17] which also prepared the SHELXS-97 input files, required for structure solution.

SHELXS-97 and SHELXD

SHELXS-97[18] was employed for the structure solutions of those structures containing smaller molecules, particularly the salts and co-crystals. The program allows the user to solve structures by direct methods or by the Patterson method. In this study only direct methods were employed for the solution of small structures.

SHELXD[18] is used for systems with large numbers of atoms. The program employs a dual-space iteration strategy, sometimes referred to as the "shake-and-bake" method. An alternative to using

this programme for cyclodextrin structures has been to use isomorphous replacement. Here, coordinates of the host are "borrowed" from an existing structure belonging to the same isostructural series.

SHELXH-97

The SHELXH-97[18] software program employs full-matrix least-squares fitting to minimise the value of $\sum w(F_o^2 - F_c^2)^2$. The agreement between the observed and calculated intensities of reflections is expressed as the residual indices R_1 and wR_2 – equations (13) and (14). The default scheme employed for the weighting, w, is given in equation (15), where P is given in equation (16) using a combination of F_o and F_c to reduce statistical bias. The 'Goodness of Fit' parameter S (equation (17)) is also based on F^2 with n the number of reflections and p the total number of refined parameters. The over-determination ratio (n/p) should be ~10 and S is expected to approach unity for well-behaved models.

$$R_1 = \frac{\sum||F_o|-|F_c||}{\sum|F_o|} \tag{13}$$

$$wR_2 = \left(\frac{\sum w(F_o^2-F_c^2)^2}{\sum w(F_o^2)^2}\right)^{\frac{1}{2}} \tag{14}$$

$$w = [\sigma^2(F_o^2) + (aP)^2 + bP]^{-1} \tag{15}$$

$$P = \frac{\max(0,F_o^2)+2F_c^2}{3} \tag{16}$$

$$S = \left(\frac{\sum w(F_o^2-F_c^2)^2}{n-p}\right)^{\frac{1}{2}} \tag{17}$$

Structure solution and refinement procedures for each structure are explained in detail in the relevant chapters.

LAYER[19] generates and displays intensity data as simulated precession photographs, which are useful for determining space group symmetry.

POV-RAY[20] is a raytracer program employed here for image generation based on the crystal structure models. All molecular structural and packing diagrams were producd using POV-RAY. (http://www.povray.org/documentation/view/3.6.0/7/)

LAZY PULVERIX[21] was used to generate calculated PXRD patterns based on atomic fractional coordinates, thermal parameters and space group data from the crystal structure model. These calculated patterns were compared with experimental patterns to identify phases and check homogeneity.

X-Seed[22] served as the graphical interface for SHELXH-97, LAYER, POV-RAY and LAZY PULVERIX.

PLATON[23] was used to determine bond angles, torsion angles and bond lengths as well as the parameters defining non-covalent interactions (e.g. hydrogen bonds, π-π stacking). Standard deviations accompanied all of the calculated parameters.

The Cambridge Structural Database (CSD)[24] was used to access relevant published structures, particularly those that incorporated the drugs that were the subject of this study.

The final crystallographic data files are provided in the following formats:

Extension	Details
.hkl	reflection data
.res	SHELX co-ordinate data
.cif	crystallographic information
.fcf	structure factor tables
.lis	Platon output
.xl	SHELX output
.sup	tabulated supplementary data

Solubility Studies

An excess amount of each co-crystal was weighed into a 20 cm^3 amber screw-cap test tube. The test tubes were filled with MilliQ water, allowing some headspace for agitation, and then sealed. Five replicates of each sample were prepared. Each test tube was fixed to a rotating axis (54 rpm) and the axis submerged into a water bath (37 °C ± 0.5 °C). The test tubes were rotated for 24 h, after which they were kept in the water bath until sampling. Samples were filtered using 0.45 μm filters. The concentrations of the filtered solutions were considered to be representative of the equilibrium solubility. These concentrations were determined by HPLC analysis.

HPLC

A Shimadzu (Kyoto, Japan) UFLC (LC-20AD) chromatographic system was utilised. The system consisted of a SIL-20AC auto-sampler fitted with a sampler cooler, a UV/VIS Photodiode Array detector (SPD-M20A) and a LC-20AD solvent delivery module. The software used was LabSolutions (LC Solutions v1.21 SP1, Shimadzu). The HPLC was equipped with a 150 × 4.6 mm Luna C18 column which contained 5 µm packing. The flow rate was set to 1.0 cm^3 min^{-1}, with the column temperature maintained at 35°C. The injection volume was set to be 1 µL and the wavelength was set to 220 nm.

A mobile phase containing 0.025 M ammonium phosphate buffer and acetonitrile (4:1) was used. The 0.025 M ammonium phosphate buffer (ACE Chemicals, B/N: 12698) was prepared by dissolving, in a volumetric flask, 2.88 g of the salt in distilled water to make an 800 cm^3 solution. The pH was adjusted to 5.0 with 1 M sodium hydroxide and the buffer solution was further diluted to 1000 cm^3.

References

1 Li Z, Yang B-S, Jiang M, Eriksson M, Spinelli E, Yee N, Senanayake C (2009) Org Process Res Dev 13: 1307

2 Milli-Q water, Millipore Corporation, Billerica, Massachusetts, USA

3 Topspin (2008) Version 2.1, Bruker BioSpin GmbH

4 MestRe-C 2.3a (1995-2000) Departimento de Química Orgánica, Universidade de Santiago de Compostela, Spain

5 Job P (1928) Ann Chim Phys 9: 113

6 Gil VMS, Oliveira NC (1990) J Chem Educ 67: 473

7 Floare C, Balibanu F, Bogdan M (2005) Studia UBB, Physica, Special Issue L. 4a: 451

8 Leavitt S, Freire E (2001) Curr Opin Struct Biol 11: 560

9 http://www.microcal.com/technology/itc.asp (accessed on 25 July 2011)

10 Wiseman T, Williston S, Brandts JF, Lin LN (1998) Anal Biochem 179: 131

11 Indyk L, Fisher HF (1998) 295: 350

12 Turnbull WB, Daranas AH (2003) J Am Chem Soc 125: 14859

13 Paratone N oil, Exxon Chemical Co., Texas, USA

14 Otwinowski Z, Minor W (1996) In: Carter CW, Sweet RM (eds) Methods in Enzymology, vol 276. Academic Press, New York, p 307

15 SAINT (2006) Version 7.60a Bruker AXS Inc., Madison, WI, USA

16 Sheldrick GM (2007) SADABS, Version 2.05, University of Göttingen, Germany

17 XPREP, Data Preparation and Reciprocal Space Exploration (1997) Version 5.1, Bruker Analytical X-ray Systems

18 Sheldrick GM (2008) Acta Crystallogr A64: 112

19 Barbour LJ (1999) J Appl Cryst 32: 351

20 POV-RAY for Windows (1996-2002) Version 3.5, The Persistence of Vision Development Team

21 Yvon K, Jeitschko W, Parthé E (1977) J Appl Cryst 46: 371

22 Barbour LJ (2003) J Supramol Chem 1: 189

23 Spek AL (2003) J Appl Cryst 36: 7

24 Cambridge Structural Database and Cambridge Structural Database System (Feb, 2011) Version 5.32, Cambridge Crystallographic Data Centre, University Chemical Laboratory, Cambridge, England

Chapter 3: Nevirapine

Introduction

Nevirapine exists as three polymorphs according to a recent patent.[1] PXRD analysis confirmed that the material with which we had been supplied was the polymorph referred to in the patent as Form II. A number of solvates of nevirapine have been reported, including five containing ethyl acetate, dichloromethane, toluene, water and 1,4-dioxane, as well as a series of linear alcohols.[2,3] An isostructural series was identified, wherein a variety of solvents was included in channels parallel to the *a*-axis. At the time of writing, only very limited discussion of attempted cyclodextrin inclusion of nevirapine existed in literature.[4]

In the single crystal structures of free nevirapine and several solvates, the nevirapine dimer (Figure 1), hydrogen bonded by the common amide-amide synthon is often present. Figure 2 shows the most relevant supramolecular synthons for the present study. These are common and were used as part of the selection criteria for co-formers in the production of nevirapine co-crystals. A variety of carboxylic acids and amides was chosen, among others (e.g. piperazine and saccharin) with less common functional groups.

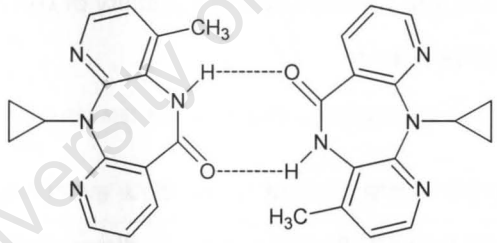

Figure 1: Scheme showing typical nevirapine dimeric hydrogen bonding.

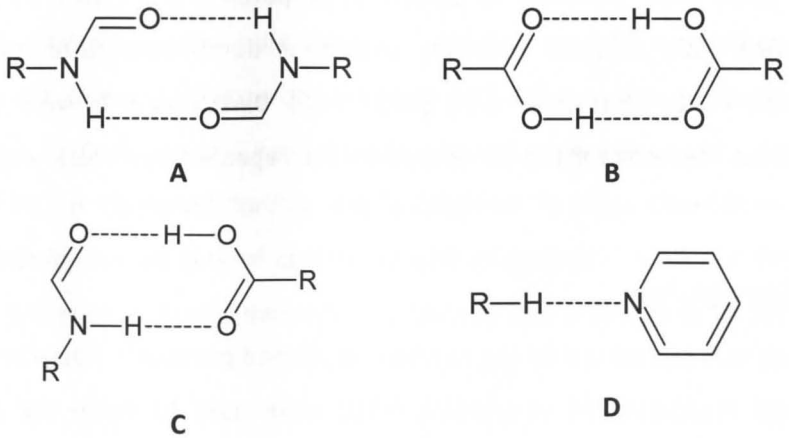

Figure 2: The relevant supramolecular synthons. These are referred to later in the chapter.

Existing co-crystals

Co-crystals of nevirapine have been prepared previously, though quite recently in our laboratory.[5] The first was a 2:1 co-crystal of nevirapine and saccharin and the second a 1:1 nevirapine-*rac*-tartaric acid co-crystal. The co-crystals were prepared by conventional slow evaporation, with single crystal X-ray structures determined for both. Attempts were made at preparing the saccharin co-crystal by co-grinding (dry and liquid-assisted) but these failed.

Thermal stability is an important property that may be manipulated by co-crystal modification. These existing co-crystals were determined to have onsets of melting of 223 °C for nevirapine-saccharin and 228 °C for nevirapine-*rac*-tartaric acid. The first melts at a temperature lower than both component melting points, while the melting point of the second is below that of the API- and above the co-former melting point.

The co-crystals were subjected to dissolution rate testing and solubility testing. Both properties were enhanced with reference to the native API and stoichiometric physical mixtures. The nevirapine-saccharin co-crystal showed a 20 % enhanced dissolution rate with respect to the physical mixture, while the drug equilibrium solubility was 46 times higher in the presence of one molar equivalent of the co-former. The dissolution rate of the nevirapine-*rac*-tartaric acid co-crystal was 10 % greater than that of the physical mixture and the equilibrium solubility of the drug was enhanced 16-fold by two molar equivalents of *rac*-tartaric acid.

Present study

During co-crystallisation attempts in the present study, slow evaporation from solutions of acetone and acetonitrile produced crystals with identical unit cell dimensions to those of the isostructural solvate series,[3] suggesting yet more isostructural solvates but because solvatomorphism was not within the scope of this research, these species were not further studied.

Three novel co-crystals were identified via screening, prepared and analysed by various methods. Crystals were grown from solution and their structures determined using single crystal XRD. Cyclodextrin inclusion was attempted with β-CD, γ-CD, DIMEB and TRIMEB with no success. Reported preparation methods for a β-CD complex were repeated but these yielded only physical mixtures.

Co-crystal Screening

Co-crystal screening was carried out by the methods explained previously (Chapter 2). The results of dry co-grinding and liquid-assisted co-grinding (LAG) were used to guide the slow evaporation experiments. The main solvents employed during liquid-assisted co-grinding were methanol and

chloroform. The screening process is summarised below along with a list of the co-formers that produced hits i.e. potential co-crystals. There were several independent hits; however, the only co-crystals that could be produced reliably were those that incorporated glutaric acid, salicylic acid and maleic acid.

Chloroform produced promising results during LAG experiments, so a number of slow evaporation experiments were carried out using chloroform as solvent. Where the solubility was too high, a non-polar solvent was incorporated into the solution, successfully producing crystals in some cases.

In the interest of achieving a high-throughput rate, the co-precipitation experiments were only analysed where single crystals were achieved. In other words, the variety of other outcomes like mixed powders, fine crystal clusters and gels were not analysed. Indeed this means that some experiments may have yielded co-crystals or a mixture of products that included a co-crystal that may have escaped detection, but to do an extensive analysis for each experiment would have drastically reduced the throughput rate.

The table below contains representative results from the dry co-grinding stage of co-crystal screening. None of the experiments conducted during this stage yielded a pure co-crystal product and there was only one case – that of the experiment with sorbic acid – in which a partial phase transformation occurred.

Table 1: Co-formers and experimental outcomes for the dry co-grinding stage of co-crystal screening of nevirapine; all experiments employed a 1:1 molar ratio.

Co-former	Product
Fumaric acid	Physical mixture
Glutaric acid	Physical mixture
L-Malic acid	Physical mixture
Maleic acid	Physical mixture
Sorbic acid	New phase + physical mixture

Methanol and chloroform were the main solvents utilised for the LAG stage of co-crystal screening, where in general a 1:1 molar mixture of co-former and API was ground in the presence of the solvent for 10 min. Table 2 shows a representative set of experiments with their outcomes. The three co-crystals to be discussed further are highlighted in blue. Chloroform was superior to methanol in facilitating the reaction of nevirapine with glutaric acid, while for the experiment with salicylic acid, the presence of excess nevirapine suggested that a change of molar ratio would be in order.

Table 2: Co-formers, solvents and experimental outcomes for the liquid-assisted co-grinding stage of co-crystal screening of nevirapine; all experiments employed a 1:1 molar ratio.

Co-former	Solvent	Product*
Adipic acid	Chloroform	New phase + adipic acid
Ascorbic acid	Chloroform	Physical mixture
Glutaric acid	Chloroform	Co-crystal
	Methanol	Co-crystal + physical mixture
Maleic acid	Chloroform	Co-crystal
Malonic acid	Chloroform	New phase
Isonicotinamide	Chloroform	Physical mixture
Nicotinamide	Chloroform	Physical mixture
Propionamide	Chloroform	New phase
Salicylic acid	Chloroform	Co-crystal + nevirapine
Sorbic acid	Methanol	New phase + physical mixture
	Chloroform	New phase + sorbic acid
Succinic acid	Chloroform	Physical mixture
Uracil	Chloroform	New phase + physical mixture

*Where the result is "co-crystal" the new phase was fully characterised later. In other cases where the PXRD result suggested potential co-crystallisation, the term "new phase" has been used.

The slow evaporation stage of screening was informed by the results from LAG experiments but a number additional solvents were employed and where warranted, co-formers that had produced no hits during either of the previous stages of screening were still included. Table 3 contains a set of representative results, showing that only pure chloroform and a 50:50 v/v mixture of chloroform and hexane yielded co-crystals.

Table 3: Co-formers, solvents, molar ratio and experimental outcomes for the slow evaporation stage of co-crystal screening of nevirapine.

Co-former	Solvent	Molar ratio	Product
Glutaric acid	Chloroform-hexane*	1:1	Co-crystal
Maleic acid	Chloroform	1:1	Co-crystal
Propionamide	Chloroform	1:1	No crystal
	Chloroform-hexane*	1:1	No crystal
	t-Amyl alcohol	1:1	No crystal
Salicylic acid	Chloroform-hexane*	1:1	Co-crystal
	Chloroform-hexane*	2:1	Co-crystal
Sorbic acid	Methanol	1:1	Solvate
	Chloroform	1:1	No crystal

*50:50 v/v

A summary of the results of co-crystal screening with nevirapine is provided in Table 4. Chloroform was used most extensively during the LAG stage of screening because it produced the best results during the initial experiments. More comprehensive lists of the co-crystal screening experiments are provided in the appendix.

Table 4: Summary of co-crystal screening outcomes.

Method	Co-formers	Hits	Pure co-crystal
Dry co-grinding	6	1	0
Chloroform LAG	30	13	3
Methanol LAG	8	2	0
Slow evaporation	25	3	2

NVPMLE: nevirapine-maleic acid 1:1 co-crystal

The co-crystal was produced by liquid-assisted grinding with chloroform, maintaining dampness with regular solvent addition. During screening, chloroform-assisted grinding yielded powdered co-crystal. In producing a larger amount, some difficulties arose in confirming the purity of the prepared co-crystal. This issue will be discussed further in the section on thermal analysis but here it involved the curious recurring appearance of a small endotherm at the melting point of nevirapine, suggesting some uncomplexed nevirapine in the batch of **NVPMLE**. A larger amount was produced by grinding nevirapine (22 mg, 0.08 mmol) and maleic acid (10 mg, 0.08 mmol) in the presence of a few drops of chloroform for 15 min. The resultant powder dried quickly under ambient conditions.

A few small crystals were produced by dissolving, with constant stirring, equimolar (0.07 mmol) amounts of nevirapine (19 mg) and maleic acid (8 mg) in 3 cm^3 chloroform at 40 °C. The solubility was poor but the suspension was stirred for 30 min and the undissolved material filtered off using a 0.45 μm microfilter. Allowing the solution to evaporate to dryness produced, in addition to powdered material, small irregular plates, one of which was used for single crystal XRD data-collection. This method was not as reliable as the aforementioned liquid-assisted grinding method.

Identification

The initial screening experiment involved grinding a small equimolar mixture of nevirapine and maleic acid for 10 min adding chloroform dropwise to keep the powder moist. After drying at room temperature, which required only a few minutes the sample was analysed by PXRD. The traces in Figure 3 show that the product of the grinding experiment is clearly a new phase. Its PXRD trace does not resemble either of the component traces. There are coincident peaks, so it was not clear whether or not there were indeed traces of either component remaining in the sample and indeed whether the 1:1 stoichiometry of the initial mixture was representative of the final, potential co-crystal.

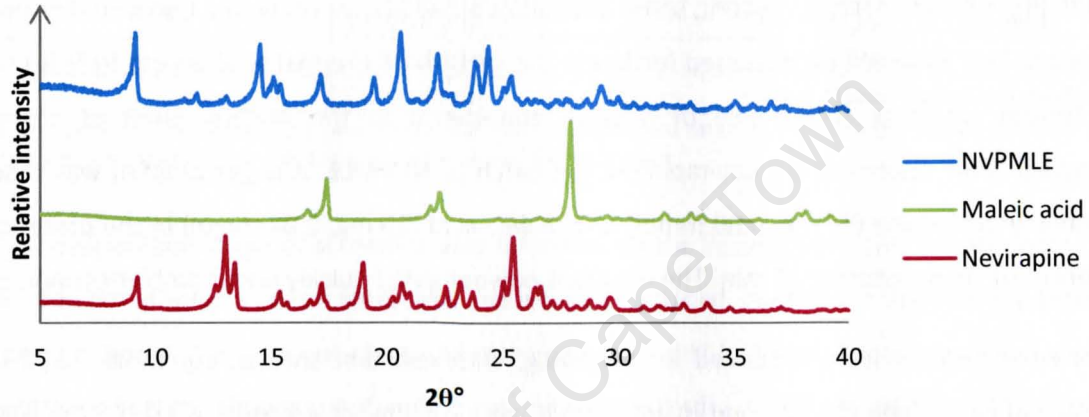

Figure 3: PXRD trace of NVPMLE compared with the traces of free nevirapine and free maleic acid.

Thermal analysis

Prior to thermal analysis it was important to consider the melting points of the free components. DSC analysis (Figure 4) confirmed that the pure nevirapine melted at 244-249 °C and the pure maleic acid at 139-145 °C. The broad peak that follows the maleic acid melt is attributed to decomposition.[6]

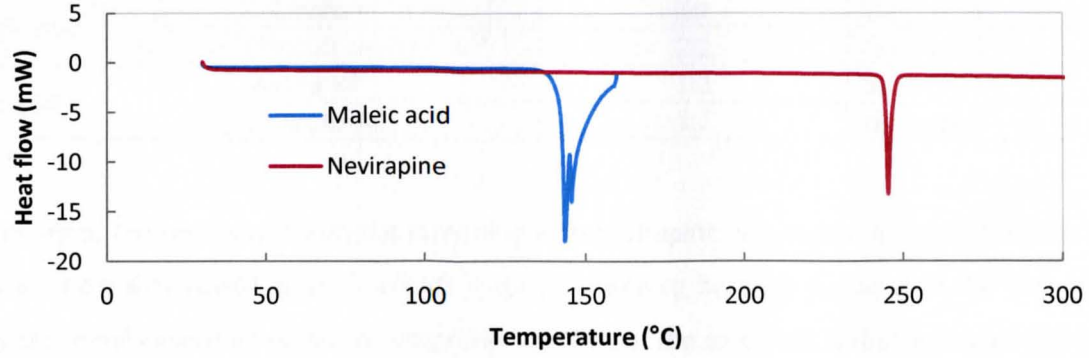

Figure 4: DSC showing nevirapine and maleic acid melting.

HSM

HSM analysis of **NVPMLE** was conducted with powdered material as larger crystals were not readily available. The sample was heated at a rate of 10 K min^{-1} The representative HSM photographs in Figure 5 show what appears as partial melting that begins at 202 °C and a final complete melt that occurs at 220-245 °C. At no point between 202 and 210 °C does the entire sample become liquid, so either the sample consists of two separate phases or the sample is initially one phase but the recrystallisation of the higher-melting species appears to be concurrent with the melt of the co-crystal.

Incidentally, the second melt concurred with the melting point of free nevirapine, suggesting that the sample contained a new phase (potential co-crystal) and some excess nevirapine.

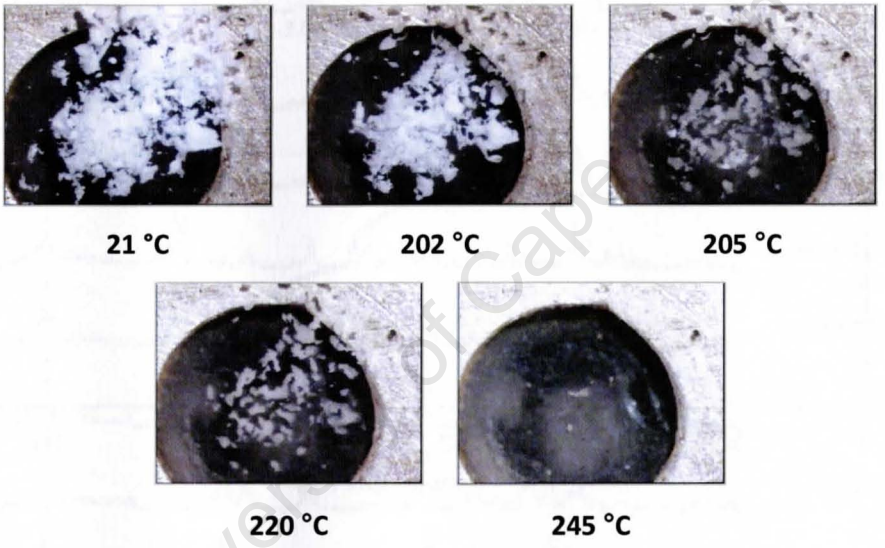

Figure 5: Representative HSM photographs of NVPMLE.

DSC and TGA

Analysis using DSC (Figure 6) provided confirmation of co-crystal formation in that the accurately determined melting point (onset 185 °C) of the new phase is unique – it differs significantly from the melting points of each of the components. Curiously, there was a reproducible endotherm at the melting point of nevirapine despite accurate weighing of the 1:1 starting materials. The possibility that nevirapine was in slight excess was ruled out because initially PXRD analysis (refer again to Figure 3) and later single crystal XRD investigation had suggested 1:1 stoichiometry.

TGA (Figure 7) also showed the decomposition of maleic acid at the co-crystal melting point. The experimentally determined mass loss of 32.6 ± 1.0 % (n = 2) is in reasonable agreement with the

30.4 % expected for 1:1 co-crystal stoichiometry. There was no apparent mass loss at lower temperatures, confirming the evidence from HSM that no included solvent was present.

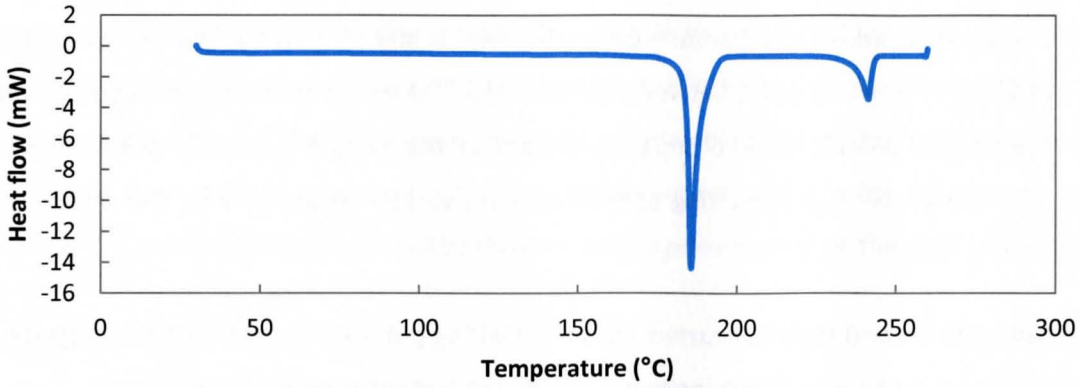

Figure 6: DSC trace for NVPMLE.

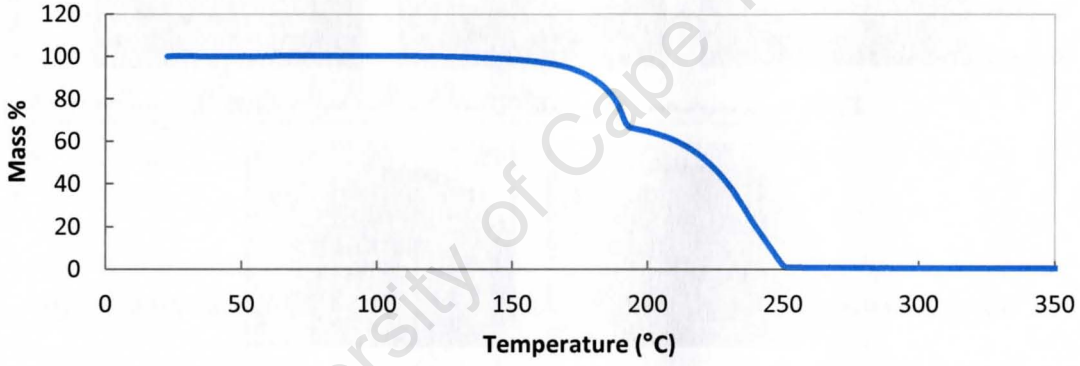

Figure 7: TGA trace for NVPMLE.

It was necessary to conduct temperature-controlled PXRD to investigate the repeated occurrence in DSC traces of the endotherm in the nevirapine melting range. This would provide some identification of the solid phase responsible for the endotherm.

Temperature-controlled PXRD

The recurrence of a melt peak that indicated the presence of free nevirapine was puzzling since there were no signs of this phase in the room temperature PXRD trace. This phenomenon persisted even when the preparative procedure for **NVPMLE** was repeated using an analytical balance (with a precision of 0.01 mg) to weigh the starting reagents. An investigation carried out by temperature-controlled PXRD analysis revealed the simultaneous recrystallisation of free nevirapine *during* the melting of the co-crystal. In Figure 8 it can be seen that at 160 °C, some peaks of **NVPMLE** are

diminished and new peaks are appearing. At 200 °C the PXRD trace of **NVPMLE** is identical to that of pure nevirapine at room temperature. It is apparent now that as the co-crystal melts, the nevirapine molecules are free to hydrogen bond in their original arrangement (as in the bulk), while the maleic acid molecules remain molten and are subsequently vaporised. Because both the co-crystal melt and nevirapine recrystallisation occur simultaneously in the range 170-200 °C and the enthalpy of recrystallisation is much smaller than the enthalpy of melting, no recrystallisation exotherm is evident in this region of the DSC trace and the later melt at 240 °C can be attributed to free nevirapine that had been liberated from the co-crystal phase.

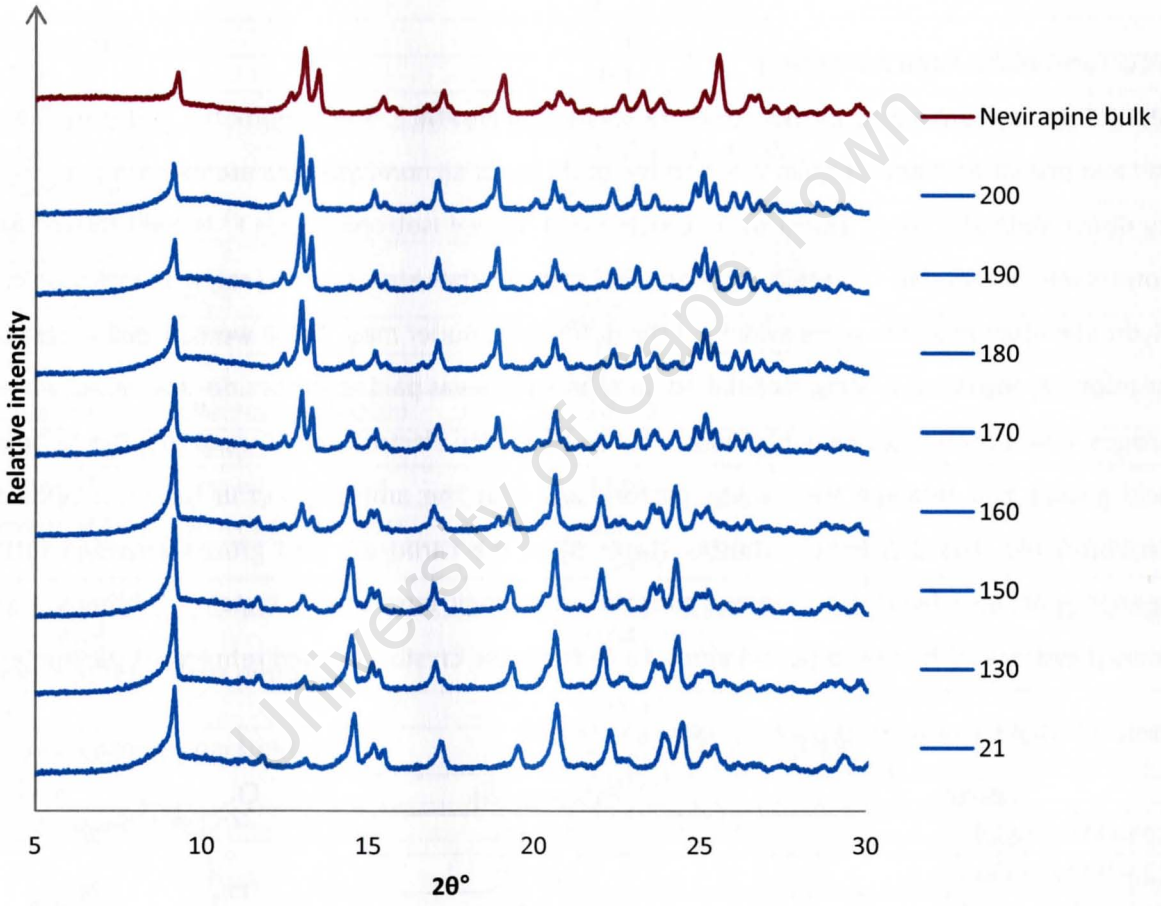

Figure 8: PXRD traces of NVPMLE recorded in the range 21-220 °C and compared with the trace for the nevirapine bulk recorded at 21 °C.

Single crystal X-ray analysis

Data-collection and space group determination

The chloroform solution produced only a few irregular plate-like crystals when allowed to evaporate to dryness. The best of these was selected for single crystal XRD analysis. The single crystal diffraction data for this crystal, as for all subsequent crystals in this chapter, were collected on a Bruker APEX DUO II four-circle diffractometer. The unit cell parameters, crystal system and space group $P2_1/n$ (alternative setting of $P2_1/c$) were determined from the X-ray diffraction data. The space group was confirmed using the program LAYER,[7] which provided evidence of the following reflection conditions: hkl: $none$; $h0l$: $h + l = 2n$; $0k0$: $k = 2n$.

Structure solution and refinement

SHELXS-97[8] was employed for the structure solution of **NVPMLE.** The asymmetric unit contains one API and one co-former molecule, of which the positions of all non-hydrogen atoms were determined by direct methods. These atoms were assigned and refined isotropically on F^2 in SHELXH-97.[8] After confirming acceptable isotropic temperature factors, the atoms were refined anisotropically. Hydrogen atom positions were evident in the difference Fourier map. These were placed in idealised positions by means of a riding model. Particular attention was paid to the amide- and carboxylic acid groups. It was confirmed, unambiguously, via the difference electron density map that the carboxylic acid groups had retained their acidic protons and that the amide group in turn had remained unprotonated. The C-O bond distances (Table 5) of the carboxylic acid groups provided further confirmation. Each hydrogen atom was assigned an isotropic temperature factor of 1.2 times (1.5 for methyl hydrogens) that of its parent atom. Table 6 lists the crystal data and refinement parameters.

Table 5: C-O bond distances for the NVPMLE maleic acid molecule

Bond	Distance (Å)
C23-O21 (single)	1.326 (2)
C23-O22 (double)	1.223 (2)
C26-O27 (double)	1.207 (2)
C26-O28 (single)	1.329 (2)

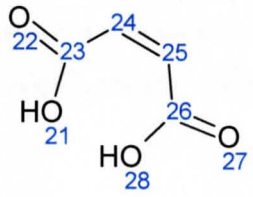

Table 6: Data-collection and refinement parameters for NVPMLE.

Formula unit	$(C_{15}H_{14}N_4O)\ (C_4H_4O_4)$
Formula mass (g mol^{-1})	382.37
Crystal system	Monoclinic
Space group	$P2_1/n$
a (Å)	7.4001(5)
b (Å)	10.4599(7)
c (Å)	23.256(2)
α (°)	90
β (°)	98.968(1)
γ (°)	90
Volume ($Å^3$)	1778.1(2)
Z	4
$Density_{calc}$ (g cm^{-3})	1.428
F(000)	800
μ(MoKα) (mm^{-1})	0.106
Crystal size (mm^3)	0.12 x 0.11 x 0.03
Temperature (K)	100(2)
Range scanned θ (°)	2.14-26.46
Index ranges	h: -9, 9 ; k: -13, 13; l:-29, 29
ϕ and ω scan angle (°)	0.5
Total number of frames	1454
Dx (mm)	40
Total number of reflections collected	18372
Number of unique reflections	3653
Number of reflections with $I > 2\sigma(I)$	2773
Number of least-squares parameters	257
R_{int}	0.0477
S	1.032
R_1 ($I > 2\sigma(I)$)	0.0413
Number of reflections omitted	2
wR_2	0.0942
Weighting scheme parameters	a = 0.0424, b = 1.0228
$(\Delta/\sigma)_{mean}$	< 0.001
Δρ excursions (e $Å^{-3}$)	0.462, -0.233

Molecular structure

The asymmetric unit (ASU), illustrated in Figure 9, consists of one nevirapine molecule and one maleic acid molecule, hydrogen bonded by the expected amide-carboxylic acid synthon **C** (Figure 2). The maleic acid molecule does not display intramolecular hydrogen bonding and the nevirapine molecule is not engaged in the self-association common in the set of known nevirapine-containing crystal structures (see Figure 1).

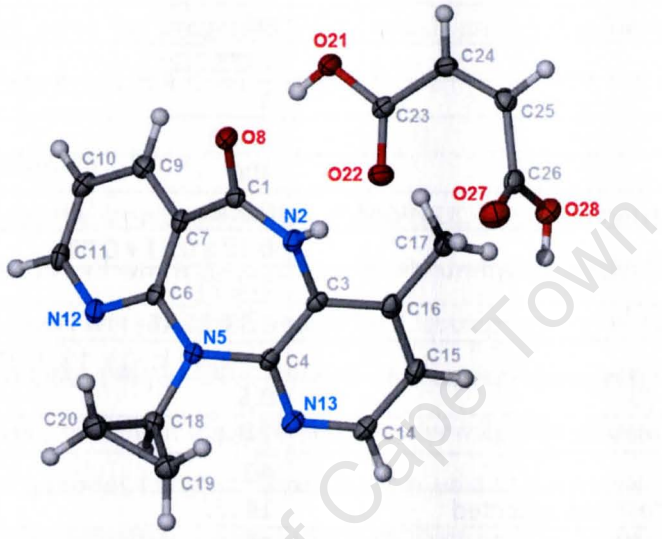

Figure 9: ASU of NVPMLE. Thermal ellipsoids are drawn at the 50 % probability level, while hydrogen atoms are presented as spheres of arbitrary radii.

Hydrogen bonding

The hydrogen bonding motif links one nevirapine molecule and one maleic acid molecule in a cyclic arrangement as represented in Figure 10. At the centre of this motif is a crystallographic centre of inversion. The amide-carboxylic acid synthon associates the two molecules of the asymmetric unit, while the pyridine nitrogen N13 is engaged in N-H···O hydrogen bonding with a carboxylic acid group of the inversion-related maleic acid molecule. Full details of these hydrogen bonds as well as those of several C-H···O and C-H···N hydrogen bonds are listed in Table 7.

There is also π-π stacking in the *a*-direction between the C3→C16 pyridine rings of inversion-related nevirapine molecules, as illustrated in Figure 11. The bonding distances of 3.875(1) and 3.671(1) Å between centroids in this case are typical of strong π-π interactions. The shorter of these, where the lateral shift is 1.60 Å, corresponds to the case where the molecules have concave surfaces facing each other.

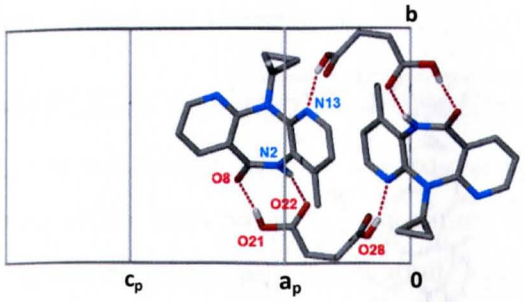

Figure 10: View normal to the plane (1 0 -4). Only the most relevant hydrogen atoms are shown.

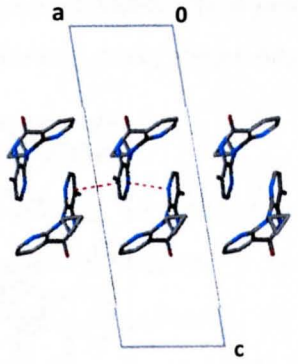

Figure 11: π-stacking in the *a*-direction (N13 ring). View down the *b*-axis with hydrogen atoms omitted.

Table 7: Hydrogen bond parameters for NVPMLE.

D-H···A	D-H (Å)	H···A (Å)	D···A (Å)	D-H···A (°)	Symmetry code
N2-H2···O22	0.88	1.97	2.821(2)	162	x, y, z
O21-H21···O8	0.84	1.77	2.607(2)	174	x, y, z
O28-H28···N13	0.84	1.94	2.748(2)	162	1-x, 1-y, -z
C11-H11···O8	0.95	2.58	3.345(2)	138	5/2-x, 1/2+y, 1/2-z
C14-H14···O22	0.95	2.56	3.376(2)	144	1-x, 1-y, -z
C17-H17B···O27	0.98	2.43	3.343(3)	154	1+x, y, z
C24-H24···O8	0.95	2.39	3.302(2)	162	3/2-x, -1/2+y, 1/2-z
C25-H25···N12	0.95	2.44	3.341(2)	158	-1+x, -1+y, z

Molecular geometry

The so-called 'butterfly angle' is the angle between the mean planes of the two nevirapine pyridine rings. It is taken as a measure of the extent to which the molecule as a whole is curved and is closely related to the puckering of the central 7-membered ring. In **NVPMLE**, the butterfly angle is 55.9(1)°. The amide group is almost planar with a C3-N2-C1-C7 torsion angle of 13.2(3)°.

The maleic acid molecule has its carboxylic acid groups oriented orthogonally with respect to one another, which is not a general occurrence for this co-former. Of the many known structures containing this molecule only one displays the same geometry for maleic acid.[9] The angle between mean planes drawn through each carboxylic acid group (O21-C23-O22 and O27-C26-O28) is 89.6(2)°. The relevant torsion angles are 0.0(3)° for O22-C23-C24-C25 and 89.4(3)° for O27-C26-C25-C24.

Crystal packing

The hydrogen bonding motif (Figure 10) is present at the *ac* and *ab* faces of the unit cell. Figure 12 shows the four motifs at the edges of the unit cell and illustrates how these pack in parallel rows

along the *b*-axis. The diagram also shows clearly the two-fold screw axis that runs parallel to the *b*-axis, while the n-glide plane is perpendicular to it.

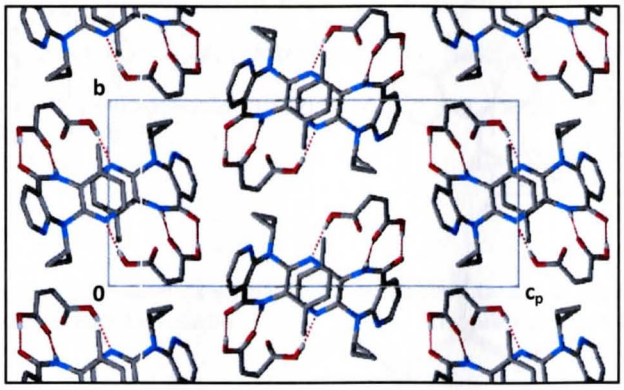

Figure 12: View along the *a*-axis of NVPMLE.

Comparative PXRD

In Figure 13 the experimental pattern for **NVPMLE** and calculated pattern from single crystal X-ray diffraction data are compared. Note that the single crystal used to generate the calculated pattern was grown by slow evaporation, while the experimental pattern was recorded using a sample prepared by liquid-assisted grinding. This is because the slow evaporation method yielded the co-crystal along with other phases, while the liquid-assisted grinding method produced the *pure* co-crystal. Nevertheless, the similarity of these PXRD patterns provides assurance that the crystal selected for single crystal XRD data-collection was representative of the material used for other methods of analysis.

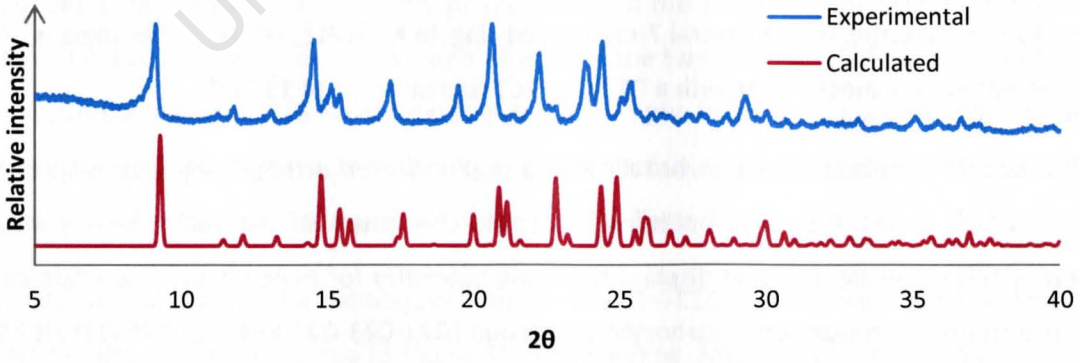

Figure 13: Comparison of experimental and calculated PXRD traces for NVPMLE.

With regard to the above PXRD comparison, the sample used for single-crystal X-ray data collection was at a lower temperature (100 K) than the sample used to record the experimental PXRD trace (room temperature). Thus, peaks corresponding to the latter sample are displaced to slightly higher

2θ values. This applies to analogous figures elsewhere in this thesis, since all single crystal X-ray data were collected at 100 or 173 K.

NVPGLT: nevirapine-glutaric acid 1:1 co-crystal

It was possible to prepare the co-crystal **NVPGLT** by liquid-assisted co-grinding and by slow evaporation from solution. Preparation by liquid-assisted co-grinding required a few drops of chloroform, which was replenished regularly to maintain a moist consistency. An equimolar (0.075 mmol) mixture of nevirapine (20 mg) and glutaric acid (10 mg) was co-ground for 20 min and allowed to dry.

Single crystals were prepared by combining 0.11 mmol each of nevirapine (30 mg) and glutaric acid (15 mg) by grinding with a few drops of chloroform for 2 min. The powder was dissolved in a 50:50 v/v chloroform:hexane mixture at 40°C by stirring for 30 min. This solution was filtered while hot and allowed to cool spontaneously at room temperature. Crystals formed after four days of slow evaporation. Subsequently, it was determined that pre-grinding is unnecessary. The co-precipitation method essentially requires equimolar amounts of nevirapine and glutaric acid dissolved by stirring at approximately 40 °C in a 50:50 v/v chloroform:hexane solution and allowed to evaporate slowly.

Identification

Initial screening by 10 min of liquid-assisted co-grinding with chloroform produced a hit for nevirapine-glutaric acid in 1:1 molar ratio. The PXRD comparison in Figure 14 shows the unique trace of the co-ground product as compared with traces for the pure starting reagents. There are no peaks in the product trace that suggest excess amounts of either component.

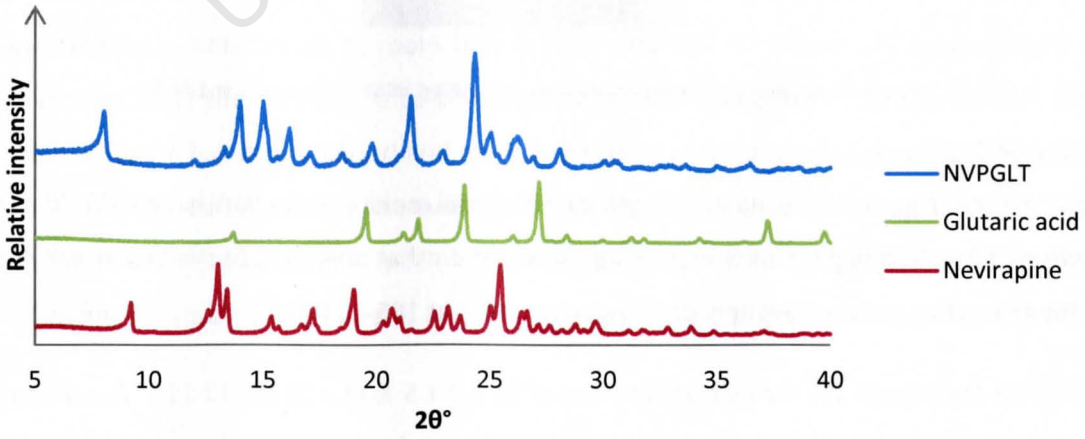

Figure 14: PXRD traces comparing NVPGLT with the starting components nevirapine and glutaric acid.

Thermal analysis

The starting materials were analysed by DSC to determine experimental melting points for comparison with thermal data for the co-crystal. The melting point of nevirapine was as for the previous example and glutaric acid melting occurred at 96-101 °C.

HSM

The hot stage temperature was ramped from room temperature at a rate of 10 K min^{-1}. The HSM photographs in Figure 15 revealed an onset of melting at 145 °C. There is sign of partial melting and immediately thereafter, the crystal becomes opaque. A second, final melting step revealed smaller crystallites that were not visible due to the crystal opacity. The recrystallisation of these after the initial melt was only observable upon magnification (Figure 16).

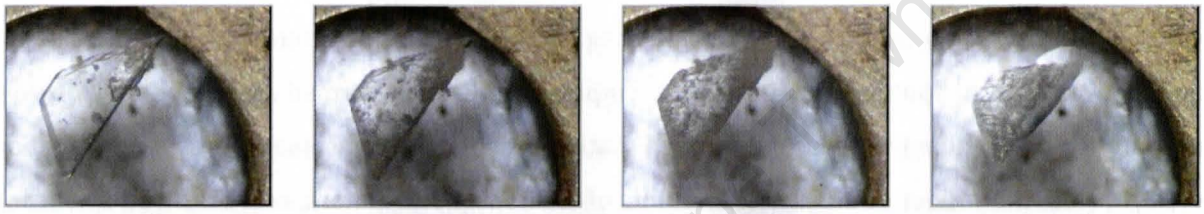

Figure 15: Representative HSM photographs of NVPGLT.

Figure 16: Formation of new crystallites. Magnified HSM photograph at 148 °C.

TGA and DSC

Analysis by DSC (Figure 17) revealed the unique co-crystal melting point with onset 137 °C and peak minimum at 140 °C along with immediate recrystallisation that is evident in the DSC trace. A second very broad melting point of the new phase was apparent at 185-220 °C.

The TGA profile (Figure 18) shows a weight loss of 31.2 ± 1.5 % (n = 2) at 110-195 °C, corresponding to the degradation of glutaric acid for a 1:1 co-crystal (theoretical value: 33.2 %), while the remaining mass (nevirapine) degrades directly thereafter. There is clearly no included solvent because there is no mass loss apparent at lower temperatures.

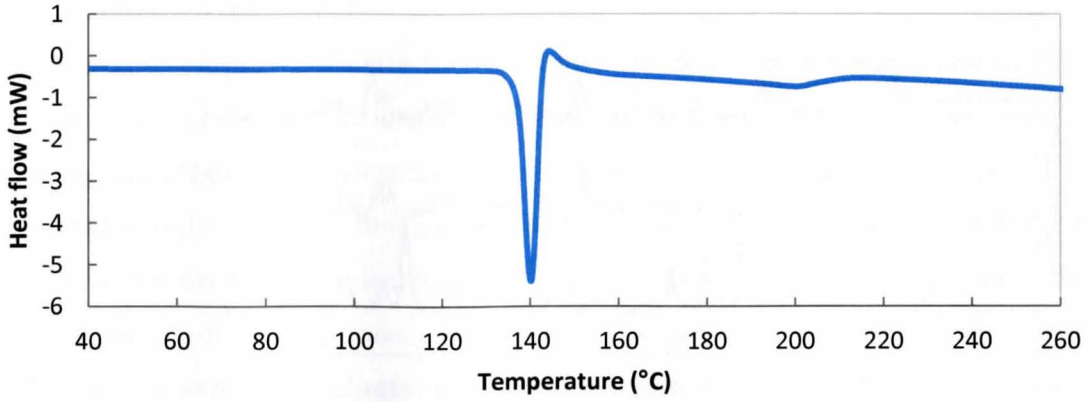

Figure 17: DSC trace for NVPGLT.

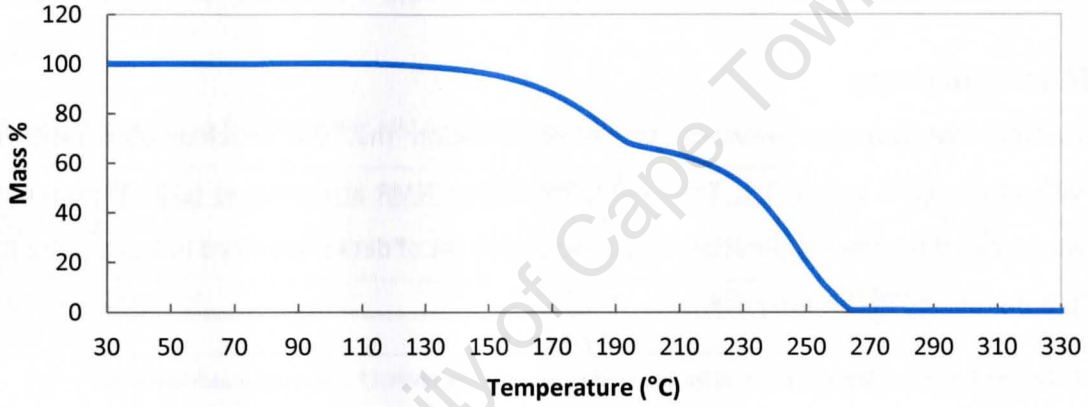

Figure 18: TGA trace for NVPGLT.

Temperature-controlled PXRD

PXRD patterns were determined at room temperature and 150 °C (Figure 19) to determine what phase is present after the melt of the co-crystal at 137 °C and subsequent recrystallisation. Clearly, at 150 °C nevirapine has recrystallised and there is no trace of solid co-crystal or pure glutaric acid. So, as in the case of **NVPMLE**, after the melting of the co-crystal and near-simultaneous degradation of the co-former, nevirapine with its much higher melting point is free to recrystallise as the original, thermodynamically stable phase used as a starting reagent for the preparation of the co-crystal.

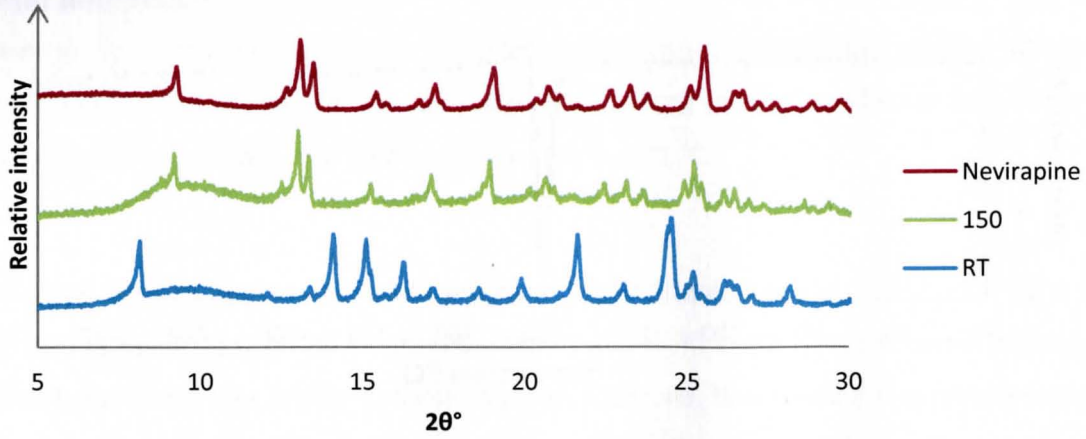

Figure 19: PXRD patterns of NVPGLT recorded at room temperature and 150 °C. The uppermost pattern was derived from our nevirapine bulk, the starting material from which the co-crystal was prepared.

NMR spectroscopy

Proton NMR spectroscopy provided further confirmation that the stoichiometric ratio in the **NVPGLT** co-crystal is indeed 1:1. The sample for proton NMR analysis was taken from a batch of crystals prepared by slow evaporation. A representative set of data is provided in Table 8 and further details are provided in the appendix.

Table 8: Selected proton NMR signals used for the confirmation of the NVPGLT co-crystal stoichiometry.

Assignment	δ (ppm)	Integral	Normalised integral
C<u>H</u> (aromatic, nevirapine)	8.57	1.0*	1
C<u>H</u> (aromatic, nevirapine)	8.23	1.1	1
C<u>H</u>$_2$ (glutaric acid)	2.01	2.2	1

*Reference integral

Single crystal X-ray analysis

Data-collection and space group determination

One of the thick plate-like crystals was selected from the chloroform-hexane mother liquor. Data-collection was carried out on the same diffractometer as for **NVPMLE**. The unit cell parameters, crystal system and space group were determined from diffraction data. Only inversion symmetry was evident and there were no systematic absences. Comparing the experimental $|E^2 - 1|$ value of 0.982 with the theoretical value of 0.968 for centrosymmetric structures confirmed that the space group is $P\bar{1}$.

Structure solution and refinement

SHELXS-978 was employed for the structure solution of **NVPGLT**. The asymmetric unit contains one API and one co-former molecule, of which the positions of all non-hydrogen atoms were determined by direct methods. These atoms were assigned and refined isotropically on F^2 in SHELXH-97.8 After confirming acceptable isotropic temperature factors, the atoms were refined anisotropically. Hydrogen atom positions were evident in the difference Fourier map. These were placed in idealised positions by means of a riding model. Again, particular attention was paid to the amide and carboxylic acid groups to check whether or not proton transfer had taken place. The carboxylic acid protons were clearly evident in the difference map, and the C-O bond distances (Table 9) confirmed that these groups had not been deprotonated. The amide, in turn, did not show evidence of ionisation. Each hydrogen atom was assigned an isotropic temperature factor of 1.2 times (1.5 for methyl hydrogens) that of its parent atom. The data-collection and refinement parameters are listed in Table 10.

Table 9: C-O bond distances for the glutaric acid molecule of NVPGLT.

Bond	Distance (Å)
C23-O21 (single)	1.323 (2)
C23-O22 (double)	1.206 (2)
C27-O28 (double)	1.216 (2)
C27-O29 (single)	1.318 (2)

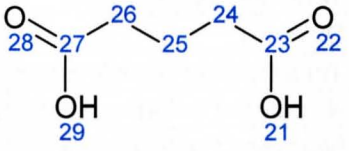

Table 10: Data-collection and refinement parameters for NVPGLT.

Formula unit	$(C_{15}H_{14}N_4O)$ $(C_5H_8O_4)$
Formula mass (g mol^{-1})	398.42
Crystal system	Triclinic
Space group	$P\bar{1}$
a (Å)	7.363(4)
b (Å)	12.292(6)
c (Å)	12.305(6)
α (°)	118.571(8)
β (°)	90.144(9)
γ (°)	98.023(8)
Volume ($Å^3$)	965.5(8)
Z	2
$Density_{calc}$ (g cm^{-3})	1.370
F(000)	420
μ(MoKα) (mm^{-1})	0.100
Crystal size (mm^3)	0.28 > 0.26 > 0.21
Temperature (K)	100(2)
Range scanned θ (°)	1.89-26.37
Index ranges	h: -9, 9; k: -15, 15; l: -15, 15
ϕ and ω scan angle (°)	0.5
Total number of frames	3777
Dx (mm)	50
Total number of reflections collected	22292
Number of unique reflections	3906
Number of reflections with $I > 2\sigma(I)$	2999
Number of least-squares parameters	266
R_{int}	0.0477
S	1.032
R_1 ($I > 2\sigma(I)$)	0.0334
Number of reflections omitted	9
wR_2	0.0798
Weighting scheme parameters	a = 0.0365, b = 0.3527
$(\Delta/\sigma)_{mean}$	< 0.001
Δρ excursions (e $Å^{-3}$)	0.264, -0.204

Molecular structure

The asymmetric unit (Figure 20) comprises one nevirapine molecule and one molecule of glutaric acid. As with the previous co-crystal, which also incorporated a dicarboxylic acid, the API and co-former hydrogen bond via the predicted supramolecular synthon **C** (see Figure 2). It is significant that here too, the predicted interaction between drug and partner molecule has replaced the generally robust amide-amide self-association of nevirapine.

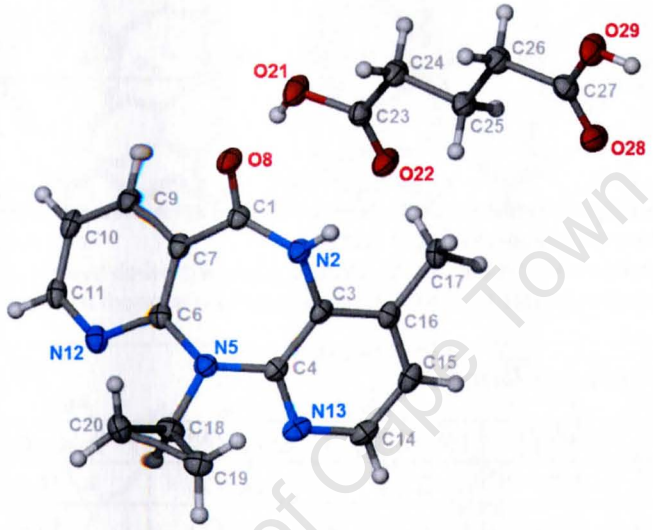

Figure 20: Asymmetric unit of NVPGLT. Thermal ellipsoids are drawn at the 50 % probability level, while hydrogen atoms are presented as spheres of arbitrary radii.

Hydrogen bonding

A representative hydrogen bonding motif is shown in Figure 21. It comprises two nevirapine molecules and two glutaric acid molecules hydrogen bonded in the sequence NVP-GLT-GLT-NVP. Synthon **C** (see Figure 2) links nevirapine molecules with glutaric acid and synthon **B** links the glutaric acid molecules in the middle, across a crystallographic centre of inversion. These four-molecule discrete units display typical hydrogen bonding interactions. It is significant that the amide-amide interaction of the nevirapine dimer is superseded by hydrogen bonding with the carboxylic acid. The pyridine nitrogens N12 and N13 do not participate in strong hydrogen bonding, in contrast to what occurs in **NVPMLE**, where these atoms play an important directing role.

In Figure 22 it can be seen that there are π-stacking interactions along the *a*-axis and as with **NVPMLE**, the nevirapine molecules are positioned so that they interlock. The butterfly shape of nevirapine is essential, so the molecules are forced to fit by being offset. The successive π-stacked molecules are related by centres of inversion in the *ab*-plane.

Hydrogen bond parameters are provided in Table 11. The longest hydrogen bond is a C-H···N bond of distance 3.5 Å and the strongest interactions are, as expected, N-H···O and O-H···O hydrogen bonds.

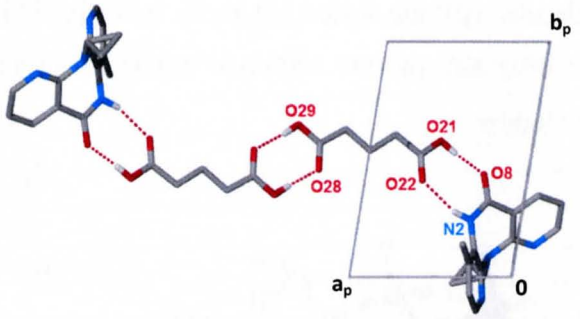

Figure 21: The primary hydrogen bonding motif, as viewed down the *c*-axis. Only the most relevant hydrogen atoms are shown.

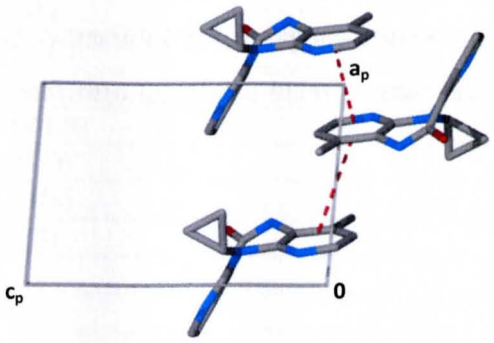

Figure 22: A view down the *b*-axis of π-stacking of the N13 ring in the *a*-direction.

Table 11: Hydrogen bond parameters for NVPGLT.

D-H···A	D-H (Å)	H···A (Å)	D···A (Å)	D-H···A (°)	Symmetry code
N2-H2···O22	0.88	2.19	3.047(2)	163	x, y, z
O21-H21···O8	0.84	1.76	2.597(2)	173	x, y, z
O29-H29···O28	0.84	1.82	2.654(2)	176	3-x, 1-y, -z
C10-H10···O8	0.95	2.58	3.103(3)	115	-x, 1-y, 1-z
C14-H14···O22	0.95	2.56	3.353(3)	141	1-x, -y, -z
C20-H20A···N12	0.99	2.55	3.475(3)	156	-x, -y, 1-z

Molecular geometry

The butterfly angle in **NVPGLT** is 55.9(1)° and the torsion angle for the amide group is 6.7(2)°. The glutaric acid molecules adopt a nearly planar conformation with a crystallographic centre of inversion at the centre of the carboxylic acid-carboxylic acid hydrogen bond.

Crystal Packing

Nevirapine molecules pack in rows along the *a*-axis, assisted by the π-π stacking interactions that were discussed earlier and illustrated in Figure 22. In Figure 23 it can be seen that the glutaric acid molecules, which are dimerically hydrogen bonded, are also arranged in rows parallel to the *a*-axis. The rows of nevirapine molecules interact with these adjacent rows of glutaric acid dimers by hydrogen bonding that is staggered in the *c*-direction (Figure 24). Rows of the four-molecule hydrogen bonding motifs are related by translation along the line [0 1 1].

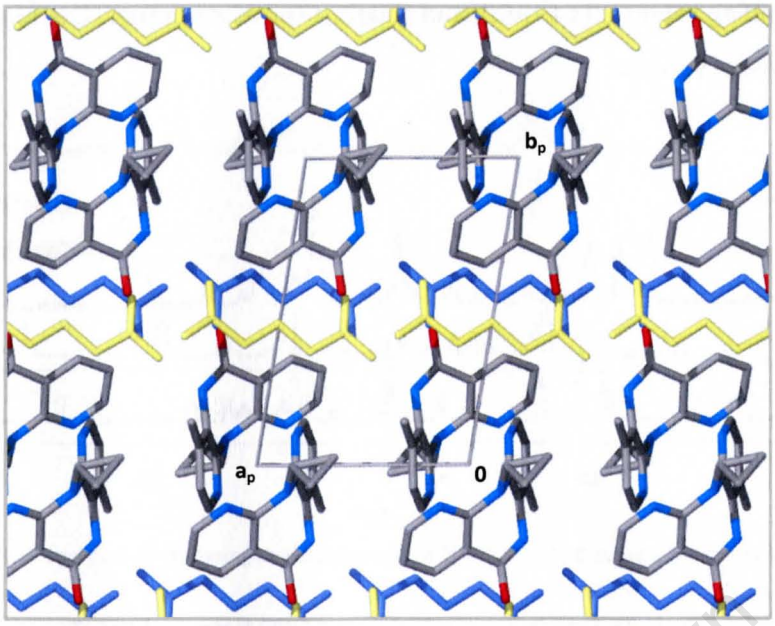

Figure 23: Packing of NVPGLT, viewed down the *c*-axis. Glutaric acid molecules are shown in different colours to distinguish between those in the foreground (yellow) and background (purple).

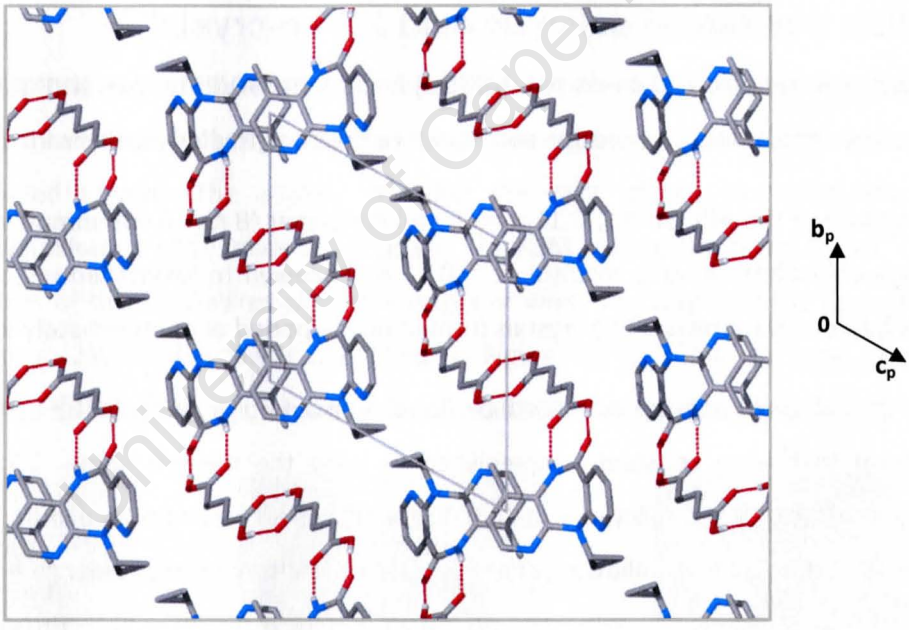

Figure 24: Packing of NVPGLT viewed down the a-axis.

Comparative PXRD

PXRD was used to identify the new form as a potential co-crystal during an early stage of screening. SCXRD confirmed that this form was indeed a co-crystal and comparison of the computed pattern from SCXRD data with the experimental pattern from liquid-assisted co-grinding confirmed that the forms produced by both preparation methods are identical. The PXRD comparison is presented in Figure 25. It is very important that the two methods produce the same phase because it means that

liquid-assisted grinding represents a quick and simple alternative preparative method that requires only a small amount of solvent.

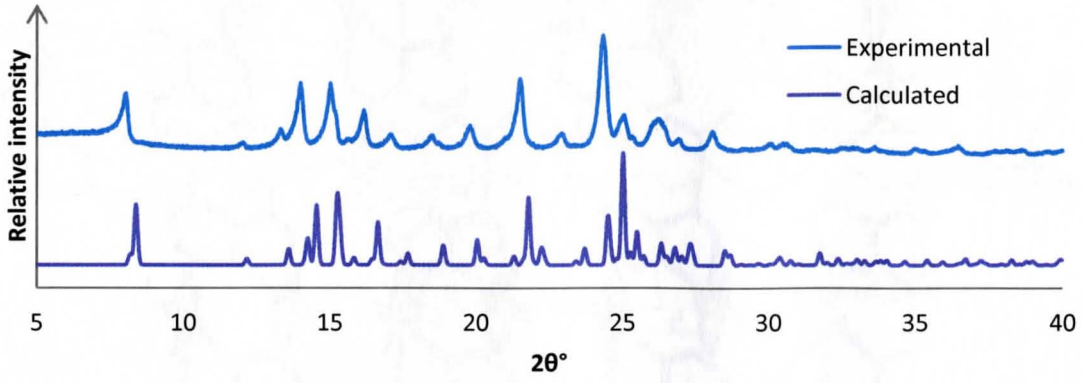

Figure 25: Experimental and calculated PXRD traces for NVPGLT.

NVPSLI: nevirapine-salicylic acid 2:1 co-crystal

The nevirapine-salicylic acid co-crystal (**NVPSLI**) is similar to **NVPMLE** and **NVPGLT** in that it may be prepared by simple slow evaporation and liquid-assisted co-grinding methods involving chloroform.

A 2:1 mixture of the API (30 mg, 0.11 mmol) and co-former (8 mg, 0.056 mmol) were dissolved in a 50:50 v/v chloroform-hexane mixture at ~40 °C and allowed to spontaneously cool to yield single crystals by slow evaporation. The crystals formed over a period of approximately four days.

The co-crystal could also be produced by liquid-assisted co-grinding (LAG) using a few drops of chloroform that were constantly replenished to keep the mixture damp. 20 mg of nevirapine (0.075 mmol) and 5 mg salicylic acid (0.038 mmol) were combined. Kneading for 10 min in the presence of chloroform and allowing drying resulted in the co-crystal powder.

Identification

The **NVPSLI** co-crystal was identified during screening by chloroform LAG. The initial screening experiment involved grinding a 1:1 mixture of 10 mg nevirapine and a one molar equivalent of salicylic acid in the presence of chloroform. The result was a new phase with excess nevirapine identified in the PXRD pattern. The experiment was repeated with a 2:1 mixture, the result of which is illustrated in Figure 26. Clearly, the product of LAG represents a unique phase and contains little or no unreacted nevirapine or salicylic acid.

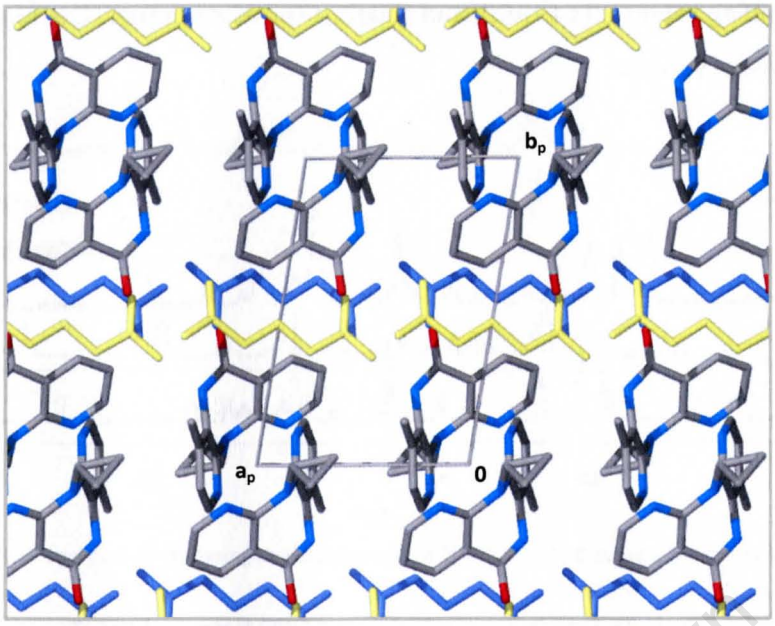

Figure 23: Packing of NVPGLT, viewed down the *c*-axis. Glutaric acid molecules are shown in different colours to distinguish between those in the foreground (yellow) and background (purple).

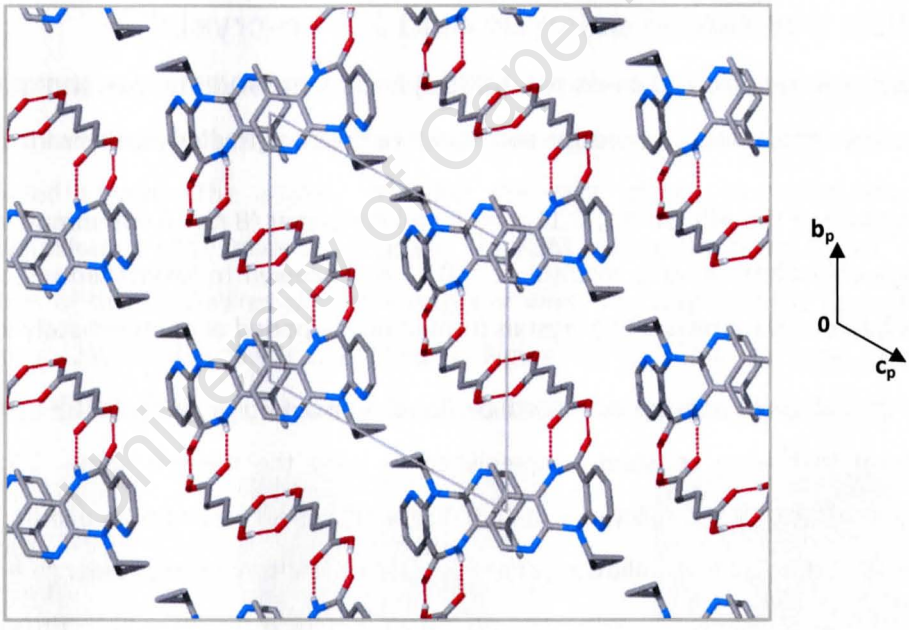

Figure 24: Packing of NVPGLT viewed down the a-axis.

Comparative PXRD

PXRD was used to identify the new form as a potential co-crystal during an early stage of screening. SCXRD confirmed that this form was indeed a co-crystal and comparison of the computed pattern from SCXRD data with the experimental pattern from liquid-assisted co-grinding confirmed that the forms produced by both preparation methods are identical. The PXRD comparison is presented in Figure 25. It is very important that the two methods produce the same phase because it means that

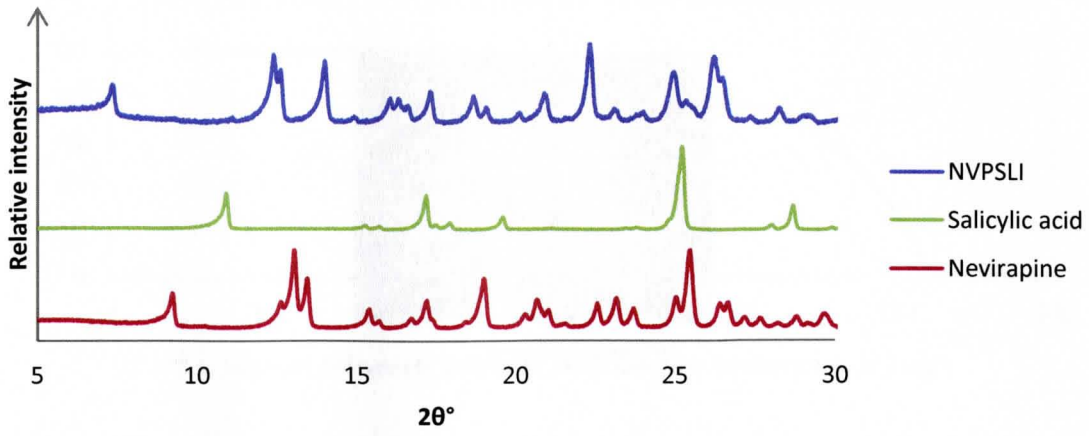

Figure 26: PXRD comparison showing the uniqueness of NVPSLI as compared with its starting reagents.

Thermal analysis

HSM

The HSM photographs in Figure 27, recorded periodically while the temperature was ramped at a rate of 10 K min^{-1}, showed no signs of bubbling at low temperature that would have suggested the presence of included solvent. The analysis revealed the melt of the co-crystal with nearly simultaneous recrystallisation of an unidentified phase. The HSM photograph taken at 225 °C clearly shows the formation of tiny crystallites along the edges of what was originally the co-crystal. The photograph taken at 230 °C has been magnified in Figure 28 to show the new crystallites. Temperature-controlled PXRD was again conducted to identify the recrystallised phase.

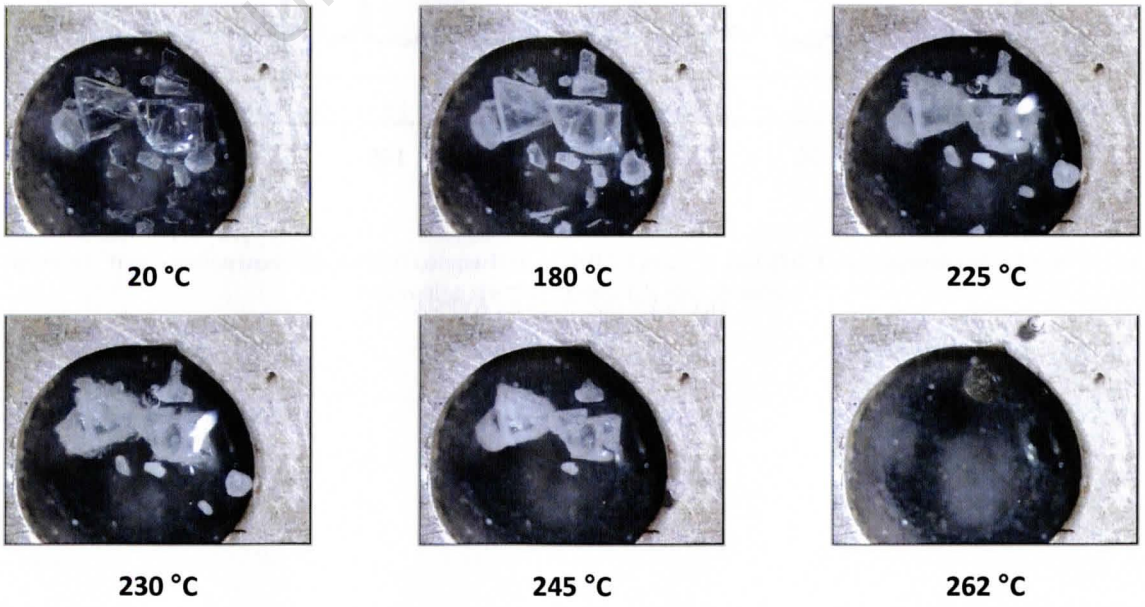

Figure 27: Representative HSM photographs of NVPSLI.

Figure 28: Formation of new crystallites. Magnified photograph recorded at 230 °C.

DSC and TGA

The DSC trace of **NVPSLI** (Figure 29) shows that the melting onset occurs at 203 °C with peak maximum at 204 °C. Thereafter, there is an erratic endotherm in the temperature range 215-240 °C.

The TGA analysis represented in Figure 30 confirms that no included solvent is present in **NVPSLI**, as was determined by hot stage microscopy. The thermogram further confirms the stoichiometry of the co-crystal – the mass loss of 20.55 ± 0.05 % (n = 2) corresponds with the loss of one molar equivalent of salicylic acid in a co-crystal of stoichiometric ratio 2:1. This experimental value is precisely the same as the expected result.

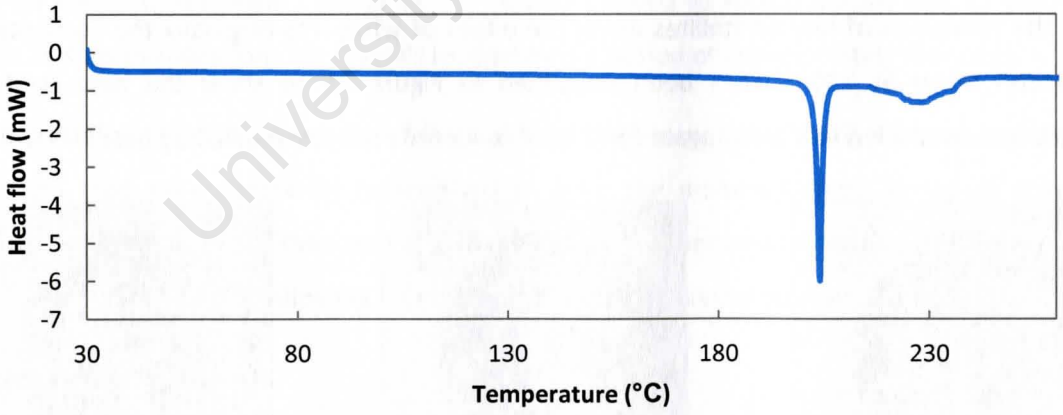

Figure 29: DSC trace for NVPSLI.

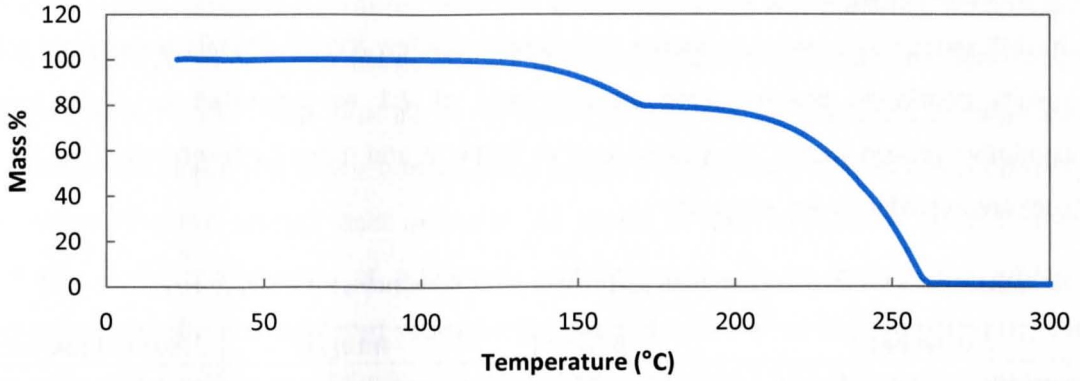

Figure 30: TGA trace for NVPSLI.

Temperature-controlled PXRD

A PXRD pattern collected at 210 °C (Figure 31) reveals that **NVPSLI** transforms to pure nevirapine in the same phase as the bulk material that was used as one of the starting reagents. Upon melting of the co-crystal, the nevirapine molecules are free to self-associate and reform the original thermodynamically stable phase, as occurs for both of the co-crystals previously discussed here.

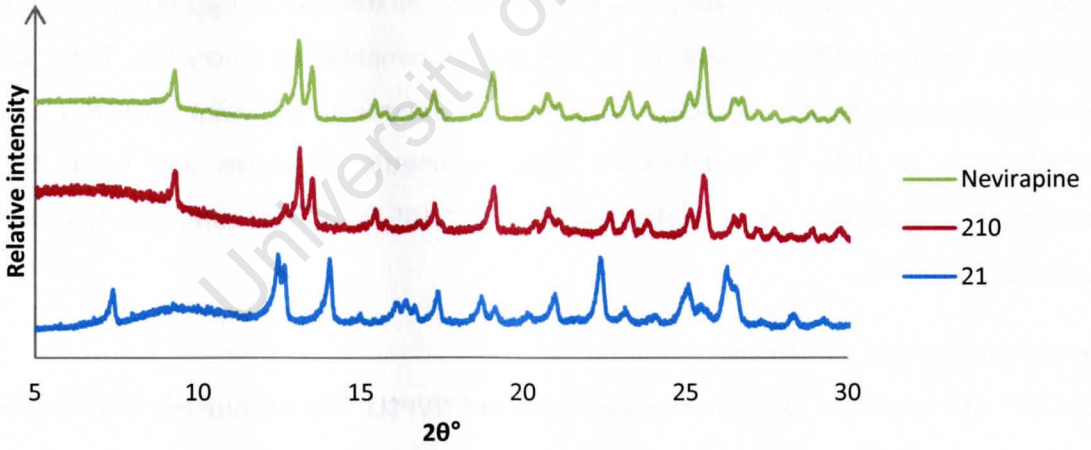

Figure 31: Temperature-controlled PXRD comparison of NVPSLI at 21 °C and 210 °C. An experimental trace for the nevirapine starting material is also shown.

NMR spectroscopy

Proton NMR spectroscopy was conducted on a sample of a few NVPSLI crystals grown from solution. The results confirmed the expected stoichiometry of 2:1 as suggested by PXRD evidence. Representative proton signals are summarised in Table 12 and more comprehensive details of the spectrum are available in the appendix.

Table 12: Selected signals from the proton NMR spectrum of NVPSLI confirming 2:1 stoichiometry.

Assignment	δ (ppm)	Integral	Normalised integral
CH (aromatic, nevirapine)	8.49	2.1	2
CH (aromatic, salicylic acid)	7.88	1.0*	1
CH (aromatic, salicylic acid)	7.42	1.0	1
CH (cyclopropyl, nevirapine)	3.71	2.1	2

*Reference integral

Single crystal X-ray analysis

Data-collection and space group determination

The thick plates were removed from their chloroform/hexane mother liquor onto a microscope slide. One was selected, placed in Paratone oil and the intensity data collected. The unit cell parameters, crystal system and space group were determined from the diffraction data, which were collected on the same diffractometer as for the two aforementioned co-crystals. There were no systematic absences and the diffraction data showed evidence of inversion symmetry only. The expected value of $|E^2 - 1|$ is 0.968 for centrosymmetric structures and 0.736 for non-centrosymmetric structures. The experimental value of 1.195 for **NVPSLI** confirmed that the space group is not $P1$ but $P\bar{1}$.

Structure solution and refinement

SHELXS-97[8] was employed for the structure solution of **NVPSLI**. The asymmetric unit contains two API molecules and one co-former molecule. The positions of all non-hydrogen atoms of the nevirapine molecules were determined by direct methods. These atoms were assigned and refined isotropically on F^2 using SHELXH-97.[8] After confirming acceptable isotropic temperature factors, the atoms were refined anisotropically. All hydrogen atom positions were evident in the difference Fourier map and the fact that no additional peaks appeared near the amide groups suggested that neither of these had been protonated, evidence that no acid-base reaction had taken place. All of the hydrogens were placed in idealised positions by means of a riding model. Each hydrogen atom was assigned an isotropic temperature factor of 1.2 times (1.5 for methyl hydrogens) that of its parent atom.

The salicylic acid molecule is disordered over two orientations and was modelled accordingly. The major component **A** has a refined site occupancy of 0.739(3). Component **A** was modelled according to the difference Fourier map with all of the non-hydrogen atoms appearing as large electron density difference peaks. The atoms bonded with realistic interatomic distances and proposed bond angles, resembling the salicylic acid molecule. All atoms of this component were first refined isotropically. Upon confirmation of acceptable isotropic temperature factors, the atoms were refined anisotropically and exhibited refined U_{iso}-values of 0.031 $Å^2$ or less. Importantly, the C-O bond lengths of the carboxylic acid differed significantly (1.238 and 1.329 Å) and the hydrogen atom of this group was identified in the electron density difference map, which confirmed that no proton transfer had occurred. In the case of component **B** (s.o.f. = 0.261(3)), all of the atoms were modelled isotropically. The substituents on the ring were allowed to refine freely but the benzene ring geometry was poor and required an AFIX 66 command, which was justified because the ring is required to be planar and have standard bond distances and angles, as exhibited by component **A**. All hydrogen atoms of both disordered components were placed using the same method as used for the nevirapine molecules. The high residual electron density difference peak of 1.30 e $Å^{-3}$ is located at the centre of the disordered salicylic acid molecules. It is an artefact that appears because of the large concentration of electron density represented by the benzene ring, which is disordered in the vicinity of that peak position.

Table 13: Data-collection and refinement parameters for NVPSLI

Formula unit	$2(C_{15}H_{14}N_4O)\ (C_7H_6O_3)$
Formula mass (g mol^{-1})	670.72
Crystal system	Triclinic
Space group	$P\bar{1}$
a (Å)	11.155(1)
b (Å)	12.619(2)
c (Å)	13.464(2)
α (°)	113.374(2)
β (°)	99.133(2)
γ (°)	107.324(2)
Volume ($Å^3$)	1575.8(3)
Z	2
$Density_{calc}$ (g cm^{-3})	1.414
F(000)	704
μ(MoKα) (mm^{-1})	0.097
Crystal size (mm^3)	0.35 x 0.14 x 0.05
Temperature (K)	100(2)
Range scanned θ (°)	2.91-28.14
Index ranges	h: -14, 14; k: -16, 16; l: -17, 17
ϕ and ω scan angle (°)	0.5
Total number of frames	2030
Dx (mm)	40
Total number of reflections collected	23138
Number of unique reflections	7552
Number of reflections with $I > 2\sigma(I)$	5331
Number of least-squares parameters	474
R_{int}	0.0296
S	1.042
R_1 ($I > 2\sigma(I)$)	0.0664
Number of reflections omitted	23
wR_2	0.1851
Weighting scheme parameters	a = 0.1248, b = 0.6966
(Δ/σ)mean	< 0.001
Δρ excursions (e $Å^{-3}$)	1.298, -0.432

Molecular structure

The asymmetric unit consists of two crystallographically independent nevirapine molecules, denoted **A** and **B** for convenience, along with one salicylic acid molecule, which is disordered over two orientations. As can be seen in Figure 33 the two positions of the salicylic acid molecule are related by a pseudo twofold axis of rotation that runs through the nearly coincident atoms C21A and C21B.

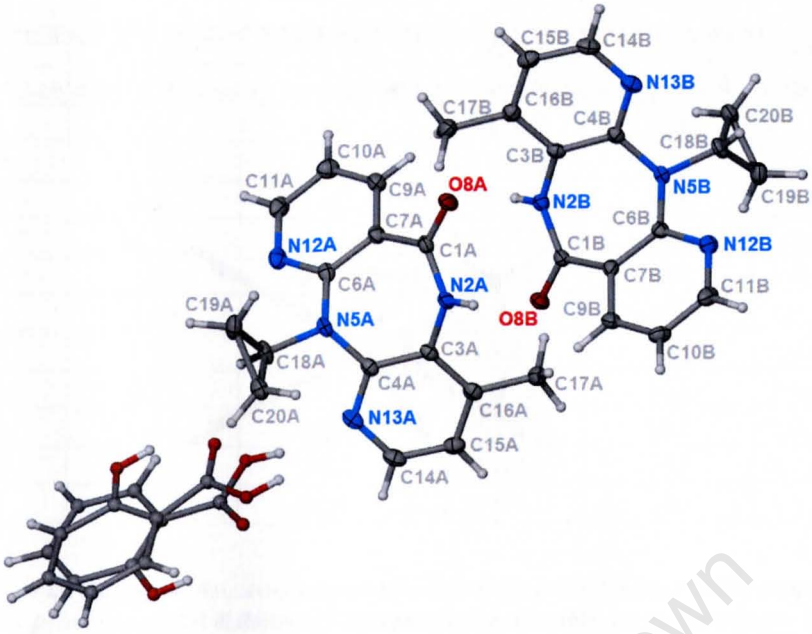

Figure 32: Asymmetric unit of NVPSLI. Thermal ellipsoids are drawn at the 50 % probability level, while hydrogen atoms and disordered guest atoms are shown as spheres of arbitrary radii.

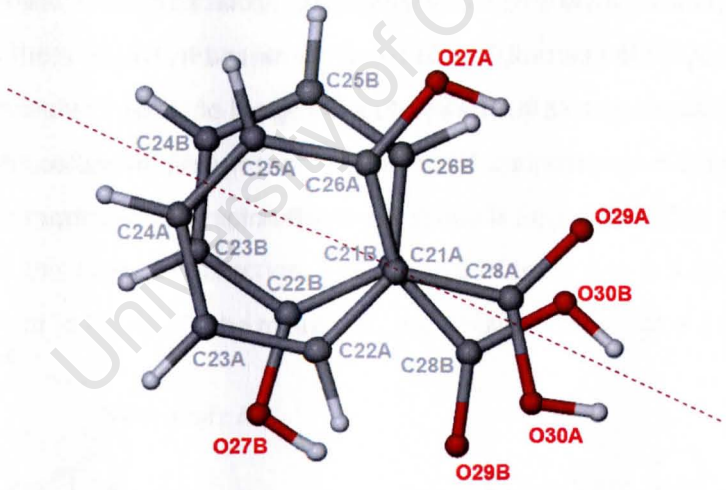

Figure 33: Disordered salicylic acid molecule. The dashed line represents a pseudo twofold rotation axis.

An overlay of the two nevirapine molecules of the asymmetric unit in Figure 34 shows that the molecules are puckered in opposite directions. The slight kink in the cyclopropyl substituent of nevirapine molecule **A** is confirmation that the two are not quite mirror images of one another.

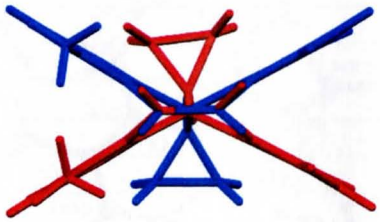

Figure 34: Overlay of the two nevirapine molecules of the asymmetric unit. Atoms C1, N2 and N5 are overlayed. Molecule A is displayed in red and B in blue.

Hydrogen bonding

Note the hydrogen bonding within the asymmetric unit that is illustrated in Figure 35. The salicylic acid molecule is internally hydrogen bonded – the hydroxyl group donating towards the carbonyl oxygen of the carboxylic acid. An example of the supramolecular synthon **D** (see Figure 2) is observable - the hydroxyl of the carboxylic acid in turn donates a hydrogen atom to the pyridine nitrogen N13 of nevirapine molecule **A**. The pyridine nitrogens of nevirapine molecule **B** are not hydrogen bonded. The two crystallographically independent nevirapine molecules are hydrogen bonded via synthon **A** to form the typical dimer. Parameters for the most important hydrogen bonds are provided in Table 14.

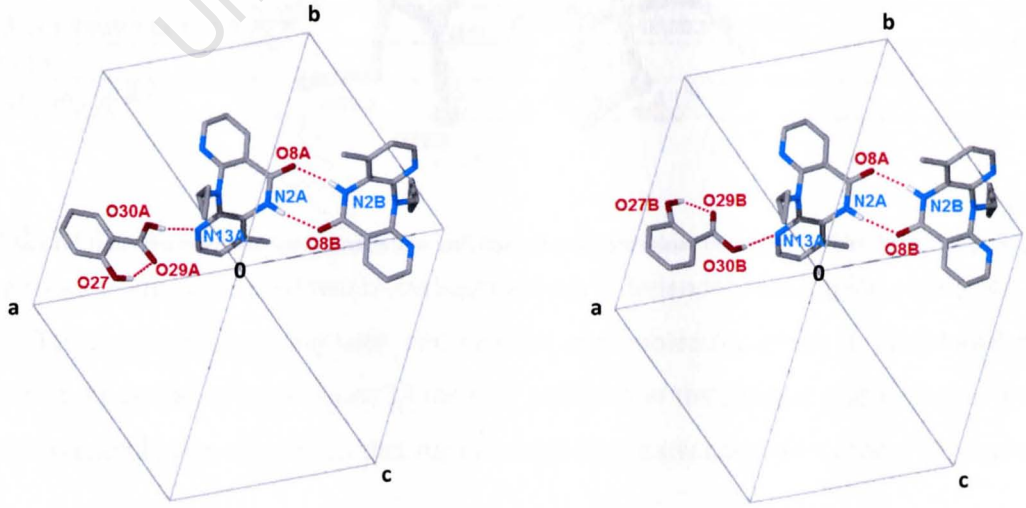

Figure 35: The primary hydrogen bonding motif. The disordered component A is shown on the left and B on the right.

Table 14: Hydrogen bond parameters for NVPSLI.

D-H···A	D-H (Å)	H···A (Å)	D···A (Å)	D-H···A (°)	Symmetry code
N2A-H2A···O8B	0.88	2.05	2.924(2)	170	x,y,z
N2B-H2B···O8A	0.88	2.05	2.921(2)	169	x,y,z
O27A-H27A···O29A	0.84	1.84	2.579(3)	145	x,y,z
O30A-H30A···N13A	0.84	1.86	2.688(3)	168	x,y,z
C14A-H14A···O8B	0.95	2.57	3.433(3)	152	1-x,1-y,1-z
C17A-H17A···O29A	0.98	2.55	3.212(3)	125	1-x,1-y,1-z
C17B-H17F···O8A	0.98	2.60	3.448(3)	145	x,y,z
C18A-H18A···O30A	1.00	2.48	3.160(3)	125	x,y,z
C19B-H19C···O27A	0.99	2.50	3.416(3)	155	1-x,1-y,1-z
O30B-H30B···N13A	0.84	2.12	2.941(16)	167	x,y,z
O27B-H27B···O29B	0.84	1.84	2.461(18)	142	x,y,z
C19A-H19B···O27B	0.99	2.53	3.378(11)	143	1-x,1-y,1-z

Multiple π-π stacking interactions further stabilise the structure. Note in Figure 36 that infinite chains of nevirapine molecules – as seen in both **NVPMLE** and **NVPGLT** – are shown on the right, while on the left is a discrete three-membered motif comprising one salicylic acid molecule 'sandwiched' between the N12 pyridine rings of two unrelated nevirapine molecules. For the interaction represented on the left, only the major component of the co-former is shown. For this major orientation, the distance between the centroids of the nevirapine molecule **A** and the co-former is shorter than the nevirapine **B**-salicylic acid distance. The average of these is 3.82 Å. For the minor position of the co-former, the nevirapine **A**-salicylic acid distance is still the shorter, while the distance between centroids of nevirapine **B** and the salicylic acid molecule is slightly greater than 4 Å, which is large for this type of interaction. The average of these two is 3.83 Å. With regard to the π-stacking on the right in Figure 36, the mean distance between centroids is 3.63 Å.

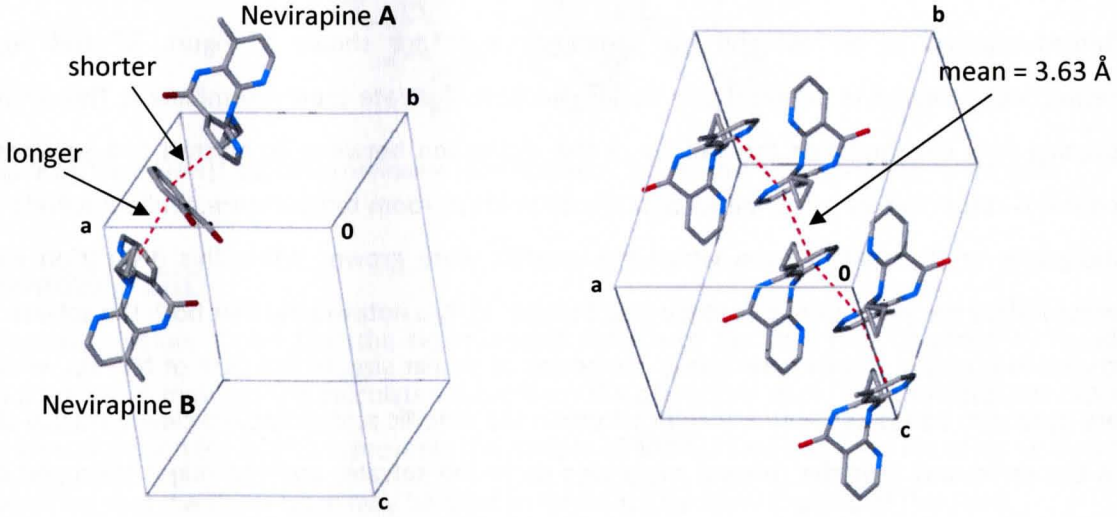

Figure 36: π-π stacking in NVPSLI. View of the *ac*-plane on the left (with only the major disordered component shown) and the *ab*-plane on the right.

Table 15: Parameters for π-stacking interactions in NVPSLI. C_g is the centre of gravity (centroid) of a given ring.

Ring #	Atoms	Interaction*	$C_gI\cdots C_gJ$	$C_gI \perp$ distance*	$C_gJ \perp$ distance	Symmetry code
1	C6A→N12A	$C_g1\cdots C_g5$	3.655(2)	3.654	3.579	1-x, 1-y, -z
2	C4A→N13A	$C_g1\cdots C_g6$	3.546(6)	3.531	3.324	1-x, 1-y, -z
3	C6B→N12B	$C_g2\cdots C_g2$	3.909(1)	3.448	3.448	1-x, 1-y, 1-z
4	C4BN→13B	$C_g2\cdots C_g4$	3.630(1)	3.507	3.536	1+x, y, z
5	C21A→C26A	$C_g3\cdots C_g5$	3.988(2)	3.578	3.479	1-x, 1-y, 1-z
6	C21B→C26B	$C_g3\cdots C_g6$	4.116(6)	3.692	3.738	1-x, 1-y, 1-z
		$C_g4\cdots C_g2$	3.630(1)	3.536	3.507	-1+x, y, z
		$C_g4\cdots C_g4$	3.712(1)	3.393	3.393	-x, 2-y, 1-z
		$C_g5\cdots C_g1$	3.655(2)	3.579	3.654	1-x, 1-y, -z
		$C_g5\cdots C_g3$	3.988(2)	3.479	3.578	1-x, 1-y, 1-z
		$C_g6\cdots C_g1$	3.546(6)	3.324	3.531	1-x, 1-y, -z
		$C_g6\cdots C_g3$	4.116(6)	3.738	3.692	1-x, 1-y, 1-z

*The length of the line drawn between C_gI and C_gJ normal to the mean plane of the atoms of ring I

Molecular geometry

The nevirapine butterfly angle is 58.2(1)° for molecule **A** and 59.4(1)° for **B**. The amide torsion angles (C3-N2-C1-C7) are 5.2(3)° and -7.3(3)° for **A** and **B** respectively. Given that the nevirapine dimer is present in **NVPSLI** but not in **NVPMLE** or **NVPGLT**, it is interesting to note that in this case the butterfly angles for both independent nevirapine molecules are greater than for the previous two co-crystals. The amide groups here are similarly planar, so it is the amide function of **NVPMLE** that is the most twisted with a torsion angle of 13.2°.

Crystal packing

NVPSLI displays a crystal packing arrangement that is similar to the one exhibited by the toluene solvate of nevirapine reported by Caira *et al.*[2] and referred to briefly at the start of this chapter. Representations of **NVPSLI** and the toluene solvate are shown in Figure 37 and Figure 38 respectively, viewed in different orientations to best illustrate their resemblance. This similarity in packing calls into question the validity of the distinction between co-crystals and solvates. A co-crystal is comprised of components that are all solids at room temperature, while a solvate contain molecules of the *solvent* from which the crystals were grown. While this distinction has been accepted for the purpose of this study (see Chapter 1), it is noteworthy that both the solvate and co-crystal in question incorporate 'guest' molecules of similar size. In the case of **NVPSLI**, while there are hydrogen bonds between API and co-former, the salicylic acid molecules clearly occupy channels in the same way that the toluene molecules do in the solvate, and the major hydrogen bonding

interactions are 'host-host' interactions forming the typical nevirapine amide-amide dimer. It is difficult to accept that the two species belong to different classes.

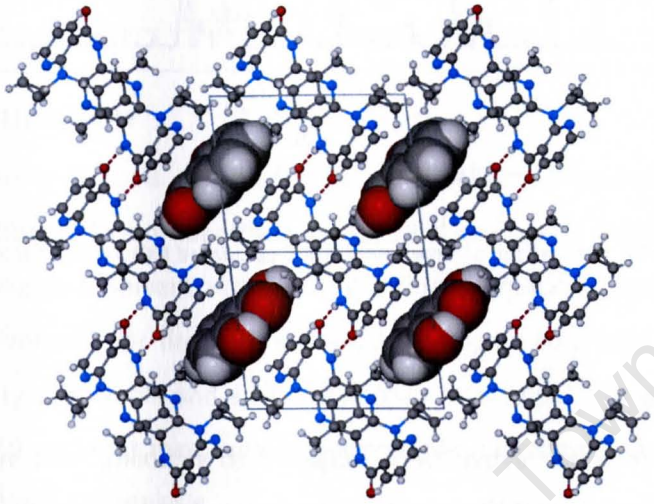

Figure 37: View down the line [1 1 0] of the NVPSLI co-crystal. Only the major disordered component is shown.

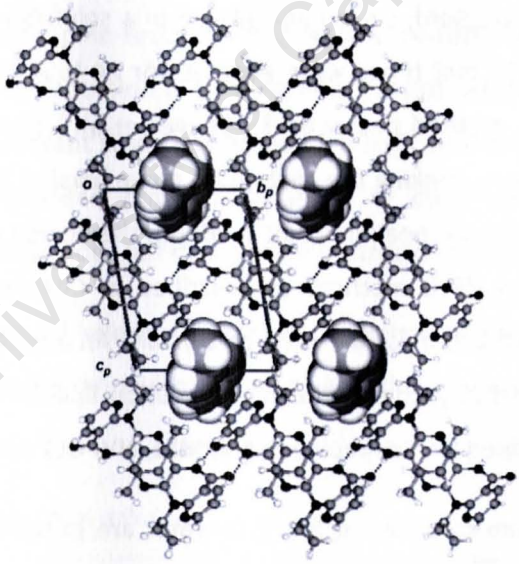

Figure 38: View down [1 0 0] of the nevirapine toluene solvate. This image is reproduced from reference 2.

Comparative PXRD

The comparison below shows that the experimental pattern of the co-crystal obtained by liquid-assisted co-grinding matches the calculated trace from the diffraction data. This provides assurance that the crystal chosen for SCXRD represents the sample of **NVPSLI** that was used for other analyses. It also confirms that the PXRD trace may be used as reference for identification of this form.

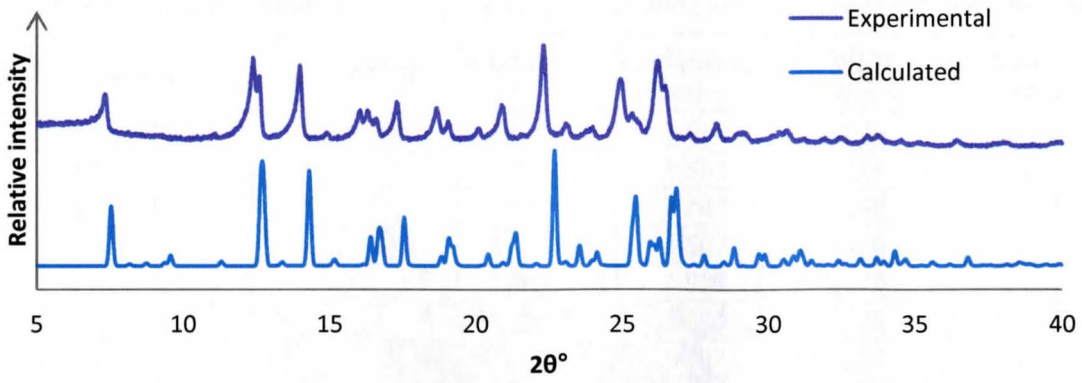

Figure 39: Comparison of experimental and calculated PXRD traces for NVPSLI.

Solubility Studies

The three co-crystals described above were subjected to solubility tests in the hope that one or more would show enhanced solubility over the nevirapine raw material. An excess amount of each co-crystal was weighed into 20 cm^3 test tubes. These were filled with MilliQ water (leaving a small amount of air to facilitate agitation), sealed and placed in a solubility bath. The bath was set at a temperature of 37 °C and the test tubes were agitated for 24 h. A UV spectroscopic method was attempted according to the method described by Stieger et al.[10] However, shifting of the λ_{max} of nevirapine occurred in all cases, making the calibration curve invalid. It was thought that, based on existing evidence of shifting of the peak in acidic medium, the acidity of the co-formers in solution caused the complication. An HPLC method, as described in Chapter 2, was employed instead. Calibration curves were constructed for all three co-crystals. An amount of co-crystal was weighed and made to volume using HPLC grade methanol. Regression lines of r^2 = 0.998524, r^2 = 0.999653 and r^2 = 0.999943 were obtained for nevirapine in **NVPMLE**, **NVPGLT** and **NVPSLI**, respectively.

The values for the equilibrium solubility at 37 °C in water are provided in Table 16. The solubility ratio is S_{cc}/S_{free} where S_{free} is the solubility of anhydrous nevirapine and S_{cc} the solubility of nevirapine for the co-crystal. Clearly, the **NVPGLT** and **NVPSLI** co-crystals showed only a minor enhancement in solubility but the **NVPMLE** showed the greatest increase – 5.3 times. This compares favourably with reported results where co-crystallisation has produced increases and decreases in equilibrium solubility.[11] Itraconazole co-crystals[12] had enhancements of 4-20 times in 0.1 M HCl but more impressive results have also been shown. For example, Good and co-workers reported 2-152 times aqueous solubility enhancements for seven carbamazepine co-crystals.[13]

Table 16: Results of solubility determination at 37 °C in water for the nevirapine standard and three co-crystals.

Form	Nevirapine solubility (mg cm^3)	Solubility ratio
Nevirapine standard[10]	0.0976 ± 0.0017	1
NVPMLE	0.515 ± 0.033	5.3
NVPGLT	0.115 ± 0.003	1.2
NVPSLI	0.110 ± 0.010	1.1

Co-crystal Comparison

Interestingly, all of the co-crystals reported here were reliably prepared by LAG and/or slow evaporation from solution and were identified as potential co-crystals during the LAG stage of co-crystal screening. This suggests solvent-assisted co-grinding is a quick method (as little as 5 minutes to reach complete conversion) for finding a potential nevirapine co-crystal. The method certainly allows for a large variety of solvents and a high co-former throughput rate, and involves very small amounts of sample (~10 mg) that may even be recoverable, depending on the method of sample preparation employed for PXRD analysis.

For convenience the abbreviations **NVSC** and **NVTTA**, as assigned by Samsodien will be used here in reference to that author's nevirapine-saccharin and nevirapine-*rac*-tartaric acid co-crystals.[5] These were described briefly in the introduction to this chapter. It is noteworthy that all of the successfully employed co-formers in the present study possessed carboxylic acid groups and none of the amides – except propionamide – provided potential evidence of co-crystallisation. Of all the known nevirapine co-crystals, only **NVSC** does not incorporate a carboxylic acid.

Table 17 provides a summary of relevant parameters related to the five nevirapine co-crystals. **NVPMLE** has the highest solubility ratio with respect to anhydrous nevirapine and **NVTTA** is the most thermally stable.

Table 17: Properties of the nevirapine co-crystals.

Co-crystal	Stoichiometry	Melting onset (°C)	Solubility ratio	Method of preparation
NVPMLE	1:1	185	5.3	LAG
NVPGLT	1:1	137	1.2	LAG/slow evaporation
NVPSLI	2:1	203	1.1	LAG/slow evaporation
NVSC	2:1	223	1.4*	Slow evaporation
NVTTA	1:1	228	1.2*	Slow evaporation

*Estimated based on the percentage dissolution after 3 hours, according to Samsodien.[5]

Interestingly, the dicarboxylic acids (maleic acid and glutaric acid) were able to prevent the formation of the typical nevirapine dimer. Both formed co-crystals in 1:1 ratio with co-operative

bonding to form a four-molecule motif. **NVTTA** also exhibits amide-carboxylic acid hydrogen bonding (synthon **C** in Figure 2), where the typical nevirapine self-association does not occur.[5] In the case of **NVPSLI**, the salicylic acid co-former behaves similarly to the solvent molecule toluene, by occupying channels in the crystal. It may be that the preferred intramolecular hydrogen bonding of salicylic acid reduces its electron donating potential to the extent that it is unable to compete with the amide-amide interaction of the API dimer.

All three of the co-crystals studied herein displayed melting points somewhere between those of the co-former and API. In general this is a common result but not predictable. There have been cases of co-crystals having melting points below, within or above the melting range of the starting reagents.[11]

The co-crystals **NVSC** and **NVTTA**[5] were not shown to exhibit the recrystallisation of nevirapine as was described here. Instead, after melting, these co-crystals decomposed. The thermal behaviour of these co-crystals in the temperature range between melting and final degradation warrants further investigation, given that all three of the co-crystals described in the present study displayed a common phenomenon.

Cyclodextrin Inclusion

There have been reports of β-CD, randomly methylated-β-CD (RAMEB) and hydroxyl-propyl-β-CD (HP-β-CD) inclusion complexes of nevirapine with accompanying solubility studies.[4] However, the PXRD evidence upon which the conclusions of complexation are based is not convincing.

Here we report a repetition of the experiment from literature along with a number of other attempts at inclusion of nevirapine in β- and γ-CD by liquid-assisted kneading and co-precipitation by slow-cooling. The kneading experiments summarised in Table 18 all involved kneading in the presence of MilliQ water (enough to maintain a wet paste) for 45 min. The products of kneading were analysed by PXRD while still moist. The co-precipitation experiments (Table 19) entailed dissolving ~15 mg of the co-former and one molar equivalent of β-CD or γ-CD in water, stirring for approximately 24 h at a temperature of 60 °C. Thereafter the solutions were filtered and allowed to cool slowly in a vacuum flask.

Table 18: Solvent-assisted kneading experiments.

Cyclodextrin	Molar ratio	Solvent
β-CD	1:1	H_2O
β-CD	1:1	30% ethanol in water (v/v)
γ-CD	1:1	H_2O

Table 19: Co-precipitation experiments by slow cooling.

Cyclodextrin	Molar ratio	Solvent
β-CD	1:1	H_2O
β-CD	1:1	30% ethanol in water (v/v)
γ-CD	1:1	H_2O
γ-CD	1:1	30% ethanol in water (v/v)

All of the attempts at cyclodextrin inclusion of nevirapine failed. In particular, even the reported method for preparation of a nevirapine-β-CD complex by methanol-assisted kneading yielded only a physical mixture. The comparison of PXRD traces in Figure 40 confirm this result and that the same occurred in the presence of water. Evidently, the authors of the paper in which the methanol-based method was used misinterpreted their PXRD data.

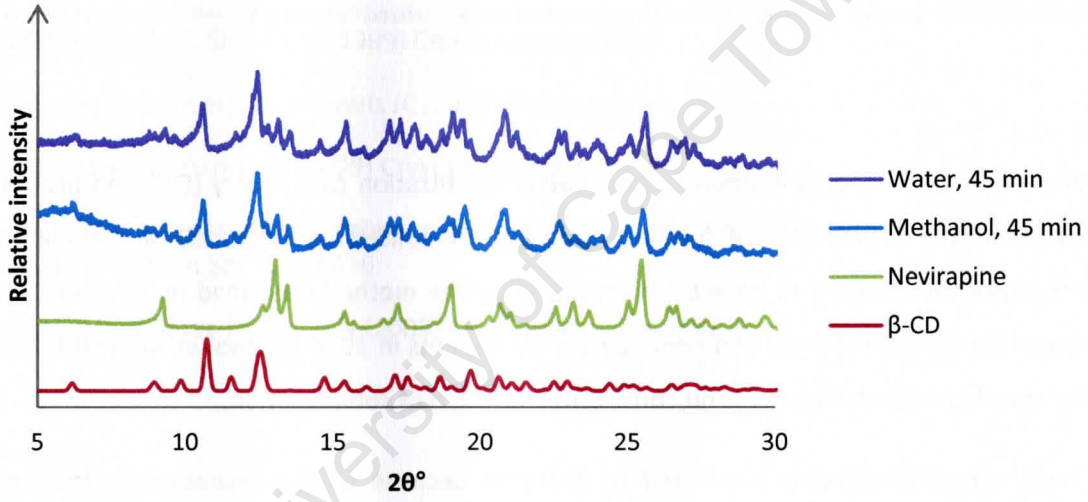

Figure 40: PXRD comparison showing traces of the products of water-assisted kneading and methanol-assisted kneading, as well as traces of the pure API and pure β-CD (computed).

Figure 41 shows that for γ-CD as well, kneading in the presence of water produces merely a physical mixture of drug and cyclodextrin.

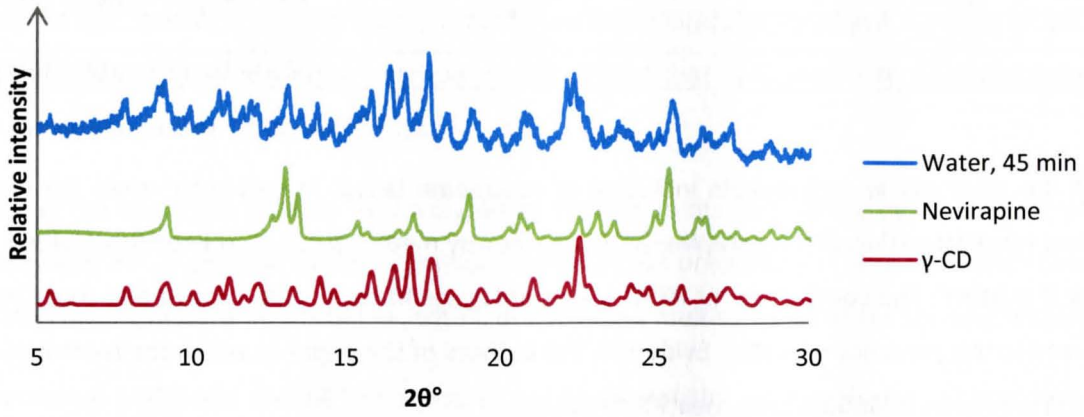

Figure 41: PXRD comparison showing traces of the product of water-assisted kneading as well as traces of the pure API and γ-CD (computed)

Solution studies included experiments using isothermal titration calorimetry (ITC) and proton NMR spectroscopy. The results thereof further supported the solid-state experimental evidence that a β-CD complex was unlikely to have been produced by the method described in literature. ITC was performed on nevirapine-β-CD and nevirapine-γ-CD systems in 30 % ethanol in water (v/v) and the results were haphazard. There was no consistent indication of complexation.

The NMR experiments were conducted in d_6-DMSO because of the exceptionally low aqueous solubility of nevirapine. No significant differences in chemical shifts were observed for either the cyclodextrin protons or nevirapine protons in the initial equimolar test for solutions of nevirapine with β-CD and γ-CD. The implication is that under these conditions, there was little or no interaction between the drug and either of the cyclodextrins.

References

1 Reguri BR, Chakka R (2006) US Patent Application 0183738

2 Caira MR, Stieger N, Liebenberg W, De Villiers MM, Samsodien H (2008) Cryst Growth Des 8: 17

3 Stieger N, Liebenberg W, Wessels JC, Samsodien H, Caira MR (2010) Struct Chem (21): 771

4 Lokamatha KM, Barathi A, Shanta Kumar SM, Rama Rao, N (2010) Research Journal of Pharmaceutical, Biological and Chemical Sciences 1: 372

5 Samsodien H (2011) Supramolecular Derivatives of Selected Bioactive Compounds: A Physicochemical Study, PhD Thesis, University of Cape Town, South Africa

6 Guo K, Sadiq G, Seaton C, Davey R, Yin Q (2010) Cryst Growth Des 10: 268

7 Barbour LJ (1999) J Appl Cryst 10: 73

8 Sheldrick GM (2008) Acta Crystallogr A64: 112

9 Audet P, Savoie R, Simard M (1999) Can J Chem 68: 2183

10 Stieger N, Liebenberg W, Wessels JC (2009) Pharmazie 64: 690

11 Schultheiss N, Newman A (2009) Cryst Growth Des 9: 2950

12 Remenar JF, Morissette SL, Peterson ML, Moulton B, MacPhee JM, Guzmán HR, Almarsson Ö (2003) J Am Chem Soc 125: 8456

13 Good DJ, Rodríguez-Hornedo N (2009) Cryst Growth Des 9: 2252

Chapter 4: Efavirenz

Introduction

There are several efavirenz polymorphs described in literature. Herein we will refer mostly to Form 1 and Form β with reference to two reported polymorphs. There are also reported co-crystals and solvates. There have been several patents claiming novel polymorphs, and X-ray structures have been published for four polymorphs, one hydrate, two solvates and two non-pharmaceutical co-crystals. References to these studies are provided below.

Tiekink *et al.* published the first known crystal structure of efavirenz in 2009.[1] Having compared its calculated PXRD trace with the traces of known polymorphs as they appear in patents, Mahapatrah and co-workers determined that it does not correspond with any of the patented forms of the drug.[2]

Form 1, the first efavirenz polymorph patented by the DuPont Pharmaceutical Company,[3] is accepted to be the most thermodynamically favourable form of the drug. Each of the other four polymorphs (Forms 2, 3, 4 and 5) described in this particular patent can be converted to Form 1. A number of patent applications followed this original one, claiming several novel polymorphs.[4,5,6] There are also methods for the preparation of an amorphous phase.[7] The bulk efavirenz (as purchased) with which the present study was conducted corresponds with Form 1. Figure 1 shows the PXRD comparison that confirms this.

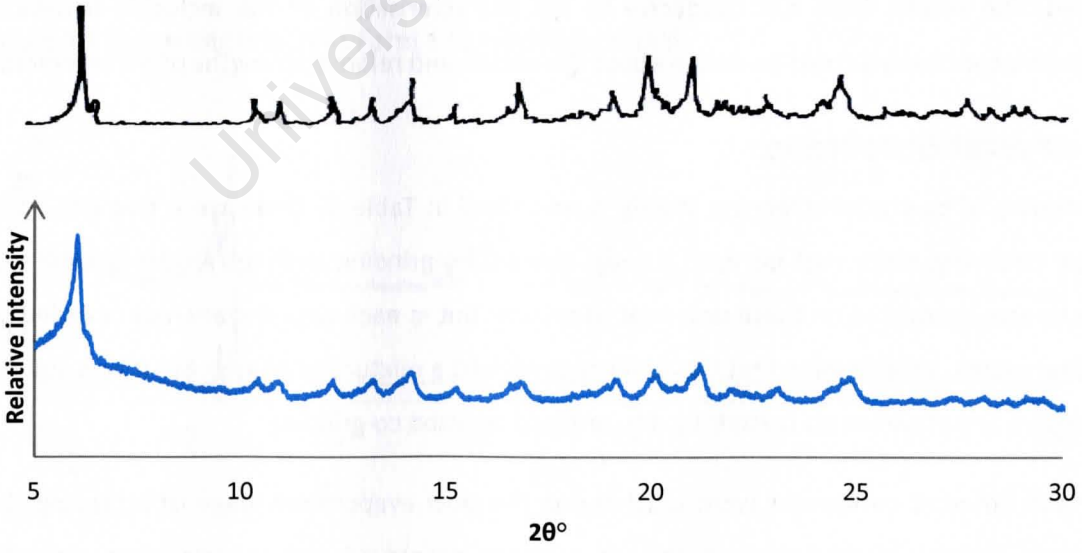

Figure 1: PXRD of the efavirenz bulk (as purchased and used in the present study; blue trace) and Form 1 as it appears in the DuPont patent application[3] (black trace).

Ravikumar and Sridhar reported X-ray structures for two forms – a monohydrate and a polymorph.[8] The polymorph corresponds with Form β, which was patented by the company Ranbaxy Laboratories.[6]

There are also reported solvates and co-crystals. Mahapatra and co-workers have determined X-ray structures of two related polymorphs and two related cyclohexane solvates. Both pairs are interconvertible by temperature-induced single-crystal to single-crystal phase transformations. One of the polymorphs has been shown to be the thermodynamically stable Form 1. In addition, the same group determined X-ray crystallographic structures of two non-pharmaceutical co-crystals with the partner molecules 1,4-cyclohexanedione and 4,4'-bipyridine.[2]

Present study

During the co-crystal screening process in this study, it became evident that liquid-assisted grinding (LAG) of efavirenz with THF and ethanol resulted in phase transitions. One of the polymorphs isolated has been identified as Form β (the structure determined by Ravikumar's group), while the other did not match reported forms. Attempts were made to recover single crystals of these forms by recrystallisation from various solvents but these were unsuccessful.

Cyclodextrin inclusion studies involved attempts at complexation using standard kneading methods and co-precipitation by slow cooling. A reported method for complex formation was investigated. Furthermore, the solution behaviour of efavirenz in the presence of various cyclodextrins was studied. The results were not conducive to full characterisation of the inclusion behaviour but qualitative conclusions could be drawn about the nature and relative strengths of the interactions.

Co-crystal Screening

A summary of co-crystal screening results is presented in Table 1. There were two hits in the co-crystal screening stage that involved solvent-assisted co-grinding with tetrahydrofuran (THF). DSC analysis was conducted on these potential co-crystals but in each case the analysis revealed several thermal events, an indication that the product contained a mixture of phases. So, it was not possible to prepare any efavirenz co-crystals by dry- or liquid-assisted co-grinding.

Fourteen different co-formers were used during the slow evaporation stage of screening. Despite the large variety of solvents and solvent mixtures employed, no crystals were yielded; only powdered and gel-like products resulted.

Table 1: Summary of the results of efavirenz co-crystal screening.

Method	Co-formers	Hits	Pure co-crystal
Dry co-grinding	18	0	0
Tetrahydrofuran LAG	19	2	0
Ethanol LAG	7	0	0
Slow evaporation	14	0	0

As mentioned above, during the co-crystal screening process, it became evident that liquid-assisted grinding with THF and ethanol resulted in phase transformations of the efavirenz component. One of the polymorphs has been identified as a known polymorphic form (Form β), while the other was unidentifiable. With regard to the unidentified form, TGA revealed the likelihood of included solvent.

Form β by Liquid-assisted Grinding

There were occurrences of phase transformation with regard to the efavirenz component during a number of co-crystallisation attempts by solvent-assisted co-grinding with ethanol. Except in the cases of possible co-crystallisation and no change, efavirenz (Form 1) was transformed to Form β during grinding with ethanol. The refined method involved grinding efavirenz with a few drops of ethanol using a pestle and mortar for at least 10 min and allowing the resultant material to dry. The PXRD traces in Figure 2 confirm that the product of this LAG preparation is in fact Form β. Previous descriptions of preparative methods for Form β have not incorporated grinding or solvent-assisted grinding. Even the most recent patent application (2009)[9] describes only solution-based methods involving seeding and freeze-drying. Thus, the method described here represents a new, rapid procedure for converting efavirenz Form 1 to efavirenz Form β.

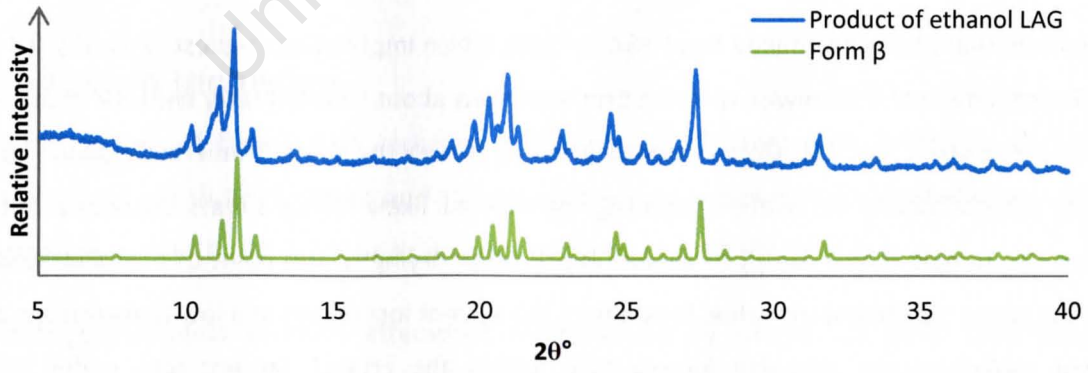

Figure 2: PXRD comparison of the product of ethanol liquid-assisted grinding (experimental) and Form β (calculated using single crystal structure obtained from the CSD[10]).

Solvate by Liquid-assisted Grinding

The second form of efavirenz, prepared by LAG using THF, is a solvate. Its PXRD pattern is not similar to any reported patterns, which makes it difficult to identify as a known form. To check whether this was an unsolvated polymorph or a solvate, the sample was subjected to TGA beyond its melting point.

The TGA experiment was conducted between room temperature and 300 °C at a heating rate of 5 K min^{-1}. The TGA trace (Figure 3) exhibits a relatively large mass loss at low temperature (~40 °C) suggesting the loss of THF or water. THF is the more likely of these two candidates because of its lower boiling point (66 °C) but, given that desolvation may occur well below or above the solvent boiling point, it cannot be concluded for certain whether THF or water is the included solvent.

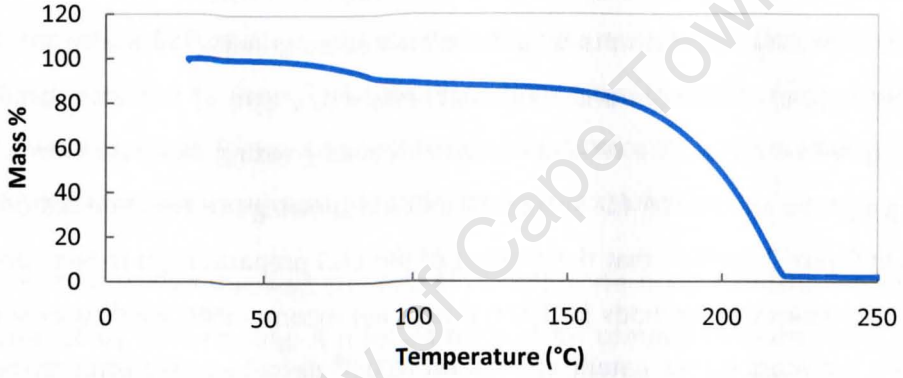

Figure 3: TGA trace of EFV solvate prepared by THF liquid-assisted grinding.

The solvent mass loss determined from TGA is ~12%, which implies a host-guest ratio of 1:0.6 if THF is included; however, it is unwise to make firm assertions about stoichiometry because of the nature of the preparation method. Liquid-assisted grinding leaves the sample inherently prone to both surface adsorption and desolvation, meaning the TGA will likely reflect a mass loss that is in excess (where the sample is still damp) or smaller (because of drying to the point of partial desolvation) than the actual stoichiometric value. In addition, the solvent loss occurs at a low temperature, so the solvent molecules are probably loosely held within the crystal. Solvent loss under ambient conditions may also result in a misleading value from TGA.

Temperature-controlled PXRD

Variable temperature PXRD analysis was carried out to investigate the desolvation process. PXRD patterns were determined at room temperature, 40, 80 and 120 °C. The comparison of patterns in Figure 4 clearly shows that as the sample is heated from 40 °C to 80 °C, it is converted from the

solvate to the thermodynamically stable Form 1 of efavirenz, the bulk material from which the solvate was initially prepared.This result is consistent with the TGA trace, where the maximum rate of solvent loss – determined by taking the derivative with respect to temperature – occurs at 83 °C.

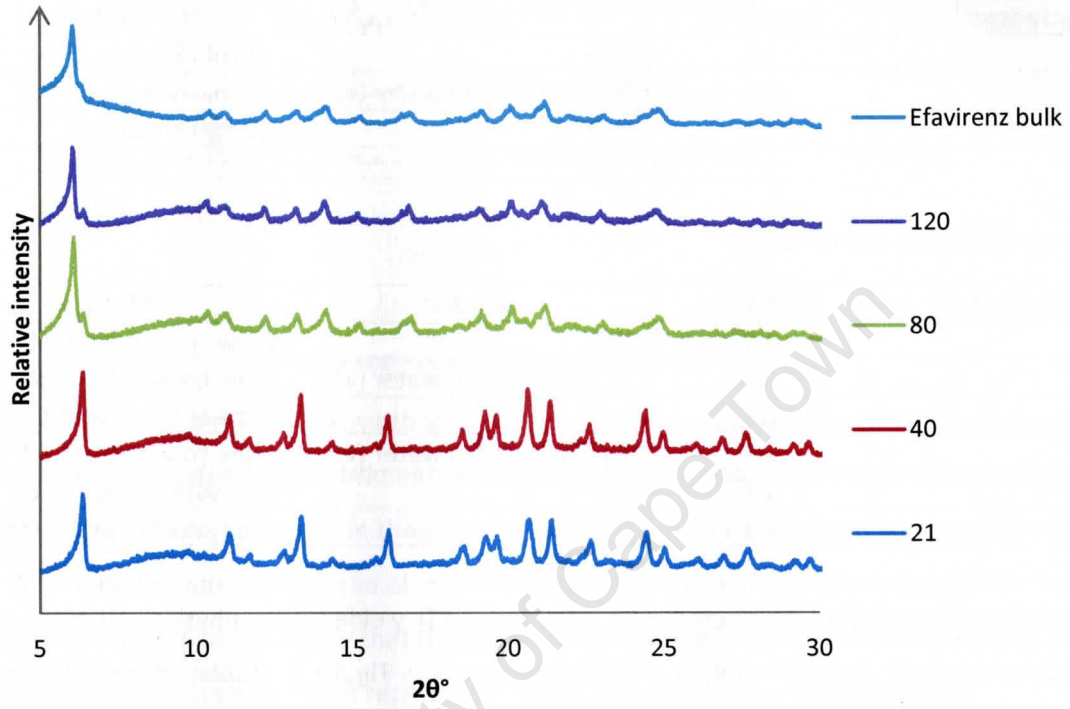

Figure 4: Variable temperature PXRD patterns for the efavirenz solvate prepared by THF liquid-assisted grinding. Temperatures are in °C.

Cyclodextrin Inclusion

There are reports of cyclodextrin inclusion complexes of efavirenz with β-CD and derivatised cyclodextrins. In particular, Sathigari and co-workers have described complexes of efavirenz with β-CD, hydroxypropyl-β-CD (HP-β-CD) and randomly methylated β-CD (RAMEB).[11]

Solid-state experiments involved attempted complexation by simple 1:1 mole ratio kneading experiments in the presence of water and ethanol. NMR spectroscopy was used to study the behaviour of efavirenz-cyclodextrin systems in solution. Here, all of the cyclodextrins used by Sathigari's group were tested along with γ-CD.

Solid-state studies

Table 2 and Table 3 summarise the attempts at cyclodextrin inclusion by kneading and co-precipitation, respectively. None of these experiments produced convincing evidence of complexation.

Table 2: Solvent-assisted kneading experiments

Cyclodextrin	Mole ratio	Solvent	Method
β-CD	1:1	H_2O	45 min knead
β-CD	1:1	50 % ethanol in water (v/v)	45 min knead
γ-CD	1:1	H_2O	45 min knead

Table 3: Co-precipitation experiments

Cyclodextrin	Mole ratio	Solvent	Method
β-CD	1:1	H_2O	Slow cooling from 60 °C
β-CD	1:1	30 % ethanol in water (v/v)	Slow cooling from 60 °C
γ-CD	1:1	H_2O	Slow cooling from 60 °C
γ-CD	1:1	30 % ethanol in water (v/v)	Slow cooling from 60 °C
DIMEB	1:1	H_2O	Recrystallisation at 60 °C
TRIMEB	1:1	H_2O	Recrystallisation at 60 °C

The kneading experiments conducted with EFV and β-CD yielded only physical mixtures of the starting components, as evidenced by PXRD comparisons in Figure 5. Displayed are experimental traces of **A**, the product of 1:1 kneading in the presence of water and **B**, the product of 1:1 kneading in the presence of 50 % ethanol in water (v/v).

Both kneading experiments were carried out for 45 min and the products sampled while still a wet paste, so as to ensure an accurate PXRD representation. Allowing the sample to dry completely may result in a different crystal form, as crystalline solvent is liberated. One of the kneading experiments was conducted according to the method described by Sathigari's group except that the kneading time was increased to 45 min for continuity and to be sure that adequate time was provided for complete conversion. Our results did not agree with those reported in the paper.

With reference to the PXRD traces in Figure 5, it is clear that the product **A** is merely a physical mixture of the starting reagents, while the kneaded material **B** is a physical mixture containing at least pure β-CD. The balance of the material represented by **B** may consist of some polymorph of efavirenz, an efavirenz solvate and/or a small amount of complexed efavirenz; it cannot be said for certain which. What is clear is that this method does not appear to be a reliable one for the preparation of an efavirenz-β-CD complex and the PXRD evidence is not by itself sufficient to conclude that such a complex exists at all. It has been shown that efavirenz readily undergoes phase

transitions when ground in the presence of some solvents. This accounts for the prominence of pure β-CD peaks with the simultaneous shrinkage of, in particular, the largest efavirenz peak at 2θ ~ 6°.

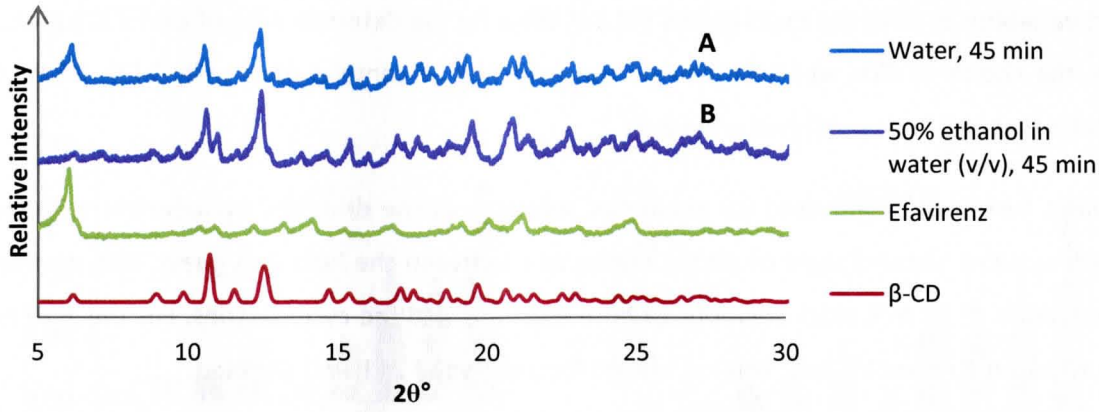

Figure 5: PXRD comparison for β-CD kneading experiments.

Similarly, with γ-CD, the kneading method produced only a physical mixture of host and guest. Here, only a single γ-CD kneading experiment was conducted, since no reported methods existed. The method employed was kneading, in the presence of water, of an equimolar mixture of efavirenz and γ-CD. The resultant material was sampled while still a wet paste and analysed using PXRD. The traces compared in Figure 6 show clearly that the product of kneading is a physical mixture of the host and guest – the trace shows only peaks represented in the traces of the pure components.

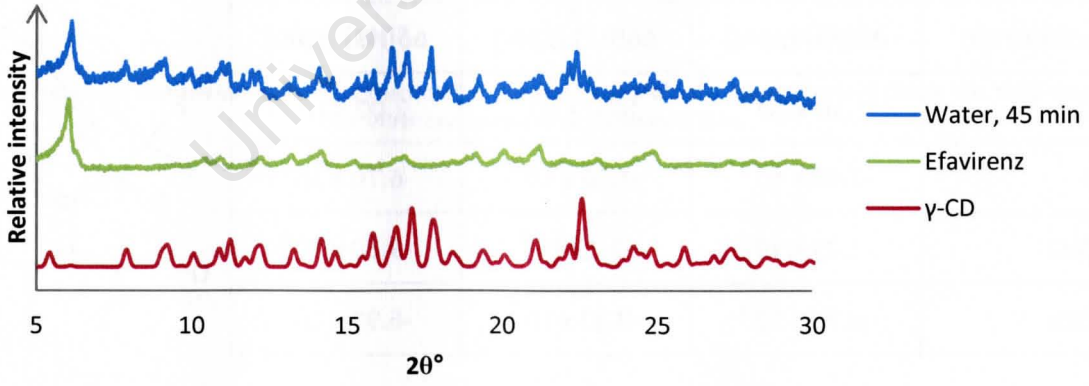

Figure 6: PXRD comparison for γ-CD kneading experiment.

Solution studies

The solution behaviour of efavirenz in the presence of cyclodextrins was investigated. Because of the extemely low aqueous solubility of the drug, its solution behaviour in water could not be studied by NMR spectroscopy. The concentration required was 10 mM (3.2 mg cm^{-3}), while the solubility of efavirenz is only 9 μg cm^{-3}. So, instead of water, and as in the case of nevirapine (Chapter 3), NMR

experiments were carried out in d_6-DMSO with the 1:1 molar ratio tests providing an initial indication of the extent of interaction between the efavirenz and cyclodextrin molecules. Again the interactions between the drug and CD appear to be weak and difficult to characterise. The chemical shift variations in all of the experiments did not allow for the determination of useful Job plots. Note that the choice of CDs was informed by the evidence of complexation with β-CD, HP-β-CD and RAMEB that had been published previously.[11]

Initially, tests were conducted for equimolar solutions of the drug and cyclodextrin to determine which systems showed signs of strong interaction between the host and guest. This involved the preparation of 10 mM stock solutions of both efavirenz and the cyclodextrins. For the 1:1 test, the solutions were mixed in equal volume, stirred for a period of 24 h and sampled.

These preliminary tests would inform the decision about which systems to include in the set of continuous variation experiments. A shortened version of the results is given in Table 4. Only the chemically induced shifts (CISs), Δδ, for the protons H1, H2 and H3 of efavirenz are shown because the values for these three were greatest. The CISs for the rest of the efavirenz protons were negligible. We were also able to determine CISs for the protons of β-CD and γ-CD. Overall, the CISs were greatest for γ-CD, HP-β-CD and RAMEB, so it was decided to carry out full continuous variation experiments with these three.

Table 4: CISs for efavirenz protons H1, H2 and H3, which showed the greatest deviations during tests that involved a host-guest molar ratio of 1.

Cyclodextrin	Δδ(H1) (ppm)	Δδ(H2) (ppm)	Δδ(H3) (ppm)
β-CD	1.10×10^{-3}	8.00×10^{-4}	2.00×10^{-4}
γ-CD	-7.40×10^{-3}	-7.70×10^{-3}	-6.70×10^{-3}
HP-β-CD	-1.01×10^{-2}	$-1.13\ 10^{-2}$	-9.30×10^{-3}
RAMEB	-6.70×10^{-3}	-8.30×10^{-3}	-6.90×10^{-3}

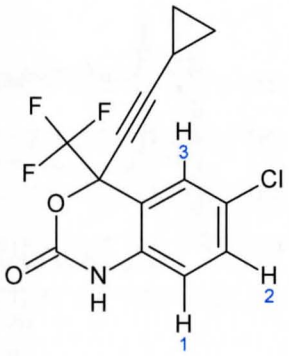

Figure 7 presents the data for continuous variation experiments carried out with the three cyclodextrins that showed the greatest absolute CISs during preliminary tests. For a system that forms an inclusion complex in solution, plotting $\Delta\delta \cdot [X]^*$ against the ratio $R = [X]/([H]_t+[G]_t)$, as described in Chapter 2 should produce a relatively smooth Job plot with a maximum where R is equal to the stoichiometric ratio of the complex. However, the results for the efavirenz-cyclodextrin systems are erratic. They suggest that there is some interaction, the strength

* [X] is the host or guest concentration, depending on which CIS values are being used

of which generally increases as the value of R is increased. However the dramatic decreases at R = 0.5 for γ-CD, R = 0.5 for HP-β-CD and R = 0.9 for RAMEB imply complicated interactions with potentially multiple modes of weak complexation.

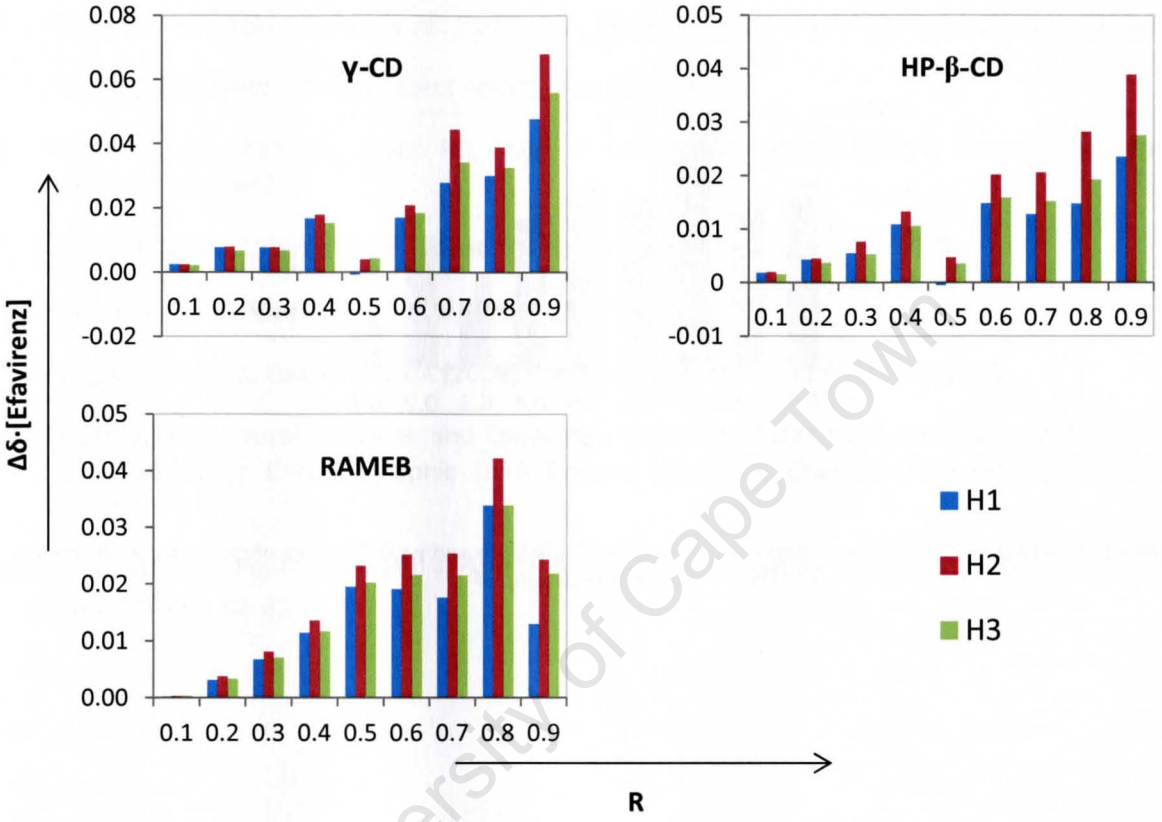

Figure 7: Results of continuous variation experiments with efavirenz and γ-CD, HP-β-CD and RAMEB. The data obtained for efavirenz protons are presented here.

The NMR peaks of the HP-β-CD and RAMEB protons could not be easily followed because of overlapping within the spectrum but the γ-CD proton signals could be tracked. The CISs for the OH2 and OH3 protons (Figure 8) of γ-CD were the greatest during preliminary tests but for ratios of 0 to 1 in steps of 0.1, the values of Δδ·[γ-CD] for these protons followed a similarly erratic pattern as for the efavirenz protons H1, H2 and H3.

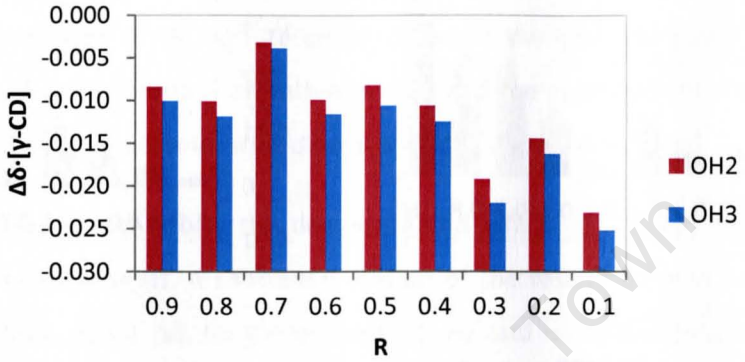

Figure 8: Results of the continuous variation experiment with efavirenz and γ-CD. The data obtained for γ-CD protons are presented here.

References

1 Cuffini S, Howie RA, Tiekink ERT, Wardell JL, Wardell SMSV (2009) Acta Crystallogr E 65: 3170

2 Mahapatra S, Thakur TS, Joseph S, Varughese S, Desiraju GR (2010) Cryst Growth Des 10: 3191

3 Radesca LA, Maurin MB, Rabel SR, Moore JR (1999) International Patent Application 64405

4 Reddy BP, Rathnakar K, Reddy RR, Reddy MD, Reddy KSC (2006) US Patent Application 0235008

5 Dova E (2008) International Patent Application 108630

6 Sharma R, Bhushan KH, Aryan RC, Singh N, Pandya B, Kumar Y (2006) International Patent Application 040643

7 Doney JA (2007) International Patent Application 014393

8 Ravikumar K, Sridhar B (2009) Mol Cryst Liq Cryst 515: 190

9 Tyagi OD, Jetti KR, Ramireddy BA (2009) International Patent Application 087679

10 Cambridge Structural Database and Cambridge Structural Database System (Feb, 2011) Version 5.32, Cambridge Crystallographic Data Centre, University Chemical Laboratory, Cambridge, England

11 Sathigari S, Chadha G, Lee Y-HP, Wright N, Parsons DL, Rangari VK, Fasina O, Babu RJ (2009) AAPS PharmSciTech 10: 81

Chapter 5: Zidovudine

Introduction

In 1987 zidovudine, or azidothymidine (AZT), became the first drug approved for AIDS therapy.[1] It is a chiral drug which is still employed, in combination therapy, as a nucleoside reverse transcriptase inhibitor against HIV-1 infection. This API has a modest aqueous solubility of 25 mg cm^{-3}, a low melting point of 106-112 °C and is basic with a pK_a of 9.7.[2,3] Represented in the figure below, the molecule possesses potential hydrogen bond donor/acceptor groups that have been highlighted.

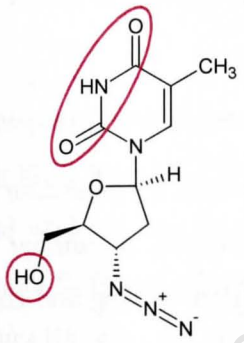

Figure 1: Zidovudine with potential hydrogen bonding groups highlighted.

The single crystal structure of zidovudine has been reported by at least three different groups[4,5,6] and a number of structures of derivatives have been determined.[7,8] There were no other polymorphs of zidovudine reported, nor solvates of zidovudine known at the time of writing. Only two co-crystals of zidovudine are known – one with lamivudine and another with 2,4,6-trinitropyrimidine, a co-former which is not pharmaceutically relevant.[9] Thus, while this drug has been in use for at least 30 years, it does not appear to have been the target of many attempts at supramolecular modification. Included in this chapter are details of co-crystal screening experiments with GRAS compounds and attempts at cyclodextrin inclusion. A new form, namely a novel β-CD complex has been discovered. Details of its preparation, analysis and the determination of its single crystal structure are presented.

Co-crystal Screening

Limited screening experiments were conducted with zidovudine. A representative selection of co-formers was used for dry co-grinding and liquid-assisted co-grinding (LAG) with ethanol. All mixtures for the co-grinding experiments were prepared in 1:1 molar ratio and co-ground for 10 min. Table 1 below provides a summary of the results of the screening experiments, showing that two hits were obtained. The set of nine co-formers employed were selected for variety in functional groups, solubilities and pK_a constants.

Table 1: Summary of the results of grinding experiments from co-crystal screening of zidovudine.

Method	Co-formers*	Hits
Dry co-grinding	9	1
Ethanol LAG	9	1

*The nine co-formers are glutaric acid; isonicotinamide; maleic acid; L-malic acid; oxalic acid dihydrate; piperazine; propionamide; saccharin and L-tartaric acid.

The first two stages of screening produced hits only with saccharin but from PXRD analysis it was evident that the resultant material was not a pure phase but a mixture of the possible co-crystal and zidovudine. Ten slow evaporation experiments, with 1:1 molar ratio and employing a different solvent or solvent mixture in each case, were subsequently conducted with saccharin as co-former. These experiments yielded no hits.

Cyclodextrin Inclusion

Attempts were made at preparing complexes of zidovudine with β-CD and γ-CD, as well as with the derivatised cyclodextrins DIMEB and TRIMEB. A number of standard methods were employed including kneading, co-precipitation by slow cooling and co-precipitation at elevated temperature, the results of which are summarised in Table 2.

Table 2: Summary of experimental results for attempted cyclodextrin inclusion of zidovudine.

Cyclodextrin	Method	Result
β-CD	30 min water-assisted kneading	Complex crystals
β-CD	Slow cooling	Physical mixture
γ-CD	30 min water-assisted kneading	Powdered complex
γ-CD	Slow cooling	γ-CD crystals
DIMEB	Elevated temperature	DIMEB crystals
TRIMEB	Elevated temperature	No crystals

Co-precipitation by slow cooling produced an inclusion complex of zidovudine with β-CD, while only pure host crystals resulted from the co-precipitation experiments with γ-CD. Kneading in the presence of water, on the other hand yielded a γ-CD complex and a zidovudine-β-CD physical mixture. The slow cooling experiments entailed dissolving 20-30 mg zidovudine and one molar equivalent of γ-CD or β-CD in 0.8-1 cm^3 Milli-Q water at elevated temperature. The resultant solutions were filtered while hot and allowed to cool slowly in a vacuum flask over a period of 2-3 days. The kneading experiments were carried out by mixing ~10 mg of zidovudine with one molar equivalent of β-CD or γ-CD and kneading for 30 min. Water was added to maintain a wet paste-like consistency throughout the period of kneading.

The solubilities of the derivatised cyclodextrins DIMEB and TRIMEB are inversely related to temperature. At room temperature and below, both are highly water-soluble and at around 60 °C their solubilities are much lower. Inclusion attempts with these potential hosts were carried out by dissolving ~20 mg zidovudine and one molar equivalent of TRIMEB or DIMEB in 5 cm^3 MilliQ water, with the vials suspended in an ice bath. The suspensions were stirred for 24 h, after which they were filtered while still cold, placed in an oven preset to 60 °C and allowed to slowly crystallise. The experiments with these cyclodextrins did not yield any complexes.

β-Cyclodextrin Inclusion Complex

Preparation of the complex

Single crystals of the zidovudine-β-CD complex (**ZIDβCD**) were grown – with great difficulty – by slow cooling. A saturated solution of 138 mg (0.11 mmol) β-CD and 29 mg (0.11 mmol) zidovudine was prepared by dissolving at 60 °C in water while stirring for 6 h. Thereafter the solution was filtered while hot and placed in a covered vacuum flask and allowed to cool over a period of 3 days. This method did not reliably produce the complex, with the host often crystallising as the free hydrate. Only high concentrations (typically ~ 0.14 mmol cm^{-3}) yielded crystals of the inclusion complex.

Kneading with β-CD in an attempt to produce the same complex was unsuccessful. Only a physical mixture resulted after 30 min of kneading. This was verified by the absence of new peaks in the PXRD pattern.

NMR spectroscopy

Proton NMR spectroscopic analysis of (Figure 2) **ZIDβCD** crystals grown by the slow cooling method revealed a host-guest stoichiometry of 1:1. As can be seen in Figure 2, the zidovudine H1 and H2 proton signals at 7.59 and 6.14 ppm integrate for 1.00 and 1.05, respectively while the β-CD H1 proton signal at 5.04 ppm has an integral value of 6.83, which correlates with the predicted value of 7 for a 1:1 complex. The minor deviation from the theoretical value is attributed to a small excess of zidovudine. As mentioned earlier, the complex crystallised only at very high concentrations, where simultaneous recrystallisation of one or both of the pure starting components often occurred.

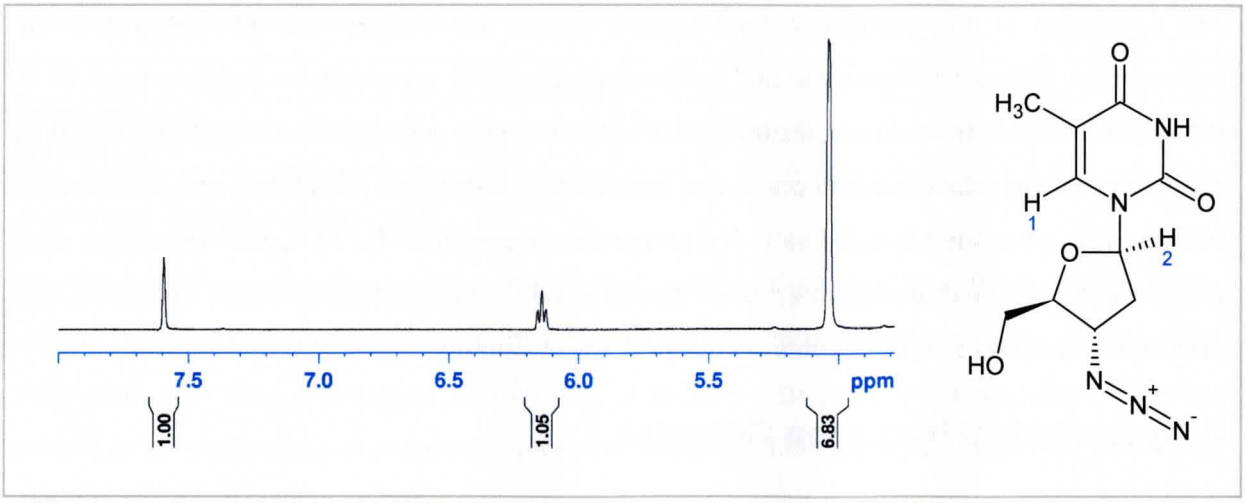

Figure 2: Partial proton NMR spectrum confirming 1:1 stoichiometry of the ZIDβCD complex.

Thermal analysis

HSM

A sample of the tiny **ZIDβCD** crystals was heated at a rate of 10 K min^{-1} during HSM analysis. The representative photographs in Figure 3 reveal important thermal events. At 60 °C the crystals begin to show signs of damage and at 85 °C, the crystals are clearly cracked. At 110 °C, bubbles appear indicating the loss of water vapour. Degradation becomes visible at approximately 240 °C and the sample is at an advanced stage of decomposition at 270 °C, where the crystals have turned dark brown. The numerous bubbles that are visible at 270 °C are likely not solvent but a volatile product of the complex degradation.

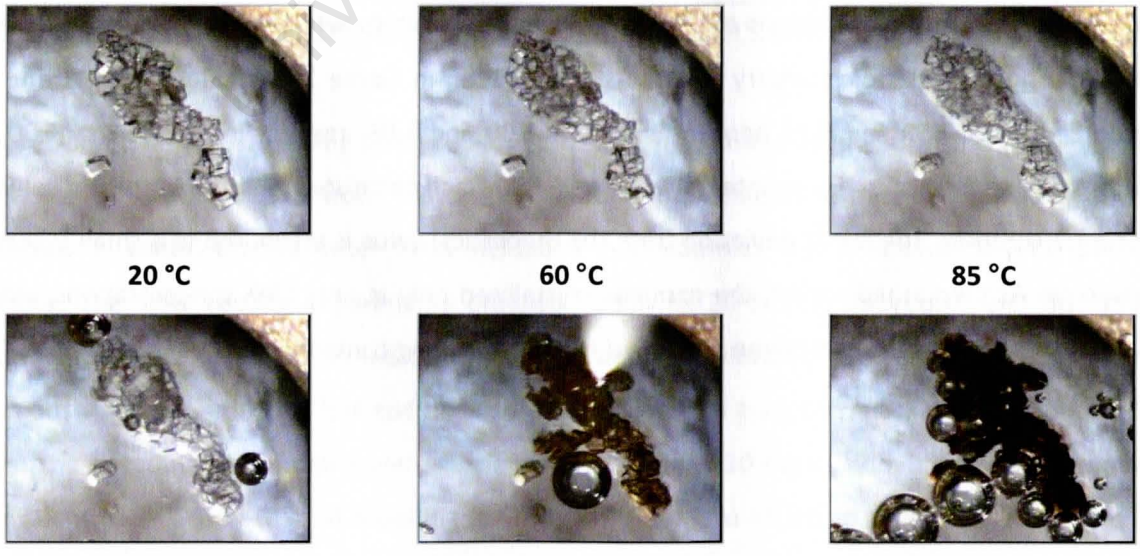

Figure 3: Representative HSM photographs of ZIDβCD.

TGA and DSC

Refer to the traces in Figure 4, both of which were generated by a temperature program with a heating rate of 10 K min^{-1}. In the TGA trace, the initial mass loss, attributed to dehydration, was determined as 9.6 ± 0.1 % (n = 2), which implies a molar equivalent of 8.3 water molecules per mole of host/guest. Thereafter, the sample mass remains constant until the onset of the first stage of decomposition at 190 °C. A second, more rapid stage of decomposition begins at 260 °C.

The DSC thermogram exhibits a number of noteworthy features. The first endotherm, occurring at 35-140 °C with peak minimum at 59 °C is the one associated with the water loss. At 190-285 °C, a large, broad exotherm with a peak maximum of 243 °C is observed. This exotherm coincides with the onset of decomposition, as observed in the TGA curve.

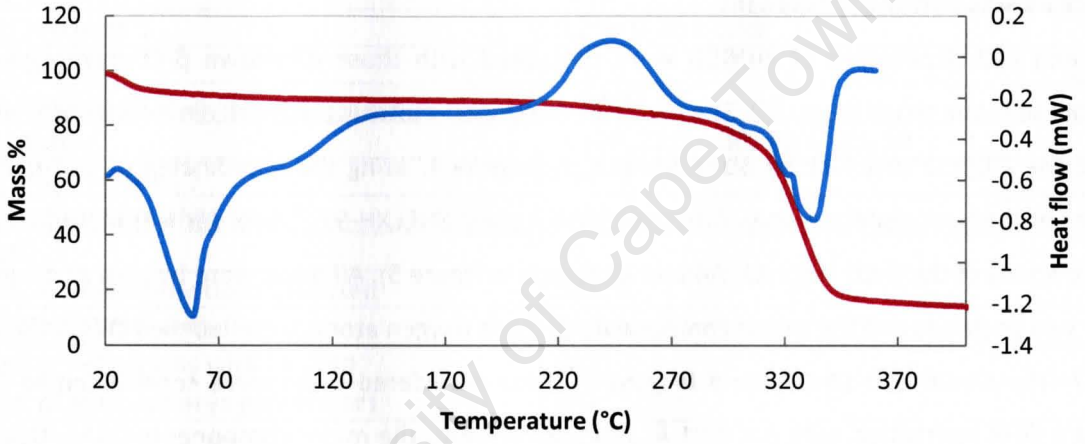

Figure 4: TGA (red) and DSC (blue) thermograms for ZIDβCD.

Considering the evidence from all three thermal analytical techniques, it is clear that 8.3 water molecules per unit of the complex are lost from room temperature to ~140 °C and that the complex degrades in two distinct stages, beginning at ~190 °C.

Single crystal X-ray diffraction

Data-collection and space group determination

Data were collected on a Bruker KAPPA APEX II DUO diffractometer. One of the tiny block-like crystals was selected from the vial and placed on a slide in Paratone oil to prevent dehydration. This was done quickly and carefully to ensure that the data collected were representative of the fully hydrated complex. X-ray diffraction data gave the unit cell dimensions and Laue symmetry of $2/m$, characteristic of the monoclinic crystal system. The following reflections conditions were identified in XPREP[10]: $hkl: h + k = 2n; (h0l: h = 2n)$, and these were confirmed using the program LAYER.[11] Thus, the space group options were $C2$, Cm or $C2/m$. The space group $C2$ was chosen because β-CD is known to be chiral, so the existence of mirror planes is impossible.

Structure solution and refinement

The unit cell dimensions of **ZIDβCD** were compared with those of known β-CD complexes that crystallise in the space group $C2$. The one with the closest matching unit cell dimensions was used to solve the ZIDβCD structure by isormorphous replacement, using the coordinates of non-hydrogen atoms of the host molecule only. After refinement using SHELXH-97,[12] disorder was identified at the O6 positions of the β-CD rings A2, A4 and A7 (labels in Figure 5). All three were treated as disordered over two positions and the minor components of these oxygen atoms were labelled O7A2, O7A4 and O7A7. The C6-O6 and C6-O7 bond lengths in these disordered cases were constrained to 1.40 Å using a DFIX instruction with σ = 0.01 Å. After refinement, the major components O6A2, O6A4 and O6A7 had site-occupancy factors of 0.71(2), 0.72(2) and 0.77(2), respectively. Hydrogen atoms of the host were placed in idealised positions for those hydrogens directly bonded to carbon atoms and an AFIX 83 instruction (hydrogen bond searching) was employed to place the hydrogens of the hydroxyl groups. The hydrogen atom positions of hydroxyl groups were inspected for potential hydrogen bonding that had not been accounted for by the riding model, and transformations carried out where necessary. Each hydrogen atom was assigned an isotropic temperature factor of 1.2 times that of its parent atom. Even after the entire host molecule had been modelled, the coordinates of the guest molecule could not be identified due to the very low values of difference electron density peaks in the host cavity. Table 3 lists the crystal data and refinement parameters.

Table 3: Data-collection and refinement parameters for ZIDβCD.

Formula unit	$(C_{42}H_{70}O_{35})$ $(C_{10}H_{13}N_5O_4)$ 7.24(H_2O)
Formula mass (g mol^{-1})	1532.67
Crystal system	Monoclinic
Space group	*C*2
a (Å)	19.103(4)
b (Å)	24.550(5)
c (Å)	15.797(3)
α (°)	90
β (°)	109.522(4)
γ (°)	90
Volume (Å^3)	6982(3)
Z	4
Density$_{calc}$ (g cm^{-3})	1.463
μ(MoKα) (mm^{-1})	0.130
F(000)	3270
Crystal size (mm^3)	0.25 x 0.26 x 0.36
Temperature (K)	173
Range scanned θ (°)	1.67-26.70
Index ranges	h: -24, 22; k: -30, 30; l: -19, 19
ϕ and ω scan angle (°)	0.5
Total number of frames	1052
Dx (mm)	40
Total number of reflections collected	23372
Number of unique reflections	14413
Number of reflections with I > 2σ(I)	9431
Number of least-squares parameters	741
R_{int}	0.0278
S	1.478
R_1 (I > 2σ(I))	0.1357
Number of reflections omitted	12
wR_2	0.3683
Weighting scheme parameters	a = 0.2
$(\Delta/\sigma)_{mean}$	< 0.001
Δρ excursions (e Å^{-3})	0.755, -0.573

The positions of three water molecules with full site-occupancy were identified and those oxygen atoms placed accordingly, while the disordered waters were placed systematically in order of the size of their difference electron density peaks. Based on the relatively high U_{iso}-values of the host atoms and the three water molecules with full site-occupancy, the U_{iso}-values of the disordered oxygen atoms were fixed at 0.1 Å^2 and the individual site-occupancy values treated as variables. The refined values for site occupancy and isotropic thermal parameters are provided in Table 4. In total, 15 water sites were identified, with a combined site-occupancy of 7.54.

Table 4: Parameters for the water sites of ZIDβCD.

Atom	s.o.f.	U_{iso} (Å^2)	Atom	s.o.f.	U_{iso} (Å^2)	Atom	s.o.f.	U_{iso} (Å^2)
O1W	1	0.075	O6W	0.51	0.10	O11W	0.18	0.10
O2W	1	0.079	O7W	0.52	0.10	O12W	0.35	0.10
O3W	1	0.091	O8W	0.35	0.10	O13W	0.37	0.10
O4W	0.68	0.10	O9W	0.29	0.10	O14W	0.13	0.10
O5W	0.44	0.10	O10W	0.38	0.10	O15W	0.34	0.10

After the final refinement the Goodness of Fit value (S) and weighted R-factor, which are available in Table 3, remained high. This is attributed to the high degree of disorder within the structure. The entire guest molecule, several water molecules as well as hydroxyl groups of the host are all disordered.

Molecular structure

The asymmetric unit, shown in Figure 5 contains one β-CD molecule and 7.2 water molecules, some of which are disordered over multiple positions. The guest molecule could not be modelled and so does not appear in the image.

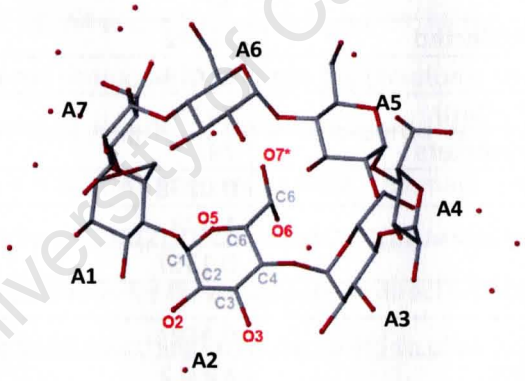

Figure 5: ASU of ZIDβCD. Hydrogens atoms have been omitted for clarity.

Figure 6 shows the electron density in the cavity of the host. These peaks appear in the difference Fourier map with a maximum value of only 0.71 e Å^{-3}. In the figure it can be seen that relative atom positions do not resemble those of a zidovudine molecule, which is evidence that the guest may be in several different orientations and impossible to model.

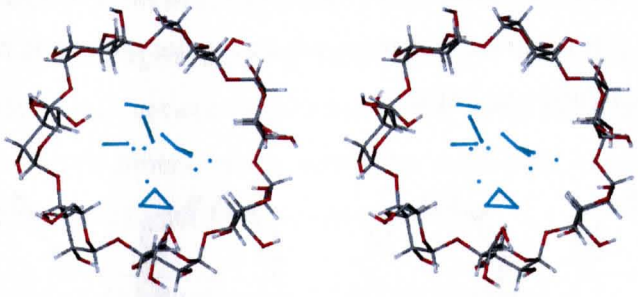

Figure 6: Stereodiagram showing the electron density in the host cavity.

Crystal packing

As mentioned earlier, the structure of **ZIDβCD** belongs to an isostructural series with space group and unit cell dimensions of a ~ 19 Å, b ~ 24.5 Å, c ~ 16 Å, β ~ 109°. Channel-type packing, the likes of which is seen in this isostructural series, has been described extensively in the literature.[13,14,15] As expected, the host molecules of **ZIDβCD** form dimers that are stacked one above the other along the *c*-axis, with a small degree of lateral shifting, making it possible for a guest molecule to be in a position anywhere along the length of a channel. The interplanar angle between the tail-to-tail cyclodextrins of adjacent dimers is 1.44° and the lateral shift between these two host molecules is 2.52 Å.

The diagrams in Figure 7 show packing as viewed down the *b*-axis, illustrating clearly the twofold axis of rotation that runs parallel to the *b*-axis and highlighting an individual dimer, as well as two adjacent dimer layers.

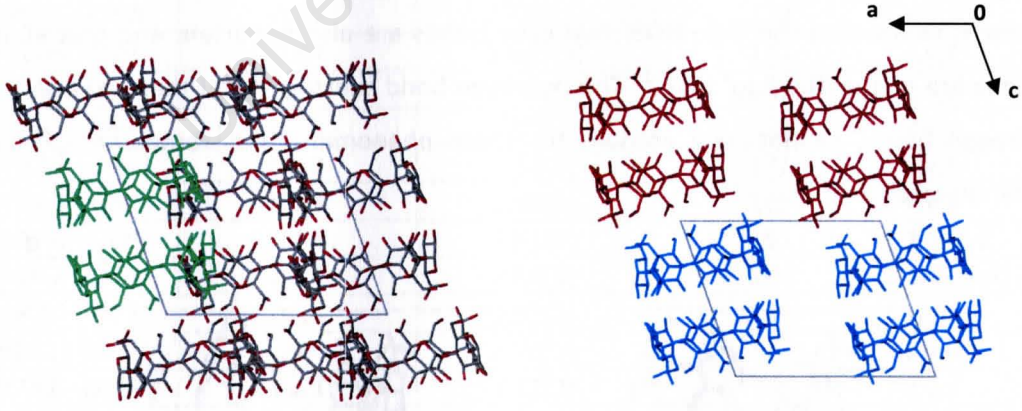

Figure 7: Packing of ZIDβCD as viewed down the *b*-axis. On the left, a single dimer is highlighted in green and on the right two layers of the dimer are shown in red and blue.

In Figure 8, a stereoview down the *c*-axis is provided, displaying the channels within which the guest molecules are included. It is apparent that there are also water molecules present in the channels. These water molecules are O9W and O10W.

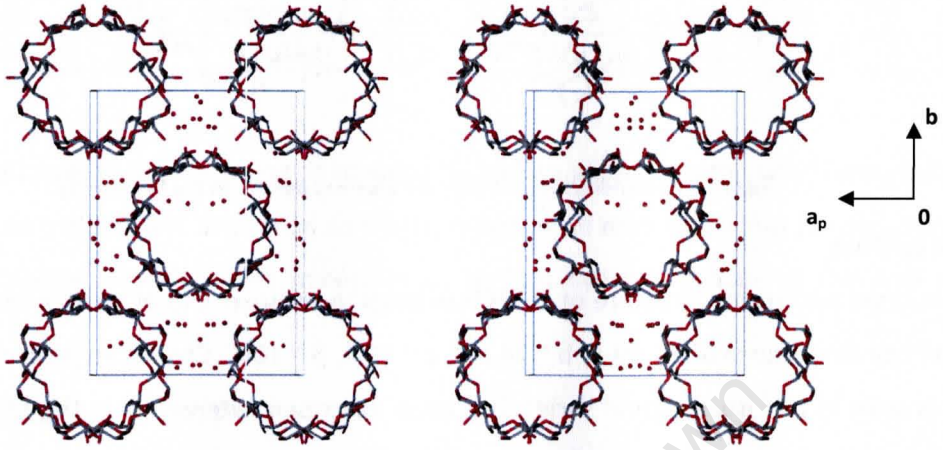

Figure 8: Stereoview down the *c*-axis, showing the packing of ZIDβCD.

Host-host hydrogen bonding

The heptagonal geometry of the host molecule is reinforced by a belt of intramolecular O2H···O3 hydrogen bonds at the secondary rim. These "flip-flop type" hydrogen bonds are a common occurrence, observable in most known β-CD structures.[16] Then, the principal hydrogen bonds that secure the dimer are intermolecular O2-H···O3′ hydrogen bonds, which are illustrated in Figure 9. The author is aware that the O-3···HO3′ hydrogen bonds are also important and that all of these interactions are of the 'flip-flop' type.[13] The hydrogen bond seeking model that was used to place the hydrogen atoms cannot fully account for these phenomena and sometimes produces an unrealistic representation.

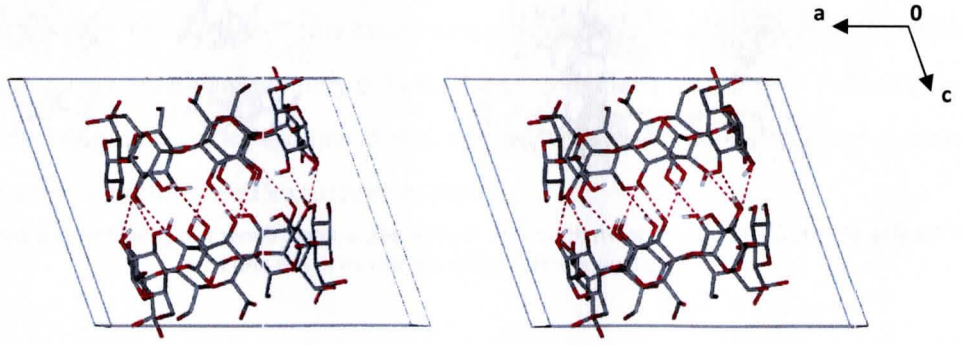

Figure 9: Stereoview down the *b*-axis showing hydrogen bonding that links the two cyclodextrins of the ZIDβCD dimer. Only the relevant hydrogen atoms are displayed.

Table 5 provides a summary of the hydrogen bonds that involve host molecules only. Details are given for three sets of hydrogen bonding interactions – intramolecular hydrogen bonds; intermolecular bonds that occur between molecules of the same dimer and intermolecular bonds between molecules of adjacent dimers, that is, within the same layer. There are no hydrogen bonds that directly connect molecules of adjacent layers of the dimer.

Table 5: A summary of ZIDβCD host-host hydrogen bonds and relevant parameters.

Interaction	Type	Number	Mean D···A distance (Å)*	Mean bond angle (°)
Intramolecular	O2-H···O3	7	2.81	153
Intermolecular (within dimer)	O2-H···O3′	4	3.08	146
	O3-H···O3′	3	2.80	170
Intermolecular (within layer)	O6-H···O6′	1	2.88	172
	C2-H···O3′	2	3.34	163

*The mean esd for all bond lengths is 0.01 Å

Hydrogen bonds involving water

The water molecules that are distributed over 15 sites are hydrogen bonded with each other, the host (and presumably the guest molecule). Parameters of the principal hydrogen bonds that have a host hydroxyl group behaving as the donor and a water molecule as the acceptor are given in Table 6.

Table 6: Parameters for interactions where a water molecule is the hydrogen bond acceptor.

Hydrogen bond	D-H (Å)	D···A (Å)	D-H···A (°)	Symmetry code
O6A1-H6A1···O1W	0.84	2.787(1)	172	x,y,z
O2A6-H2A6···O2W	0.84	2.655(9)	117	x,y,z
06A3-H6A3···O3W	0.84	2.748(1)	167	x,y,z
O6A7-H6A7···O6W	0.84	2.80(3)	151	x,y,z
O7A7-H7A7···O6W	0.84	2.52(3)	171	x,y,z
O6A6-H6A6···O8W	0.84	2.96(3)	166	x,y,z
O6A4-H6A4···O8W	0.84	2.81(3)	151	1-x,y,-z
O6A2-H6A2···O8W	0.84	2.84(3)	164	1/2-x,y-1/2,-z
O7A4-H7A4···O9W	0.84	2.93(3)	155	x,y,z
O2A2-H2A2···O13W	0.84	2.76(3)	122	x,y,z
O7A2-H7A2···O15W	0.84	2.52(3)	148	x,y,z

There are 23 close contacts between water molecules and oxygen atoms of the host with distances in the range 2.61-3.21 Å and a mean distance of 2.93 Å. There are 8 close contacts between adjacent water molecules with a distance range of 2.71-3.16 Å. The mean distance for the set of water-water close contacts is 2.88 Å.

The water molecules that are found in the interstitial cavity are represented in Figure 10. The magnified portion of the diagram has the water molecules on the left labelled. Those on the right of the diagram are related to the labelled atoms by a twofold symmetry axis running vertically through the middle of the image. Atoms O9W and O10W are positioned in the channels, O9W near the primary rim and O10W at the head-to-head interface of the dimer. O9W is in close contact with one of the host hydroxyl groups so it may be acting as bridge between host and guest, while O10W is not in close contact with any host molecules, so may be interacting with the disordered guest only.

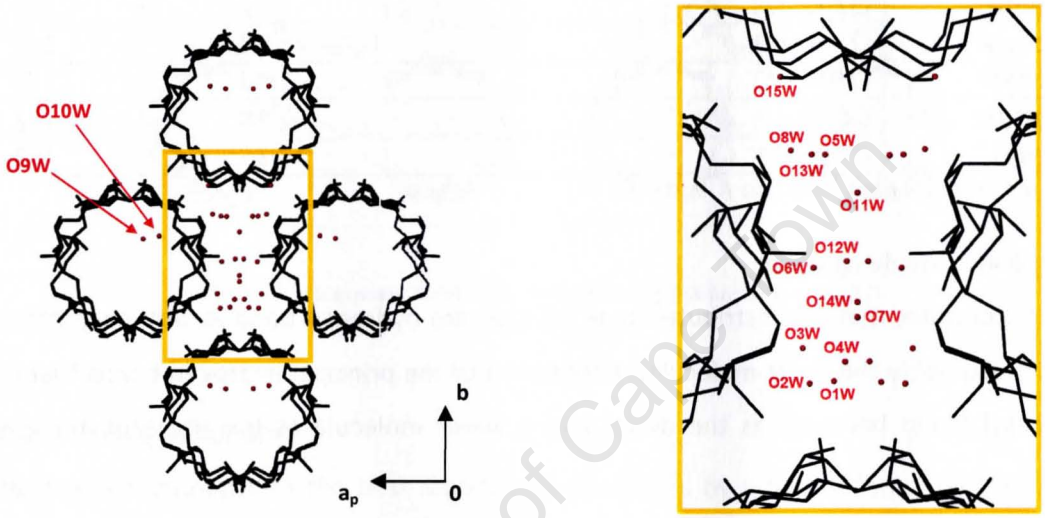

Figure 10: Diagram highlighting the positions of water molecules in the interstitial space. The twofold axis runs vertically through the centre of each image.

Host molecular geometry

Table 7 provides parameters (defined in Chapter 1) that describe the conformation of the host molecule. The I-values are the lengths of the sides of the O4-polygon, r is the centroid-O4 distance, ϕ the torsion angle O4(n-2)-O4(n-1)-O4(n)-O4(n+1) and d the deviation of each atom from the O4 mean plane. Also provided are the distances between consecutive inter-glucose hydroxyls of the secondary rim, D_3, and the tilt angles τ_1 and τ_2. The glucose residues are all found to be in the usual $^4C_1$ chair conformation The primary hydroxyl groups that have full site-occupancy are all in the (-)-gauche conformation. All of the three disordered primary hydroxyl groups have their major components in the (-)-gauche conformation and minor components in the (+)-gauche conformation. Figure 11 is a graphical representation of the pseudo heptagonal symmetry of the host. The predicted polygon angle for a regular heptagon is 128.6° and the maximum deviation from this value for the current host is -2.6°.

Table 7: Geometrical parameters for the host molecule of ZIDβCD.

Residue	I (Å)	r (Å)	d (Å)	ϕ (°)	D_3 (Å)	τ_1 (°)	τ_2 (°)
A1	4.315	5.028	-0.007(4)	1.4	2.892(7)	7.0(2)	8.5(1)
A2	4.459	4.954	-0.023(5)	0.4	2.832(9)	12.5(3)	14.5(2)
A3	4.335	5.087	0.021(5)	-1.5	2.787(1)	9.4(2)	11.6(3)
A4	4.396	5.088	0.002(4)	1.0	2.859(9)	7.2(3)	8.3(3)
A5	4.298	4.978	-0.003(4)	-0.5	2.756(7)	3.4(2)	4.6(2)
A6	4.443	4.974	-0.021(4)	1.2	2.753(9)	9.6(2)	9.7(1)
A7	4.350	5.147	0.032(4)	-2.1	2.779(9)	12.5(2)	13.2(1)

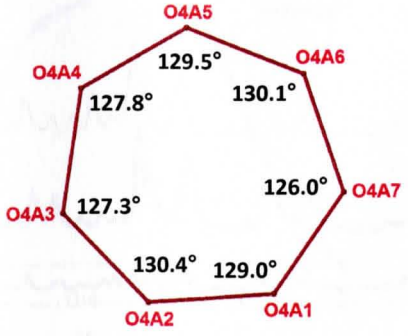

Figure 11: Diagram showing the O4(n-1)-O4n-O4(n+1) angles.

Comparative PXRD

Figure 12 provides a comparison of the experimental PXRD trace of **ZIDβCD** with the computed PXRD trace derived from the single crystal structure. The dominant peaks in the computed pattern match those in the experimental trace. Beyond ~13° there are only very low intensity peaks in the calculated trace, mainly because the guest molecule was not modelled.

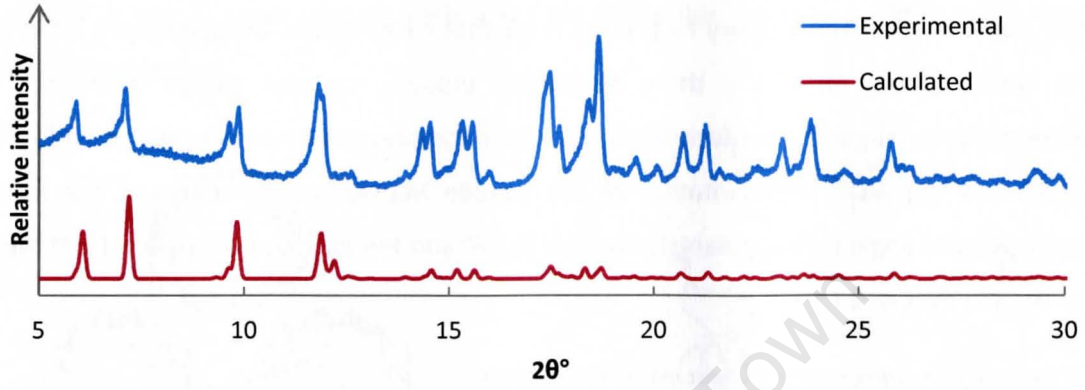

Figure 12: Experimental and calculated PXRD traces of ZIDβCD.

The experimental trace of **ZIDβCD** was also compared with the computed traces for the structures with CSD reference codes ZUZXOH and AJUVEG.[17] ZUZXOH is the structure from which coordinates of the host were 'borrowed' for the isomorphous replacement structure solution of **ZIDβCD**. AJUVEG is a structure from the same isostructural series, where the guest has been modelled. The peaks beyond ~13° in the experimental trace appear to match those of the calculated trace for AJUVEG.

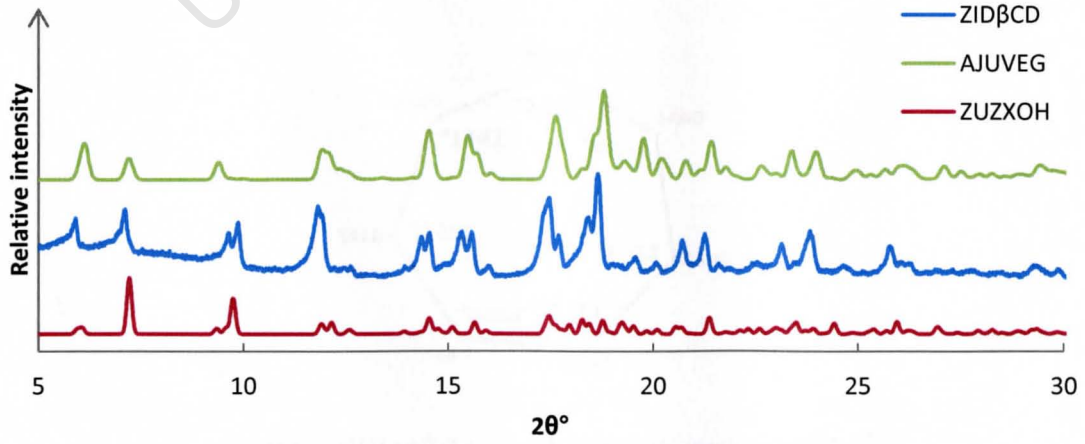

Figure 13: Experimental PXRD trace of ZIDβCD compared with the calculated traces for the reported structures with CSD reference codes ZUZXOH and AJUVEG. The reported structures belong to the same isostructural series.

Solution-state NMR spectroscopy

Continuous variation experiments (see Chapter 2) were conducted to characterise zidovudine-β-CD complexation in solution, with proton NMR spectroscopy used to track changes in chemical shifts due to complexation. Stock solutions of concentration 10 mM were prepared of zidovudine and β-CD in D_2O. These solutions were mixed to a constant volume of 2 cm^3 to give a series of 11 samples, each with R in the range 0-1, where R = $[X]/([H]_t+[G]_t)$. For each of the samples, a proton NMR spectrum was collected and the chemically induced shifts (CISs) of the host and guest protons determined. The resultant Job plots are illustrated in Figure 14. The CIS, Δδ, multiplied by the host/guest concentration [X] is plotted against R. For the zidovudine protons, significant shifting was observed for three protons, while for the host protons, only H3 exhibited shifting. Overall, the CISs were very small, which is indicative of weak complexation.

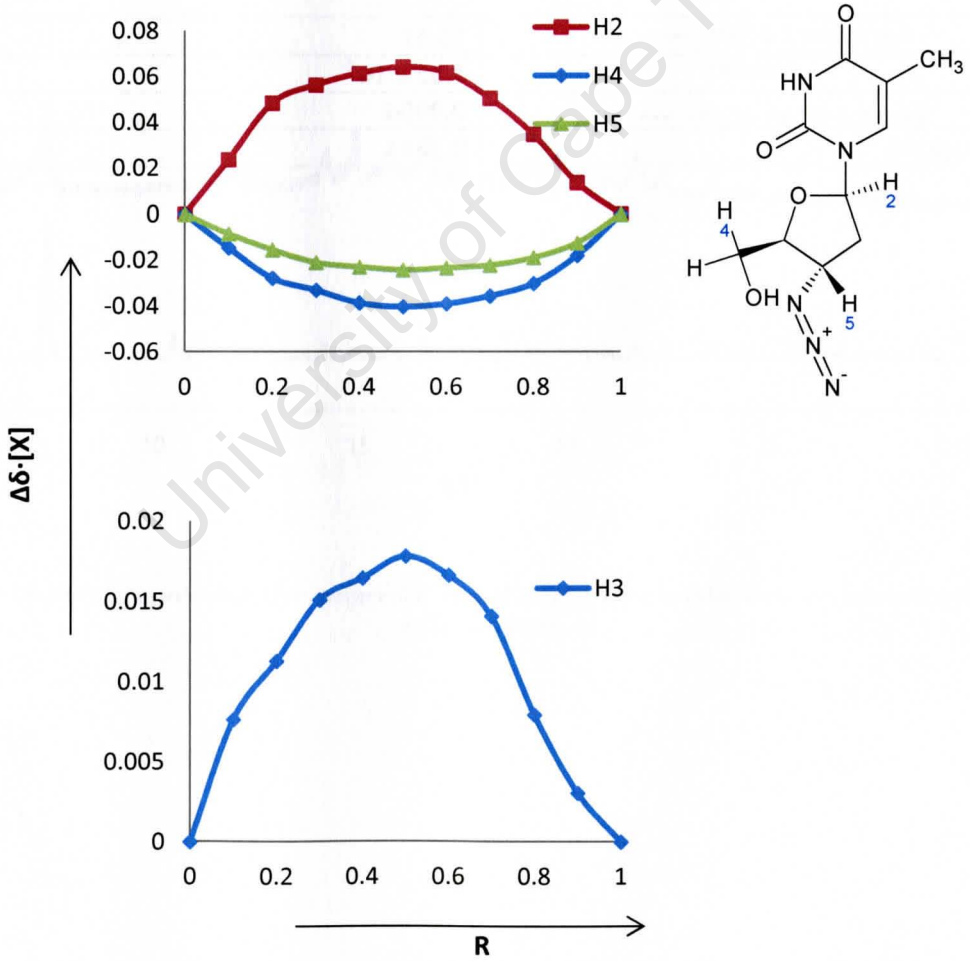

Figure 14: Job plots for zidovudine interaction with β-CD in solution.

The program ConstEQ[18] was used for an initial determination of the association constant but the fitting procedure did not converge. An additional continuous variation experiment was carried out where the concentration of zidovudine was fixed at 0.5 mM and the β-CD concentration varied from 0 to 12.5 mM so that the R values for the data set had a range of 0-25. Using this new dataset, the association constant was determined in ConstEQV (see Chapter 2), applying the regression analysis to the set of Δδ values for the zidovudine proton H2 (diagram in Figure 14). The results of these calculations are provided in Table 8. E is the error loss function and r is the correlation coefficient. The magnitude of Δδ·[X] reached a maximum at R = 0.5 for all four Job plots, which indicates that the stoichiometry in solution is 1:1. The association constant of 15.47 is extremely small, suggesting only very weak interaction between the host and guest. Given that the H3 host protons were shifted the most in the original continuous variation experiment, the interaction most likely occurs at the secondary rim.

Table 8: Binding parameters for ZIDβCD in solution determined using ConstEQV.

K	15.47
E	1.52×10^{-6}
r	0.9994
ΔδH2 (ZID; ppm)	0.2641

γ-Cyclodextrin Inclusion Complex

An inclusion complex (**ZIDγCD**) of zidovudine with γ-CD was prepared by kneading. All of the attempts to produce the complex by co-precipitation and slow cooling failed. These experiments yielded only crystals of the free host. The successful preparation method entailed 12 mg (0.045 mmol) of zidovudine and 64 mg (0.045 mmol) of γ-CD, combined in a mortar. The mixture was kneaded for 30 min, adding drops of MilliQ water periodically to maintain a wet paste-like consistency.

Comparative PXRD

The material obtained from kneading was subjected to PXRD analysis and the resultant trace compared directly with a trace representing the most common known packing arrangement for γ-CD complexes (Figure 15). Since the major features of both patterns are identical, it can be deduced that the **ZIDγCD** complex is of the channel-type, crystallising in the space group $P42_12$.

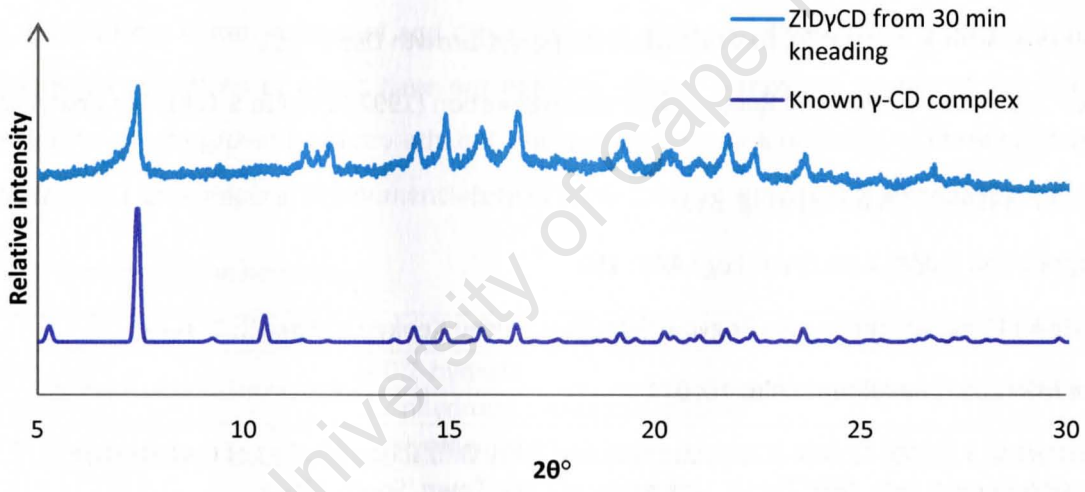

Figure 15: PXRD comparison of the experimental trace of ZIDγCD and a calculated trace representing known γ-CD complexes.

References

1 http://www.fda.gov/ForConsumers/ByAudience/ForPatientAdvocates/HIVandAIDSActivities/ucm151074.htm (accessed on 20 July 2011)

2 O' Neil MJ, Heckelman PE, Koch CB, Roman KJ (eds) (2006) Merck Index, 14th edition, New Jersey, USA

3 Gennaro AR (1995) Remington: The Science and Practice of Pharmacy, 19th edition, vol 2. Mack Publishing, Easton, Pennsylvania, USA, p 1336

4 Birnbaum GI, Giziewicz J, Gabe EJ, Lin T-S, Prusoff WH (1987) Can J Chem 65: 2135

5 Camerman A, Mastraopaolo D, Camerman N (1987) Proc Natl Acad Sci USA 84: 8239

6 Dyer I, Low JN, Tollin P, Wilson HR, Howie RA (1988) Acta Crystallogr C44: 767

7 Raviolo MA, Williams PAM, Etcheverry SB, Piro OE, Castellano EE, Gualdesi MS, Briñón MC (2010) J Mol Struct 970: 59

8 Van Roey P, Salerno JM, Duax WL, Chu CK, Ahn MK, Schinazi RF (1988) J Am Chem Soc 110: 2277

9 Bhatt PM, Azim Y, Thakur TS, Desiraju GR (2009) Cryst Growth Des 9: 951

10 XPREP, Data Preparation and Reciprocal Space Exploration (1997) Version 5.1, Bruker Analytical X-ray Systems

11 Barbour LJ (1999) J Appl Cryst 32: 351

12 Sheldrick GM (2008) Acta Crystallogr A64: 112

13 Harata K (1993) Seimei Kogaku Kogyo Gijutsu Kenkyushu Kenkyu Hokoku 1: 1

14 Caira MR (2001) Rev Roum Chim 46: 371

15 Lubhelwana S (2005) Crystal Isostructurality and X-ray Diffraction Studies of Cyclodextrin Inclusion Compounds, MSc Thesis, University of Cape Town, South Africa

16 Mentzafos D, Mavridis IM, Le Bas G, Tsoucaris G (1991) Acta Crystallogr B47: 746

17 Cambridge Structural Database and Cambridge Structural Database System (Feb, 2011) Version 5.32, Cambridge Crystallographic Data Centre, University Chemical Laboratory, Cambridge, England

18 Floare C, Balibanu F, Bogdan M (2005) Studia UBB, Physica, Special Issue L. 4a: 451

Chapter 6: Lamivudine

Introduction

Lamivudine (2*R*,5*S* enantiomer) is a chiral drug. At 70 mg cm^{-3}, the aqueous solubility of lamivudine is far greater than those of nevirapine and efavirenz. Still, an improvement in solubility is desirable. In addition there are other physicochemical properties like thermal stability, hardness and compressibility that may be enhanced in some way by supramolecular modification. Thus, lamivudine was subjected to various attempts at preparing novel co-crystals and cyclodextrin inclusion complexes, with the expectation that the experiments might result in these desired forms or new polymorphs, hydrates, solvates or salts.

Existing forms

Crystal structures have been reported for pure lamivudine and two lamivudine hydrates. The first of these hydrates has five lamivudine molecules in the asymmetric unit and a lamivudine-water ratio of 5:1, grown from water, methanol and other aqueous alcohols.[1] The second is a hemihydrate, the preparation conditions of which have not been described. Tetragonal crystals of the solvent-free lamivudine can be grown from dry ethanol, n-propanol and some mixtures of these with non-polar solvents.[2] For convenience, the nomenclature in Table 1 will be used in reference to these forms.

Table 1: Common forms of lamivudine.

Label	Description	Reference
Form I	0.2-hydrate	1
Form II	Anhydrous, tetragonal crystals	1
Form III	Hemihydrate	2

Lamivudine salts and co-crystals have been reported in the literature. The salts are lamivudine maleate, lamivudine saccharinate and lamivudine 3,5-dinitrosalicylate while the co-crystal is a monohydrated lamivudine-zidovudine co-crystal. There is also a description of a "co-crystal" with 4-quinoline, which by definition in this thesis is a solvate.[3,4]

A complex of lamivudine with β-CD has been claimed by Lloret Perez and co-worker.[5] The patent describes preparation by kneading of at least 0.5 molar equivalents of a cyclodextrin (primarily β-CD but other cyclodextrins are encompassed by the patent) with one molar equivalent of lamivudine. A PXRD trace (see Figure 31 in this chapter) was provided as evidence of the patented form. At the time of writing there were no other reported accounts of lamivudine complexes with native or derivatised cyclodetrins.

Present study

It was confirmed that the bulk material that we were using was the reported anhydrous Form II by comparing the PXRD pattern of our starting material with those of the known forms. The same batch was tested for purity by NMR analysis and DSC (to confirm melting point). Both tests were consistent with a high degree of purity of the starting material.

The present study reveals six novel pharmaceutically acceptable, multi-component molecular crystals, two of which are cyclodextrin inclusion complexes. Note that the term 'multi-component molecular crystal' is employed here in reference to co-crystals *and* salts. Two pharmaceutical salts were analysed by single crystal X-ray diffraction to determine their crystal structures. Of the cyclodextrin complexes, only that with β-CD could be prepared as single crystals and the X-ray structure solved. The γ-CD complex of lamivudine could only be produced by kneading.

Co-crystal Screening

Again, co-formers were chosen on the basis of hydrogen bonding groups that could potentially form robust synthons with lamivudine. The lamivudine molecule possesses a number of features that suggest it would be well-suited to this type of modification. Its molecular structure is presented below with the important potential hydrogen bond donor/acceptor groups highlighted.

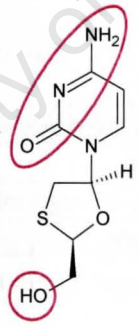

Figure 1: Lamivudine with potential hydrogen bonding groups highlighted.

Having encountered salt forms of this API in the literature, it was important to consider the pK_a of the co-former. In general, co-formers were not excluded on the basis of an unfavourable pK_a value but emphasis was certainly placed on those with more suitable pK_a constants during the screening process.

The outcomes of co-crystal screening with lamivudine are summarised in Table 2. Several hits resulted from the initial dry co-grinding experiments, so this method was employed extensively. A few liquid-assisted grinding experiments were also carried out, as well as slow evaporation with co-

formers of a variety of pK_a constants in attempts to produce co-crystals as opposed to salts. Nevertheless, novel salts were identified and studied.

Table 2: Summary of lamivudine co-crystal screening experiments and their outcomes.

Method	Co-formers	Hits	Pure salt/co-crystal
Dry co-grinding	30	10	4
Ethanol LAG	3	0	0
Slow evaporation	10	4	4

A number of our attempts to grow lamivudine co-crystal and salt single crystals produced single crystals of the host in reported Forms I and II. Form II crystallised when a mixture of ethanol and propanol with less polar solvents like pentane, hexane or cyclohexane was used. None of our experiments yielded crystals of Form III, the hemihydrate.

LAMSUC: product of reaction between lamivudine and succinic acid

Preparation of the reaction product

A new phase, referred to here as **LAMSUC** is produced when combining lamivudine with succinic acid by co-precipitation or dry co-grinding. One reliable method of preparation involved 22 mg (0.096 mmol) lamivudine and 11 mg (0.093 mmol) succinic acid dissolved in 1.5 cm^3 1-propanol at ~40 °C. The resultant solution was allowed to cool spontaneously to room temperature and slowly evaporate. Fibrous crystals appeared after approximately 10 days.

Identification

LAMSUC was identified during the dry co-grinding screening stage. A small equimolar mixture of lamivudine and succinic acid was co-ground for 5 min and the resultant material subjected to PXRD analysis. In Figure 2 it can be seen that the product of co-grinding is not a physical mixture of starting reagents. Some peaks in the trace for **LAMSUC** appear to coincide with peaks in the pure lamivudine trace but it will be shown that these are not due to excess lamivudine in the product.

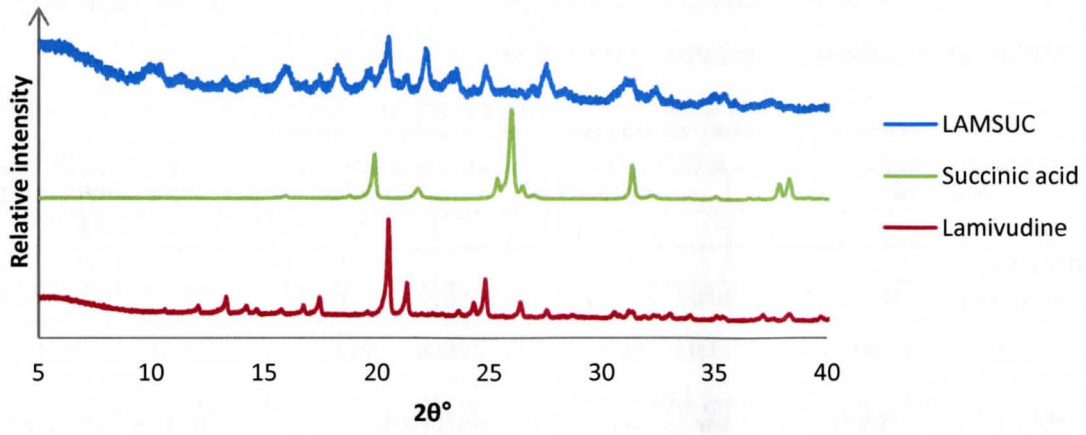

Figure 2: The PXRD trace of LAMSUC compared with traces of free succinic acid and lamivudine.

The products obtained from dry co-grinding and slow evaporation were compared by PXRD analysis (Figure 3) to confirm that they represented the same phase. Indeed it can be seen that the peaks of the two traces match and so it was concluded that **LAMSUC** may be prepared by either method.

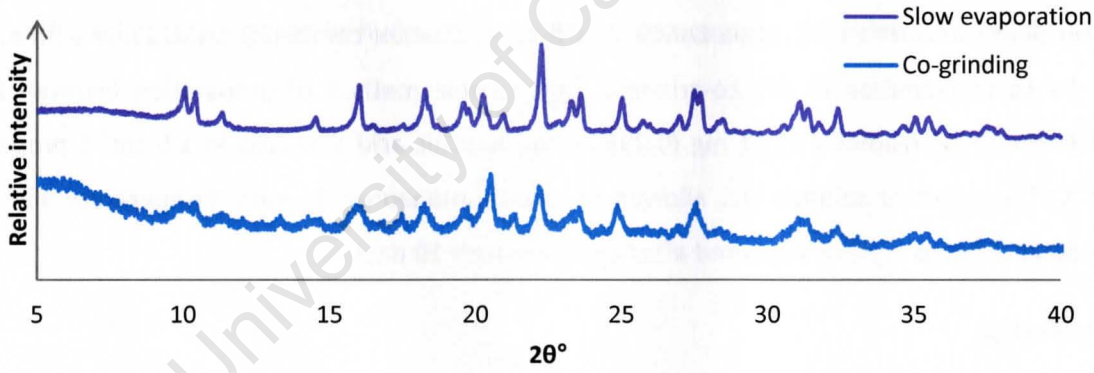

Figure 3: PXRD Comparison showing LAMSUC produced by dry co-grinding and slow evaporation.

Thermal analysis

HSM

A clump of **LAMSUC** crystallites was heated at a rate of 10 K min^{-1} during HSM analysis. The selected photographs in Figure 4 show the loss of solvent vapour, onset of melting, the melted product and discolouration at the onset of degradation. The onset of melting at 131 °C coincides with the initial appearance of bubbles that correspond with solvent loss. Given the fact that **LAMSUC** is obtainable

from neat co-grinding, it may be deduced that the solvent that is incorporated is water. Atmospheric water vapour is incorporated during the dry co-grinding process.

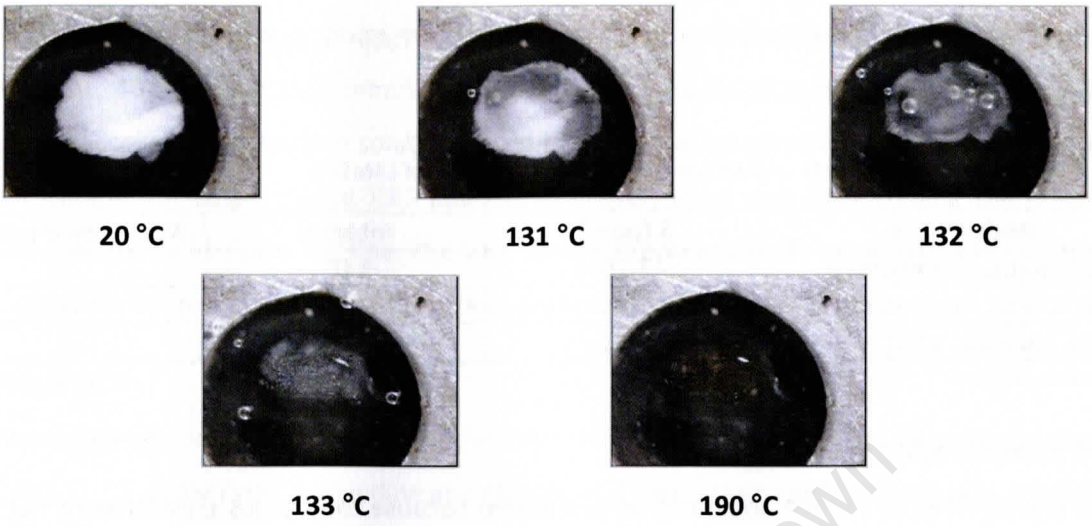

Figure 4: Representative HSM photographs for LAMSUC.

TGA and DSC

The DSC and TGA traces in Figure 5 were recorded using a sample obtained by slow evaporation and show what appears to be a two-step loss of solvent. The first stage of solvent loss occurs over a broad range of 60-120 °C. The sample was dried very well on filter paper but it is still possible that this initial mass loss relates to solvent adsorbed on the crystallite surfaces. The second mass loss is sharper at onset 123 °C with peak minimum 124 °C. This event occurred identically for samples obtained from two slow evaporation experiments that employed different solvents (ethanol and 1-propanol) with different boiling points, which is further evidence that the solvent present in **LAMSUC** is water.

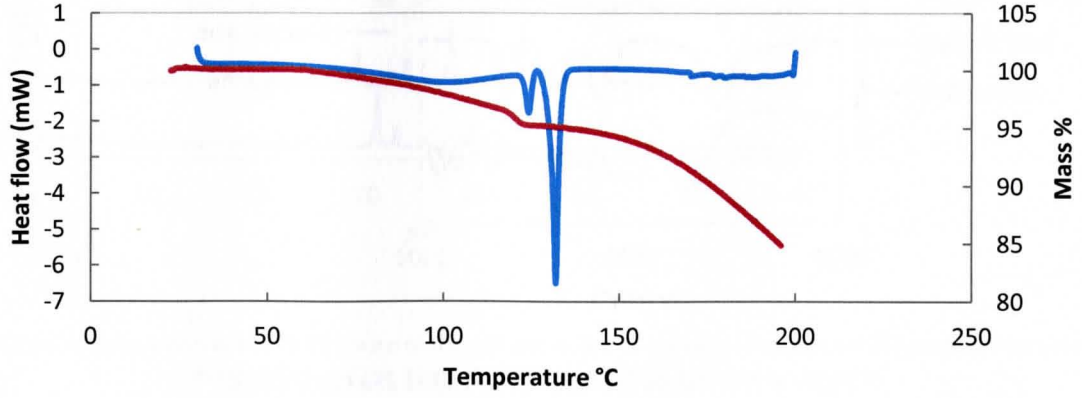

Figure 5: DSC (blue) and TGA (red) traces for LAMSUC.

NMR spectroscopy

Proton NMR spectroscopy was used to determine the stoichiometry of **LAMSUC**. The sample for analysis was taken from a batch prepared by slow evaporation from 1-propanol. The resultant spectrum, an abbreviated summary of which is provided in Table 3, suggests a lamivudine-succinic acid stoichiometric ratio of 1:1.

Table 3 Summary of the NMR data used to determine the stoichiometry of LAMSUC.

Assignment	δ (ppm)	Integral	Normalised integral
CH (aromatic, lamivudine)	7.79	1.0*	1
CH (aromatic, lamivudine)	5.74	1.0	1
2 x CH_2 (succinic acid)	2.41	4.0	1

*Reference integral

FTIR spectroscopy

Single crystal X-ray diffraction could not be performed because the fibrous crystals were not large enough. Infrared spectroscopy (Figure 6) was employed in determining whether **LAMSUC** was a salt or co-crystal; in other words, to determine whether or not an acid-base reaction had taken place during the formation of this new phase. It can be seen that there are prominent peaks, associated with carbonyl stretching, at 1713 and 1651 cm^{-1}. The absence of a strong carboxylate peak at around 1500 cm^{-1} suggests that no acid-base reaction took place in the formation of **LAMSUC**. Thus, the IR spectrum indicates the species is most likely a co-crystal and not a salt but further investigation is necessary to confirm this conclusion.

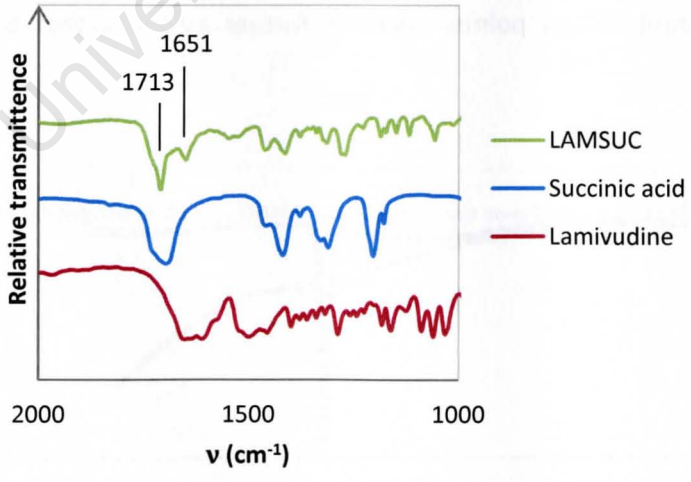

Figure 6: FTIR spectra of LAMSUC, lamivudine and succinic acid.

LAMGLT: product of reaction between lamivudine and glutaric acid

Preparation of the reaction product

LAMGLT was grown by slow evaporation from an acetonitrile solution. The solution was prepared by dissolving, at ~40 °C, 23 mg (0.10 mmol) lamivudine and 13 mg (0.098 mmol) glutaric acid in 2 cm^3 of the solvent. Slow cooling, another solution-based method, was employed in an effort to grow larger crystals suitable for single crystal XRD analysis. However, even with slow cooling the crystalline material produced was extremely fine. The slow cooling preparation was carried out over a period of three days with the solution cooled from a temperature of ~60 °C.

Identification

The lamivudine-glutaric acid reaction product was identified during the dry co-grinding stage of screening. In 1:1 molar ratio, lamivudine and glutaric acid were co-ground for 5 minutes. After only a few minutes of grinding, the consistency of the mixture changed – the co-ground material became sticky and quite difficult to remove from the mortar. PXRD analysis (Figure 7) indicated that a reaction had taken place since the product of co-grinding was not a physical mixture of the starting reagents. A later PXRD comparison with the product obtained by slow evaporation (also shown in Figure 7) revealed that the co-grinding product was a mixture of phases that contained **LAMGLT**.

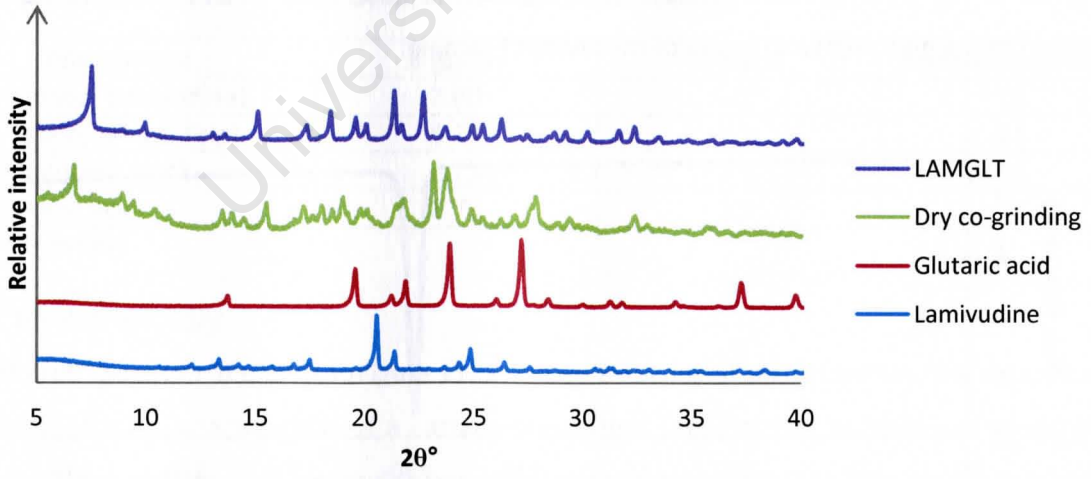

Figure 7: Comparison of the PXRD traces of the product of dry co-grinding (5 min), LAMGLT prepared by slow evaporation and the starting reagents – glutaric acid and lamivudine.

Thermal analysis

HSM

A clump of the fine, thread-like crystals of **LAMGLT** was analysed by hot stage microscopy. The crystals were heated at a rate of 10 K min^{-1}. The photographs in Figure 8 provide evidence of melting at an onset temperature of 137 °C. The melting point is very sharp – the crystals are completely melted at 138 °C.

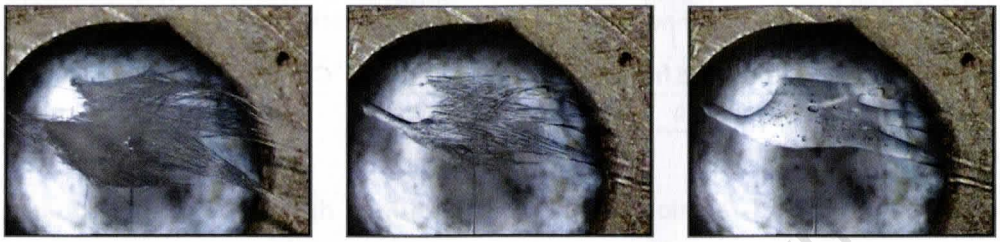

Figure 8: Representative photographs for the HSM analysis of LAMGLT.

DSC and TGA

The samples used for DSC and TG analysis were prepared by slow evaporation. DSC (Figure 9) revealed melting at onset 127.3 °C with a peak minimum at 129.0 °C. The hot stage does not heat efficiently at its centre, which accounts for the deviation between values obtained by the two different methods. The melting point determined by DSC analysis is far more accurate. This sharpness of the melting endotherm and the fact that no other thermal events are evident is an indication of the high degree of purity of the **LAMGLT** sample.

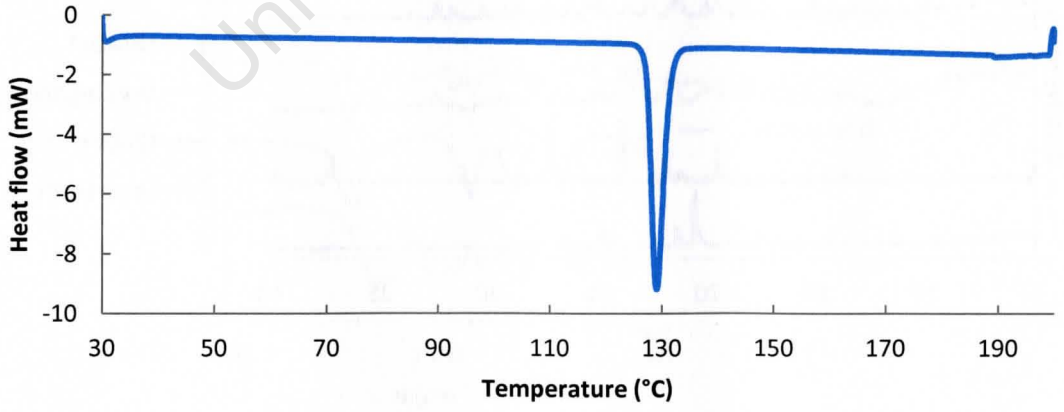

Figure 9: DSC trace for LAMGLT.

TGA (Figure 10) confirmed the absence of included solvent and showed that the sample begins to degrade at 170 °C.

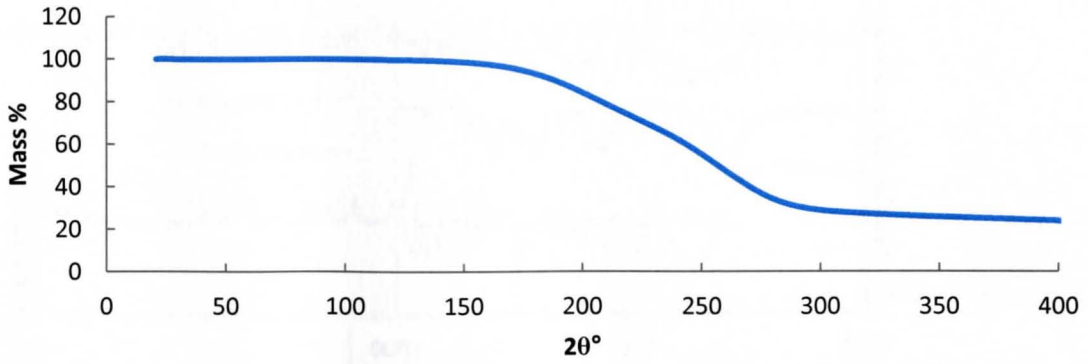

Figure 10: TGA trace for LAMGLT.

NMR spectroscopy

A sample of **LAMGLT** prepared by slow evaporation was removed from the mother liquor and dried on filter paper before being dissolved in $CDCl_3$ and analysed by proton NMR spectrocopy. The results of the experiment were used to determine the stoichiometry of the reaction product, which is 1:1 according to the representative set of data provided in Table 4.

Table 4: Selected proton NMR signals for LAMGLT confirming 1:1 stoichiometry.

Assignment	δ (ppm)	Integral	Normalised integral
C<u>H</u> (aromatic, lamivudine)	7.80	1.0*	1
C<u>H</u> (cytosine, lamivudine)	6.21	0.9	1
2 x C<u>H</u>$_2$ (glutaric acid)	2.25	3.8	1
C<u>H</u>$_2$ (glutaric acid)	1.73	1.9	1

*Reference integral

FTIR spectroscopy

The infrared spectrum of LAMGLT (Figure 11) provided evidence of salt formation. The existence of a peak at 1539 cm^{-1}, characteristic of a carboxylate stretch suggests that at least one of the acidic protons of the glutaric acid molecules has been transferred to the API. The absorption peak at 1674 cm^{-1} is evidence that a carbonyl group is still present. This information does not allow us to predict the precise extent of proton transfer, given the existence of a C=O function on the lamivudine molecule and the density of peaks in this region of interest, but it can be deduced that at least one acid-base reaction has taken place. Thus, **LAMGLT** is most probably a salt and not a co-crystal.

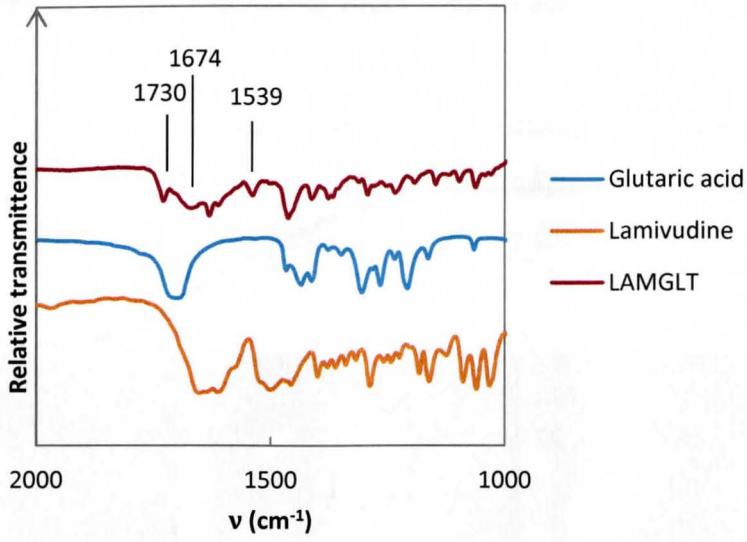

Figure 11: FTIR spectra of LAMGLT, Glutaric acid and Lamivudine.

LAMOXL: lamivudine-oxalic acid salt

Preparation of the salt

The lamivudine-oxalic acid 2:1 salt **LAMOXL** was prepared by co-precipitation from a solution of 0.11 mmol (25 mg) lamivudine and 0.055 mmol (7 mg) oxalic acid dihydrate in 1 cm^3 of 50:50 v/v ethanol in water. The solution was prepared by dissolving the starting reagents at 50 °C with continuous stirring. It was allowed to cool spontaneously and slowly evaporate. Crystals of the salt formed within one day. The salt could also be prepared by slow evaporation from a solution of 50:50 v/v 1-propanol in water.

Grinding experiments did not produce **LAMOXL**. The product of different co-grinding experiments was affected by the reagent stoichiometry, the solvent added and period of grinding. Thus, these were not investigated further. All of the material used for analysis was prepared by the reliable slow evaporation method described above.

Identification

The initial screening experiment that suggested the potential existence of a lamivudine-oxalic acid co-crystal or salt involved neat co-grinding of a small equimolar mixture of lamivudine and oxalic acid dihydrate. Figure 12 contains the PXRD trace of the resultant material compared with traces for the starting reagents. The pattern for the material obtained from co-grinding exhibits peaks that are represented in the traces for the starting reagents, indicating that it is a mixture of phases that probably contains unreacted lamivudine and oxalic acid dihydrate. The time of grinding was

extended and the molar ratio varied in the hope of finding a method that produced a quantitative conversion to the new phase, but in each case PXRD and thermal analysis revealed that the product was a mixture of forms. Nevertheless, this initial set of tests suggested a co-crystal or salt of lamivudine could be prepared using oxalic acid as the partner molecule.

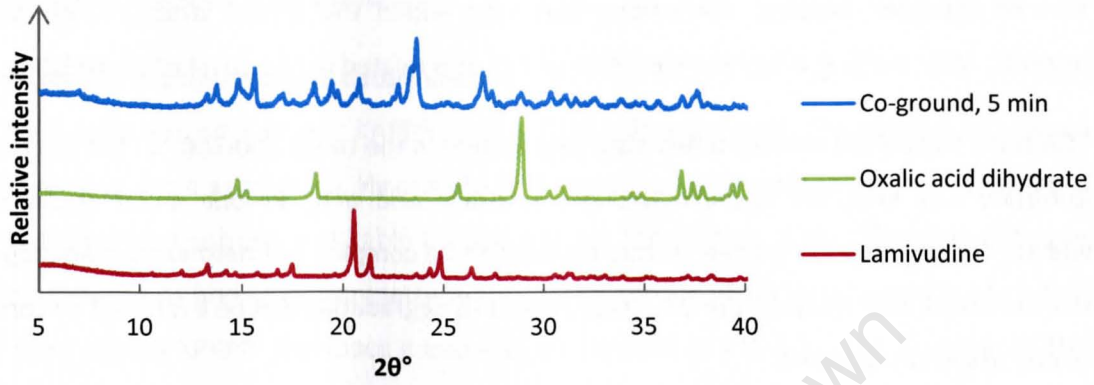

Figure 12: PXRD trace of co-ground lamivudine and oxalic acid dihydrate. The product trace is compared here with traces of the pure starting reagents.

Thermal analysis

HSM

The hot stage microscope is used to observe thermal events directly. A large portion of one of the **LAMOXL** crystals was cut for the analysis. Representative photographs are shown in Figure 13 for the onset of melting, start of degradation and the further degradation. The first sign of melting occurs at 210 °C. Thereafter, at approximately 216 °C the crystal becomes discoloured and bubbles begin to form rapidly. Bubbles are most often associated with the loss of solvent vapour but the high temperature at which they are released from **LAMOXL** suggests the gas is more likely a product of degradation.

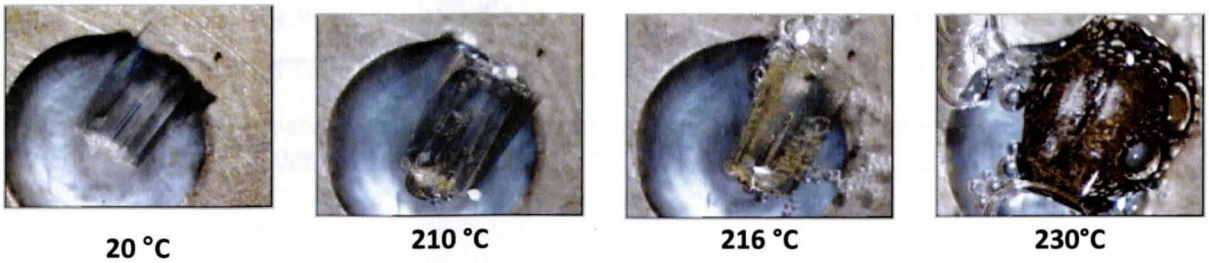

Figure 13: Representative HSM photographs for LAMOXL.

DSC and TGA

DSC analysis (Figure 14) provided confirmation of the purity of the co-crystal, since no heat transfer was apparent that could be associated with melting of the pure co-former or free API. The unique melting point of the product is much higher than for both starting components, an expected result of salt formation. The sum of electrostatic interactions of the salt product is evidently greater than the sum of hydrogen bonding interactions that exist within the crystal structures of the free components. After melting, a broad endotherm occurs. It is related to the onset of degradation.

The TGA trace (Figure 15) exhibits a two-step degradation in the range 200-300 °C. The fractions do not correlate well with, for example the loss of oxalic acid only, or one molar equivalent of lamivudine. The degradation process is thus assumed to be complex and neither the two-step mass loss nor the broad endotherm in the DSC trace related to degradation can be explained by complete loss of one of the components.

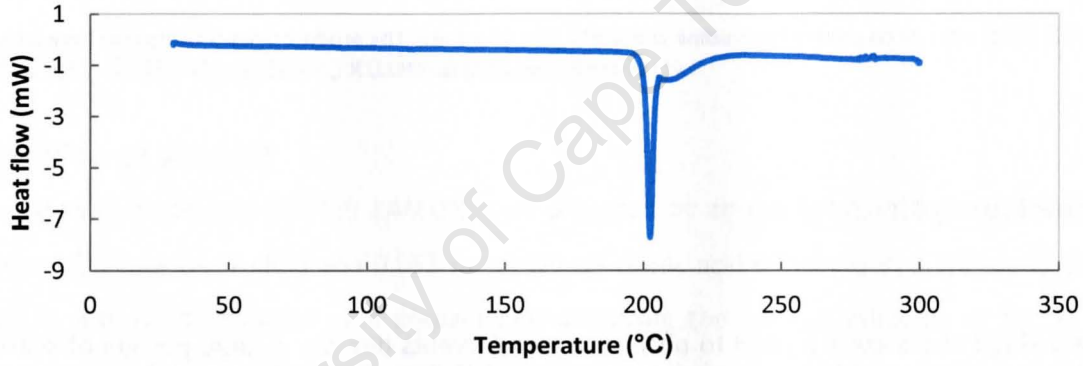

Figure 14: DSC trace for LAMOXL.

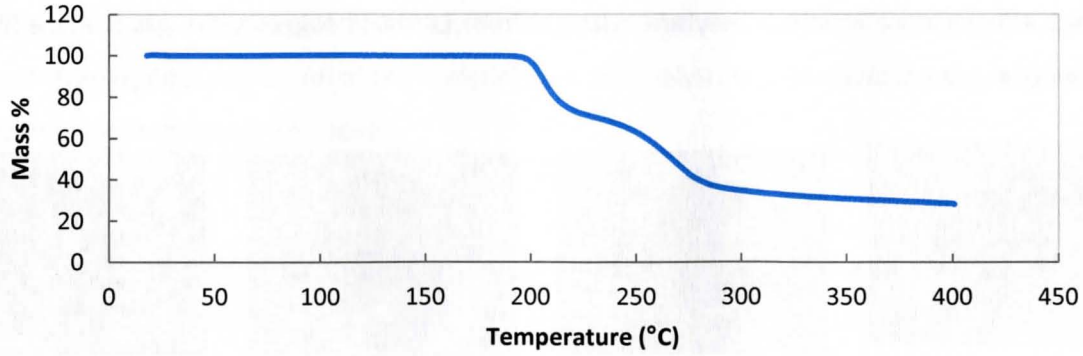

Figure 15: TGA trace for LAMOXL.

In summary, the melting point of the new species is significantly higher than the melting points of both free components. The degradation is a complex two-step process, the onset of which produces a broad endotherm in the DSC trace immediately after melting. The second step of degradation could not be observed using HSM or DSC but TGA revealed that it begins at ~250 °C.

Single crystal X-ray diffraction

Data-collection and space group determination

Data were collected on a Bruker KAPPA APEX II DUO diffractometer. The striated rectangular rod crystals grew as large aggregates. Having placed a sample under Paratone oil to prevent the loss of potentially included solvent, a suitable portion was cut for analysis. X-ray diffraction data gave the unit cell dimensions and Laue symmetry mmm, characteristic of the orthorhombic crystal system. Using the program XPREP[6] the space group was determined as $P2_12_12_1$. The program LAYER[7] was employed to confirm this assignment – the following systematic absences were observed: $hkl: none; h00: h = 2n + 1; 0k0: k = 2n + 1; 00l: l = 2n + 1.$

Structure solution and refinement

SHELXS-97[8] was employed for the structure solution of **LAMOXL**. The asymmetric unit contains two lamivudine ions and one oxalate ion. Following their location, non-hydrogen atoms were assigned and refined isotropically on F^2 in SHELXH-97.[8] Upon confirming acceptable isotropic temperature factors, the atoms were refined anisotropically. It was clearly evident from the difference Fourier map that the oxalic acid had been deprotonated to yield a dicarboxylate ion, while each lamivudine molecule had been protonated at the N3-position. Measuring the carboxylate C-O distances, which were significantly alike with an average value of 1.256 Å, provided further confirmation of the acid-base reaction. Hydrogen atoms were placed by means of a riding model, except for those of the primary amines (position N8), which were placed directly, according to peak positions in the difference Fourier map. The N-H distances of these two groups (at N8) were constrained at 0.88 Å using a DFIX instruction with σ = 0.01 Å. After refinement, the N-H distances ranged from 0.875 to 0.885 Å and each of the hydrogen atoms had a temperature factor in the range 0.032-0.048 $Å^2$. Each hydrogen atom placed using a riding model was assigned an isotropic temperature factor of 1.2 times that of its parent atom. The crystal structure and refinement parameters are listed in Table 5.

Table 5: Data-collection and refinement parameters for LAMOXL.

Formula unit	$2(C_8H_{12}N_3O_3S^+)\ (C_2O_4^{2-})$
Formula mass (g mol^{-1})	548.55
Crystal system	Orthorhombic
Space group	$P2_12_12_1$
a (Å)	6.6768(5)
b (Å)	9.1379(7)
c (Å)	37.688(3)
α (°)	90
β (°)	90
γ (°)	90
Volume ($Å^3$)	2299.4(3)
Z	4
$Density_{calc}$ (g cm^{-3})	1.585
μ(MoKα) (mm^{-1})	0.301
F(000)	1144
Crystal size (mm^3)	0.20 x 0.18 x 0.10
Temperature (K)	173(2)
Range scanned θ (°)	1.89-26.37
Index ranges	h: -9, 9 ; k: -15, 15; l:-15, 15
ϕ and ω scan angle (°)	0.5
Total number of frames	1520
Dx (mm)	48
Total number of reflections collected	22292
Number of unique reflections	3906
Number of reflections with $I > 2\sigma(I)$	2999
Number of least-squares parameters	343
R_{int}	0.0391
S	1.020
R_1 ($I > 2\sigma(I)$)	0.0413
Number of reflections omitted	4
wR_2	0.0835
Weighting scheme parameters	a = 0.0427, b = 0.2685
$(\Delta/\sigma)_{mean}$	<0.001
Δρ excursions (e $Å^{-3}$)	0.301, -0.274
Absolute structure parameter[9]	-0.07(5)

Molecular structure

The asymmetric unit consists of one oxalate ion of formal charge 2- and two crystallographically independent lamivudine cations. Both lamivudine ions in the asymmetric unit possess a proton that has been fully transferred to the nitrogen atom N3.

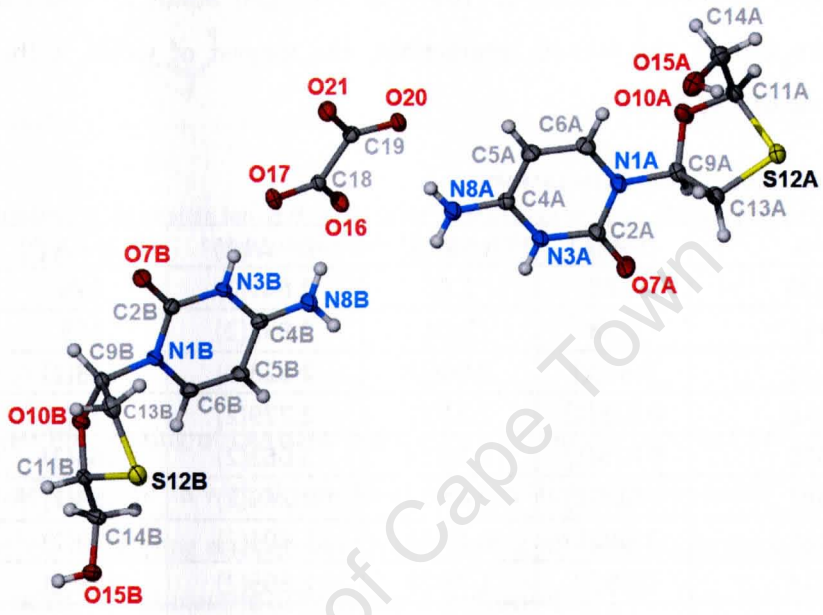

Figure 16: Asymmetric unit of LAMOXL

The deprotonation of both carboxylic acid groups is consistent with the tentative model that predicts salt or co-crystal formation based on the ΔpK_a of API and partner molecule, but only because the ΔpK_a values for the present systems fall within the range $0 < \Delta pK_a < 3$ where the model predicts that *either* a co-crystal *or* a salt will form. In the case of oxalic acid, the values are pK_{a1}=1.3 and pK_{a2}=4.1. The pK_a of lamivudine is 4.3, so the values of ΔpK_a with respect to both proton transfer steps are 3.0 and 0.2. The list of C-O bond distances in Table 6 for the oxalate ion confirms that both carboxylic acid groups were deprotonated.

Table 6: C-O bond distances for the oxalate ion of LAMOXL.

Bond	Distance (Å)
C18-O16	1.250(2)
C18-O17	1.263(2)
C19-O20	1.249(2)
C19-O21	1.261(2)

Hydrogen bonding

There are no strong hydrogen bonds between adjacent lamivudine molecules. Within the framework, lamivudine ions are linked only via oxalate ions. The parameters for all of the hydrogen bonding interactions are provided in Table 7. The mean bond length for O-H···O hydrogen bonds is 2.80 Å, while the average of the N-H···O hydrogen bond distances is 2.88 Å. Short D···A distances are observed, as expected, for the charge-assisted hydrogen bonds. For example, N8B-H8D···O16 has a hydrogen bond length of 2.655(2) Å. The only hydrogen bonds between adjacent lamivudine molecules are C-H···O and N-H···O interactions, the longest of which is the C14A-H14B···O15B hydrogen bond of 3.433(2) Å.

Table 7: Hydrogen bond parameters for LAMOXL

D-H···A	D-H (Å)	H···A (Å)	D···A (Å)	D-H···A (°)	Symmetry code
N3A-H3A···O20	0.88	1.96	2.841(2)	176	-1+x,y,z
N3B-H3B···O17	0.88	2.04	2.858(2)	155	x,y,z
N8A-H8A···O21	0.87(2)	2.00(2)	2.823(2)	158(2)	-1+x,y,z
N8A-H8B···O16	0.875(1)	2.21(2)	2.779(2)	122(2)	x,y,z
N8A-H8B···O20	0.875(1)	2.22(1)	3.063(2)	163(2)	x,y,z
N8B-H8C···O17	0.886(1)	2.41(1)	3.249(2)	158(2)	-1+x,y,z
N8B-H8C···O21	0.886(1)	2.17(2)	2.801(2)	128(2)	-1+x,y,z
N8B-H8D···O16	0.88(2)	1.78(2)	2.655(2)	173(2)	x,y,z
O15A-H15A···O21	0.84	2.00	2.837(2)	171	-1/2+x,3/2-y,1-z
O15B-H15B···O17	0.84	1.98	2.771(2)	157	1-x,-1/2+y,1/2-z
C5A-H5A···O7A	0.95	2.27	2.985(2)	132	1+x,y,z
C5B-H5B···O7B	0.95	2.47	3.108(2)	125	-1+x,y,z
C6B-H6B···O7B	0.95	2.55	3.155(2)	122	-1+x,y,z
C13B-H13C···O15B	0.99	2.37	3.234(2)	146	1+x,y,z
C13B-H13D···O10B	0.99	2.41	3.298(2)	149	1-x,1/2+y,1/2-z
C14A-H14B···O15B	0.99	2.56	3.433(2)	147	1/2-x,1-y,1/2+z

Each oxalate ion is directly hydrogen bonded with six lamivudine cations (Figure 17). The N-H···O hydrogen bonds are illustrated separately from the O-H···O hydrogen bonds for clarity. The oxygen atoms O16, O20 engage in bifurcated hydrogen bonds while O17 and O21 are involved in trifurcated hydrogen bonds. This behaviour as an acceptor of multiple hydrogen bonds is typical of carboxylate ions.[10]

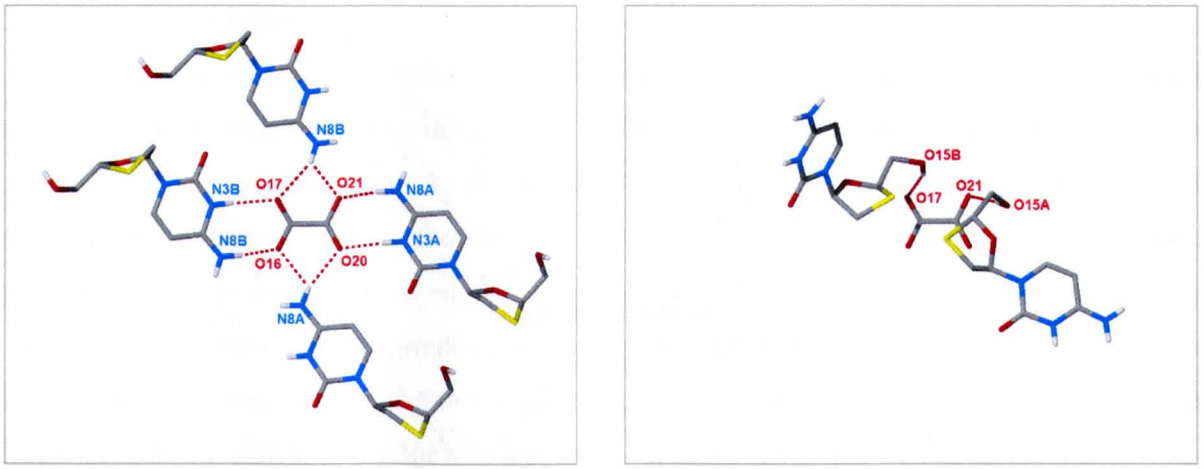

Figure 17: Hydrogen bonding of the oxalate ion. N-H···O hydrogen bonds are shown on the left and O-H···O hydrogen bonds are illustrated on the right.

Crystal packing

The similarity between the packing of **LAMOXL** and the two previously reported salts of lamivudine can be seen in comparing Figure 18 with the packing diagrams from a recent paper[4] that have been reproduced in Figure 19. The zig-zag arrangement is common to all three but in the case of **LAMOXL**, the lamivudine molecules are not stacked directly above one another.

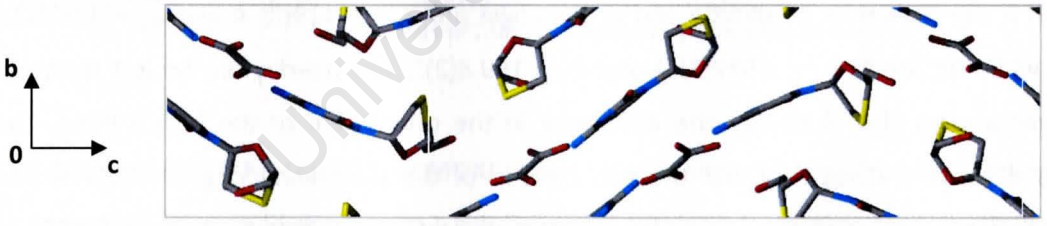

Figure 18: Crystal packing of LAMOXL. View of the *bc*-face of the unit cell.

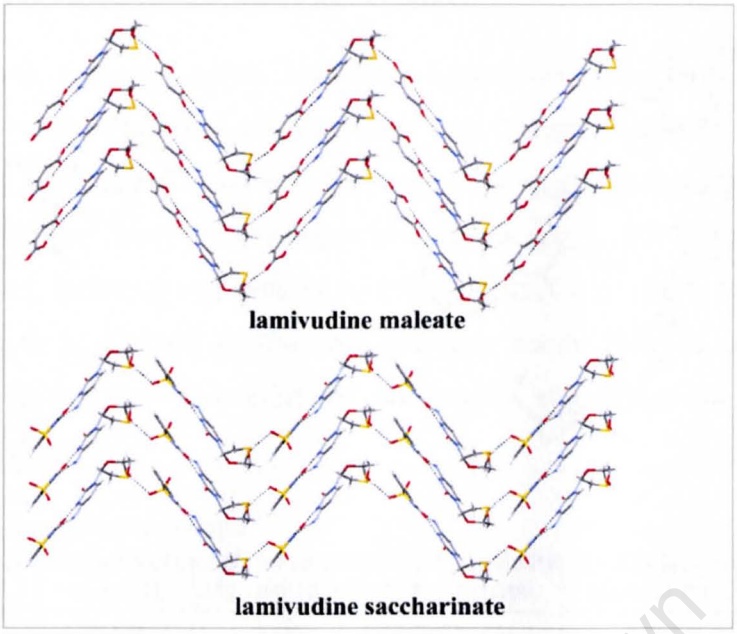

Figure 19: View of the *bc*-face of the maleate and saccharinate salts, reproduced from reference 4.

Molecular geometry

Given that the pyrimidine fragment of lamivudine is necessarily virtually planar, predictably, the main geometrical differences in the two crystallographically-independent lamivudine ions of the asymmetric unit exist with respect to the five-membered cytosine ring. Puckering analysis was carried out according to the methods described by Kilpatrick *et al.*[11] and Cremer and Pople.[12] With respect to ion **A** the maximum amplitude and phase angle are q_2 = 0.429(2) Å and ϕ_2 = 338.8(2)° respectively, while for ion **B**, q_2 = 0.527(2) Å and ϕ_2 = 169.8(2)°. The overlay on the left (cytosine fragments overlapping) also illustrates the difference in the orientation of the N1-C9 bond. The perpendicular distance between C9 and the mean plane of the pyrimidine ring is -0.187 Å and 0.226 Å for ions **A** and **B** respectively. The hydroxyl group orientations are also markedly different.

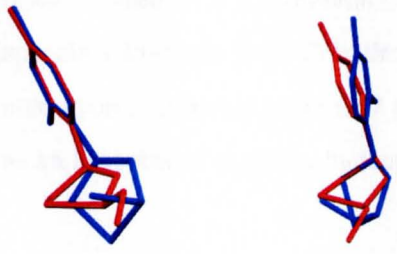

Figure 20: Overlay of independent lamivudine ions of the asymmetric unit. Ion A is presented in red, while B is in blue. On the left, the ions have been positioned so that the pyrimidine rings are overlapping, while on the right, the orientation is such that the atoms O10, C9 and C13 of both ions are coincident.

Comparative PXRD

It was not possible to produce **LAMOXL** by dry or liquid-assisted co-grinding. Multiple dry co-grinding experiments were attempted with different molar ratios and periods of grinding. The experimental patterns of the dry grinding products are shown to differ from that of **LAMOXL** (prepared by slow evaporation) in Figure 21. The product compositions are complex and inconsistent between experiments. The product of the 5 min grinding method exhibits peaks that correlate with those in the uppermost pattern (20 min grinding) and the trace of **LAMOXL**, implying that there are similar phases present. Based on these PXRD data there are very likely other salt forms that may be prepared from lamivudine and oxalic acid dihydrate.

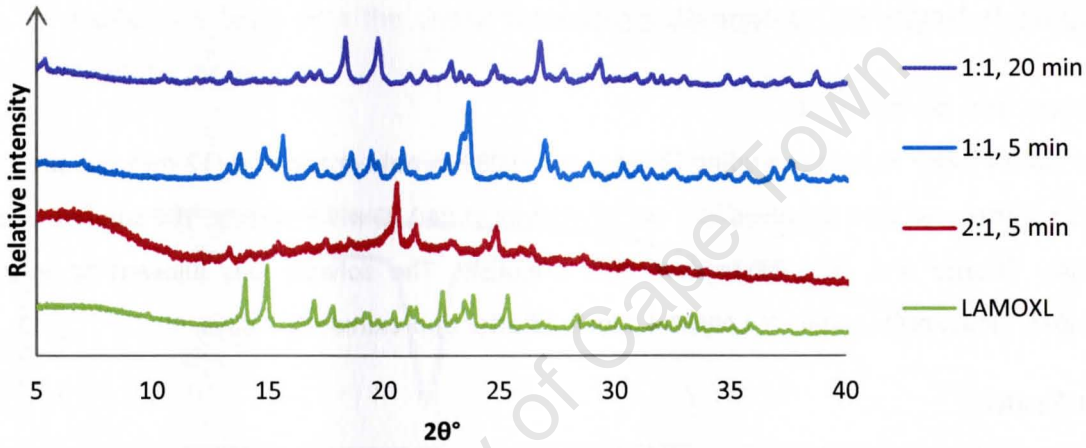

Figure 21: The products of dry co-grinding experiments (molar ratios and periods of grinding) are compared with the PXRD trace of LAMOXL prepared by slow evaporation.

The experimental PXRD trace for **LAMOXL** is presented along with the computed pattern in Figure 22 to show that upon mild grinding this salt form is stable and to confirm that the PXRD trace can be used for identification. It also provides assurance that the crystal selected for single crystal X-ray analysis is representative of the bulk material prepared by slow evaporation.

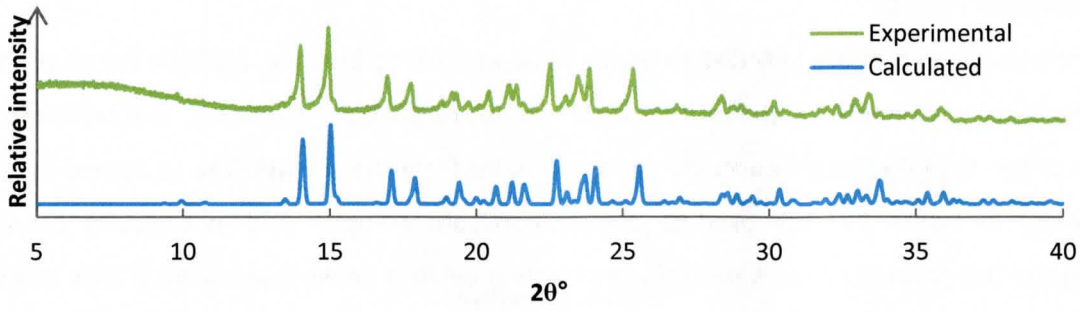

Figure 22: Comparison of experimental and calculated PXRD patterns for LAMOXL.

LAMMLI: lamivudine-malic acid salt

Preparation of the salt

A mixture of 0.087 mmol lamivudine (20 mg) and 0.089 mmol L-malic acid (12 mg) was pre-ground for 15 minutes and then dissolved in 1 cm^3 of ethanol at ~40 °C while stirring. The solution was then carefully filtered and allowed to cool spontaneously. The solvent was allowed to evaporate extremely slowly and crystals of **LAMMLI** appeared after approximately 7 days.

Identification

The screening experiment that revealed the new form was carried out by dry co-grinding a small equimolar mixture of lamivudine and L-malic acid for 5 min and analysing the product using PXRD. In Figure 23 the PXRD trace of the reaction product is compared with those of the starting reagents to show that the reaction product represents a new phase and does not appear to contain excess lamivudine or L-malic acid.

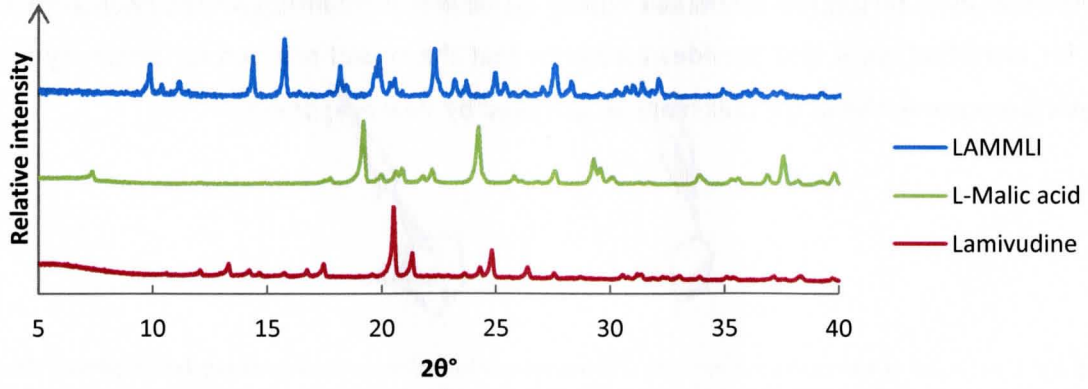

Figure 23: PXRD comparison of the traces for LAMMLI, lamivudine and L-malic acid.

Thermal analysis

TGA and DSC

TG analysis, conducted in triplicate, revealed a solvent loss of 4.5 ± 0.2 % at onset 79 °C. After the desolvation event, the sample mass continues to decrease at a very slow rate until decomposition at approximately 140 °C. Initially the TGA programme that was used involved heating at 10 K min^{-1} but this rate did not allow resolution of the melting and decomposition events. A heating rate of 1 K min^{-1} was required to achieve the necessary resolution.

The DSC curve exhibits a single, exceptionally broad endotherm at 85-105 °C associated with melting. The onset of melting appears to be coincident with the solvent loss as seen in the TGA trace, the implication being that the crystal collapses (and begins to melt) precisely when the included solvent is expelled.

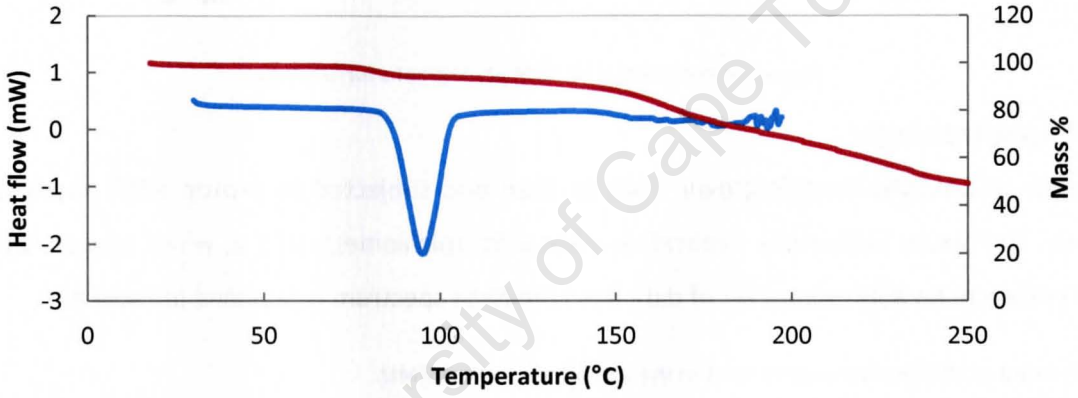

Figure 24: TGA (red) and DSC (blue) traces for LAMMLI.

In summary, TG and DSC analyses revealed the presence of included solvent. Given that **LAMMLI** may be prepared by both co-precipitation and dry kneading, the solvent of crystallisation is most likely water, since water may be absorbed from the atmosphere in neat grinding experiments.[13] The melting of **LAMMLI** occurs over a broad range at relatively low temperature. In fact the onset of melting occurs well below the melting points of both starting reagents. Decomposition occurs directly after melting and accelerates greatly at ~140 °C.

HSM

A sample of aggregated **LAMMLI** crystals was subjected to a 10 K min^{-1} heating using the HSM apparatus. Photos were taken to illustrate the only visible thermal event – melting. During HSM analysis melting occurred over a broad range of 77-90 °C. Having established that the crystal had

included water, we expected to see the release of water but this is not evident for two important reasons. Subsequent analysis – the results of which are presented later in this chapter – showed that water is indeed the solvent of crystallisation. It represents a very small fraction of the total mass of **LAMMLI** – 4.5 ± 0.2 % as determined by thermogravimetry. Secondly, the collapse of the hydrate by melting occurs well below the boiling point of water. We are only able to observe the release of solvent as it is vaporised and forms bubbles in the silicone oil medium.

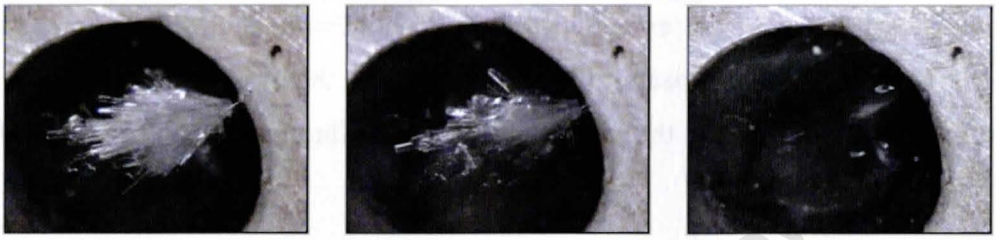

Figure 25: Representative HSM photographs for LAMMLI.

NMR spectroscopy

A sample of **LAMMLI** crystals grown from solution was subjected to proton NMR spectroscopic analysis. The results indicated a lamivudine-malic acid stoichiometry of 1:1, which concurs with the PXRD evidence. An abbreviated set of data from the NMR spectrum is provided in Table 8.

Table 8: Selected NMR signals used to confirm the stoichiometry of LAMMLI.

Assignment	δ (ppm)	Integral	Normalised integral
CH (aromatic, lamivudine)	7.81	1.0*	1
CH (aromatic, lamivudine)	5.75	0.9	1
CH (L-malic acid)	4.26	1.0	1

*Reference integral

Single crystal X-ray diffraction

Data-collection and space group determination

The needle-like crystals grew as aggregates. Having placed one under Paratone oil to prevent the loss of potentially included solvent, a suitable portion was cut for analysis. X-ray diffraction data were collected on a Bruker KAPPA APEX II DUO diffractometer. The data were used to determine the unit cell dimensions and identify the crystal system as being orthorhombic (Laue symmetry: mmm). The space group $P2_12_12_1$ was determined using XPREP and confirmed using the program LAYER to observe the following systematic absences: $hkl: none;\ h00: h = 2n+1;\ 0k0: k = 2n+1;\ 00l: l = 2n+1.$

Structure solution and refinement

SHELXS-97 was employed for the structure solution of **LAMMLI**. The asymmetric unit contains one lamivudine ion and one L-malate ion. Non-hydrogen atoms were located in the difference Fourier map, assigned, and refined isotropically on F^2 in SHELXH-97. Upon confirming acceptable isotropic temperature factors, these atoms were refined anisotropically. Guided by peaks in the difference Fourier map, hydrogen atoms were placed by means of a riding model. Importantly, it was clearly evident from the difference Fourier map that the L-malic acid had been deprotonated, while the lamivudine had been protonated at the N3-position. Each hydrogen atom was assigned an isotropic temperature factor of 1.2 times that of its parent atom. The single water molecule in the asymmetric unit was identified by the large peak of the oxygen atom. Hydrogens of the water molecule were also evident in the difference Fourier map. These were placed according to peak positions and the O-H bond distances constrained to 0.84 Å with σ = 0.01 Å. Both O-H bond lengths refined to 0.83 Å.

Table 9: Data-collection and refinement parameters for LAMMLI.

Formula unit	$(C_8H_{12}N_3O_3S^+)$ $(C_4H_5O_5^-)$ (H_2O)
Formula mass (g mol^{-1})	381.36
Crystal system	Orthorhombic
Space group	$P2_12_12_1$
a (Å)	5.1651(3)
b (Å)	16.9225(8)
c (Å)	17.7735(9)
α (°)	90
β (°)	90
γ (°)	90
Volume ($Å^3$)	1553.5(1)
Z	4
$Density_{calc}$ (g cm^{-3})	1.631
μ(MoKα) (mm^{-1})	0.266
F(000)	800
Crystal size (mm^3)	0.17 x 0.10 x 0.07
Temperature (K)	173(2)
Range scanned θ (°)	2.29-28.31
Index ranges	h: -9, 9 ; k: -13, 13; l:-29, 29
ϕ and ω scan angle (°)	0.5
Total number of frames	1671
Dx (mm)	40
Total number of reflections collected	22453
Number of unique reflections	3870
Number of reflections with $I > 2\sigma(I)$	3512
Number of least-squares parameters	246
R_{int}	0.0404
S	1.033
R_1 ($I > 2\sigma(I)$)	0.0293
Number of reflections omitted	2
wR_2	0.0675
Weighting scheme parameters	a = 0.0378, b = 0.2294
$(\Delta/\sigma)_{mean}$	<0.001
Δρ excursions (e $Å^{-3}$)	0.251, -0.175
Absolute structure parameter9	0.04(6)

Molecular structure

There are one lamivudine ion and one malate ion in the asymmetric unit. There is also one water molecule present. Referring back to the thermal analysis that showed a water content of 4.5 %, it can be seen that this correlates well with the theoretical value of 4.7 % based on the crystal structure. The standard deviation of 0.2 % and the low temperature of dehydration account for the small discrepancy between the experimental and theoretical values.

The difference Fourier map clearly revealed the protonation of the lamivudine molecule at atom N3. The deprotonation of the dicarboxylic malic acid molecule at one end is consistent with the tentative model for the prediction of salt formation that was described in Chapter 1, given that pK_a (L-malic acid) = 3.4, 5.2 and pK_a (lamivudine) = 4.3. The pK_a of the more acidic carboxylic acid group results in a ΔpK_a value that is between zero and three but the value of ΔpK_a with respect to the second carboxylic acid group is less than zero. Thus, the model correctly predicts that the first carboxylic acid group may or may not react (in this case it *does*) and that the second –COOH group will not be deprotonated.

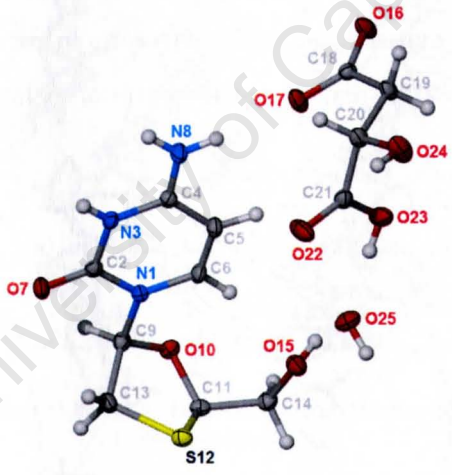

Figure 26: Asymmetric unit of LAMMLI.

Hydrogen bonding

The hydrogen bonding pattern is again complex (see Table 10 for hydrogen bond parameters), owing largely to the existence of the strongly electron-donating carboxylate group of the counterion. As expected, the O-H···O hydrogen bonds are numerous with an average D···A distance of 2.87 Å and an angular range of 133-178°. There are three unique N-H···O hydrogen bonds with bonding angles 158°, 175° and 179° and a mean D···A distance of 2.79 Å, which is short because all three of these hydrogen bonds are charge-assisted. The three C-H···O hydrogen bonds are of mean bond distance 3.30 Å with smaller angles, as is often the case.

Table 10: Hydrogen bond parameters for LAMMLI.

D-H···A	D-H (Å)	H···A (Å)	D···A (Å)	D-H···A (°)	Symmetry code
N3-H3···O16	0.82(2)	1.87(2)	2.68(2)	175(2)	1/2+x,3/2-y,1-z
N8-H8A···O17	0.88	1.91	2.79(2)	179	1/2+x,3/2-y,1-z
N8-H8B···O17	0.88	2.05	2.886(2)	158	x,y,z
O15-H15···O22	0.76(2)	2.20(2)	2.767(2)	133(2)	-1+x,y,z
O15-H15···O25	0.76(2)	2.42(2)	3.034(2)	139(2)	-1+x,y,z
O23-H23···O25	0.84	1.74	2.575(2)	178	x,y,z
O24-H24···O23	0.93(3)	1.99(3)	2.911(2)	168(3)	1+x,y,z
O25-H25A···O15	0.83(1)	2.45(2)	3.177(2)	147(3)	x,y,z
O25-H25B···O16	0.83(2)	1.90(2)	2.725(2)	176(2)	1-x,1/2+y,3/2-z
C6-H6···O15	0.95	2.26	3.159(2)	157	x,y,z
C14-H14A···O24	0,99	2.43	3.371(2)	159	1-x,1/2+y,3/2-z
C19-H19B···O15	0.99	2.54	3.367(2)	141	1-x,-1/2+y,3/2-z

Refer to Figure 27, which illustrates the hydrogen bonding pattern with respect to the malate ion. Malate ions are connected via the hydrogen bond O24-H···O23. Furthermore, each malate ion is hydrogen bonded to three lamivudine ions and two water molecules. As in the case of **LAMOXL**, there are no hydrogen bonds that link adjacent API units. In other words, the hydrogen bond connections are all of the form malate-malate, malate-water or malate-lamivudine.

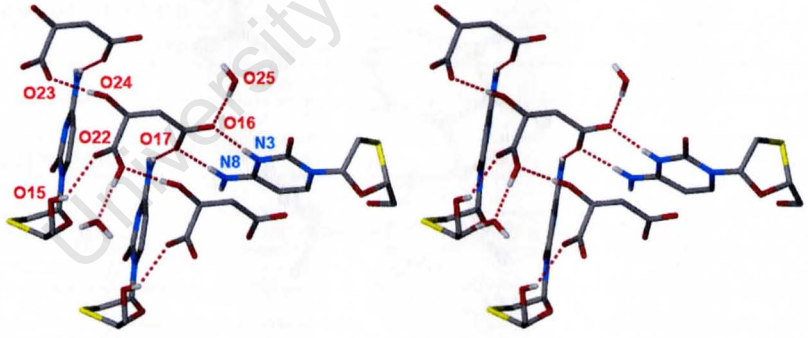

Figure 27: Stereodiagram showing hydrogen bonding with respect to the malate ion. Irrelevant hydrogen atoms have been omitted for clarity.

Crystal packing

The 2_1 screw-axes that characterise the space group $P2_12_12_1$ are clearly visible in Figure 28. In the *b*-direction the lamivudine ions pack in an alternating head-to-head and tail-to-tail arrangement, while along the *c*-axis successive lamivudine ions are separated by a water molecule. Figure 29 shows how the salt former and API pack in rows along the *a*-axis. Looking down the *c*-axis, the API ions pack one behind the other, while the malate ions are staggered.

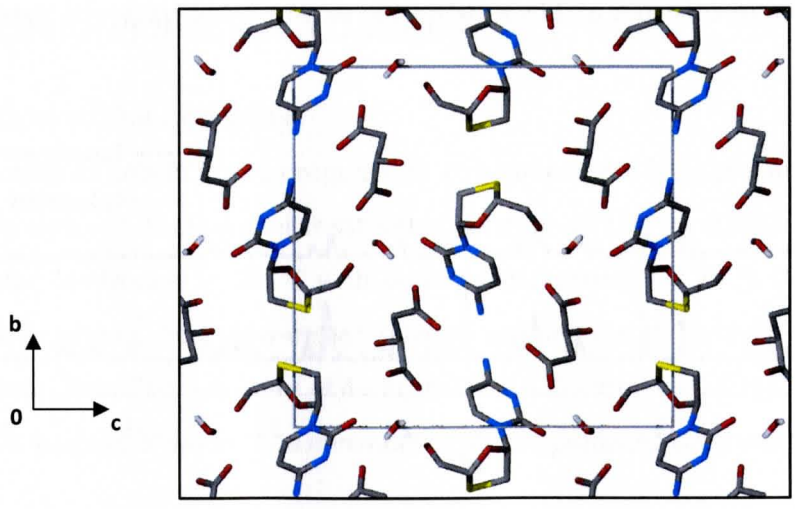

Figure 28: Crystal packing of LAMMLI. View down the a-axis. The only hydrogens shown are those of the water molecules.

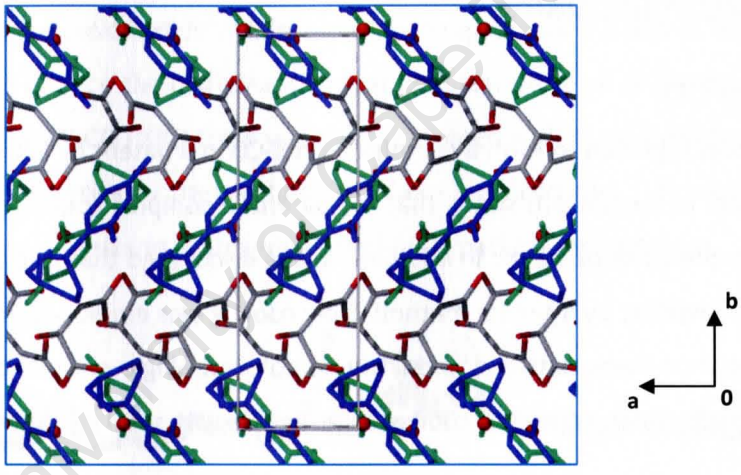

Figure 29: View down the c-axis. Alternate layers of the API are shown in different colours. Hydrogen atoms have been omitted for clarity.

Molecular geometry

The cytosine ring of the lamivudine ion (see Figure 26 for atom labels) is in the usual envelope conformation with S12 the flap atom. The puckering parameters are q_2 = 0.489(1) Å and ϕ_2 = 168.1(2)°. The torsion angles about the C11-C14 bond (at which the hydroxyl group is attached) are 65.7(2)° (O10-C11-C14-O15) and -54.9(2)° (S12-C11-C14-O15) and the angle between the mean planes of the six-membered and five-membered rings is 78.03(4)°.

Comparative PXRD

Below is a PXRD comparison showing that the sample of **LAMMLI** prepared by dry co-grinding and used for analysis was indeed identical to the sample from which the single crystal was selected for data-collection. The calculated pattern is shifted slightly to higher 2θ values because the single

crystal diffraction data were collected at 173 K, while the experimental trace was determined at room temperature.

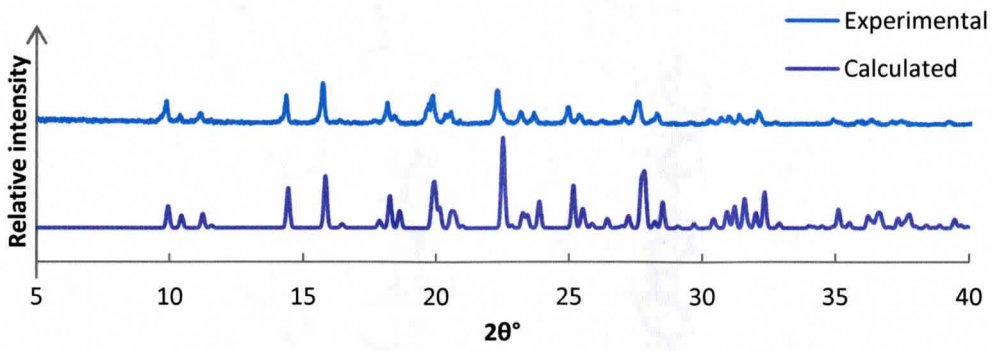

Figure 30: PXRD comparison of the experimental and calculated traces for LAMMLI.

Cyclodextrin Inclusion

β-CD and γ-CD

Lamivudine was reported to form a complex with β-CD in a patent by Lloret Perez and co-worker.[5] It was confirmed, in the present study, that the patented complex could be prepared by kneading for 90 min in the presence of water. In addition, it was discovered that it is possible to produce a γ-CD complex of lamivudine by a similar method. Slow cooling was employed in an attempt to grow single crystals of both of these native cyclodextrin complexes. Single crystals of the β-CD complex were successfully prepared but the slow cooling experiments with γ-CD yielded only powdered material.

DIMEB and TRIMEB

In the present study, attempts were made to complex lamivudine with DIMEB and TRIMEB. The experiments involved dissolving an equimolar mixture of the API and cyclodextrin in a water at low temperature (ice bath), while stirring for approximately 24 h. Subsequently the solutions were placed in an oven preset to 60°C and allowed to crystallise. The DIMEB experiments produced only pure DIMEB single crystals; the API remained in solution. Experiments with TRIMEB did not yield crystals even after several weeks.

β-Cyclodextrin Inclusion Complex

Preparation of the complex

The β-CD complex **LAMβCD** was prepared by slow cooling and kneading in water. The slow cooling experiment involved heating a near-saturated solution of 110 mg (0.087 mmol) β-CD and 20 mg (0.087 mmol) lamivudine to 60 °C with simultaneous stirring for 24 h. Good single crystals were obtained only when a clear slow-cooled solution was allowed to slowly evaporate over a period of several weeks. Kneading a mixture of 44 mg β-CD (0.035 mmol) and 8 mg lamivudine (0.035 mmol) with a small quantity of water for a minimum of 30 min produced the same complex.

The complex prepared here by slow cooling and kneading was compared with that of the complex claimed by Lloret Perez and co-worker using PXRD analysis.[5] Observe the comparison of PXRD traces in Figure 31. Firstly, note that the products of both the slow cooling and kneading methods are identical. The method described in the aforementioned patent combined lamivudine with "at least about 0.5 molar equivalents of cyclodextrin". Unfortunately the quality of the patent trace is low but according to the available evidence the complexes appear identical, since all of the dominant peaks in the patterns match. The **LAMβCD** PXRD trace was then compared with representative patterns for the known β-CD isostructural series by the method that Caira has described.[14] However, it did not match any of these, and thus appears to represent a novel β-CD packing arrangement.

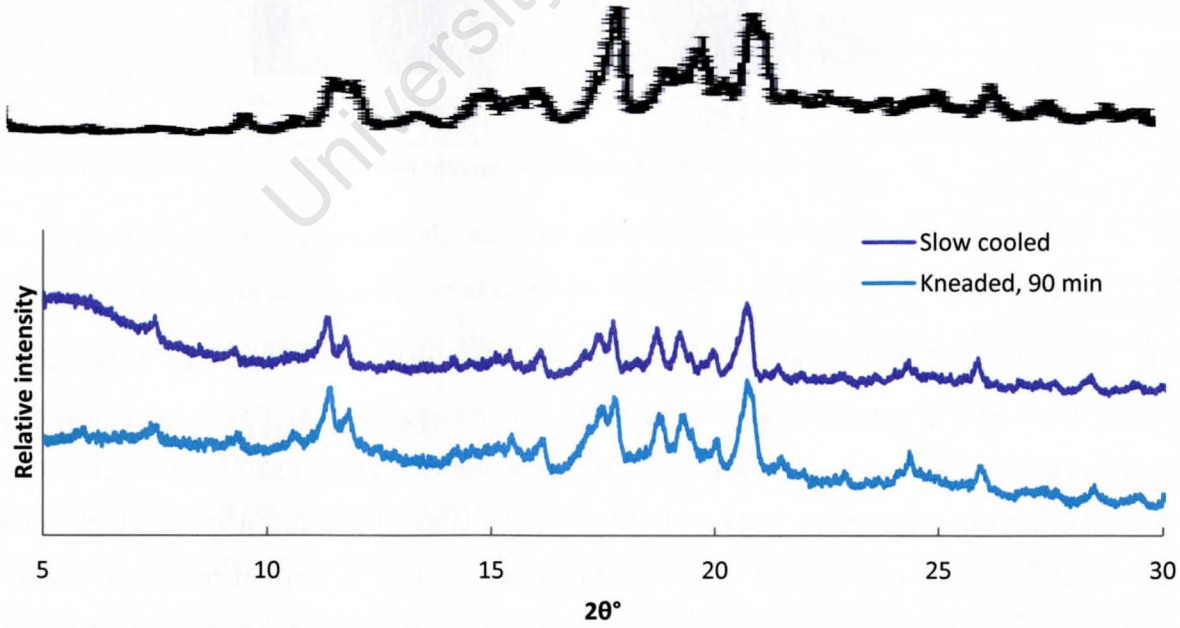

Figure 31: PXRD traces of the complex obtained by kneading and slow cooling (below) compared with the trace of the patented form (above), reproduced from reference 5.

Thermal analysis

HSM

A sample of **LAMβCD** crystals was heated at a rate of 10 K min^{-1} on the hot stage and representative photographs recorded. The first signs of bubbling, related to the loss of waters of crystallisation, appeared at 65 °C. At 260 °C the crystals began to decompose, indicated by the colour change from colourless to brown. Extensive decomposition at 295 °C can be seen by the dark brown colour of the crystals and the evolution of some gas that is likely a product of degradation.

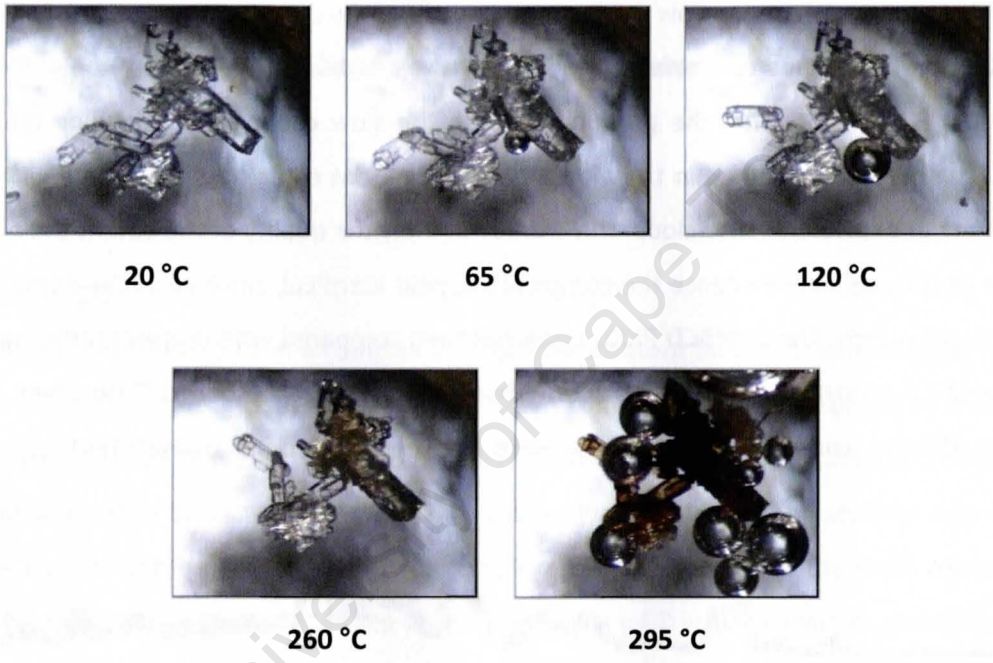

Figure 32: Representative HSM photographs for LAMβCD.

TGA and DSC

The TGA and DSC traces appear in Figure 33. TGA revealed a two-step mass loss of 10.9 ± 0.3 % (n = 2) associated with dehydration. The onset of dehydration is evident from the profile as a large mass loss beginning at 245 °C and accelerating rapidly at 310°C. The trace obtained from DSC analysis displayed a large endotherm at the start of the run and a second, smaller endotherm beginning immediately thereafter and ending at 135 °C. Both of these are related to dehydration, which is a two-step process as evidenced by the TGA trace. A third endotherm, associated with degradation of the complex is apparent at 295-345 °C.

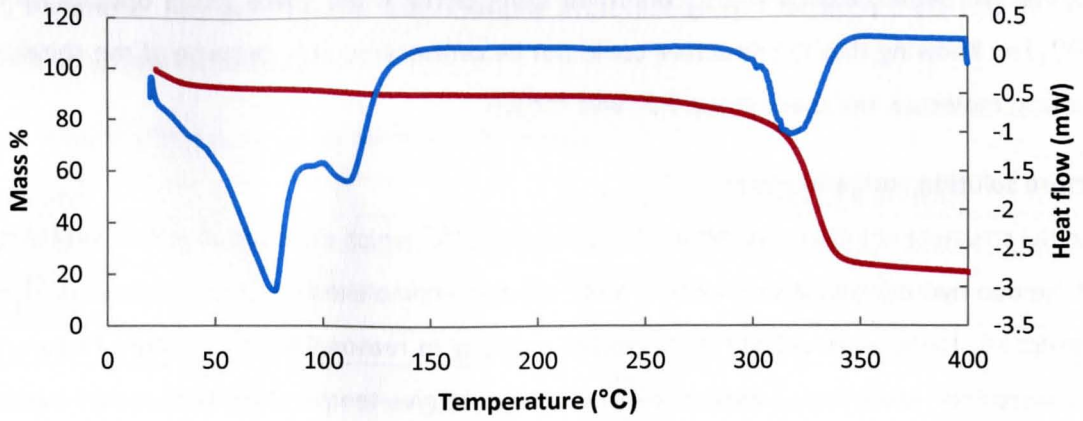

Figure 33: TGA (red) and DSC (blue) traces for LAMβCD.

NMR spectroscopy

Proton NMR spectroscopy was used to determine the host-guest stoichiometry of the complex. A representative set of data used for calculation of the stoichiometry is listed in Table 11. Most often, β-CD complexes with non-solvent guest molecules are found to have stoichiometries of 1:1 or 2:1; however, in this case 1:1.46 appeared to be the approximate host-guest stoichiometry.

Table 11: Data from a proton NMR spectrum of LAMβCD, used to determine the stoichiometry of the complex.

Assignment	δ (ppm)	Integral	Normalised integral
aromatic CH (guest)	7.83	1.00*	1.46
cytosine CH (guest)	6.29	1.00	1.46
7 x CH1 (host)	5.01	4.8	1

*Reference integral

The NMR experiment was repeated, this time with a crystal that had been grown from a highly concentrated solution of the pre-ground complex. The second experiment gave a similar result and, taking both experiments into account, the mean host-guest stoichiometry is 1:1.48 ± 0.05 (n = 2).

Single crystal X-ray diffraction

Data-collection and space group determination

One of the elongated plate-like crystals was removed from the aqueous mother liquor and placed directly into Paratone oil to prevent the loss of any waters of crystallisation. The data were collected using a Bruker KAPPA APEX II DUO diffractometer (details provided in Chapter 2). From the X-ray diffraction data, the unit cell dimensions were determined along with Laue symmetry, which was $2/m$, indicating the monoclinic system. Based on the reflection conditions

$hkl: none;\ h0l: none;\ 0k0: k = 2n$ (confirmed using LAYER[7]), the space group options were $P2_1$ and $P2_1/m$. Knowing that the structure could not be centrosymmetric because of the chiral nature of the host molecule, the space group $P2_1$ was chosen.

Structure solution and refinement

The initial structure solution was carried out using SHELXD,[8] which employs *ab initio* direct methods. All of the non-hydrogen atoms of the host molecule and a complexed guest molecule were identified and assigned. These were refined isotropically, resulting in reasonable temperature factors. These atoms were then modelled as anisotropic and refined to give temperature factors that indicated a low degree of thermal motion. In fact the highest U_{iso} value was 0.057(1) Å^2 for an O6 atom of the cyclodextrin, which is remarkably low for a group of this type. The next greatest electron density peaks were inspected for typical hydrogen bonding distances and, where appropriate, the oxygen atoms of water molecules were placed. Water molecules O1W-O5W were placed with full site-occupancy and refined isotropically. All five atoms exhibited relatively low temperature factors and were refined anisotropically to assist identification of the disordered waters. Atoms 06AW and O6BW, and atoms O7AW and O7BW were initially assigned as disordered pairs. Later these were assigned the same global U_{iso} of 0.05 Å^2 as for the rest of the eight water positions that appeared to have partial site-occupancy. After isotropic refinement and settling of the site-occupancy factors, the temperature factors of O6AW, O6BW, O7AW, O7BW and O8W were again treated as variables and allowed to refine freely, while for the other seven disordered atoms, the temperature factors were treated as variables but the site-occupancies had to be fixed. The hydrogens of the host and guest molecules were placed in idealised positions. For the hydroxyl groups, a hydrogen bond searching model was employed. All of the hydrogens were refined isotropically with temperature factors set at 1.2 times those of their parent atoms. The hydrogens of water atoms were not placed.

All of the residual electron density in the interstitial spaces was treated as water because the connectivity of the electron density peaks did not resemble any portion of the lamivudine molecule. The TGA data were used as a guide for the modelling of these water molecules, so that their total number in the model (9.7) was in reasonable agreement with the predicted value of 9.3. The apparent absence of approximately half a guest molecule, as expected according to NMR spectroscopic evidence, is addressed in detail in a later section of this chapter. Nevertheless the final weighted R-factor, at 7 %, is excellent for a cyclodextrin inclusion complex and the Goodness of Fit parameter, S, is very close to 1. The crystal data and refinement parameters are listed in Table 12 and Table 13 provides s.o.f. and U_{iso} values for the water sites. Note that the absolute structure

(Flack) parameter has been quoted but is largely irrelevant given that both β-CD and lamivudine have known absolute configurations.

Table 12: Data-collection and refinement parameters for LAMβCD.

Formula unit	$(C_{42}H_{70}O_{35})$ $(C_8H_{11}N_3O_3S)$ 9.66(H_2O)
Formula mass (g mol^{-1})	1538.27
Crystal system	Monoclinic
Space group	$P2_1$
a (Å)	15.270(1)
b (Å)	10.1453(8)
c (Å)	23.746(2)
α (°)	90
β (°)	100.250(2)
γ (°)	90
Volume ($Å^3$)	3620.0(5)
Z	2
$Density_{calc}$ (g cm^{-3})	1.411
F(000)	1637
μ(MoKα) (mm^{-1})	0.153
Crystal size (mm^3)	0.36 x 0.11 x 0.07
Temperature (K)	173(2)
Range scanned θ (°)	2.19-28.32
Index ranges	h: -20, 20; k: -13, 13; l: -31, 31
ϕ and ω scan angle (°)	0.5
Total number of frames	1500
Dx (mm)	40
Total number of reflections collected	41216
Number of unique reflections	17977
Number of reflections with I > 2σ(I)	14434
Number of least-squares parameters	927
R_{int}	0.0421
S	1.037
R_1 (I > 2σ(I))	0.0700
Number of reflections omitted	1
wR_2	0.1860
Weighting scheme parameters	a = 0.1206, b = 3.1427
(Δ/σ)mean	< 0.001
Δρ excursions (e $Å^{-3}$)	1.032, -0.656
Absolute structure parameter9	-0.05(14)

Table 13: Site-occupancy factors and thermal parameters for the LAMβCD water sites.

Atom	s.o.f.	U_{iso} (Å^2)	Atom	s.o.f.	U_{iso} (Å^2)
O1W	1	0.0277(8)	O8W	0.55(2)	0.064(3)
O2W	1	0.038(1)	O9AW	0.43	0.052(2)
O3W	1	0.065 (2)	O9BW	0.33	0.051(3)
O4W	1	0.051(1)	O9CW	0.23	0.059(5)
O5W	1	0.076(2)	10W	0.21	0.084(7)
O6AW	0.53(2)	0.066(4)	11A	0.50	0.054(2)
O6BW	0.37(2)	0.065(5)	11B	0.22	0.058(5)
O7AW	0.62(2)	0.058(3)	11C	0.23	0.066(5)
O7BW	0.44(2)	0.078(5)			

Molecular structure

The asymmetric unit is illustrated in Figure 34, showing clearly the mode of guest inclusion. The cytosine ring is inserted into the host cavity with its hydroxyl group at the secondary rim. The pyrimidine ring protrudes from the primary rim. The red spheres in the image represent the 17 water molecule sites, five of which have full site-occupancy.

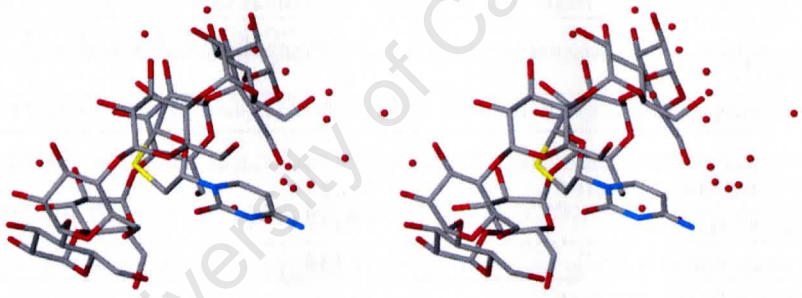

Figure 34: Stereodiagram showing the asymmetric unit of LAMβCD as viewed down the *a*-axis. Hydrogen atoms are omitted for clarity.

The host and guest molecules are represented separately in Figure 35 to show the labelling of atoms and the relative sizes of thermal ellipsoids. The relatively small ellipsoids of the host atoms, as compared with other β-CD complexes, are indicative of an unusually low degree of thermal motion.

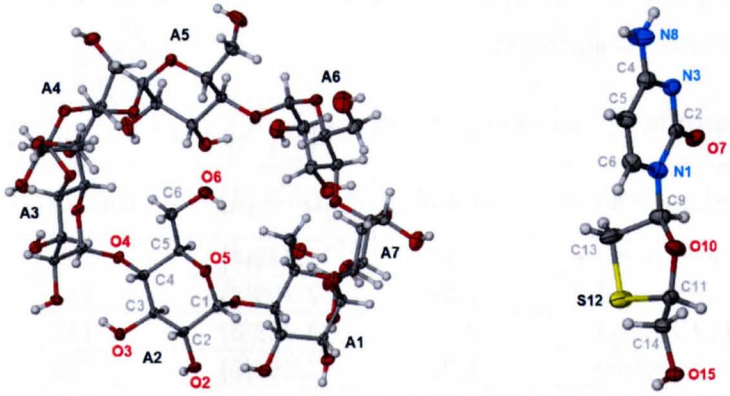

Figure 35: The host and guest molecules of LAMβCD. Thermal ellipsoids are drawn at the 50% probability level and hydrogen atoms are drawn as spheres with arbitrary radii.

Hydrogen bonding: host-host

The host-host hydrogen bond parameters are summarised in Table 14. The primary intramolecular interactions of the host molecule form a hydrogen bonding 'belt' at the secondary rim (similarly to **ZIDβCD**). All of these hydrogen bonds are of the form O3An-H···O2A(n+1). It is important to mention here that the hydrogen bond seeking model cannot fully account for the 'flip-flop' hydrogen bonding of the secondary hydroxyls,[15] so in this regard the model may in some respects be unrealistic. Some artefacts may occur, like the fact that in this case O2A2-H appears not to have a hydrogen bond acceptor. The host geometry is such that O6An-H···O5An hydrogen bonds are also present. There are five C-H···O hydrogen bonds and three O-H···O interactions linking adjacent host molecules.

Table 14: A summary of host-host hydrogen bond parameters.

Interaction	Type	Number	Mean D···A distance (Å)	Mean bond angle (°)
Intramolecular	O3-H···O2	6	2.846(4)	164
	C6-H···O5	3	3.324(5)	144
Intermolecular	O6-H···O2′	1	2.727(4)	149
	O2-H···O3′	1	2.747(4)	131
	O6-H···O6′	1	2.755(4)	167
	C-H···O′	5	3.403(4)	154

Hydrogen bonds between the host and guest

The guest molecule is not merely included within the cyclodextrin cavity, but rather plays a very important directing role through hydrogen bonding with the host atoms of adjacent complexes. There are five principal hydrogen bonds between the host and guest (Table 15), three of which are O-H···O interactions. The other two are N-H···O and C-H···O hydrogen bonds. The O2A5-H2A5···O7

bond angle is particularly low for this type of interaction but this is because the donor appears to interact with *two* acceptors – O7 and O3A5.

Table 15: Parameters for the hydrogen bonds between the host and guest.

Interaction	Hydrogen bond	H···A (Å)	D···A (Å)	D-H···A (°)	Symmetry code
Host-guest	O6A2-H26···O15	1.94	2.743(4)	159	x,-1+y,z
	O2A5-H2A5···O7	2.04	2.709(4)	136	x,1+y,z
	C2A5-H20···N3	2.56	3.323(6)	132	x,1+y,z
Guest-host	N8-H8B···O6A5	1.99	2.859(6)	169	1-x,-1/2y,2-z
	O15-H15···O3A2	1.95	2.743(4)	157	1-x,1/2+y,1-z

Figure 36 and Figure 37 illustrate the host-guest O-H···O and N-H···O hydrogen bonds respectively. It can be seen that the interactions are complex – the host and guest are co-operatively responsible for the overall packing arrangement. It can be seen from the stereodiagrams that the monomeric complexes pack extremely close to one another in a herringbone arrangement. The β-CD A2 residue is nearly inserted into the cavity of an adjacent host molecule at the secondary rim.

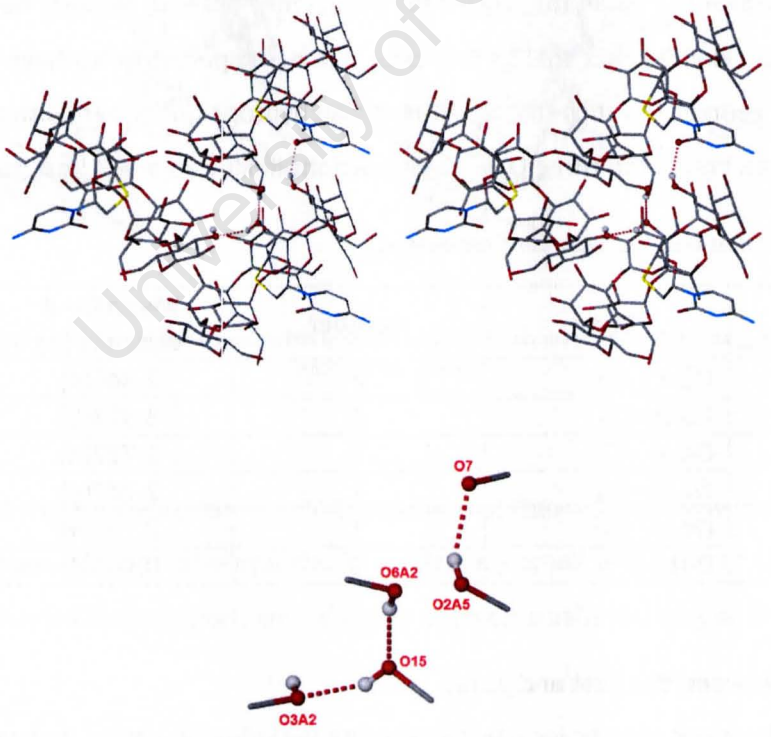

Figure 36: An illustration of the O-H···O hydrogen bonds between the host and guest. Above is a stereodiagram and below, the most relevant atoms are magnified.

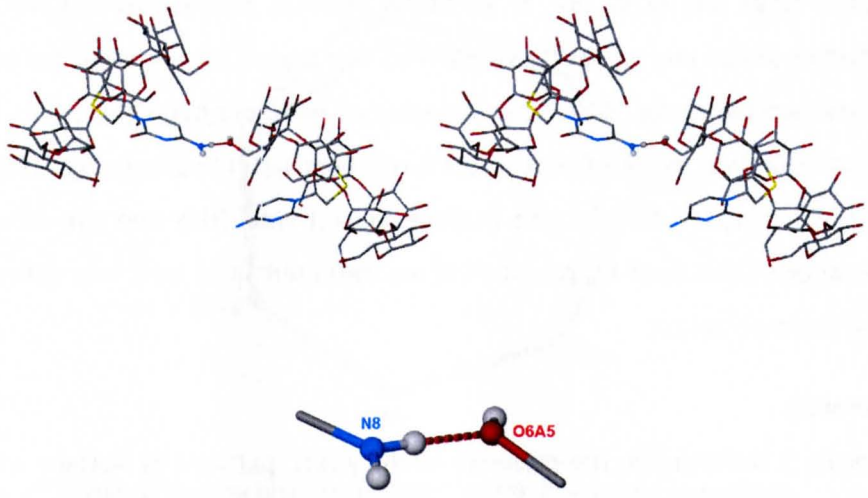

Figure 37: An illustration of the guest-host N-H···O hydrogen bond. Above is a stereodiagram and below, the most relevant atoms are magnified.

Hydrogen bonds involving water

There were 17 water molecule sites identified. Parameters for the 7 host-water and single guest-water hydrogen bonds are listed in Table 16. Of the sites that have full occupancy, three are hydrogen bond acceptors where host atoms are the donors. O5W is the hydrogen bond acceptor for the only guest-water hydrogen bond. O3W is the only water molecule with full site-occupancy that is not directly hydrogen bonded with the host or guest.

Table 16: Parameters for host-water and guest-water hydrogen bonds.

D-H···A	H···A (Å)	D···A (Å)	D-H···A (°)	Symmetry code
O2A1-H2A1···O1W	2.31	3.071(4)	151	x,y,z
N8-H8A···O5W	2.21	3.045(8)	159	x,y,z
O6A3-H6A3···O1W	2.07	2.894(4)	169	x,y,z
O6A6-H28···O6AW	2.08	2.68(1)	128	x,y,z
O6A5-H6A5···O7AW	2.20	2.832(9)	132	x,y,z
O6A5-H6A5···O7BW	1.80	2.59(1)	156	x,y,z
O2A6-H2A6···O6AW	2.38	3.01(1)	132	x,y,z
O2A6-H2A6···O6BW	1.84	2.76(1)	171	x,1+y,z
O2A7-H2A7···O2W	1.84	2.676(4)	174	x,y,z
O6A7-H6A7···O4W	1.90	2.716(5)	164	x,y,z

There are 11 close contacts between water molecules and host atoms. The distances of these contacts are in the range 2.72-3.15 Å and their average value is 2.86 Å. Eighteen close contacts between water molecules exist with a mean distance of 2.77 Å and a range of 2.50-3.04 Å.

Water molecules O1W and O2W are of particular interest because both have unusually low temperature factors (0.028 and 0.038 $Å^2$ respectively). The reason for this is related to the hydrogen bonding of these two molecules. O1W is an acceptor of two host hydrogen bonds and is in close contact with two other host oxygen atoms. There is one host-water hydrogen bond for which O2W is the hydrogen bond acceptor. O2W is also in close contact with O4W and two other host oxygen atoms. Thus, it appears that both O1W and O2W are 'tethered' in at least four different directions, restricting their thermal motion.

Molecular geometry

The host molecule is distorted by the presence of the guest, particularly because of the extensive network of host-guest hydrogen bonds. The relevant geometrical parameters, as defined in Chapter 2, are listed in Table 17. Note in particular the large tilt angles – the maximum values of τ_1 and τ_2 are 22.6 and 25.5° respectively. The reason for these large values may be that, as mentioned previously, the host molecules of **LAMβCD** pack very closely to one another, to the extent that the A2 glucopyranoside residue is practically inserted at the secondary rim of an adjacent cyclodextrin. The torsion angle ϕ for residue A6 is large at -23.8° and the deviations (d) of O4 atoms from the mean plane of the O4 polygon are, on average, an order of magnitude greater than the corresponding values for the **ZIBβCD** structure.

Table 17: Geometrical parameters for the β-CD molecule of LAMβCD.

Residue	l (Å)	r (Å)	d (Å)	α	ϕ (°)	D_3 (Å)	τ_1 (°)	τ_2 (°)
A1	4.427	4.970	0.301(2)	128.2	12.0	2.953(4)	22.20(7)	21.2(2)
A2	4.402	5.046	0.053(2)	129.0	-7.1	2.914(4)	22.61(7)	25.5(2)
A3	4.335	5.141	-0.297(2)	125.0	-7.8	2.808(4)	3.06(8)	7.7(2)
A4	4.320	4.900	0.005(2)	130.6	5.1	2.946(4)	6.93(8)	8.6(1)
A5	4.483	4.931	0.414(2)	129.4	16.4	2.702(4)	4.74(7)	6.5(3)
A6	4.213	5.165	-0.301(2)	123.9	-23.8	2.755(4)	15.27(9)	20.5(2)
A7	4.414	4.986	-0.175(2)	129.7	6.3	3.184(5)	1.95(8)	2.2(1)

Figure 38 illustrates the large deviation from heptagonal symmetry of the **LAMβCD** host molecule by comparing its O4 polygon with a regular heptagon. The dramatic compression of the O4A6 angle is obvious.

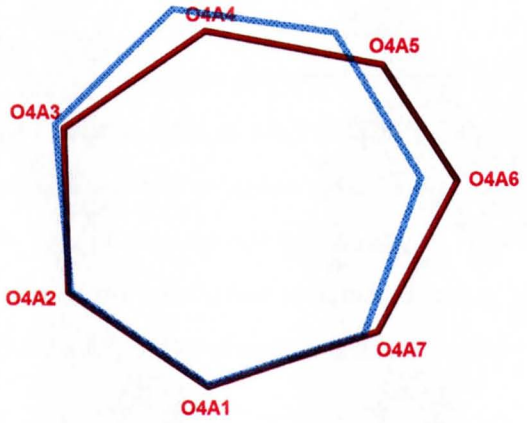

Figure 38: Overlay of the O4 polygon of LAMβCD and a regular heptagon.

With regard to the guest molecule, the pyrimidine ring is nearly planar as usual, while the cytosine ring is puckered in the usual envelope conformation, with C9 the flap atom (Figure 35). The maximum amplitude, q_2 = 0.421(4) Å and the phase angle, ϕ_2 = 290.5(6)°. The six-membered and five-membered rings are almost orthogonal to one another – the angle between the mean planes of these rings is 81.5(2)°. The torsion angles about the C11-C14 bond (about which the hydroxyl group may rotate) are -158.8(3)° (O10-C11-C14-O15) and 83.6(4)° (S12-C11-C14-O15).

Crystal packing

Notice in Figure 39 how the herringbone crystal packing of **LAMβCD** is similar to the crystal packing in two other structures, which are referred to here according to their CSD[16] reference codes – POBRON, where the only guest molecules are water atoms and SUYLON, which is the structure of a monosubstituted cyclodextrin (6-deoxy-6-[(1*R*,2*S*)-2-hydroxyindan-1-yl]amino-β-cyclodextrin) where the substituent is included within an adjacent molecule to form an infinite chain of tilted cyclodextrins stacked along the *b*-axis. In all three cases the packing arrangement may be classified as cage type. The cyclodextrins interlock to form 'herringbone' rows along the twofold screw-axis. It is particularly interesting that despite the similarities in packing, the nature of the complex in all three cases is very different. In the first case it is a hydrate, in the second a self-included complex and in the case of **LAMβCD**, a standard inclusion complex.

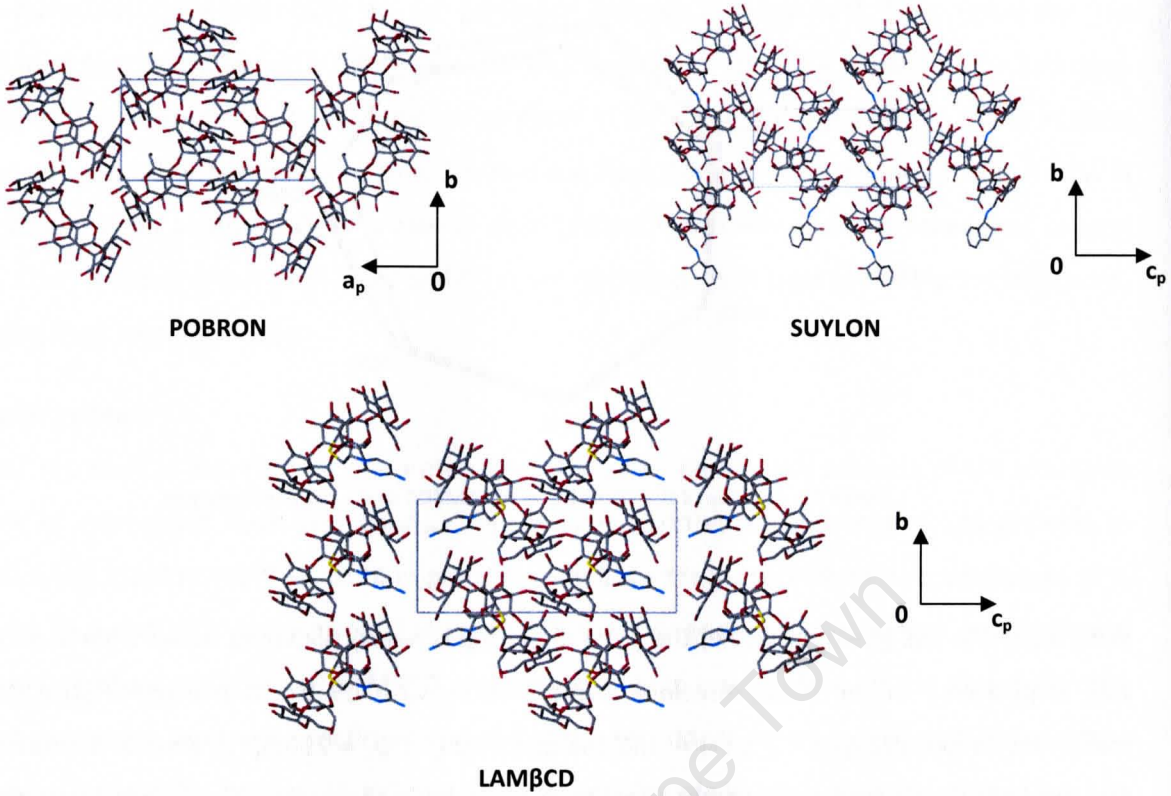

Figure 39: Diagram showing the similarity in packing arrangements between POBRON, SUYLON and LAMβCD.

The space-filling models in Figure 40 show how the guest molecule of **LAMβCD** fills the cyclodextrin cavity and how the monomeric complex units interlock and stack along the *b*-axis. The image on the right illustrates particularly how adjacent host molecules are positioned so that there are virtually no voids between them.

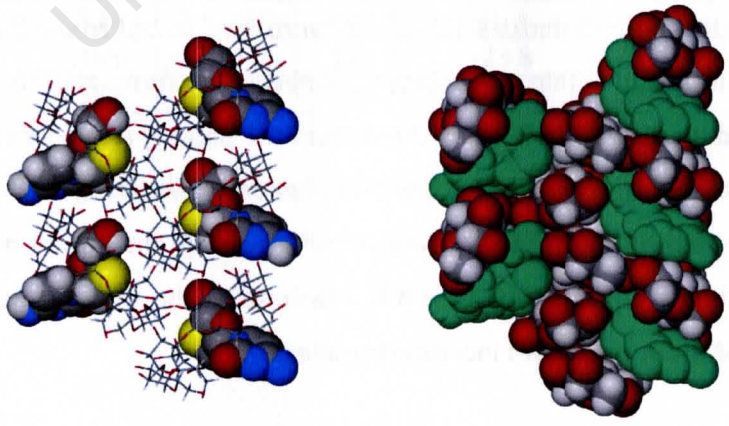

Figure 40: Space-filling models that further illustrate the crystal packing of LAMβCD.

The missing guest

The single crystal X-ray model that has just been discussed accounts for 1:1 host-guest stoichiometry but NMR data indicated a stoichiometric ratio of 1:1.5 for **LAMβCD**. Figure 41 shows the interstitial channel with water molecules represented as green spheres and bonded where the interatomic distances are smaller than the sum of the van der Waals radii. It is clear that none of the bonded fragments resembles any portion of the lamivudine molecule. Most of the residual electron density (the maximum peak height is 1.03 e $Å^{-3}$) of this structure is located within the illustrated space.

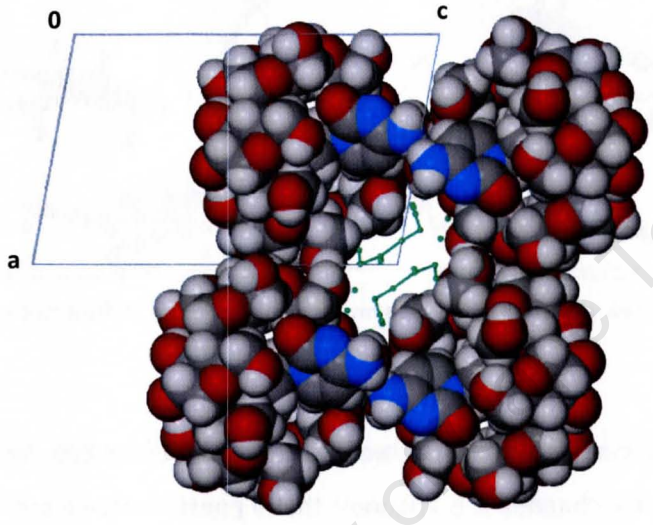

Figure 41: A view down the *a*-axis, showing the interstitial channel. Water molecules are represented as green spheres, bonded where the interatomic distance is smaller than the sum of the van der Waals radii.

A set of putative water molecules with low site-occupancy factors was removed from the model to simulate a void where a partial lamivudine guest molecule might be located. The atoms removed were O9AW, O9BW, O9CW, O10W, O11A, O11B and O11C. All of these water molecules had site-occupancy factors of less than 0.5 and none of them had been unequivocally identified as hydrogen bond acceptors. The hypothesis was that these oxygen atoms had accounted for density that in reality might represent the partial 'missing guest'.

The programme WebLab Viewer[17] was used to simulate the channel and the guest molecule. Two layers of the complex were generated and the guest orientated longitudinally to the channel. The guest was further orientated so that it was roughly in the middle of the two complex layers i.e. so that no portion of the guest would protrude from the top or bottom of the simulated channel. Thereafter it was translated and rotated to find the best fit. Two conformations of the guest were tested and the results of those tests are illustrated in Figure 42 and Figure 43.

First, the conformation of the modelled guest of **LAMβCD** was tested (Figure 42, left). It was possible to position the molecule such that the only close contact that formed was between an H atom of lamivudine (at C14) and water molecule O8W, which has a site-occupancy of 0.55. The 1.94 Å contact represents a possible C-H···O hydrogen bond. A second, more compact conformation of the lamivudine molecule was also tested (Figure 42, right). In this case it was possible to position the molecule within the channel without the occurrence of any close contacts.

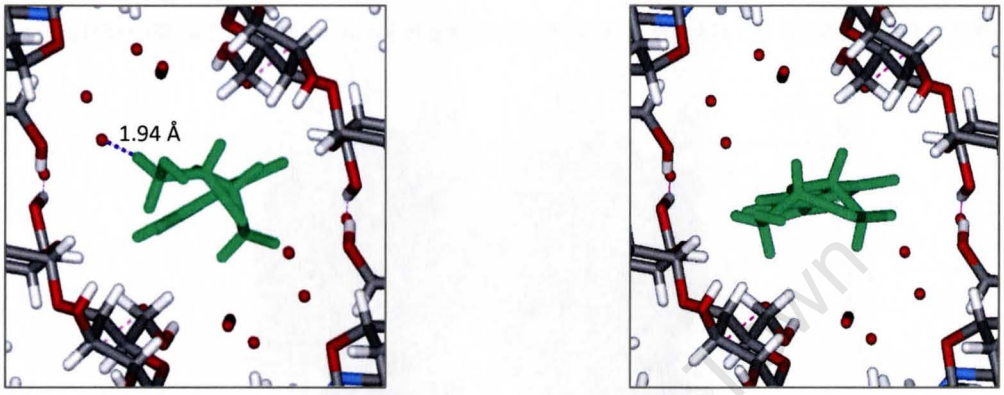

Figure 42: WebLab Viewer image of the simulated 'missing guest' in stick mode.

In Figure 43, space-filling models illustrate how the simulated guest molecules of both conformations fill the interstitial channel. It is apparent that a guest molecule could well be present in this space and the available evidence suggests that such a molecule would exhibit low s.o.f.s for the individual atoms and may be disordered over multiple positions.

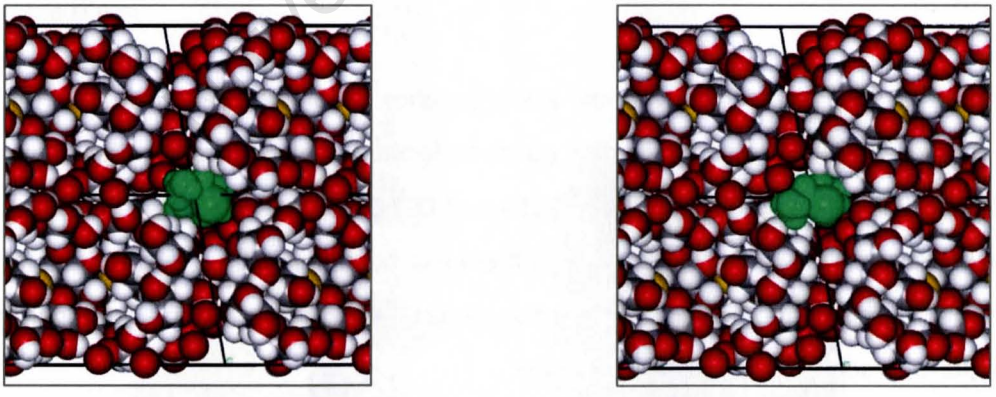

Figure 43: WebLab Viewer image of the simulated 'missing guest' in space-filling mode.

Comparative PXRD

The PXRD traces in Figure 44 demonstrate the similarity between the experimental trace for **LAMβCD** and the trace computed from the single crystal X-ray structure. Despite some incompleteness of the structure – i.e. significant electron density unaccounted for and the problem of an unmodelled partial guest – there is only one peak at 2θ ~ 21° in the computed pattern that is not present in the experimental trace. The variations in intensity at low 2θ values may be attributed to the aforementioned factors and/or preferred orientation effects.

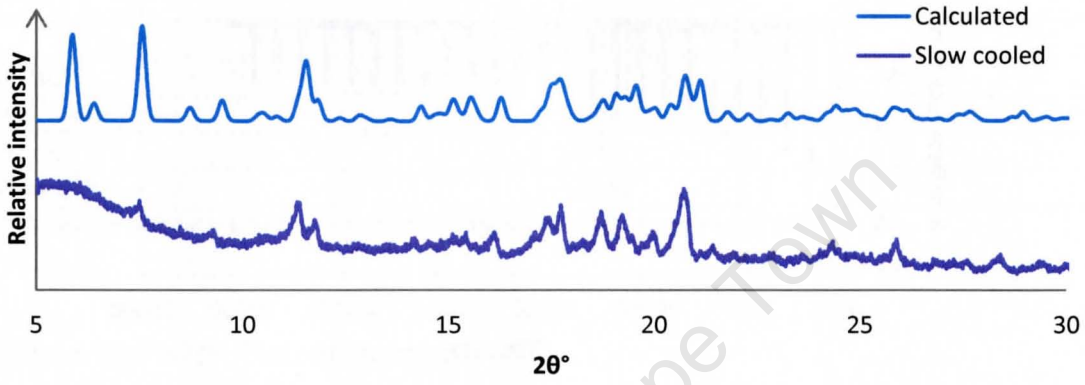

Figure 44: PXRD comparison of the experimental and computed traces for LAMβCD.

ITC

ITC was performed on the lamivudine-β-CD system in solution. A 15 mM β-CD solution was titrated against a 0.75 mM LAM solution at a temperature of 298 K. 10 μL aliquots were injected at 1.2 s intervals. The raw data are provided in Figure 45 and the integrated data from which the binding parameters were derived, are represented by the curve in Figure 46.

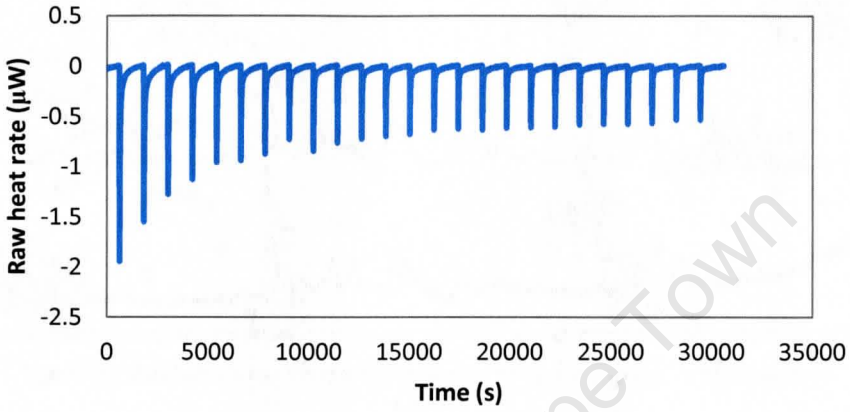

Figure 45: Raw ITC data for lamivudine in the presence of β-CD.

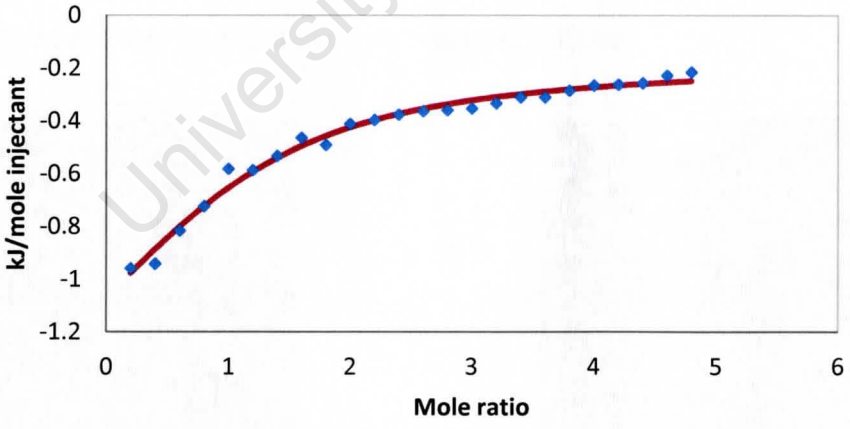

Figure 46: Integrated ITC data for lamivudine in the presence of β-CD compared with the calculated curve.

The binding parameters, determined directly from the ITC data, and calculated thermodynamic parameters are listed in Table 18. Chapter 2 contains the equations that were used to calculate ΔS^0 and ΔG^0. The stoichiometry in solution appears to be 1:1 (n = 1) and the association constant of 511 suggests that the interactions between the host and guest are relatively weak in solution. The thermodynamic data imply that the inclusion reaction is both enthalpy- and entropy-driven.

Table 18: Binding and thermodynamic parameters for the lamivudine-β-CD complex in solution.

Parameter	Value*
n	1
K	511(39)
ΔH^0 (kJ mol^{-1})	-3.7(1)
ΔS^0 (kJ K^{-1} mol^{-1})	0.039
$T\Delta S^0$ (kJ mol^{-1})	11752
ΔG^0 (kJ mol^{-1})	-15452

*The energy values without e.s.d.s were not directly measured but calculated using K and ΔH

Solution-state NMR Spectroscopy

The lamivudine-β-CD system in solution was analysed by proton NMR spectroscopy and Job plots produced according to the method described in Chapter 2. Stock solutions of 10 mM were prepared of lamivudine and β-CD in D_2O. These solutions were mixed to a constant volume of 2 cm^3 to give ratios in the range 0-1 with increments of 0.1, where the ratio is defined as $R = [X]/([H]_t+[G]_t)$. Figure 47 shows the Job plots of $\Delta\delta \cdot [X]$ against R, where $\Delta\delta$ is the induced chemical shift and [X] is the concentration of the host or guest, depending on which protons are being measured.

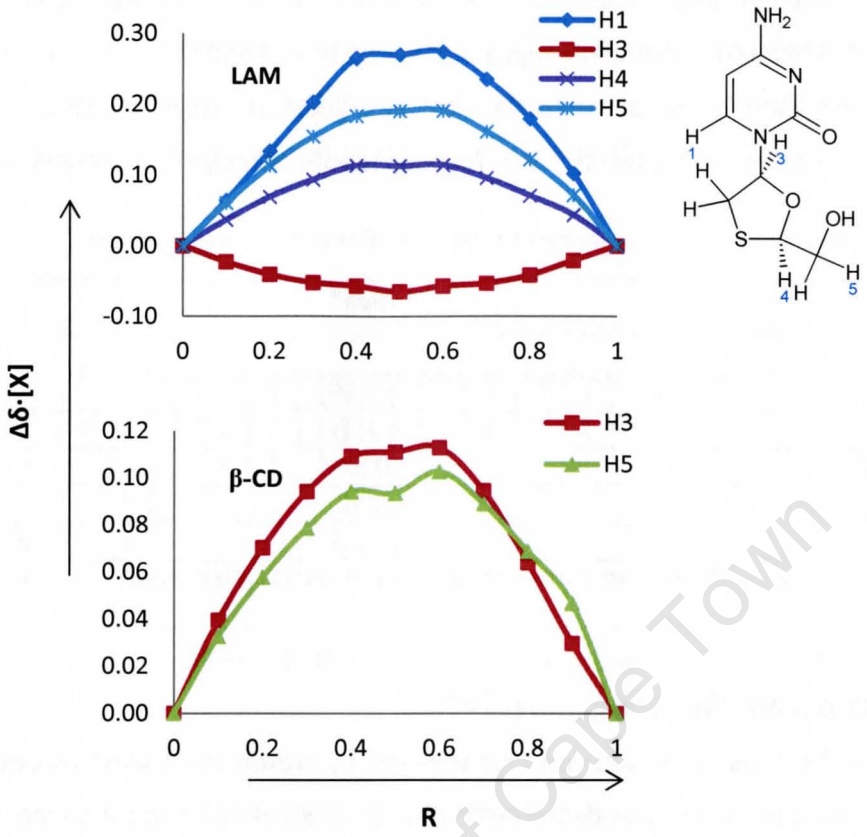

Figure 47: Job plots for lamivudine-β-CD in D_2O.

The results of the continuous variation experiment show that the average stoichiometry in solution is 1:1, but the fact that there are absolute maxima at R = 0.6 indicates that the system is intricate, with multiple modes of guest inclusion. Mostly, the H3 and H5 protons of β-CD experience the greatest increase in shielding, in which case the guest must penetrate at the secondary rim. The two dominant modes of inclusion are likely to involve:

1. Insertion of the cytosine fragment at the secondary rim, resulting in greater shielding of lamivudine protons H4 and H5
2. Insertion at the secondary rim, with the central portion of the lamivudine molecule (including protons H1 and H3) most affected

Using ConstEQ[18] as described in Chapter 2 with six protons of the lamivudine-β-CD complex in solution considered (two of the cyclodextrin and four of the drug), the association constant was determined. Table 19 provides K along with the error loss function (E) and the correlation coefficient (r). The Δδ values for the relevant protons are provided for a possible 1:1 complex. Each of these protons was included in the Job plots discussed earlier. The association constant determined using

NMR spectroscopy is fairly small, but importantly, is similar to the value determined by a rather different method, ITC, where K = 511 (Table 15). These association constants imply that the host-guest interactions are of moderate to weak strength.

Table 19: Association parameters for lamivudine-β-CD in D_2O assuming 1:1 complexation.

K	978.5
E	3.33×10^{-4}
r	0.9947
ΔδH3 (β-CD; ppm)	0.03950
ΔδH5 (β-CD; ppm)	0.03348
ΔδH1 (LAM; ppm)	0.08167
ΔδH3 (LAM; ppm)	-0.02227
ΔδH4 (LAM; ppm)	0.03864
ΔδH5 (LAM; ppm)	0.06398

γ-Cyclodextrin Complex

A lamivudine complex (**LAMγCD**) with γ-CD was prepared by kneading and slow cooling. The kneading experiment involved 20 mg (0.087 mmol) lamivudine and 124 mg (0.087 mmol) γ-CD. The reagents were mixed in a mortar and kneaded for a period of 30 min in the presence of a small amount of water. The slow cooling method was carried out by dissolving an equimolar (0.13 mmol) mixture of 30 mg lamivudine and 186 mg γ-CD in 1 cm^3 water at a temperature of 50 °C. The temperature was maintained and the solution stirred for approximately 6 h. Thereafter, the solution was passed through a 0.45 μm microfilter and cooled slowly over a period of three days in a covered vacuum flask. Powdered **LAMγCD** was obtained.

The slow cooling method is generally useful for growing larger crystals but in this case the product was always a powder. The complex was identified by PXRD analysis (Figure 48), which revealed that **LAMγCD** has the tetragonal crystal structure that is commonly observed for γ-CD inclusion complexes.

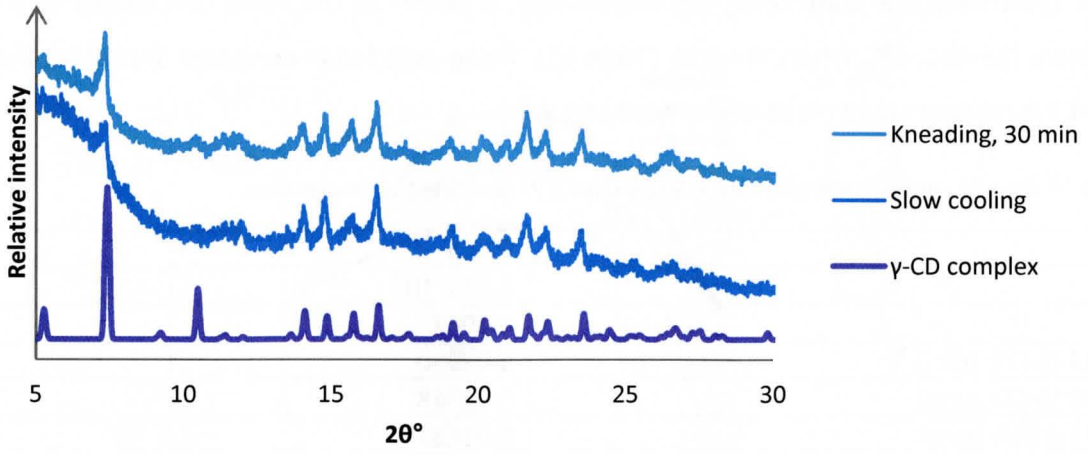

Figure 48: PXRD comparison of traces for LAMγCD prepared by different methods and a calculated trace representing the known γ-CD inclusion complexes.

References

1 Harris RK, Yeung RR, Lamont RB, Lancaster RW, Lynn SM, Staniforth SE (1997) J Chem Soc, Perkin Trans 2 12: 2653

2 Bhattacharya A, Roy BN, Singh GP, Srivastava D, Mukherjee AK (2010) Acta Crystallogr C66: 329

3 Bhatt PM, Azim Y, Thakur TS, Desiraju GR (2009) Cryst Growth Des 9: 951

4 Martins FT, Paparidis N, Doriguetto AC, Ellena J (2009) Cryst Growth Des 9: 5283

5 Lloret Perez S, Puigvert Colomer M (2009) International Patent Application 031026.

6 XPREP, Data Preparation and Reciprocal Space Exploration (1997) Version 5.1, Bruker Analytical X-ray Systems

7 Barbour LJ (1999) J Appl Cryst 32: 351

8 Sheldrick GM (2008) Acta Crystallogr A64: 112

9 Flack HD (1983) Acta Crystallogr A39: 876

10 Aakeröy CB, Fasulo ME, Desper J (2007) Mol Pharmaceutics 4: 317

11 Kilpatrick JE, Pitzer KS, Spitzer R (1947) J Am Chem Soc 69: 2483

12 Cremer D, Pople JA (1974) J Am Chem Soc 97: 1354

13 Karki S, Friščić T, Jones W, Motherwell WDS (2007) Mol Pharmaceutics 4: 347

14 Caira MR (2001) Rev Roum Chim 46: 371

15 Harata K (1993) Seimei Kogaku Kogyo Gijutsi Kenkyusho Kenkyu Hokoku 1: 1

16 Cambridge Structural Database and Cambridge Structural Database System (Feb, 2011) Version 5.32, Cambridge Crystallographic Data Centre, University Chemical Laboratory, Cambridge, England

17 WebLab ViewerPro 3.7. 2000, San Diego, CA: Molecular Simulations, Inc.

18 Floare C, Balibanu F, Bogdan M (2005) Studia UBB, Physica, Special Issue L. 4a: 451

Chapter 7: Conclusion

A total of nine new pharmaceutical co-crystals, salts, and cyclodextrin inclusion complexes of the selected antiretroviral drugs were discovered by supramolecular methods and isolated. Single crystal X-ray structures were determined for seven of these.

Co-crystal Screening

Co-crystal screening was carried out with nevirapine, efavirenz, zidovudine and lamivudine. The methods employed were dry co-grinding, liquid-assisted co-grinding and co-precipitation by the well-known slow evaporation procedure. PXRD together with thermal analysis, specifically HSM, TGA and DSC analysis, were used to identify co-crystals and, where co-crystallisation had occurred, to determine whether a sample contained only the co-crystal or a mixture of phases.

No co-crystals of efavirenz or zidovudine were isolated. Three co-crystals of nevirapine were prepared and these were labelled **NVPMLE**, **NVPGLT** and **NVPSLI**. For lamivudine, two novel pharmaceutical salts (**LAMOXL** and **LAMMLI**) and two other multi-component molecular crystals (**LAMGLT** and **LAMSUC**) were obtained by co-crystal screening and isolated. Proton NMR spectroscopy, X-ray diffraction, and thermal analysis methods were used to characterise these new forms. Where single crystals were obtained, three-dimensional X-ray analysis was used to determine the crystal structures and where this was not possible, the powdered samples were analysed by FTIR spectroscopy to investigate whether these were salts or co-crystals.

Cyclodextrin Inclusion

Cyclodextrin inclusion was attempted with each of the APIs using β-CD, γ-CD, DIMEB and TRIMEB. For the native cyclodextrins, attempts were made at preparing solid-state complexes by water-assisted kneading and co-precipitation. PXRD analysis and the isostructural series method described by Caira[1] was employed extensively for the identification of complexes.

There was no convincing evidence of complexation in any of the inclusion attempts with nevirapine and efavirenz. A lamivudine-β-CD complex (**LAMβCD**) was prepared by kneading in the presence of water and by slow cooling. Zidovudine was successfully included in β-CD by slow cooling and the solid-state complex (**ZIDβCD**) isolated; however, kneading methods produced only physical mixtures. A γ-CD inclusion complex of lamivudine was prepared by water-assisted kneading with but co-precipitation attempts yielded only crystals of the pure host. Single crystals were obtained of **LAMβCD** and **ZIDβCD** and the X-ray crystal structures of these inclusion complexes elucidated accordingly.

For the derivatised cyclodextrins, only co-precipitation at elevated temperature (60 °C) was attempted. All of the attempts at inclusion in DIMEB and TRIMEB were unsuccessful. The DIMEB experiments yielded only pure DIMEB crystals. In the case of the TRIMEB experiments, the solutions were not concentrated enough and did not crystallise after more than five months at 60 °C.

Cyclodextrin complexation in solution was also investigated. The continuous variation method was employed using proton NMR spectroscopy. For nevirapine, lamivudine and zidovudine, preliminary NMR test runs were carried out with β-CD and γ-CD. In the case of efavirenz, tests were conducted with β-CD, γ-CD, RAMEB and HP-β-CD, the derivatised CDs having been included because complexation with these had been reported by Sathigari and co-workers.[2] Based on the preliminary tests, full continuous variation experiments were conducted for lamivudine with β-CD, zidovudine with β-CD, and efavirenz with γ-CD, RAMEB and HP-β-CD. From the resultant data, association constants were determined for the lamivudine-β-CD and zidovudine-β-CD complexes, while for efavirenz, the data displayed no clear trends and were not conducive to carrying out the necessary calculations. ITC was employed for further characterisation of the inclusion behaviour of the lamivudine-β-CD complex in aqueous solution.

Nevirapine

The three new nevirapine co-crystals **NVPMLE**, **NVPGLT** and **NVPSLI** incorporate the carboxylic acids maleic acid, glutaric acid and salicylic acid, respectively. All three were prepared by liquid-assisted grinding, using chloroform as the solvent. This appears to be a very robust method. In scaling up from very small quantities of ~10 mg to larger quantities of ~10 g, only the duration of grinding and amount of solvent were increased appropriately. No other modifications to the preparative method were required. Furthermore, the co-crystallisation reaction was successful regardless of the pestle and mortar used – a small, smooth pestle and mortar were used for small batches, while large batches were prepared with a much bigger, textured pestle and mortar.

NVPGLT and **NVPSLI** could be reliably prepared by slow evaporation from a 50:50 v/v chloroform:hexane solution. Crystals of **NVPMLE** were obtained by slow evaporation but the result was not reproducible. Using the single crystals obtained, the X-ray crystal structures of all three co-crystals were determined with residual indices in the range $0.035 < R_1 < 0.066$ and Goodness of Fit parameters of $1.007 < S < 1.042$, implying excellent correlation between the data and the respective models.

Remarkably, nevirapine recrystallised upon melting of each of the co-crystals. It is a factor that should be carefully considered and further investigated if co-crystals of nevirapine are to be

commercialised. As in the cases where drugs have inadvertently undergone polymorphic phase transitions,[3] or transformed between anhydrous and hydrated forms, co-crystals of nevirapine may potentially revert to a mixture of free nevirapine and the co-former, especially if exposed to high temperature.

The aqueous solubility of the co-crystals was investigated. Two of the co-crystals showed only modest solubility increases for nevirapine, a similar result as was observed in a previous study for the saccharin and *rac*-tartaric acid co-crystals of nevirapine.[4] **NVPMLE**, on the other hand showed a fivefold drug solubility enhancement as compared with anhydrous nevirapine.

Interestingly, there are distinct similarities between the **NVPSLI** co-crystal and a previously reported toluene solvate of nevirapine.[5] Given that the salicylic acid and toluene molecules are of similar shape and size, to distinguish the two crystal forms as belonging to separate categories – one a solvate and the other a co-crystal – on the basis of one being a solid at room temperature and the other a liquid, seems illogical. As explained in Chapter 1, the definition of a co-crystal for the purpose of this dissertation includes the condition that the co-former be a solid at room temperature. However, the similarities between the crystal structure of **NVPSLI** and that of the nevirapine toluene solvate lend credence to Bond's assertion that the distinction between co-crystals and solvates is "contrived and inappropriate".[6]

Efavirenz

Though the experiments with efavirenz did not yield any co-crystals or cyclodextrin inclusion complexes, a known polymorph was prepared by liquid-assisted grinding and a solvate, also prepared by liquid-assisted grinding, was discovered.

Form β[7] of efavirenz was prepared from Form 1 by a simple, 10 min liquid-assisted grinding procedure, using ethanol as the solvent. The most recent patent application (2009),[8] claiming improved methods for the preparation of Form β, describes the use of solution-based methods involving seeding and freeze-drying. Previous descriptions of preparative methods for Form β have not included any grinding or solvent-assisted grinding procedures. Thus, the method described in this thesis represents a novel procedure for converting efavirenz Form 1 to efavirenz Form β.

The drug-solvent stoichiometry of the solvate was determined to be 1:0.6 by TG analysis, assuming that the included solvent is THF. However, this is only a tentative conclusion because the solvate could be prepared only by liquid-assisted grinding and desolvation occurred at low temperature (~40 °C). An accurate determination of stoichiometry would require the solvate to be prepared by a solution-based method and the sample analysed immediately upon removal from the mother liquor

to minimise solvent loss. Temperature-controlled PXRD analysis revealed that upon desolvation, the solvate reverts to efavirenz Form 1, the phase from which it was prepared.

Zidovudine

ZIDβCD, a novel 1:1 zidovudine-β-CD complex was prepared and characterised. Single crystals were grown with great difficulty. The slow cooling method had a low degree of reproducibility, with most of the experiments resuting in crystals of the pure host. The complex crystallises in the space group $C2$ with unit cell dimensions that place it in the isostructural series 11.[1] Its structure was determined by isomorphous replacement, using the coordinates of the structure with CSD reference code ZUZXOH. As is commonly the case with the $C2$ channel type structures of β-CD inclusion complexes, the guest was highly disordered and could not be modelled. The crystal structure included 7.2 water molecules distributed over 15 positions and this was in reasonable agreement with the value of 8.3 obtained from TG analysis, given the level of disorder present in the structure.

The complexation between β-CD and zidovudine in aqueous solution was investigated by NMR spectroscopy. The chemically induced shift values were very low and suggested only weak complexation. Job plots gave a host-guest stoichiometry of 1:1 and calculations using the program ConstEQ[9] yielded an association constant of K = 15 which is very low and confirms that the host-guest binding interaction in solution is extremely weak. This accounts for the difficulty with which crystals of the complex were obtained from solution.

Lamivudine

The two multi-component molecular crystals of lamivudine, **LAMGLT** and **LAMSUC**, were prepared using glutaric acid and succinic acid respectively. Both could be prepared by dry co-grinding and slow evaporation. Single crystals could not be grown, so the extent of ionisation could not be determined by single crystal X-ray diffraction analysis. FTIR evidence suggests that **LAMGLT** may be a salt and **LAMSUC** a co-crystal, but further investigation is required since the IR spectra were not conclusive.

LAMOXL and **LAMMLI**, the two additional salts were prepared by slow evaporation and their single crystal structures determined. Both salt formers are carboxylic acids and both salts crystallise in the space group $P2_12_12_1$, as is the case for the previously reported saccharinate and maleate salts.[10,11] However, only **LAMOXL** shows some similarities in crystal packing when compared with these previously reported forms.

As in the case of **ZIDβCD**, the **LAMβCD** single crystals were not easily obtained. The crystals of the complex formed only at very high reagent concentrations. The single crystal X-ray structure was solved but reconciling the X-ray data with other analytical data proved a challenge. Proton NMR data

yielded a host-guest stoichiometry of 1:1.5 but only one guest molecule (that included in the host cavity) could be modelled using the single crystal X-ray data. After the host-guest complex was modelled, all of the residual electron density difference peaks were treated as water molecules. These were modelled as such, using TG analysis as a guide for the number of expected water molecules. Nevertheless, an investigation using the program WebLab Viewer[12] revealed that the space occupied by dubious water molecules is large enough to accommodate a lamivudine molecule, which is probably disordered over multiple positions, such that it appears in the Fourier difference map as a diffuse scattering of low electron density peaks.

The **LAMβCD** structure represents a novel packing arrangement for native β-CD inclusion complexes. It is most similar to the structures of the series containing free hydrated β-CD, and may be considered a variation thereof, with elongation of the *c*-axis. In comparing with the modified CDs as well, the structure of **LAMβCD** is most similar to the crystal structure of a monosubstituted β-CD with CSD reference code SUYLON[13,14] but of course the two cannot be isostructural. The crystal packing of **LAMβCD** is highly dependent on a complex set of at least five host-guest hydrogen bonding interactions. The host is significantly distorted from its usually pseudo-heptagonal symmetry. In particular, some of the tilt angles τ_1 and τ_2 are very large (> 20°) because of the intricate host-guest hydrogen bonding. Adjacent complex units pack very closely, with the A2 residue of one host molecule nearly inserted at the secondary rim of another.

The lamivudine-βCD complex was analysed in aqueous solution by proton NMR spectroscopy and ITC. The Job plots from continuous variation experiments indicate a host-guest stoichiometry of 1:1 but there are consistent abnormalities in the curves that suggest the interactions in solution are much more complicated than conventional guest inclusion. The association constants determined from continuous variation and ITC differ, which is not uncommon,[15] but both suggest moderate to weak binding. From continuous variation, K = 979 and from ITC, K = 511.

Suggestions for Future Work

To date, five nevirapine co-crystals have been discovered. Given the 2000+ food additives and pharmaceutical excipients[16] that may be potential co-formers, as well as the dramatic influence that different solvents may have on the success rate of screening experiments, additional screening will surely yield more co-crystals. The saccharin and *rac*-tartaric acid co-crystals of nevirapine were shown to have enhanced nevirapine dissolution rates as compared with physical mixtures of the drug and co-former.[4] Similar experiments could be conducted with **NVPMLE**, **NVPGLT** and **NVPSLI** for comparison.

The inclusion complex **ZIDβCD** was not investigated by ITC. While the association constant has already been determined by proton NMR spectroscopy, analysis of the system by ITC could provide validation of the conclusion that the host-guest binding in solution is extremely weak.

LAMGLT, **LAMSUC**, **LAMOXL** and **LAMMLI** should also be tested to determine whether these exhibit improved lamivudine solubility and dissolution rates. Further analytical investigation of **LAMGLT** and **LAMSUC** is required to confirm whether these are in fact a salt and a co-crystal respectively. Alternatively, other solvents or solvent combinations could be employed in an effort to grow larger crystals for single crystal X-ray diffraction analysis.

References

1 Caira MR (2001) Rev Roum Chim 46: 371

2 Sathigari S, Chadha G, Lee Y-HP, Wright N, Parsons DL, Rangari VK, Fasina O, Babu RJ (2009) AAPS PharmSciTech 10: 81

3 Bauer J, Spanton S, Henry R, Quick J, Dziki W, Porter W, Morris J (2001) Pharm Res 18: 859

4 Samsodien H (2010) Supramolecular Derivatives of Selected Bioactive Compounds: A Physicochemical Study, PhD Thesis, University of Cape Town, South Africa

5 Caira MR, Stieger N, Liebenberg W, De Villiers MM, Samsodien H (2008) Cryst Growth Des 8: 17

6 Bond AD (2007) CrystEngComm 9: 833

7 Sharma R, Bhushan KH, Aryan RC, Singh N, Pandya B, Kumar Y (2006) International Patent Application 040643

8 Tyagi OD, Jetti KR, Ramireddy BA (2009) International Patent Application 087679

9 Floare C, Balibanu F, Bogdan M (2005) Studia UBB, Physica, Special Issue L. 4a: 451

10 Bhatt PM, Azim Y, Thakur TS, Desiraju GR (2009) Cryst Growth Des 9: 951

11 Martins FT, Paparidis N, Doriguetto AC, Ellena J (2009) Cryst Growth Des 9: 5283

12 WebLab ViewerPro 3.7. 2000, San Diego, CA: Molecular Simulations, Inc.

13 Cambridge Structural Database and Cambridge Structural Database System (Feb, 2011) Version 5.32, Cambridge Crystallographic Data Centre, University Chemical Laboratory, Cambridge, England

14 Harata K, Takenaka Y, Yoshida N (2001) J Chem Soc, Perkin Trans 2 (9):1667

15 Loftsson T, Másson M, Brewster ME (2004) J Pharm Sci 93: 1091

16 Trask AV (2007) Mol Pharmaceutics 4: 301